Version 4.0
December 2011

Cosmic Origins Spectrograph Instrument Handbook for Cycle 20

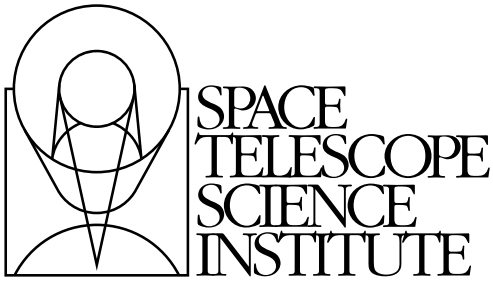

Space Telescope Science Institute
3700 San Martin Drive
Baltimore, Maryland 21218
help@stsci.edu

Operated by the Association of Universities for Research in Astronomy, Inc., for the National Aeronautics and Space Administration

User Support

For prompt answers to any question, please contact the STScI Help Desk.

- Send e-mail to: help@stsci.edu.
- Phone: 410-338-1082.
- Within the USA, you may call toll free: 1-800-544-8125.

World Wide Web

Information and other resources are available on the STScI COS World Wide Web site:

http://www.stsci.edu/instruments/cos

COS Handbook History

Version	Date	Editors
4.0	December 2011	Dixon, W. V.
3.0	December 2010	Dixon, W. V.
2.0	January 2010	Dixon, W. V., and Niemi, S.-M.
1.0	December 2007	Soderblom, D. R.

Additional Contributors

Please see the acknowledgments.

Citation

In publications, please refer to this document as
Dixon, W. V., et al. 2011, Cosmic Origins Spectrograph Instrument Handbook, Version 4.0 (Baltimore: STScI)

Send comments or corrections to:
Space Telescope Science Institute
3700 San Martin Drive
Baltimore, Maryland 21218
E-mail:help@stsci.edu

Table of Contents

Acknowledgments

The technical and operational information contained in this handbook is the summary of the experience gained by members of the STScI COS Team and by the COS IDT at the University of Colorado in Boulder.

Current and former members of the STScI COS Team include Alessandra Aloisi (lead), Tom Ake, Rossy Diaz, Van Dixon, Tom Donaldson, Linda Dressel, Scott Friedman, Parviz Ghavamian, Paul Goudfrooij, George Hartig, Phil Hodge, Mary Beth Kaiser, Tony Keyes, Claus Leitherer, Chris Long, Matt McMaster, Melissa McGrath, Derck Massa, Sami Niemi, Cristina Oliveira, Rachel Osten, Charles Proffitt, David Sahnow, Ken Sembach, Brittany Shaw, Ed Smith, David Soderblom, Katya Verner, Nolan Walborn, Alan Welty, Tom Wheeler, Brian York, and Wei Zheng. All of these individuals contributed to this volume, as did Russ Makidon.

The COS IDT includes James Green (Principal Investigator), Cynthia Froning (Project Scientist), Steven Penton, Steven Osterman (Instrument Scientist), Stéphane Béland, Eric Burgh, Charles Danforth, Kevin France, and Brian Keeney, all of whom provided information and assistance. COS co-investigators are Dennis Ebbets (Ball Aerospace), Sara R. Heap (GSFC), Claus Leitherer (STScI), Jeffrey Linsky (University of Colorado), Blair D. Savage (University of Wisconsin-Madison), Ken Sembach (STScI), J. Michael Shull (University of Colorado), Oswald Siegmund (University of California, Berkeley), Theodore P. Snow (University of Colorado), John Spencer and Alan Stern (Southwest Research Institute), and John T. Stocke (University of Colorado). K. Brownsberger, J. Morse, and E. Wilkinson have also been part of the COS IDT and have made significant contributions.

The prime contractor for COS is Ball Aerospace, Boulder, Colorado. The XDL detector was built at UC Berkeley by O. Siegmund, J. McPhate, J. Vallerga, and B. Welsh.

The Editor thanks Susan Rose (Senior Technical Editor) for her contributions to the production of this handbook.

References and Additional Information

This document relies heavily on information provided by the COS team in Boulder. The primary documents used are

Morse, J. 2004, Cosmic Origins Spectrograph Science Operations Requirements Document (referred to as OP-01);

Wilkinson, E. 2002, COS Calibration Requirements and Procedures, rev. B. (referred to as AV-03); and

Wilkinson, E. 2008, COS Prelaunch Calibration Data (referred to as AV-04).

We also used the *STIS Instrument Handbook* (Kim Quijano et al. 2007, v8.0).

CHAPTER 1:

An Introduction to COS

In this chapter…

1.1 Overview

The Cosmic Origins Spectrograph (COS) was installed on the *Hubble Space Telescope (HST)* in May 2009. Working at far-ultraviolet wavelengths, COS was designed to study the origins of large-scale structure in the Universe, the formation and evolution of galaxies, the origin of stellar and planetary systems, and the cold interstellar medium. COS significantly enhances the spectroscopic capabilities of *HST* at ultraviolet wavelengths, providing observers with unparalleled opportunities for observing faint sources of ultraviolet light.

COS offers two independent observing channels, an FUV detector sensitive to wavelengths between 900 and 2150 Å and an NUV detector for wavelengths from 1650 to 3200 Å. Both channels are equipped with medium-resolution (R ~ 20,000) and low-resolution (R ~ 3000) gratings. In addition, the NUV channel can be used in imaging mode for both target acquisitions and scientific observations. The COS field of view is approximately 2.5 arcsec in diameter.

In this chapter, we provide a brief overview of COS operations, tables of instrument and detector parameters, a list of frequently-asked questions, and a guide to using this handbook.

1.2 Observing with COS

1.2.1 Target Acquisitions

The COS entrance apertures are 2.5 arcsec in diameter. To ensure that the target is centered in the aperture, a target-acquisition procedure must be performed at the beginning of each visit. For moving targets, acquisition should be repeated at the beginning of each orbit.

The COS flight software provides two methods for acquiring and centering a target in the aperture. The first method obtains a direct image of the aperture with the NUV channel and moves the telescope to the center of light. The second method centers the target using its dispersed spectrum and can be performed with either the NUV or FUV channel. For both methods, a target's center of light can be computed from a single exposure or from a series of exposures that map out a grid on the sky. Acquisitions are described in Chapter 8.

1.2.2 Observing Modes: Spectroscopic and Imaging

While COS was designed as a spectrograph, the NUV channel can be used for imaging observations. With a plate scale of 23.5 mas per pixel, COS provides the highest spatial sampling of any instrument aboard *HST*. The image is corrected for the telescope's spherical aberration, but is degraded by zonal (polishing) errors on its primary and secondary mirrors (see Chapter 3). The NUV imaging count-rate limit of 50 counts per second per pixel (Table 10.1) corresponds to a *Galex* NUV magnitude of 17.6.

1.2.3 Observing Modes: TIME-TAG and ACCUM

COS provides two observing modes, `TIME-TAG` and `ACCUM`. In `TIME-TAG` mode, the position, arrival time, and (for FUV) pulse height of each detected photon are recorded in the memory buffer. In `ACCUM` mode, only the location of arriving photons is recorded.

`TIME-TAG` mode is preferred, because it allows for more sophisticated data reduction. For example, an observer may compare data from the night and day sides of the orbit or compute the count rate of an object whose intensity varies on short time scales. `TIME-TAG` observations through the PSA allow the taking of occasional wavelength-calibration spectra during an exposure. These spectra are used by the COS data-reduction pipeline **calcos** to correct drifts in the spectrum due to small motions of the Optics Select Mechanism (OSM). `ACCUM` mode is designed for observations of targets too bright for `TIME-TAG` mode. Because the lower information content of `ACCUM` data reduces their utility for archival researchers, its use must be justified for each target.

Both `TIME-TAG` and `ACCUM` modes may be used with either the FUV or NUV channel. For more information comparing `TIME-TAG` and `ACCUM`, see Section 5.2.

1.2.4 Typical Observing Sequences

In the majority of cases, the following sequence of events will produce high-quality data:

- Acquire the object using `ACQ/IMAGE`. This should take about three minutes. See the examples in Chapter 9.
- Obtain spectra in `TIME-TAG` mode using multiple `FP-POS` settings and `FLASH=YES` so the spectra can be corrected for flat-field anomalies and OSM drifts. The COS Exposure Time Calculator (ETC) provides a means of calculating essential parameters such as the `BUFFER-TIME`.
- Obtain additional spectra during subsequent orbits to achieve the desired signal-to-noise ratio or wavelength coverage.

1.3 COS Quick Reference Guide

Table 1.1: COS Instrument Characteristics

Property	FUV channel	NUV channel
Entrance apertures	2.5 arcsec round: clear (PSA) or attenuated (BOA)	
Detector plate scale	0.1 arcsec per pixel 1 arcsec per resel (G130M cross-dispersion)	23.5 mas per pixel 70.5 mas per resel (imaging mode)

Table 1.2: COS Detector Characteristics

		FUV XDL	NUV MAMA
Photocathode		CsI (opaque)	Cs_2Te (semi-transparent)
Window		None	MgF_2 (re-entrant)
Wavelength range		< 900 – 2150 Å	1650 – 3200 Å
Active area		85 × 10 mm (two)	25.6 × 25.6 mm
Pixel format (full detector)		16384 × 1024 (two)	1024 × 1024
Image size recorded per spectrum		16384 × 128 (two, `ACCUM`) 16384 × 1024 (two, `TIME-TAG`)	1024 × 1024
Pixel size		6 × 24 µm	25 × 25 µm
Spectral resolution element size (= resel)		6 × 10 pix	3 × 3 pix
Quantum efficiency		~26% at 1335 Å ~12% at 1560 Å	~10% at 2200 Å ~8% at 2800 Å
Typical dark-count rate (away from SAA)[1]		1.25 cnt s^{-1} cm^{-2} 1.8×10^{-6} cnt s^{-1} pix^{-1} 1.1×10^{-4} cnt s^{-1} $resel^{-1}$	128 cnt s^{-1} cm^{-2} 8.0×10^{-4} cnt s^{-1} pix^{-1} 7.2×10^{-3} cnt s^{-1} $resel^{-1}$
Detector global count rate limit[2]	TIME-TAG mode	30,000 cnt s^{-1} (but counts lost at rates above ~21,000 cnt s^{-1})	
	ACCUM mode	~60,000 cnt s^{-1} per segment	~170,000 cnt s^{-1}
Local count-rate limit[2]		~1.67 cnt s^{-1} pix^{-1} ~100 cnt s^{-1} $resel^{-1}$	~200 cnt s^{-1} pix^{-1} ~1800 cnt s^{-1} $resel^{-1}$
Screening limits for bright objects		see Table 10.1	
Dead-time constant		7.4 µsec	280 nsec

1. FUV dark rates were measured in 2010 September; NUV values are projections to the middle of Cycle 20 (2013 April).
2. Count rates higher than these limits will trigger a detector shut-down. Bright-object screening limits are lower. See Chapter 10.

Table 1.3: COS Calibration Accuracies

Property	FUV channel	NUV channel
Wavelength zero point: M gratings	15 km s^{-1}	15 km s^{-1}
Wavelength zero point: L gratings	150 km s^{-1}	175 km s^{-1}
Wavelength scale	15 km s^{-1}	15 km s^{-1}
Absolute photometry	5%	5%
Relative photometry (same object at a different time)	2%	2%
Flat field quality (spectral S/N) per resel, using standard techniques	35:1[1]	100:1
Flat field quality (spectral S/N) per resel, goal	100:1	100:1

1. S/N of 100:1 is possible; see Section 5.8.1.

Table 1.4: Useful Figures and Tables

Topic	Source	Content
Usage planning	Table 5.1	Grating parameters
	Table 5.4	FUV grating wavelength ranges
	Table 5.5	NUV grating wavelength ranges
	Table 10.1	Count-rate screening limits
Aperture parameters and PSFs	Figure 3.2	BOA transmission
	Figure 3.6	Model LSFs for the COS FUV Channel
	Figure 4.8	Model LSFs for the COS NUV Channel
	Figure 3.7	Resolving Power of FUV Gratings
	Figure 6.4	Cross section of the COS imaging PSF
	Figure 8.5	Relative transmission of the COS PSA in the NUV
	Figure 13.28	*HST* focal plane and COS aperture
Effective Area	Figure 5.1	FUV spectroscopy
	Figure 5.2	NUV spectroscopy
	Figure 6.3	NUV imaging
Acquisitions	Figure 8.1	Example of 3 × 3 spiral search pattern
	Figure 8.2	Point-source images with all apertures and mirrors
	Figure 8.3	ACQ/IMAGE exposure times
	Figure 8.4	Dispersed-light exposure times
Detector characteristics	Figure 4.1	FUV XDL detector schematic layout
	Figure 4.7	NUV MAMA detector layout
	Table 7.1	Detector background count rates
Overheads and observing parameters	Table 5.2	TAGFLASH exposure durations
	Table 9.1	Overhead estimates for Phase I proposals
	Table 9.2	Generic observatory overhead times
	Table 9.3	Overhead times for OSM1 movements
	Table 9.4	Overhead times for OSM2 movements
	Table 9.5	Science exposure overhead times
Celestial backgrounds	Figure 7.1	Sky background versus wavelength
	Figure 7.2	Moon, Earth and zodiacal-light background levels
	Figure 7.3	Galactic extinction model
	Table 7.3	Earthshine and zodiacal light fluxes
	Table 7.4	Strengths of airglow lines
Data quality	Figure 5.9	FUV flat-field example
	Figure 5.11	NUV flat-field example

1.4 COS FAQ

Table 1.5: COS Frequently-Asked Questions

Question	Answer
Should I use COS or STIS? Does COS have an imaging mode?	Section 2.5 Chapter 6
What detectors are available? What apertures? What gratings? What are their properties?	Chapter 4 Section 3.1.2 Tables 5.1, 5.4, 5.5
What do COS images look like? What do COS spectra look like? Do the spectra have gaps?	Figure 6.1 Figures 4.2, 4.7 Section 5.5
What is the difference between ACCUM and TIME-TAG mode? How do I estimate the BUFFER-TIME for TIME-TAG exposures? How do I obtain wavelength-calibration exposures?	Section 5.2 Section 5.4 Section 5.7
What are the science impacts of the COS line-spread function? What are the COS sensitivity and resolution below 1150 Å? Which COS gratings suffer from second-order contamination?	Section 3.3 Figures 5.3, 5.5, 5.6 Section 5.1.3
How accurate is COS absolute/relative photometry? How accurate are the COS wavelength scale and zero point?	Section 5.1.9 Section 5.1.10
How do I plan a successful target acquisition?	Chapter 8
What are the bright-object limits? How do I confirm that my target/field is safe to observe?	Table 10.1 Section 10.5
How much time should I request for my observations?	Chapter 9

1.5 Purpose of This Handbook

The *COS Instrument Handbook* describes the design, performance, operation, and calibration of COS. It is meant to be the principal reference manual for users of the Cosmic Origins Spectrograph. This handbook is written and maintained at STScI. While it presents the best available information about COS, tabulated parameters are likely to evolve as we learn more about its on-orbit performance.

The handbook is designed for readers who are

- preparing a Phase I proposal to observe with *HST*;
- writing a Phase II program once a proposal has been accepted; or
- analyzing data from observations that have already been made.

This handbook is not meant to be the primary reference for COS data reduction or analysis; that information is provided in the *COS Data Handbook*. For quick reference, information on COS data products is provided in Chapter 11.

Document Conventions

This document follows the usual STScI conventions:

- Terms, words, or phrases that are to be entered by the user in a literal way in an *HST* proposal are shown in a typewriter or Courier font, such as "`COS/FUV`" or "`TIME-TAG`."
- Names of software packages or commands (such as **calcos**) are shown in boldface.

Wavelengths in this handbook and in COS data products are always as measured in vacuum and are quoted in Ångstroms (Å).

CHAPTER 2:

Special Considerations for Cycle 20

In this chapter…

2.1 COS Observations below 1150 Å with R > 10,000

A new G130M central-wavelength setting, 1222 Å, will be available for Cycle 20. It spans the 1065–1365 Å bandpass, providing an effective area similar to that of G130M/1096, but with considerably higher resolution. Preliminary measurements (derived from low signal-to-noise data) indicate that the resolving power of this mode is R > 13,000 at 1135 Å and R > 10,000 at 1340 Å, but predicted values exceed 14,000 at 1065 Å and 17,000 at 1135 Å (see Figure 5.5). An additional feature of this setting is that it places the Lyman α airglow line in the gap between detector segments A and B, eliminating this source of damaging high-intensity flux.

This observing mode will facilitate studies of

- Ly β, O VI, and Ly α absorption in the low-redshift IGM (z = 0.125);
- the He II Ly α forest at the epoch of He II re-ionization (z = 2.51–2.73);
- molecular hydrogen in planetary nebulae and in translucent clouds; and
- high-ionization AGN outflows at low redshifts.

2.2 Time-Dependent Sensitivity Changes

During Cycle 17, the throughput of some COS modes—the bare-aluminum NUV G225M and G285M gratings and the FUV channels—was found to be declining with time significantly more rapidly than had been expected. Since that time, the decline of the G225M and G285M grating throughputs has continued at approximately the same rate, but the rate of decline of the FUV channels has become considerably more modest (Section 5.1.4).

In addition, the FUV detector is beginning to show evidence of gain sag in some parts of the detector. The COS instrument team is working on operational changes to mitigate these effects, but for some observations, it is possible that gain sag may affect the data quality and S/N achieved, especially if multiple FP-POS positions are not employed. See Section 4.1.6 for details.

Despite these challenges, the COS FUV sensitivity is still outstanding, and COS remains the instrument of choice for most spectroscopic observations of faint FUV targets.

The figures and tables in this handbook were constructed using projected instrumental sensitivities for the middle of Cycle 20 (2013 April). Observers are reminded to use the COS Exposure Time Calculator (ETC; see Chapter 7) to design their proposals; it will be updated as the instrument sensitivity evolves.

2.3 Non-Optimal Observing Scenarios

To optimize the scientific return of COS, we recommend that all observations be performed in TIME-TAG mode, employ the default wavelength-calibration procedures (i.e., `TAGFLASH=YES`), and obtain data at all four FP-POS positions of each CENWAVE setting (for the FUV gratings). Observers who wish to employ non-optimal observing techniques must justify their observing strategy in the "Description of Observations" section of their Phase I proposal.

2.4 SNAP Programs with COS

The COS photon-counting detectors can be harmed by exposure to bright light. Because all COS observations must be checked at STScI by an Instrument Scientist to confirm that both the intended target and all nearby objects lie within safe-brightness limits, the total number of targets accepted for all COS and STIS MAMA SNAP programs will be limited to 150 per cycle. For more information on this and other policies pertaining to *HST* observing, please see the *Call for Proposals*.

2.5 Should I Use COS or STIS?

With the installation of COS and the repair of STIS, *HST* has two spectrographs with significant overlap in spectral range and resolving power. Each has unique capabilities, and the decision of which to use will be driven by the science goals of the program and the nature of the target to be observed.

In the far-UV (from about 1100 to 1800 Å), the throughput of the COS FUV channel exceeds that of the STIS FUV MAMA by factors of 10 to 30, and the combination of the spectroscopic resolving power (~20,000) and wavelength coverage (300 to 370 Å per setting) of the medium-resolution COS FUV modes results in a discovery space (throughput times wavelength coverage) for observations of faint FUV point sources that is at least 10 times greater for most targets than that of STIS modes with comparable resolution, and as much as 70 times greater for faint, background-limited point sources.

Because of its MgF_2 windows, the STIS FUV MAMA is insensitive to wavelengths below ~ 1150 Å. The COS FUV XDL detector is windowless and provides useful throughput to at least 900 Å. See Section 5.1.2 for details.

In the near-UV (approximately 1700 to 3200 Å), COS and STIS have complementary capabilities. To accommodate the NUV detector format, the COS NUV spectrum is split into three non-contiguous stripes, each of which covers a relatively small range in wavelength. Obtaining a full NUV spectrum of an object requires several set-ups and exposures (6 or more for the medium-resolution gratings and 4 for G230L). When broad NUV wavelength coverage is needed, obtaining a single STIS spectrum may be more efficient than taking separate COS spectra. Users should also consider that the STIS NUV modes have produced a large set of existing observations, while the COS NUV modes have so far seen limited use. As a result, the calibration of the STIS NUV modes is likely to be superior to that of comparable COS modes for the foreseeable future.

Because the dark rate of the COS NUV detector is substantially lower than that of STIS, COS will often be superior for faint sources, even when more exposures are required to achieve full wavelength coverage. As of September 2011, the mean dark rate of the STIS NUV MAMA was about 2.7×10^{-3} counts/pixel/s, about twice the typical pre-SM4 value. The COS dark rate has been increasing with time, but even if current trends continue, the projected mean value of 8.0×10^{-4} counts/pixel/s for April 2013 will still be a fraction of the rate for STIS. Observers are advised to perform detailed calculations using both the COS and STIS ETCs and to consider carefully the relative instrument overheads to determine which combination of instruments and modes is best for their science.

For observations of extended sources, the spatial resolution offered by STIS must be weighed against the superior sensitivity of COS. One of the primary design goals of STIS was to provide spatially-resolved spectra in the UV, optical, and near-IR. The STIS long slits, when used with the first-order gratings, allow spatially-resolved observations that exploit the intrinsically high resolution of *HST* over the full width of the detectors (approximately 0.05 arcsec per 2-pixel spatial resolution element over a

length of 25 arcsec with the NUV and FUV MAMAs, and ~ 0.1 arcsec per 2-pixel spatial-resolution element over a length of 52 arcsec with the CCD).

COS was optimized for point-source observations. While COS has relatively large entrance apertures (2.5 arcsec diameter), flux from regions more than 0.5 arcsec from the aperture center is significantly vignetted. These large apertures also mean that objects extended in the dispersion direction will yield spectra with lower spectral resolution. In addition, the optical design of the FUV channel limits the achievable spatial resolution; measured values of the FWHM in the spatial dimension vary between about 0.25 and 1.5 arcsec, depending on grating and wavelength (Section 5.1.8). The COS NUV channel uses a different optical design and has a spatial resolution comparable to that of the STIS first-order NUV modes (~ 0.05 arcsec), with somewhat better sampling; however, for sources extending more than 1 arcsec in the spatial direction, the various NUV spectral segments will begin to overlap.

The line-spread functions (LSFs) of both instruments exhibit non-Gaussian wings due to mid-frequency zonal (polishing) errors in the Optical Telescope Assembly (OTA). Using STIS, one can minimize their effects through the use of narrow apertures. On COS, narrow apertures are not available. The broad wings of the its LSF, especially in the short wavelengths of the FUV band, can limit the ability of COS to resolve faint, narrow features and blend closely-spaced lines. Studies that require accurate knowledge of the line profile will require full consideration of the COS LSF (Section 3.3). The non-Gaussian wings of the COS LSF should have only modest impact on science programs targeting broad lines and continuum sources.

Both COS detectors and the STIS MAMA detectors are prohibited from observing objects that exceed specific brightness levels (see Chapter 10 in this handbook and Sections 13.8 and 14.8 of the *STIS Instrument Handbook*). Some brightness limits have been established for the health and safety of the instrument, while others are practical limits that are set to ensure good data quality. Because STIS is less sensitive than COS, the brightness limits for STIS tend to be significantly less stringent. In the NUV range, the STIS G230LB and G230MB gratings can also be used with the STIS CCD, which has no bright-object limitations. STIS also has a number of small and neutral-density apertures that can be used with the MAMA detectors to attenuate the light of a too-bright object. COS has only a single neutral-density filter that attenuates by a factor of about 200 but also degrades the spectral resolution by a factor of 3 to 5. In most cases, some combination of STIS gratings and apertures will be a better choice for observing a UV-bright object than COS with its neutral-density filter. Users are advised to compare results from the COS and STIS ETCs when deciding on an appropriate strategy for their target.

The STIS high-dispersion echelle modes E140H and E230H have resolving powers of ~114,000 (or even R ~ 200,000 with the 0.1 × 0.03 aperture and specialized data reduction; see Section 12.6, "Improving the Sampling of the Line Spread Function," of the *STIS Instrument Handbook*), significantly higher than the best COS resolution. Also, STIS can obtain spectra in the optical and near-IR at wavelengths up to 10,200 Å, while the maximum wavelength observable by COS is about 3,200 Å.

Both STIS and COS can perform observations in `TIME-TAG` mode, whereby the time of each photon's arrival is recorded. STIS is capable of a much finer time

resolution (125 microseconds vs. 32 milliseconds for COS), although few programs require such a high sampling rate. Due to its lower sensitivity, STIS may be able to observe a target in TIME-TAG mode that is too bright for TIME-TAG observations with COS. On the other hand, TIME-TAG data acquired with the COS FUV detector includes information on the pulse-height distribution, while TIME-TAG data acquired with the STIS and COS MAMAs do not. Pulse-height information can be valuable in identifying and rejecting background counts in the spectra of faint sources.

CHAPTER 3:

Description and Performance of the COS Optics

In this chapter…

3.1 The Optical Design of COS

In most spectrographs, the light from the telescope is focused onto a slit, which then re-imaged onto the detector. In such a design, the slit width and the way that the slit is illuminated determine the resolving power and line-spread function (LSF). COS is different: it is essentially a slitless spectrograph with an extremely small field of view. In this section, the light from the *HST* Optical Telescope Assembly (OTA) is followed as it progresses through COS to each optical element and mechanism. The optical path and mechanism locations are shown in Figure 3.1.

3.1.1 External Shutter

The external shutter is located at the front of the COS enclosure. When closed, the shutter blocks all external light from entering the COS instrument and prevents light from the COS internal lamps from exiting the instrument. The opening and closing of the external shutter do not define the duration of an exposure, as the shutter may be opened before an exposure begins to allow for target acquisition and bright-object checking.

Figure 3.1: The COS Optical Path and the Locations of the Mechanisms

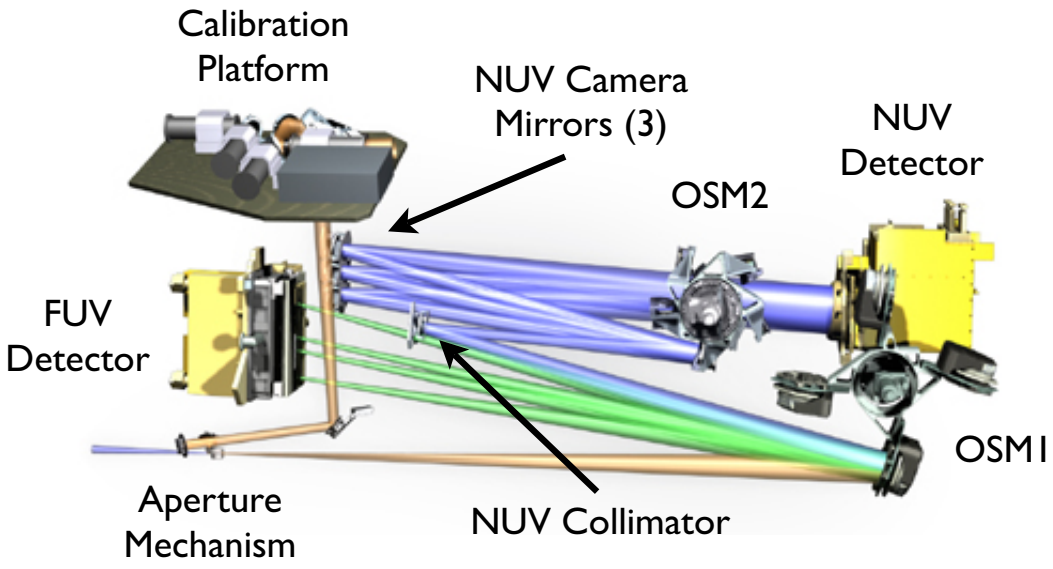

The optical path is drawn to scale, with all elements in proportion and in their correct relative locations.

3.1.2 The Apertures and Aperture Mechanism

After passing through the external shutter, the light from the OTA first encounters one of the COS entrance apertures (Table 3.1), which are mounted on the Aperture Mechanism (ApM). Selecting an aperture can involve movement of the Aperture Mechanism.

Primary Science Aperture

The Primary Science Aperture (PSA) is a field stop 2.5 arcsec (700 μm) in diameter. It is located, not at the *HST* focal surface, but near the point of the circle of least confusion. The aperture transmits ≥ 95% of the light from a well-centered, aberrated point-source image delivered by the *HST* optics. The PSA is used for almost all COS observations. It is in place, ready to use, at the start of a new visit. Note that, when the PSA is in place, the Wavelength Calibration Aperture (WCA; see below) is also in place and available to acquire simultaneous wavelength-calibration spectra. External light entering the PSA and internal light entering the WCA are dispersed by the same grating. Thus, for a given grating and central-wavelength setting, no additional motion of the Aperture Mechanism is required to obtain a wavelength-calibration exposure.

Table 3.1: COS Entrance Apertures

Aperture	Full Name	Purpose	Size (mm)
PSA	Primary Science Aperture	science aperture	0.700 circular
BOA	Bright Object Aperture	science aperture with ND2 filter	0.700 circular
WCA	Wavelength Calibration Aperture	wavecals with Pt-Ne lamp	0.020 × 0.100
FCA	Flat-Field Calibration Aperture	flat field with deuterium lamp	0.750 × 1.750

Wavelength Calibration Aperture

The Wavelength Calibration Aperture (WCA) is offset from the PSA by 2.5 mm (about 9 arcsec) in the cross-dispersion direction. The WCA is illuminated by one of two Pt-Ne wavelength-calibration (wavecal) lamps; it does not receive light from external sources. The wavecal spectrum is used by **calcos** to assign wavelengths to the science spectra obtained through either the PSA or BOA. During target acquisitions, light from the Pt-Ne lamps provides a reference from which the location of the target aperture is determined.

Bright Object Aperture

Like the PSA, the Bright Object Aperture (BOA) is 2.5 arcsec (700 μm) in diameter, but it incorporates a neutral-density (ND2) filter. The transmission of the ND2 filter varies with wavelength (Figure 3.2) but is roughly 0.6%. The BOA is offset from the PSA by 3.7 mm (about 13 arcsec) in the cross-dispersion direction. For scientific observations, the aperture block is shifted, via movement of the Aperture Mechanism, to place the BOA in the position normally occupied by the PSA. Thus, spectra obtained through either the PSA or BOA use the same optical path and detector region (for a given channel), and so may employ the same flat-field calibrations. *Moving the BOA into place for scientific use shifts the WCA as well, precluding simultaneous use of the WCA for a wavecal exposure*. After an observation through the BOA, the Aperture Mechanism must be moved to properly position the WC A, so that a wavecal exposure may be obtained.

Flat-Field Calibration Aperture

The Flat-Field Calibration Aperture (FCA) is used to obtain flat-field exposures using one of the two deuterium hollow-cathode flat-field calibration lamps. The FCA is used only for calibration and is not available to general observers.

Figure 3.2: Transmission of the COS BOA as a Function of Wavelength

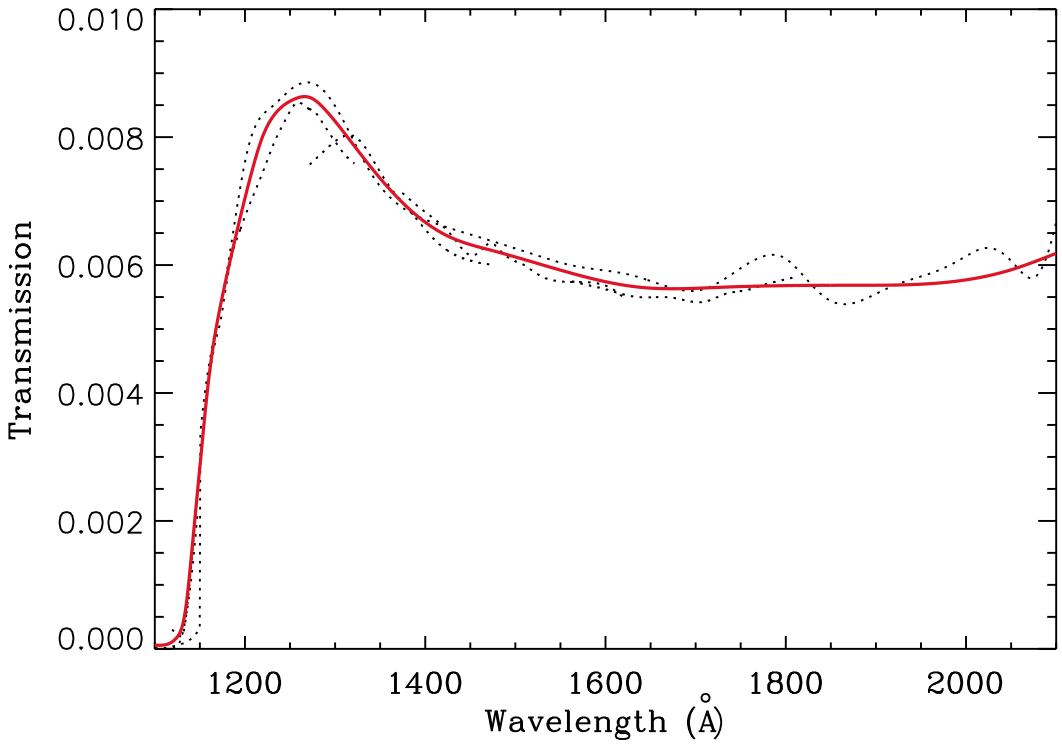

Dashed lines represent the ratio of BOA to PSA spectra of the standard star LDS749b obtained using all three FUV gratings. The thick red curve is a spline fit to the dashed curves.

3.1.3 Gratings and Mirrors: The Optics Select Mechanisms

After passing through one of the COS apertures, light next encounters the Optics Select Mechanism 1 (OSM1), a rotating mechanism that can bring one of four optical elements into the beam. One of these, NUV Collimating Mirror 1 (NCM1), is a flat mirror that directs the beam to the NUV channel. The other three elements are the G130M, G160M, and G140L gratings for the FUV channel. As a consequence of this design, the FUV and NUV channels cannot be used simultaneously.

Figure 3.3: The COS FUV Optical Path

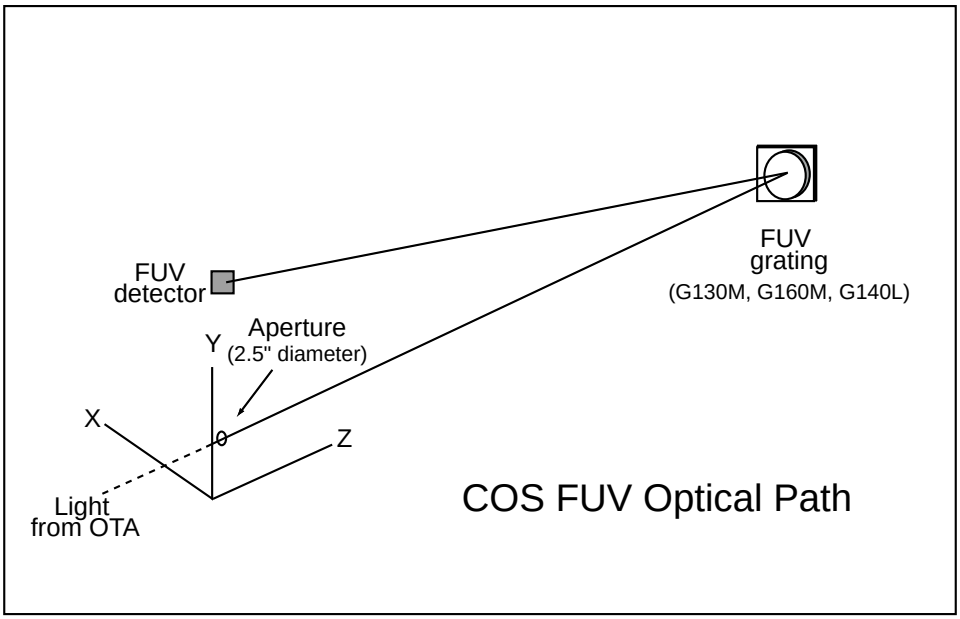

FUV Channel Optical Design

The COS FUV optical path is illustrated schematically in Figure 3.3. To maximize throughput, a single FUV grating is used to disperse the light, remove the spherical aberration introduced by the *HST* primary mirror, and focus the beam onto the detector. Because the FUV gratings introduce astigmatism in the direction perpendicular to dispersion, the height of the spectrum varies with wavelength (Section 5.1.8). Given the location of OSM1 in the *HST* optical path, it is possible for the FUV gratings to disperse, focus, and correct the beam optimally only for a point source that is centered in the aperture. Performance is degraded when the source is moved away from the aperture center. Fortunately, this degradation is low for displacements up to about 0.4 arcsec (Section 8.8).

The COS FUV channel provides spectra from 900 to 2150 Å at low and moderate spectral resolution (Section 5.1). The FUV detector is described fully in Chapter 4, but it is important to note that it consists of two independent detector segments with a small physical gap between them. Light falling into the gap is not recorded. Though the gap prevents a continuous spectrum from being obtained at a single central-wavelength setting, the missing wavelengths can be recovered by obtaining additional exposures at other central-wavelength settings (corresponding to small rotations of the OSM1 mechanism; see Section 5.5).

Figure 3.4: The COS NUV Optical Path for Spectroscopic Observations

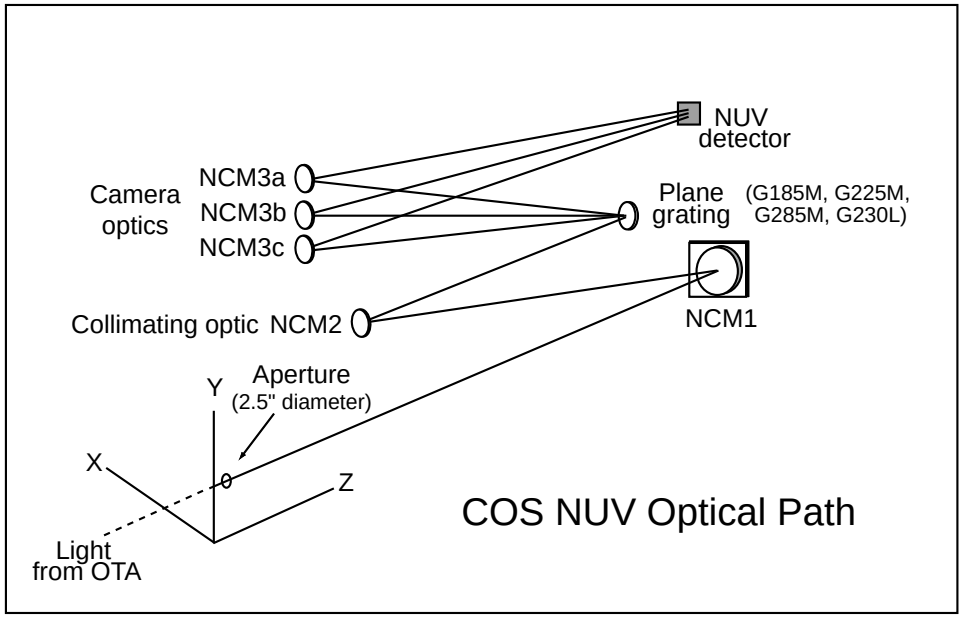

OSM2 and the NUV Channel

The COS NUV channel, illustrated schematically in Figure 3.4, provides coverage from about 1650 to 3200 Å at low and moderate spectral resolution. If the NUV channel is to be used, OSM1 is turned to place mirror NCM1 in the beam. NCM1 corrects the beam for the spherical aberration of *HST*, magnifies it by a factor of four, and directs it to the NUV Collimating Mirror 2 (NCM2). The NCM2 collimates the light and directs it to Optics Select Mechanism 2 (OSM2). OSM2 holds five optical elements: the four NUV diffraction gratings (G185M, G225M, G285M, and G230L) and a mirror for target acquisitions or imaging.

To accommodate the NUV detector format, dispersed light from the NUV gratings is imaged onto the detector by three parallel mirrors (NCM3a, 3b, 3c). For the medium-dispersion gratings, the spectra appear as three non-contiguous 35–40 Å stripes on the MAMA detector, providing 105–120 Å wavelength coverage per exposure. The low-dispersion grating provides ~ 400 Å per stripe. The layout of the stripes is shown in Figure 4.7. The gratings can be shifted via slight rotations of OSM2 to cover the entire NUV wavelength band. The NCM3 mirrors are spaced such that several correctly-chosen exposures will produce a complete spectrum, from the low end of the short-wavelength stripe to the high end of the long-wavelength stripe.

Imaging with the NUV Mirror

For imaging observations, OSM2 is turned to place a mirror in the light path, rather than a grating (Figure 3.5). When used in direct specular reflection, this mirror is designated as `MIRRORA`. For bright targets, the flux can be attenuated by adjusting OSM1 so that the order-sorting filter in front of the mirror reflects the light onto the detector. This configuration is referred to as `MIRRORB`. COS imaging is described in Chapter 6.

Figure 3.5: COS NUV Optical Path for Imaging Observations

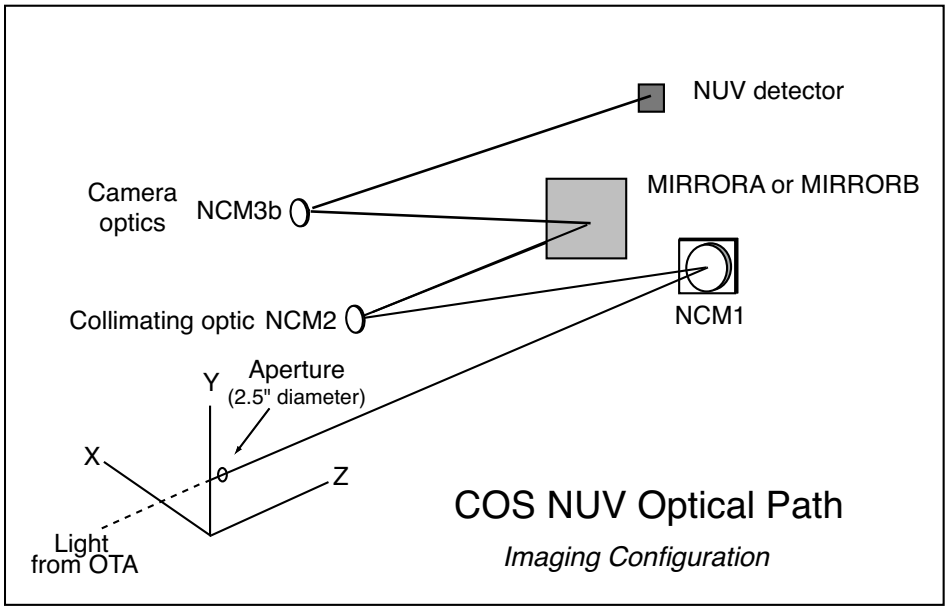

3.2 Size of a Resolution Element

Throughout this document, we assume that a resolution element (resel) spans 6 × 10 pixels on the FUV detector (in the dispersion and cross-dispersion directions, respectively) and 3 × 3 pixels on the NUV detector (Table 1.2). These values were determined before launch; even then, it was known that the true size of a resel would vary with wavelength. Preliminary analysis of in-flight data suggests that the FUV resel is somewhat larger than previously assumed (see the discussion of the line-spread function in Section 3.3), while the NUV resel is smaller. We will continue to refine our analysis of the instrument parameters. In the mean time, keep in mind that the *COS Exposure Time Calculator* (ETC) uses the pre-flight resel sizes in all of its calculations. Users who adopt a larger or smaller resel should adjust the ETC results accordingly.

3.3 The COS Line-Spread Function

The COS optics correct for the spherical aberration of the *HST* primary mirror, but not for the mid-frequency wavefront errors (MFWFEs) due to zonal (polishing) irregularities in the *HST* primary and secondary mirrors. As a result, the COS spectroscopic line-spread function (LSF) has extended wings and a core that is slightly broader and shallower than a Gaussian. The extended wings of its LSF limit the ability of COS to detect faint, narrow spectral features. The effect is greater at short

wavelengths, and it may have consequences for some COS FUV science. The most severely impacted programs are likely to be those that

- rely on models of the shapes of narrow lines;
- search for very weak lines;
- aim to measure line strengths in complex spectra with overlapping or nearly overlapping lines; or
- require precise estimates of residual intensity in very strong or saturated lines.

3.3.1 Non-Gaussianity of the COS LSF

Initial results from an analysis of the on-orbit COS LSF are reported by Ghavamian et al. (2009) in COS ISR 2009-01. They find that model LSFs incorporating *HST* MFWFEs are required to reproduce the absorption features observed in stellar spectra obtained with COS. Figure 3.6 shows two model LSFs computed for grating G130M at 1309 Å. The solid line represents a model incorporating the spherical aberration of the *HST* OTA; it is well-fit by a Gaussian with FWHM = 6.5 pixels. The dotted line represents a model that also includes the MFWFEs. It has a FWHM of 7.9 pixels, slightly larger than that of the solid curve, and broad non-Gaussian wings. These wings can hinder the detection of closely-spaced narrow spectral features. Model LSFs for all of the COS gratings are available on the COS Web site.

Figure 3.6: Model Line-Spread Functions for the COS FUV Channel

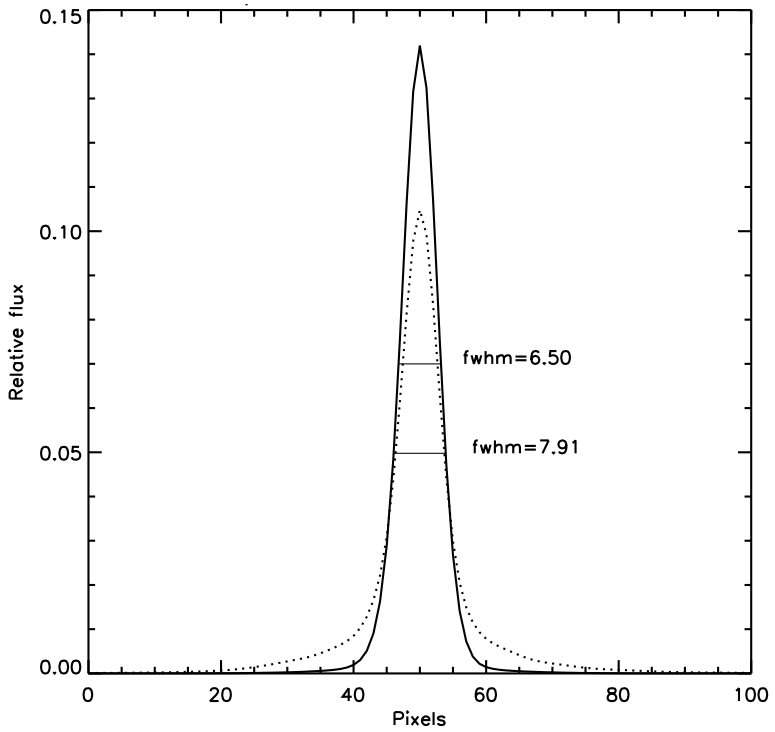

Model LSFs for G130M at 1309 Å, normalized to a sum of unity. The solid line represents a model LSF that incorporates the spherical aberration of the OTA; it is well-fit by a Gaussian with FWHM = 6.5 pixels. The dotted line represents a model that also includes the *HST* mid-frequency wave-front errors. It shows a larger FWHM and broad, non-Gaussian wings.

3.3.2 Quantifying the Resolution

When a substantial fraction of the power in an LSF is transferred to its extended wings, traditional measures of resolution, such as the FWHM of the line core, can be misleading. For example, an observer assuming that the resolving power R = 16,000 quoted for the G130M grating represents the FWHM of a Gaussian would mistakenly conclude that COS can resolve two closely-spaced narrow absorption features, when in fact it cannot. Nevertheless, the FWHM is a convenient tool, and we use it to describe the COS gratings in tables throughout this handbook. When using these tables, keep in mind that the quoted resolving power R is computed from the empirically-determined FWHM of the line core, and careful modeling may be needed to determine the feasibility of a particular observation or to analyze its result.

Figure 3.7 shows the resolving power of the FUV gratings for two cases: the first assumes a Gaussian LSF of FWHM = 6.5 pixels, with no MFWFEs from the *HST* OTA (dotted lines); the second is an LSF model with the MFWFEs included (solid lines). In the latter case, the FWHM of the LSF is calculated directly from the line profile by taking the width at half the peak (from Table 1 of COS ISR 2009-01). The MFWFEs reduce the resolving power of the G130M and G160M gratings by ~20%. The G140L profile is least affected by the MFWFEs, due to its lower dispersion. Preliminary measurements of the resolving power of the G130M grating at $\lambda < 1150$ Å are presented in Section 5.1.4.

Figure 3.7: Resolving Power of FUV Gratings

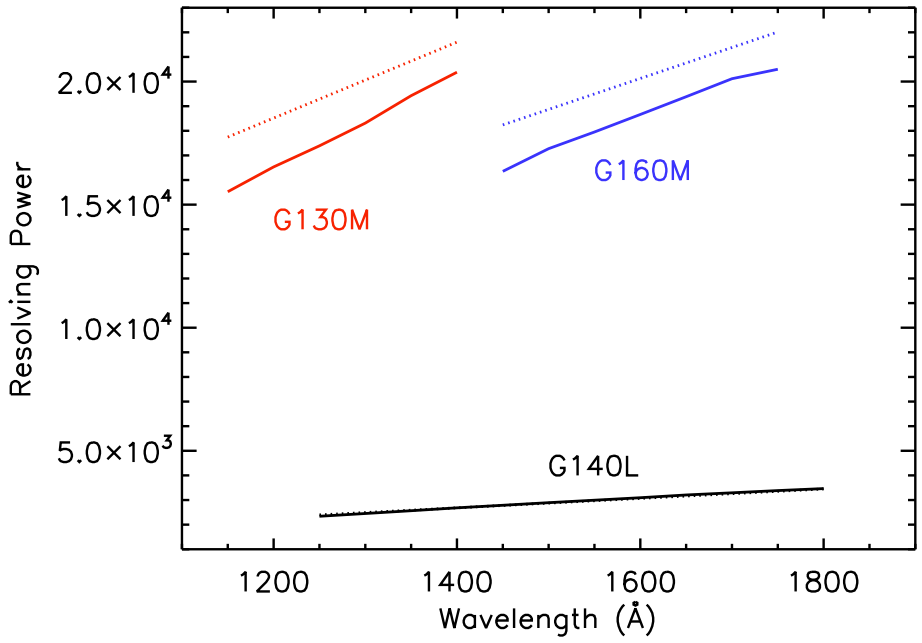

The resolving power (R = λ/FWHM) for the three gratings of the COS FUV channel for observations through the PSA aperture. The dotted lines represent a Gaussian with FWHM = 6.5 pixels. The solid lines are the values predicted by the LSF model with the on-orbit MFWFEs included. (The dotted and solid lines for G140L nearly overlap.)

3.3.3 Impact on Equivalent Width Measurements

The broad core and extended wings of the COS LSF increase the limiting equivalent width for absorption features in COS spectra. Figure 3.8 shows the limiting equivalent widths as a function of wavelength for a 3σ FUV detection of absorption features at S/N = 10 per pixel. A series of Gaussian spectral features with nominal Doppler parameters of b = 0, 10, 25, 50 and 100 km/s have been convolved with both a Gaussian instrumental LSF and the modeled on-orbit COS LSF for the G130M and G160M gratings. The results are similar for the NUV gratings, although the effect of the MFWFEs is more moderate for the long-wavelength G285M grating.

Figure 3.8: Limiting Equivalent Width of FUV Medium-Resolution Gratings

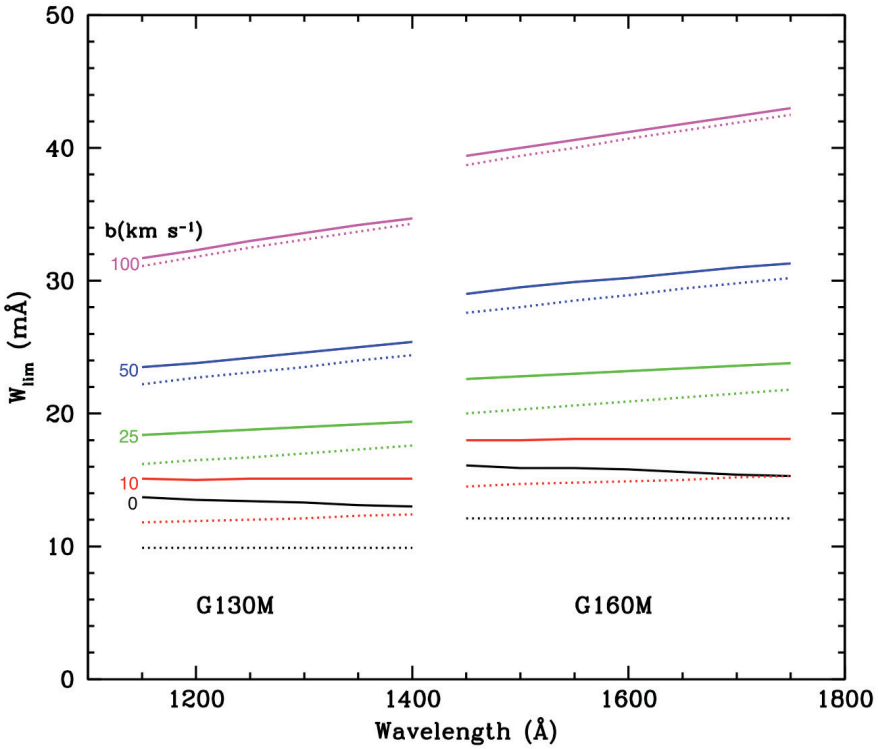

Limiting equivalent width as a function of wavelength for 3σ detections of absorption features at a S/N of 10 per pixel. Solid lines represent the full on-orbit LSFs including MFWFEs. Dashed lines represent Gaussian LSFs without MFWFEs. The colors correspond to features with intrinsic Doppler parameters b = 0 km/s (black), 10 km/s (red), 25 km/s (green), 50 km/s (blue) and 100 km/s (magenta).

3.3.4 Extended Wings of the COS LSF

While the LSF models of Ghavamian et al. (2009) successfully characterize the basic profile and integrated properties of narrow spectral features in COS spectra, scientific investigations that depend on characterizing the depth of saturated or nearly-saturated absorption features may require a more careful treatment of the light scattered into the wings of the LSF. To address this concern, Kriss (2011) has developed empirical LSF models for the G130M and G160M gratings. These models

differ in two ways from the preliminary models discussed above. First, while the preliminary models extend only ± 50 pixels from the line center, the new models extend ± 100 pixels, the full width of the geocoronal Lyman α line. Second, the new models include scattering due to the micro-roughness of the surface of the primary mirror, an effect that transfers an additional 3% of the light from the center of the line into its extended wings (Figure 3.9). For details, see COS ISR 2011-01. Both the LSF models computed by Ghavamian et al. (2009) and the empirical models of Kriss (2011) are available on the COS Web site.

Figure 3.9: Comparison of LSF Models for Medium-Resolution FUV Gratings

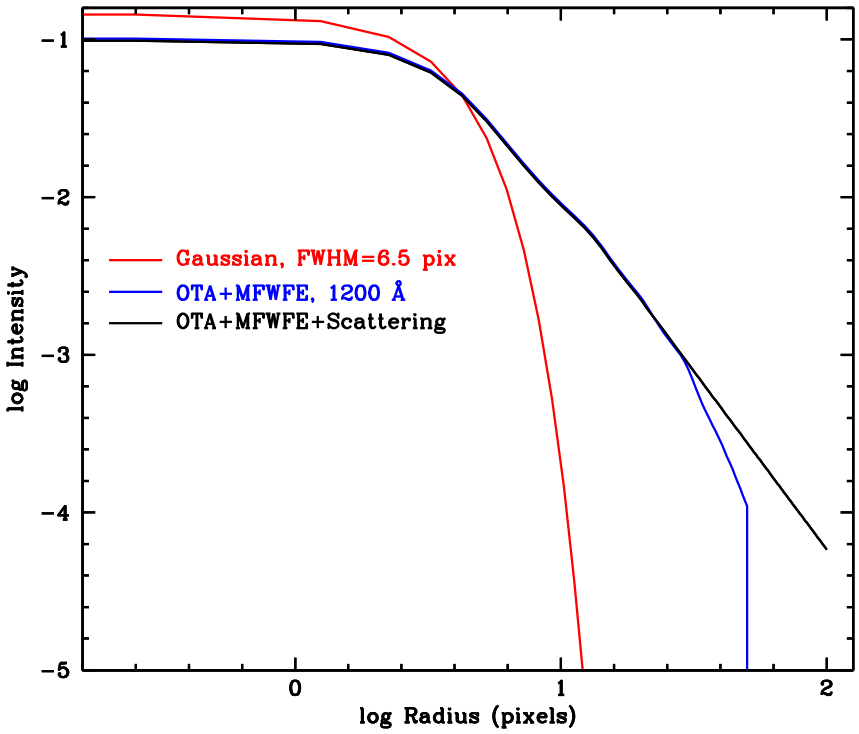

Comparison between a simple Gaussian LSF model (red line, FWHM = 6.5 pixels), the LSF profile from Ghavamian et al. (2009) that includes MFWFEs from the *HST* OTA (blue line, calculated at 1200 Å), and the new LSF that includes power-law scattering wings of index -2.25 extending ± 100 pixels from line center (black line). Figure taken from Kriss (2011).

3.3.5 Enclosed Energy of COS LSF

Figure 3.10 shows the fraction of enclosed energy within the LSF, measured from the center of the profile, for both the FUV and NUV channels. The differences between the modeled on-orbit LSFs (MFWFEs included) and the Gaussian LSFs without MFWFEs are apparent in both spectroscopic channels. Though inclusion of the MFWFEs at longer NUV wavelengths widens the FWHM of the on-orbit LSF models only slightly, the wider wings decrease noticeably the spectral purity and the contrast level of the observed spectra.

Figure 3.10: Enclosed Energy Fraction of the COS Line-Spread Function

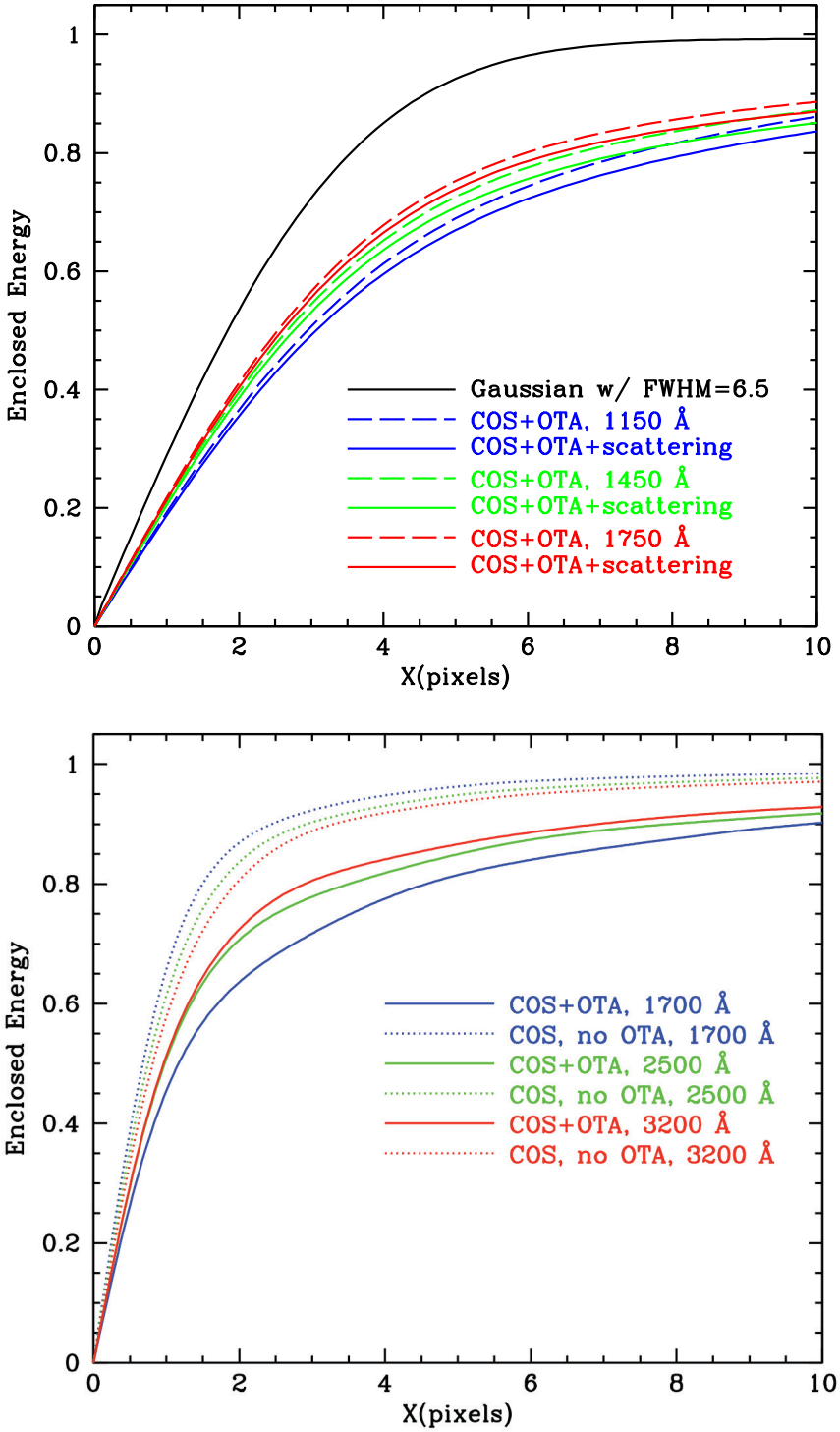

The enclosed energy fraction of the COS LSF for an unresolved spectral feature as measured from the center of the profile (collapsed along the cross-dispersion direction). In the top panel are plotted a Gaussian with FWHM = 6.5 Å and FUV model profiles with and without scattering due to micro roughness on the surface of the *HST* primary mirror (Kriss 2011). In the bottom panel, NUV model profiles with and without the effects of the OTA MFWFEs are shown (Ghavamian et al. 2009).

Table 3.2: Distance from Line Center (in Pixels) Versus Enclosed Energy Fraction and Wavelength for the G130M Grating

Enclosed Energy Fraction	Wavelength (Å)						
	1150	**1200**	**1250**	**1300**	**1350**	**1400**	**1450**
0.90	14.9	15.0	15.0	14.9	14.8	14.7	14.4
0.95	24.3	24.4	24.4	24.5	24.4	24.3	23.8
0.99	58.1	58.3	58.3	58.4	58.3	58.2	57.5

Table 3.3: Distance from Line Center (in Pixels) Versus Enclosed Energy Fraction and Wavelength for the G160M Grating

Enclosed Energy Fraction	Wavelength (Å)						
	1450	**1500**	**1550**	**1600**	**1650**	**1700**	**1750**
0.90	14.7	14.6	14.4	14.2	14.0	13.6	13.2
0.95	24.5	24.3	24.0	23.8	23.5	23.1	22.6
0.99	58.3	58.1	57.8	57.4	57.0	56.3	55.6

Table 3.4: Distance from Line Center (in Pixels) Versus Enclosed Energy Fraction and Wavelength for the G140L Grating

Enclosed Energy Fraction	Wavelength (Å)											
	1250	**1300**	**1350**	**1400**	**1450**	**1500**	**1550**	**1600**	**1650**	**1700**	**1750**	**1800**
0.90	12.1	12.1	12.1	12.1	12.1	12.1	12.0	11.9	11.8	11.7	11.6	11.4
0.95	17.9	18.1	18.2	18.4	18.5	18.6	18.7	18.7	18.7	18.7	18.7	18.7
0.99	30.5	30.7	31.0	31.3	31.6	31.9	32.1	32.4	32.6	32.9	33.2	33.3

Table 3.2, Table 3.3, and Table 3.4 present the enclosed-energy fractions for gratings G130M, G160M, and G140L, respectively. The G140L data are taken from Ghavamian et al. (2009) and do not include the effects micro-roughness. In contrast to the medium-resolution gratings, the LSF of G140L becomes decidedly more concentrated with increasing wavelength.

CHAPTER 4:

Description and Performance of the COS Detectors

In this chapter…

4.1 The FUV XDL Detector

4.1.1 XDL Properties

The COS FUV detector is a windowless cross delay line (XDL) device that is similar to the detectors used on the *Far Ultraviolet Spectroscopic Explorer (FUSE)*. The XDL is a photon-counting micro-channel plate (MCP) detector with two independently-operable segments. Each segment has an active area of 85 × 10 mm; they are placed end to end and separated by a 9-mm gap. When the locations of detected photons are digitized, they are placed into a pair of arrays (one per detector), each 16384 × 1024 pixels, though the active area of the detector is considerably smaller. Individual pixels span 6 × 24 µm. The long dimension of the array is in the direction of dispersion; increasing pixel number (the detector's *x* axis in user coordinates) corresponds to increasing wavelength. The XDL format is shown schematically in Figure 4.1. Detector parameters are listed in Table 1.2.

The FUV XDL is optimized for the 1150-to-1775 Å bandpass, with a cesium iodide photocathode on the front MCP. The front surfaces of the MCPs are curved with a radius of 826 mm to match the curvature of the focal plane. When photons strike the photocathode, they produce photoelectrons that are multiplied by a stack of MCPs. The charge cloud that comes out of the MCP stack, several millimeters in diameter,

lands on the delay-line anode. There is one anode for each detector segment, and each anode has separate traces for the dispersion (x) and cross-dispersion (y) axes. The location of an event in each axis is determined by measuring the relative arrival times of the collected charge pulse at each end of the delay-line anode for that axis. The results of this analog measurement are digitized to 14 bits in x and 10 bits in y. In `TIME-TAG` mode, the total charge collected from the event, called the pulse height, is saved as a 5-bit number.

Figure 4.1: The FUV XDL Detector.

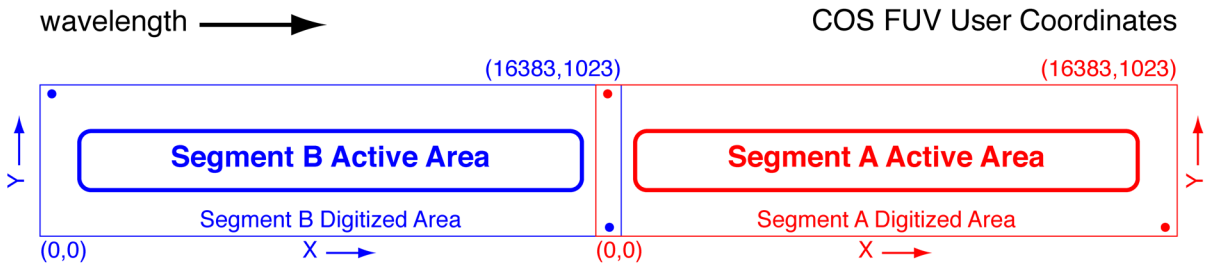

This diagram is drawn to scale, and the slight curvature at the corners is also present on the masks of the flight detectors. Wavelength increases in the direction of the increasing x coordinate. The red and blue dots show the approximate locations of the stim pulses on each segment. The numbers in parentheses show the pixel coordinates at the corner of the segment's digitized area; the two digitized areas overlap in the region of the inter-segment gap.

The detector electronics generate pulses that emulate counts located near the corners of the anode, outside the active area of the MCPs. These "stim pulses" (see Section 4.1.5) provide a means of tracking and correcting thermal distortions.

The XDL's quantum efficiency is improved by the presence of a series of wires, called the quantum-efficiency (DQE) grid, placed above the detector (*i.e.,* in the light path). These wires create shadows in the spectrum that are flagged by **calcos** during data reduction. The XDL also includes an ion-repeller grid that reduces the background rate by preventing low-energy thermal ions from entering the open-faced detector. They act as a 95% transmission neutral-density filter.

4.1.2 XDL Spectrum Response

COS is considerably more sensitive than STIS and earlier-generation *HST* instruments at comparable spectral resolutions in the FUV. Effective areas for the COS FUV gratings are shown in Figure 5.1. The time-dependent changes in the sensitivity of the COS FUV channel are discussed in Section 5.1.4.

4.1.3 XDL Background Rate

The XDL detectors have extremely low dark rates, on the order of 10^{-6} counts/s/pixel; see Section 7.4.1.

Figure 4.2: Example of a COS FUV Spectrum

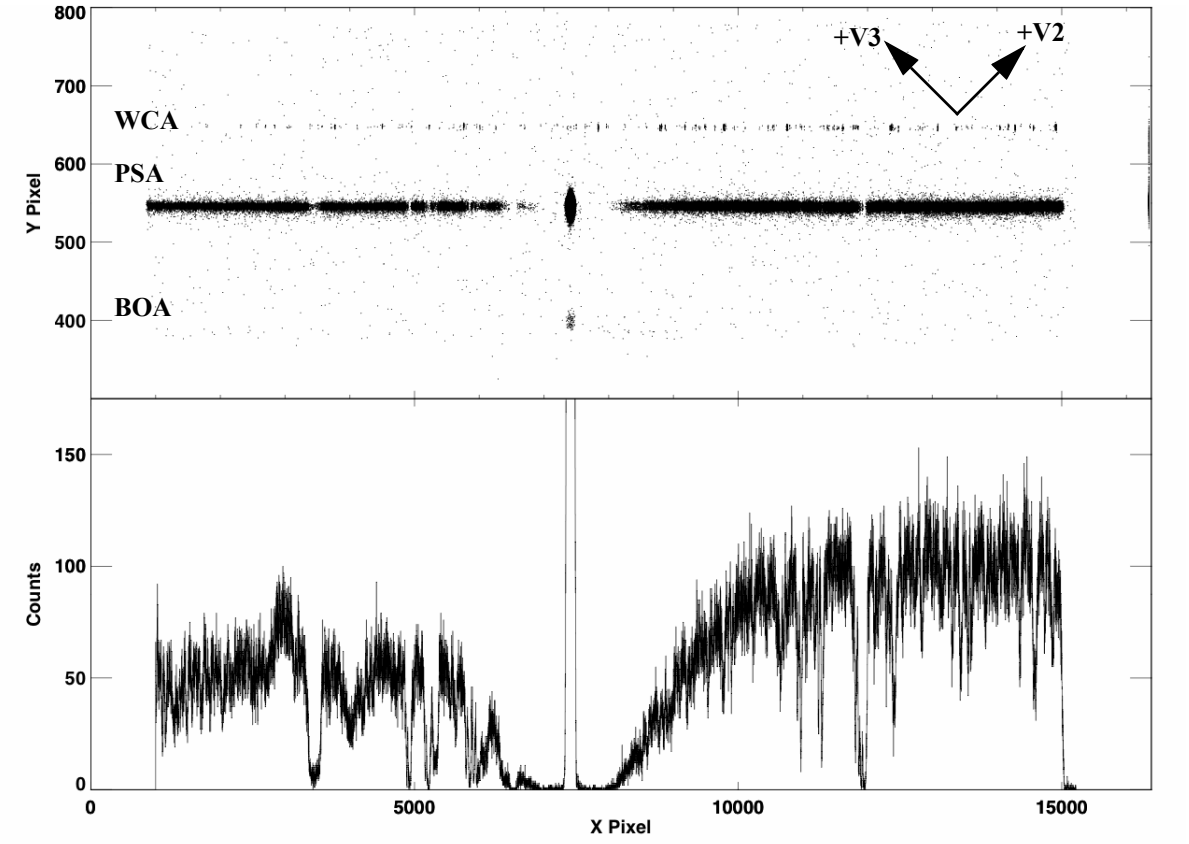

Upper panel: A stellar spectrum obtained with segment B of the COS FUV detector using the G130M grating at a central wavelength of 1309 Å. The wavelength calibration (WCA) spectrum is on top, and the stellar spectrum (PSA) is below. Both the PSA and BOA are open to the sky when the COS shutter is open, so Lyman α airglow through the BOA is also visible below the PSA (near Y = 400). The *HST* +V2 and +V3 axes are over plotted. Note that the size of the active area of the MCP is smaller than the overall digitized area (16384 $\times$ 1024). Lower panel: the extracted stellar spectrum from the PSA.

4.1.4 XDL Read-out Format

The FUV channel creates one spectral stripe on each detector segment for the science spectrum and another for the wavelength-calibration spectrum. The aperture not being used for science may also create a spectrum. If so, it will appear below the science spectrum if the PSA is being used, above it if the target lies in the BOA. Since the non-target aperture is usually observing blank sky, it will normally be visible only if Lyman α falls in the spectral range. Figure 4.2 shows an example of an FUV spectrum obtained on orbit with segment B. The upper panel shows the two-dimensional image; the lower panel shows the extracted PSA spectrum. Note the difference in the *x* and *y* axis scales in the upper figure.

Although the gap between the two FUV detector segments prevents the recording of an uninterrupted spectrum, it can be made useful. For example, when the G140L

grating is used with a central wavelength of 1280 Å, the bright Lyman α airglow feature falls in the gap. For suggestions on spanning the gap, see Section 5.5.

Should a high count rate on one of the segments be a safety concern, the detector can be operated in single-segment mode, whereby the high voltage on one segment is lowered to a value that prevents it from detecting light. This adjustment is required for central wavelength 1105 Å on G140L, since the zero-order light falling on segment B is too bright.

4.1.5 Stim Pulses

The signals from the XDL anodes are processed by Time-to-Digital Converters (TDCs). Each TDC contains a circuit that produces two alternating, periodic, negative-polarity pulses that are capacitively coupled to both ends of the delay-line anode. These stim pulses emulate counts located near the corners of the anode, beyond the active area of the detector. Stim pulses provide a means for **calcos** to correct the temperature-dependent shift and stretch of the image during an exposure, and they provide a first-order check on the dead-time correction. They are recorded in both `TIME-TAG` and `ACCUM` modes and appear in the data files.

Four stim-pulse rates are used: 0 (i.e., off), 2, 30, and 2000 Hz per segment. These rates, which are only approximate, are *not* user selectable. Exposures longer than 100 sec will use the 2 Hz rate, those between 10 and 100 sec use 30 Hz, and those shorter than 10 seconds use 2000 Hz.

4.1.6 Pulse-height Distributions

The XDL detectors convert each ultraviolet photon into a shower of electrons, from which the detector electronics calculate the *x* and *y* coordinates and the total charge, or pulse height. The pulse height for an event at a particular location on the detector depends on the high voltage across the MCPs and the local properties of the MCPs at that location; it is not related to the energy of the incident photon. A histogram of pulse heights for multiple events is called a pulse-height distribution (PHD).

The PHD from photon events is typically peaked at the average gain of the MCPs with a width determined by the MCP characteristics. Background events, both internal to the detector and induced by cosmic-rays, tend to have a falling exponential PHD, with most events having low pulse heights. On-board charge-threshold discriminators filter out very large and small pulses to reduce the background and improve the signal-to-noise ratio. In TIME-TAG mode, the pulse height is recorded for each detected photon event. By rejecting low pulse-height events, **calcos** further reduces the background rate. In ACCUM mode, only the integrated pulse-height distribution is recorded (Section 5.2.2), so pulse-height filtering is not possible.

Figure 4.3: Spectra Showing the Effects of Gain Sag on FUV Detector Segment B

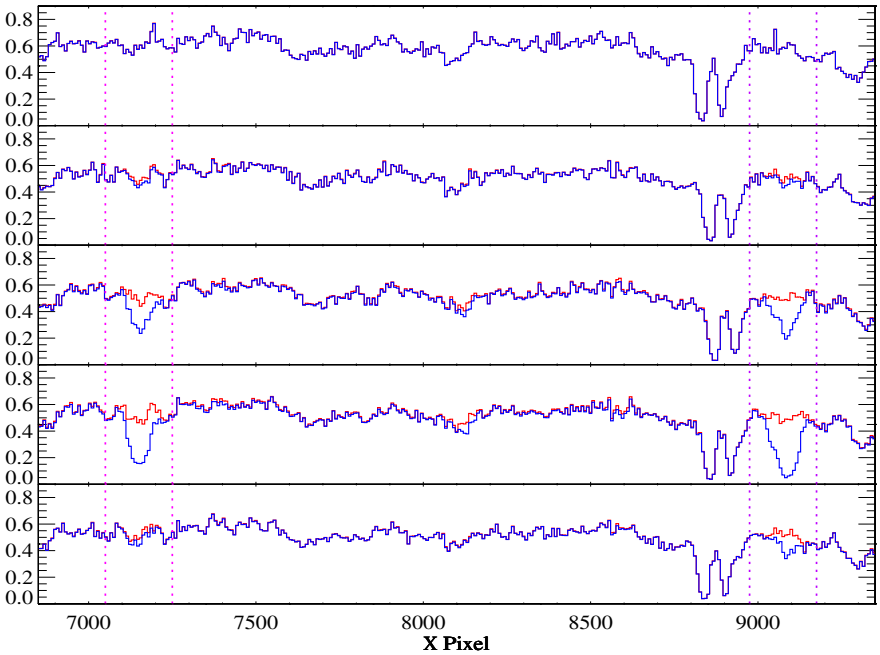

Count-rate spectra (G160M/1623/FP=4) of a target observed five times over 19 months: from top to bottom, September 2009, June 2010, September 2010, January 2011, and May 2011. The blue curve includes only photon events with pulse heights in the range 4-30; the red curve includes pulse heights 2-30. The spectral features near pixels 7200 and 9011 are not astrophysical, but represent the effect of gain sag on regions of the detector illuminated by Lyman α in other observing modes. These features become more pronounced with time until March 2011, when the segment B high voltage was raised.

Gain Sag

Prolonged exposure to light causes the XDL detectors to become less efficient at photon-to-electron conversion, a phenomenon called "gain sag." As a result, the peak of the PHD in each region of the detector shifts to lower values as the total (time-integrated) illumination of that region increases. As long as all pulse heights are above the minimum threshold imposed by **calcos**, there is no loss in sensitivity. But if the pulse height drops low enough that photon events from the target fall below the threshold, these events are discarded and the throughput decreases. Since the amount of gain sag increases with the total amount of previous illumination, gain sag appears first in regions of the detector that are illuminated by bright airglow lines, but eventually affects the entire spectrum. Figure 4.3 shows the effect of gain sag on Segment B of the COS FUV detector. These data were obtained using the grating setting G160M/1623/FP=4. A portion of the extracted spectrum from the same object taken at five different times is shown. The blue curve was constructed using only photon events with pulse heights in the range 4-30 (the limits used by **calcos** until December 2010), while the red curve includes pulse heights of 2-30 (the present limits). Two regions that suffer the most serious gain sag are marked: the region near pixel 7200 is illuminated by Lyman α when grating setting G130M/1309/FP=3 is used, and that near pixel 9100 is illuminated by Lyman α when the setting is

G130M/1291/FP=3. Initially, the pulse heights were well above either threshold, so the blue and red curves are indistinguishable. As time progressed, all of the pulse heights decreased, but the two Lyman α regions decreased faster, causing the blue spectra to exhibit spurious absorption features. This trend continued until the segment B high voltage was raised in March 2011. The bottom plot shows that increasing the voltage has recovered some of the lost gain, but not all of it.

More details on the gain sag can be found in the *COS Data Handbook* and COS ISR 2011-05.

Detector Walk

As the pulse height of a photon event decreases, the detector electronics begin to systematically miscalculate its position. On the COS FUV detector, this effect, called detector walk, is significant only in the *y* (cross-dispersion) direction. The shift is approximately 0.5 pixel per pulse-height bin, which means that the entire spectrum may be shifted by several pixels, and the low-gain Lyman α regions may be noticeably shifted relative to the rest of the spectrum (Figure 4.4). **Calcos** applies a *y*-walk correction to TIME-TAG data, but the effect remains uncorrected in ACCUM mode, where no pulse-height information is available. The spectral extraction should remain unaffected.

Figure 4.4: Y Walk on the FUV Detector

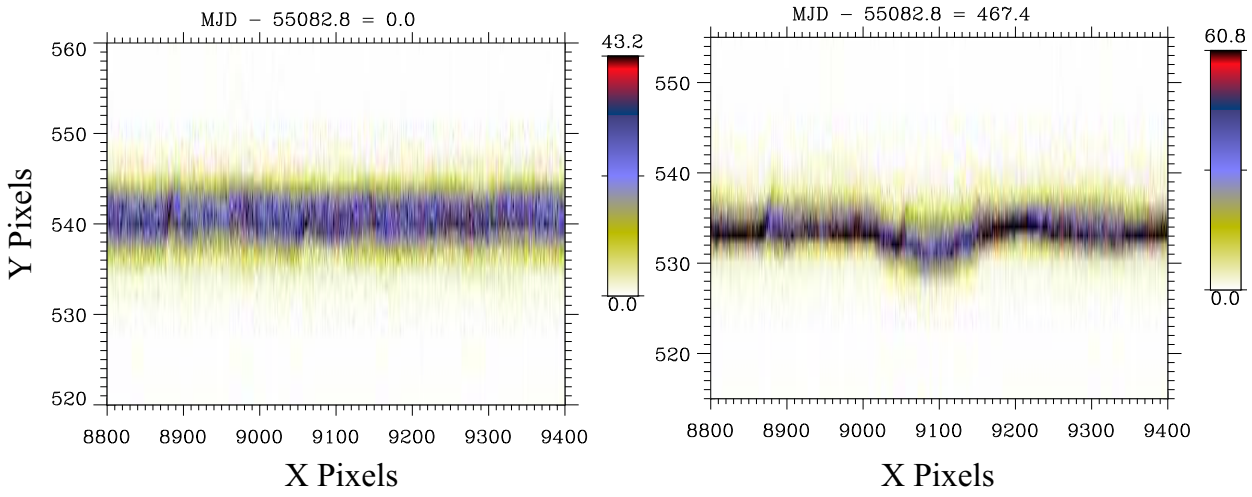

Spectral images taken in 2009 September (left) and 2010 December (right) showing the effect of *y* walk. While the entire spectrum has shifted by about 8 pixels, the region near X = 9100, where the geocoronal Lyman α feature falls when G130M/1291/FP-POS=3 is employed, is particularly affected.

Future Plans

As described above, the lower pulse height threshold in **calcos** was decreased from 4 to 2, and the high voltage on Segment B was increased to minimize gain-sag effects. These changes resulted in a small increase (~7%) in the detector background. In addition, beginning in Cycle 19, we have eliminated the default FP-POS position and

required observers to use more than one position in order to distribute the damage on the detector (Section 5.8.2). These steps will delay the onset of the Lyman α holes, but because the gain will continue to sag, the holes will eventually reappear, and in time the entire spectrum will show similar effects.

In the near future, we plan to flag low-gain pixels and exclude them when combining spectra taken at multiple FP-POS positions, and we hope to implement time- and position-dependent pulse-height thresholds within **calcos**.

In the long term, we plan to move the spectra onto a previously-unused portion of the detector by offsetting the aperture mechanism in the cross-dispersion direction. The initial calibration activity for moving to one of these additional lifetime positions began in mid-2011, and this activity will continue for many months. A final decision on when to move to a new lifetime position will be made after the optical, mechanical, and operational impacts are evaluated. Until then, some areas on the detector may become more difficult to calibrate; if such changes are likely to affect the data analysis, the *COS Data Handbook* and periodic STANs will document the changes.

It is expected that future modifications to **calcos** and its associated reference files will make any changes to the position of the spectrum on the detector transparent for data analysis. Some modifications to target-acquisition strategies may be required.

4.1.7 Non-linear Photon Counting Effects (Dead Time)

The electronics that control the COS detectors have a finite response time t, called the dead time, that limits the rate at which photon events can be processed. If two photons arrive within time t, the second photon will not be processed. For the FUV channel, three factors limit the detected count rate. The first is the Fast Event Counter (FEC) for each segment, which has a dead time of 300 ns. The FEC dead time matters only at count rates well above what is usable, introducing a 1% error at a count rate of 33,500 per segment per second.

The second factor is the time required to digitize a detected event. For a given true count rate C, the detected count rate D is

$$D = \frac{C}{1 + C \cdot t}$$

where t is the dead-time constant. For the COS FUV detector, t = 7.4 μs, so the apparent count rate deviates from the true count rate by 1% when C = 1,350 counts/s and by 10% when C = 15,000 counts/s. Note that, when the effect is near the 10% level, then the FUV detector is near its global count-rate limit (see Table 10.1), so non-linear effects are relatively small.

Finally, the Detector Interface Board (DIB) combines the count streams from the two FUV segments and writes them to a single data buffer. The DIB is limited to processing about 250,000 counts/s in ACCUM mode and only 30,000 counts/s in TIME-TAG mode (the highest rate allowed for TIME-TAG mode). The DIB interrogates the A and B segments alternately; because of this, a count rate that is high in one segment but not the other could cause a loss of data from both segments. Tests have shown that the DIB is lossless up to a combined rate for both segments of 20,000 counts/s; the loss is 100 counts/s at a rate of 40,000 counts/s. Thus, this effect is less

than 0.3% at the highest allowable rates. Furthermore, information in the engineering data characterizes this effect.

While dead-time corrections are automatically made in the **calcos** pipeline, they are not included in the ETC, which will over-predict count rates for bright targets.

4.1.8 Spatial Variation of the Dark Rate

The dark rate varies spatially over the FUV detector. Figure 4.5 shows the sum of approximately 80,000 seconds of dark exposures taken over a five-month period in 2011. With the standard lower pulse-height threshold of 2, segment A is relatively featureless away from the edges of the active area, except for a few small spots with a higher rate. Segment B shows several large regions with a slightly elevated rate; they are enhanced by less than a factor of two over the quieter regions.

For most TIME-TAG observations, these features will have a negligible effect on the extracted spectra, because the variation is small and the overall rate is low (see Table 7.1). In ACCUM mode, where no lower pulse-height threshold is used, additional features appear. Since ACCUM mode is used only for bright targets, these features should constitute a negligible fraction of the total counts.

Figure 4.5: FUV Detector Dark Features

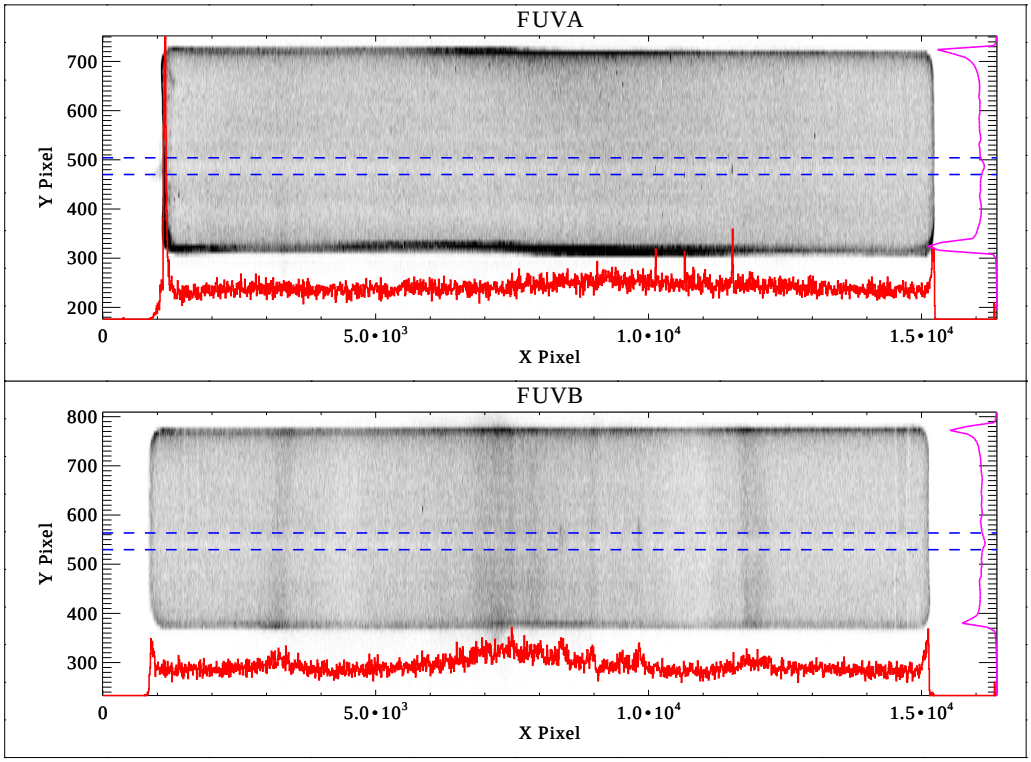

Summed raw dark frames show spatial variation on the detector. The approximate position of the G130M extraction window is marked in blue, and a sum of the dark counts in this extraction window as a function of x pixel is shown in red below the image. A sum as a function of y pixel is shown in purple on the right side of the figure. Segment A is nearly featureless aside from a few small hot spots, while segment B shows larger variations. Both segments show a slightly lower dark rate in the region where the spectra fall; this is due to gain sag. The data are binned by 8 pixels in each dimension for display purposes.

4.2 The NUV MAMA Detector

4.2.1 MAMA Properties

The COS NUV detector is a Multi-Anode Micro-channel Array (MAMA) identical to that used for the NUV in STIS. (In fact, it is the STIS NUV flight spare.) The COS MAMA has a semi-transparent cesium telluride photocathode on a magnesium fluoride window and is sensitive to photons with wavelengths from 1150 to 3200 Å. The NUV optics focus light through the MgF_2 window onto the Cs_2Te photocathode. A photoelectron generated by the photocathode then falls onto a curved-channel micro-channel plate (MCP), which generates a cloud of electrons. The active area of the coded anode array is 25.6 mm square and is divided into 1024 × 1024 pixels on 25 µm centers. The spatial resolution at 2500 Å is 35 µm FWHM. Detector parameters are listed in Table 1.2.

4.2.2 MAMA Spectrum Response

The inherent spectral response of the COS NUV MAMA is essentially identical to that of the STIS NUV MAMA. However, the overall optical train of COS differs from STIS, so the throughputs are different (Figure 5.2).

4.2.3 MAMA Dark Rate

A sum of dark exposures taken away from the SAA shows a relatively featureless background, with slight enhancements at two of the corners. Although the early dark rate was lower than had been measured on the ground, the rate has steadily increased since launch, as shown in Figure 4.6. As of 2011 September, the rate is approximately 5.0×10^{-4} counts/s/pixel. If the current trend continues, then the mean NUV dark rate will increase to about 8.0×10^{-4} counts/s/pixel by 2013 April.

Figure 4.6: NUV Detector Dark Rate versus Time

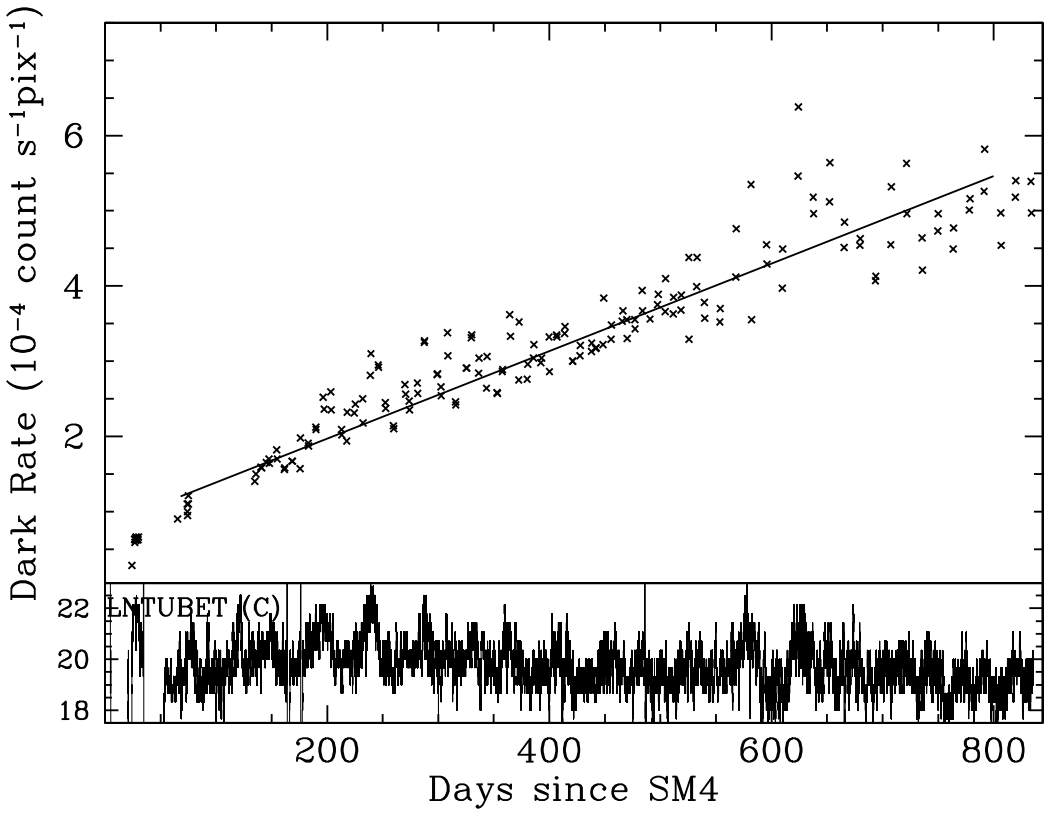

Measured dark rate as a function of time, through September 2011, excluding SAA-impacted periods. The best-fit line shows that the dark rate increases by ~ 200 counts/s per year. The cause of this increase is not understood. In the lower panel, the detector temperature (LNTUBET) is plotted to demonstrate the temperature dependence of the dark rate.

Figure 4.7: Example of a COS NUV Spectrum.

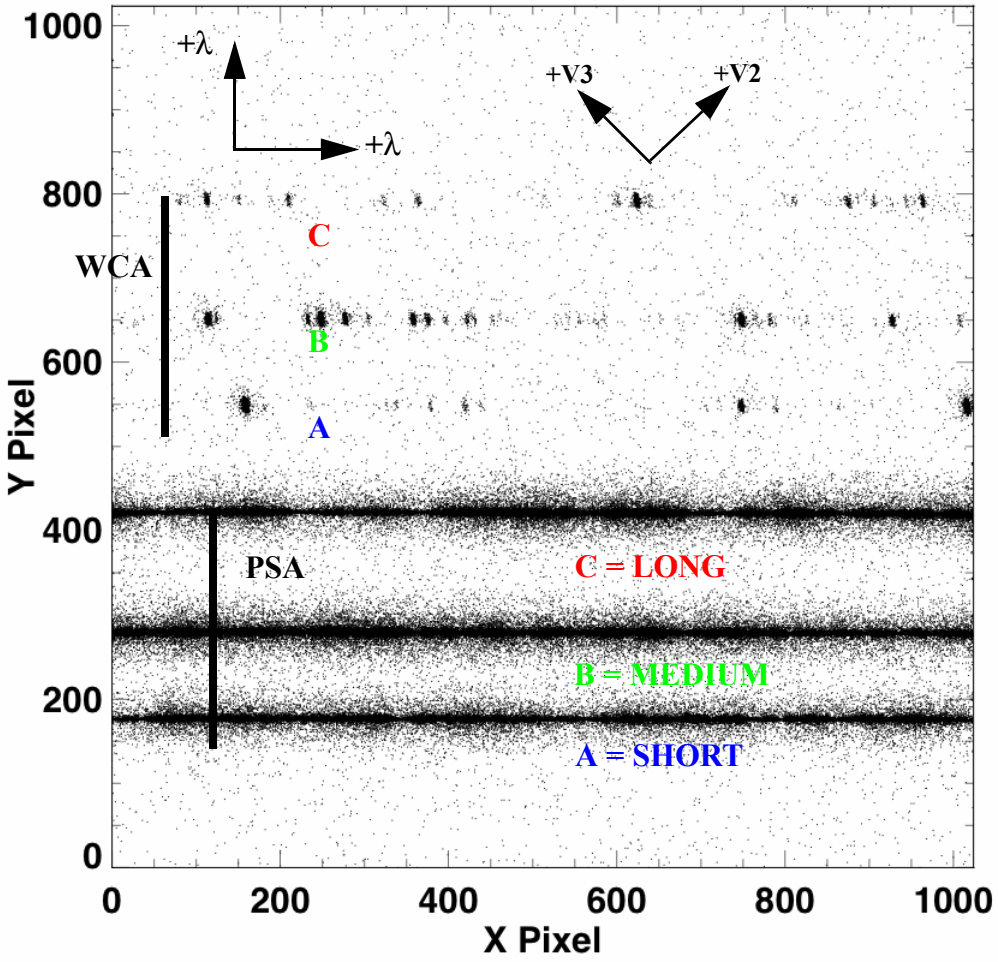

A COS NUV spectrum obtained in `TIME-TAG` mode with `FLASH=YES`. The stellar spectrum (labeled PSA) is on the bottom, and the wavelength-calibration spectrum (labeled WCA) on the top; each has three stripes. From bottom to top, these stripes are designated A, B, and C, as illustrated. Wavelength increases to the right and toward the top of the chip. The *HST* +V2 and +V3 axes are also shown. The SHORT, MEDIUM, and LONG designations are used in Phase II with the ACQ/PEAKXD command and the STRIPE Optional Parameter.

4.2.4 MAMA Read-out Format

The NUV channel creates six spectral stripes on the MAMA detector, three for the science data and three for the wavelength-calibration data. Stripes are separated by 94 to 143 pixels (2.1 to 3.3 arcsec), center to center, in the cross-dispersion direction. The NUV detector is read out as a 1024 × 1024 array, but in all other respects the data are handled in the same way as for the FUV detector. As noted, no pulse-height information is provided for MAMA data. An NUV spectrum obtained in TAGFLASH mode is shown in Figure 4.7.

Figure 4.8: Model LSFs for the COS NUV Channel

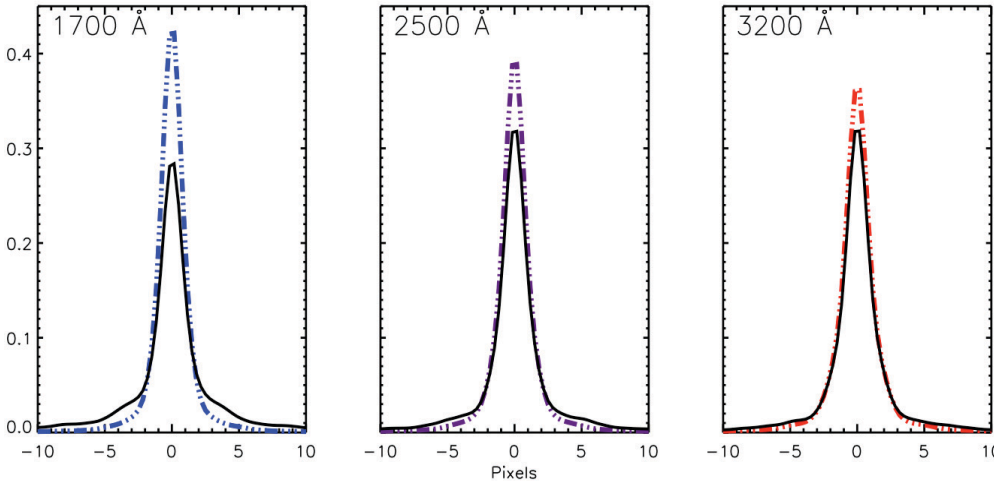

LSFs including the MFWFEs are plotted as solid lines, those without as dotted lines.

4.2.5 MAMA Dead Time

The dead time for the COS NUV MAMA is 280 ns, the same as for the STIS NUV MAMA. The 1% level of non-linearity is reached for C = 36,000 counts/s.

4.2.6 Non-Gaussian Wings in the MAMA PSF

While most NUV observations should be minimally affected by the mid-frequency wavefront errors (MFWFEs) discussed in Section 3.3, they will reflect the point-spread function of the COS MAMA detector, which exhibits faint, extended wings that are unrelated to the telescope optics. While the telescope-induced wings weaken as wavelength increases, the detector wings become stronger with increasing wavelength. Figure 4.8 shows model NUV detector LSFs with and without the MFWFEs at various wavelengths. Beyond 2500 Å, the detector wings dominate.

CHAPTER 5:

Spectroscopy with COS

In this chapter…

5.1 The Capabilities of COS

The two detectors and seven diffraction gratings (three for FUV, four for NUV) of COS enable high-sensitivity spectroscopy at low and moderate resolution across the FUV and NUV bands. The bandpass and resolution of each grating are presented in Table 5.1.

For each exposure, the observer selects a detector (FUV or NUV); a grating, central wavelength, and FP-POS setting; one of the two apertures (PSA or BOA); and a data-taking mode (TIME-TAG or ACCUM). Chapter 13 provides detailed specifications for each grating and aperture. Note that the two channels cannot be used simultaneously, as the NUV channel is fed by a mirror on the FUV optics select mechanism (OSM1).

Table 5.1: COS Grating Parameters

Grating	Approximate Wavelength Range (Å)	Bandpass per Exposure and FUV Gap[1] (Å)	Inferred PSA Resolving Power $R = \lambda/\mathrm{FWHM}$[2]	Approximate BOA Resolving Power	Dispersion (mÅ pixel^{-1})
FUV Channel					
G130M	900 – 1236	295 / 16	3000 – 1000[3]	—	9.97
	1065 – 1365	296 / 15.7	13,000 – 10,000[3]	—	9.97
	1150 – 1450	292 / 14.3	16,000 – 21,000	5900	9.97
G160M	1405 – 1775	360 / 18.1	16,000 – 21,000	4400	12.23
G140L	< 900 – 2150	> 1150 / 112	1500 – 4000	1100	80.3
NUV Channel					
G185M	1700 – 2100	3 × 35	16,000 – 20,000	3500	37
G225M	2100 – 2500	3 × 35	20,000 – 24,000	4600	33
G285M	2500 – 3200	3 × 41	20,000 – 24,000	5000	40
G230L	1650 – 3200[4]	(1 or 2) × 398	2100 – 3900	500	390

1. Width of gap between FUV detector segments; see Section 5.5.
2. Empirically-determined FWHM of the LSF, which is not Gaussian. *R* increases approximately linearly with wavelength.
3. *R* falls with increasing wavelength.
4. Some shorter wavelengths are recorded in second-order light. They are listed in Table 5.5.

5.1.1 First-Order Sensitivity

COS is considerably more sensitive than STIS and earlier-generation *HST* instruments at comparable spectral resolutions, particularly in the far ultraviolet. Effective areas for targets observed through the PSA are shown in Figure 5.1 and Figure 5.2. Note that the COS sensitivity changes with time (Section 5.1.5); plots and tables in this handbook are based on predictions for the middle of Cycle 20 (2013 April). Please consult the COS Web pages for updated information.

While the figures and tables in this handbook can be used to estimate of count rates and exposure times, we recommend the use of the COS ETC in all cases, because it properly computes instrument throughput, accounts for detector and astronomical backgrounds, and checks for violations of local and global count-rate limits.

Figure 5.1: Effective Areas for the FUV Channel through the PSA

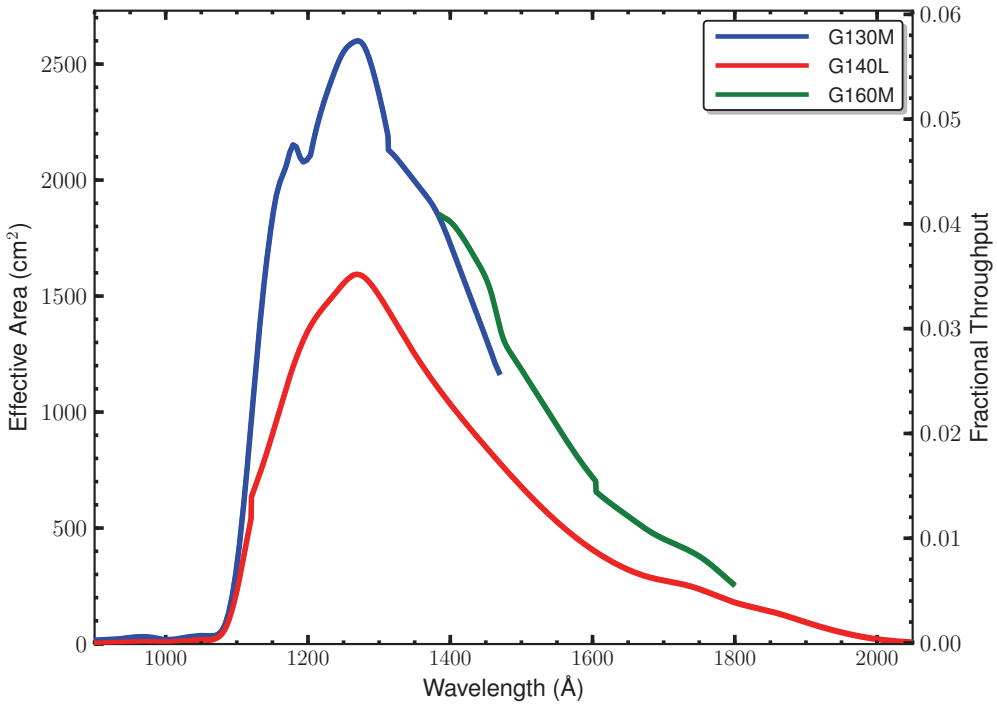

Figure 5.2: Effective Areas for the NUV Channel through the PSA

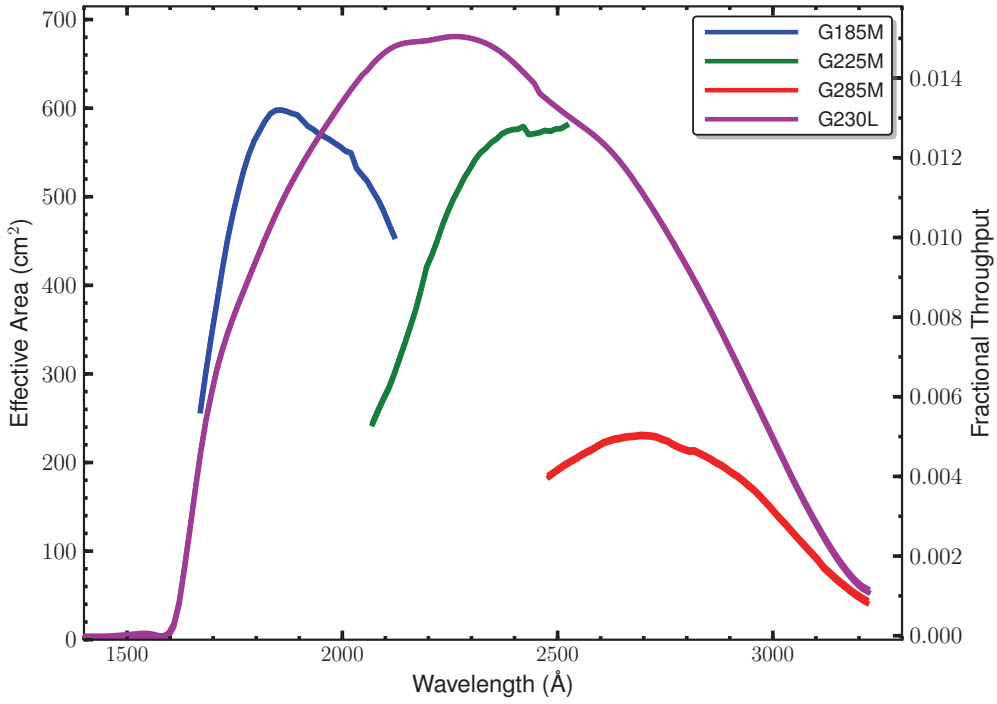

Figure 5.3: Effective Area at Wavelengths below 1400 Å

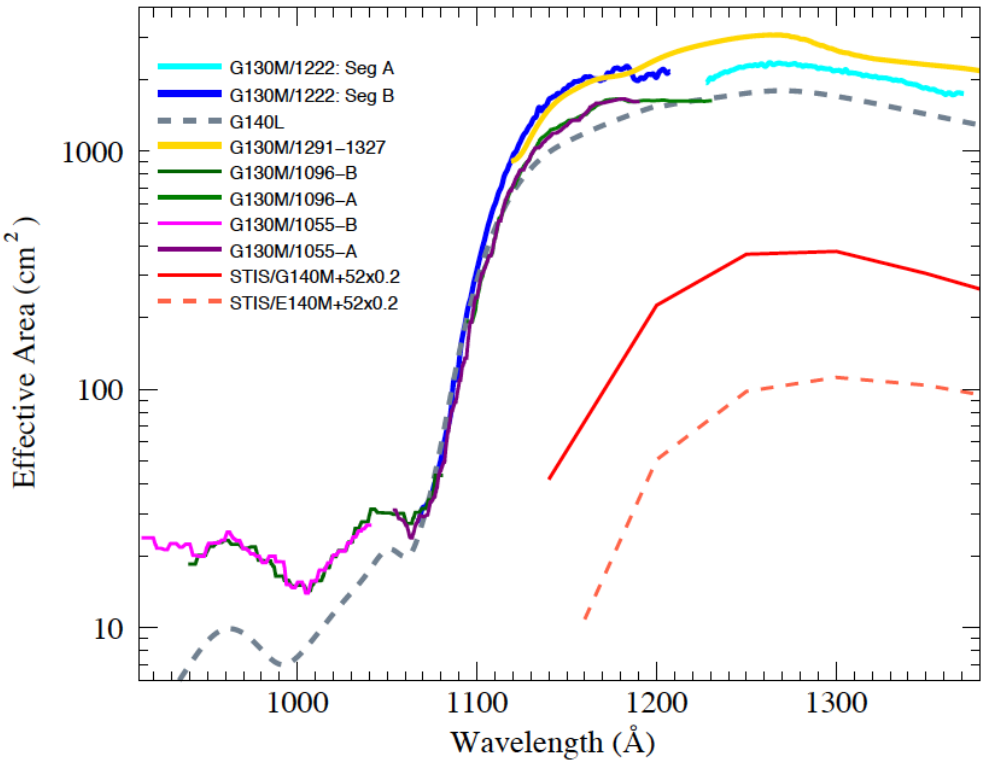

The effective areas of the various G130M central-wavelength settings are compared with those of G140L and STIS. Effective areas are not well characterized below 920 Å.

5.1.2 Sensitivity below 1150 Å

Figure 5.3 compares the effective areas of the G130M and G140L gratings at the short-wavelength end of the COS bandpass. From this figure, we can draw two fundamental conclusions: First, COS can obtain useful spectra at wavelengths between 900 and 1150 Å. Second, the contrast between the throughput at 1070 and 1150 Å is roughly a factor of 100.

When G140L is used with `CENWAVE=1280`, wavelengths as long as 1200 Å can fall on detector segment B. For many targets, the count rate at 1150 Å will exceed the local bright limit, while the count rate at shorter wavelengths is perfectly safe. Consequently, turning segment A off and using `FP-POS=4` is the recommended approach for observing bright objects below 1150 Å with the G140L grating.

When grating G130M is used with `CENWAVE=1055`, segment B records wavelengths shortward of ~1050 Å, depending on the FP-POS setting employed (Section 13.3). Using this grating mode with segment A turned off further reduces the danger of high count rates at longer wavelengths (but at the cost of some wavelength accuracy; see Section 5.7.4). Note that both the sensitivity and resolving power (Section 5.1.4) of G130M are greater than those of G140L in this wavelength range.

Figure 5.4: Second-Order Light in G230L Spectrum

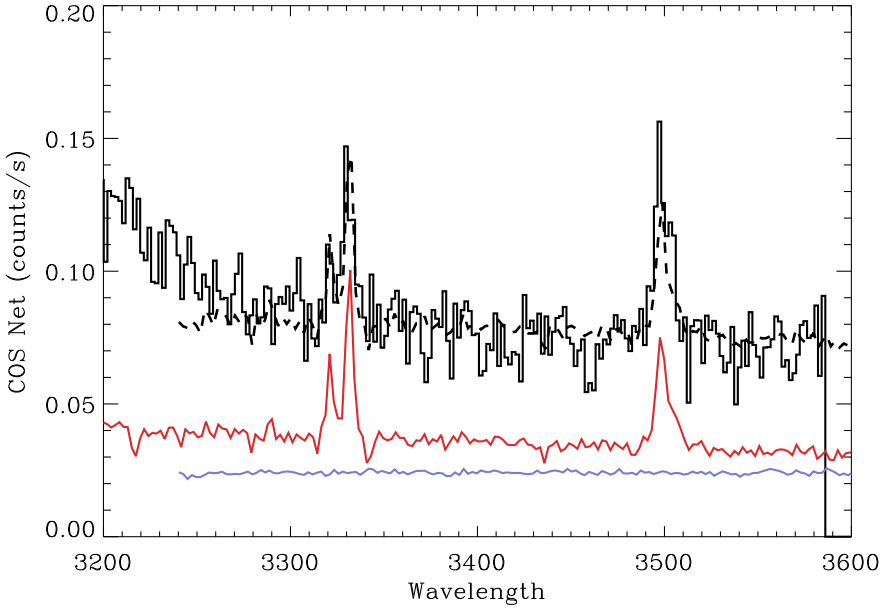

Black curve is stripe B of the G230L CENWAVE = 3360 spectrum of NGC 6833. Blue curve is an FOS spectrum over the same wavelength range (units are Ångstroms). Red curve is an FOS spectrum of the 1600 - 1800 Å region, plotted as $f(2\lambda)$. The FOS spectra have been rescaled by arbitrary amounts for display purposes. The dashed curve, a combination of the two FOS spectra, reasonably reproduces the COS spectrum.

5.1.3 Second-Order Sensitivity

Because the MAMA detector is sensitive to wavelengths as short as 1150 Å, NUV spectra longward of 2300 Å are vulnerable to contamination from second-order light. To mitigate this problem, the COS NUV optics were designed to provide peak reflectivities between 1600 and 2000 Å. Gratings G225M and G285M are coated with bare aluminum, which when oxidized has poor reflectivity below 1800 Å. After six reflections (two MgF_2 mirrors in the *HST* OTA and four bare-Al optics in COS), light from below 1250 Å is attenuated by 99%. Mounted directly on gratings G230L and G285M are order-sorting filters that block most light from below 1700 Å.

For G230L, stripes B and C are still affected by second-order flux. When `CENWAVE=3360`, stripe B is contaminated by second-order light beyond 3200 Å. In a spectrum of the planetary nebula NGC 6833 obtained with `CENWAVE=3360`, second-order light accounts for roughly 40% of the flux at 3320 Å and more that 50% at 3500 Å (Figure 5.4). Above 1700 Å, stripe C is more sensitive to second-order light than first-order by design (Table 5.5), but on-orbit observations reveal that first-order light is detectable at a level of 5% from wavelengths greater than 3700 Å at all central-wavelength settings (COS ISR 2010-01).

In the FUV channel, second-order light is present at long wavelengths ($\lambda > 2150$ Å) in spectra taken with G140L `CENWAVE=1280` FUVA. These photons are rejected by the COS pipeline during processing but available in the "net counts" column of the `*x1d*.fits` files.

Figure 5.5: Resolving Power of G130M/1222

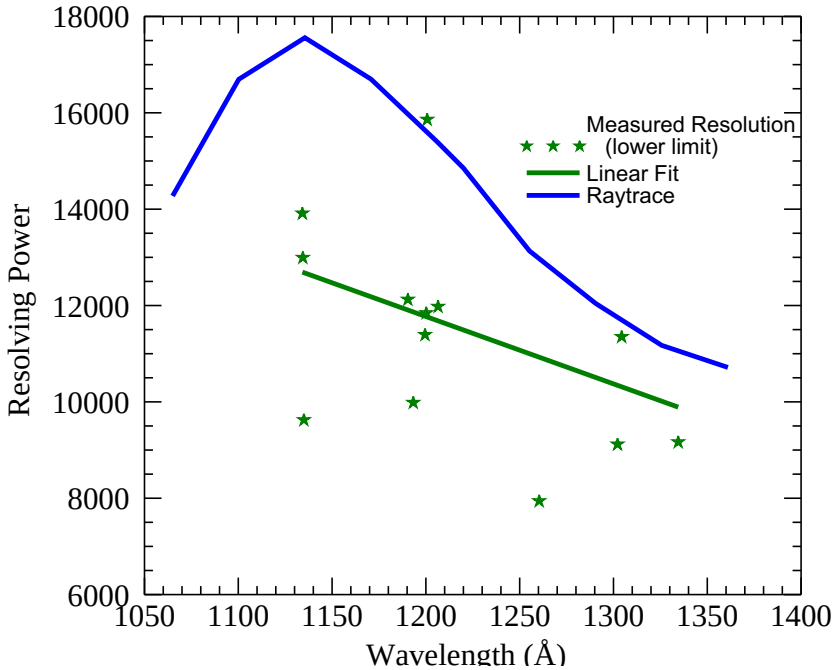

Green stars denote preliminary (low S/N) measurements of the resolving power ($R = \lambda/\mathrm{FWHM}$) of the G130M grating with `CENWAVE=1222`, which should be considered lower limits. The solid green line is a fit to the data. The light blue line represents ray-trace estimates of the resolving power in this mode.

5.1.4 Spectroscopic Resolving Power

The spectroscopic resolving power ($R = \lambda/\mathrm{FWHM}$) of each COS grating is listed in Table 5.1 and plotted as a function of wavelength for the FUV gratings in Figure 3.7. These values correspond to the FWHM of the model line-spread functions (LSFs) that are described in Section 3.3. Preliminary measurements and model predictions of the resolving power for the new 1222 Å central-wavelength setting of G130M are shown in Figure 5.5. (Derived from low signal-to-noise data, these measurements should be considered lower limits on R.) Measured values for the 1055 and 1086 Å central-wavelength settings of G130M are presented in Figure 5.6. Note that the resolving power decreases with increasing wavelength for these three central wavelengths of grating G130M.

Because the COS LSF is not a Gaussian, simple rules relating R to the observability of narrow spectral features may not apply. Careful modeling of the LSF may be required to determine the feasibility of an observation.

Figure 5.6: Resolving Power of G130M/1055, G130M/1096, and G140L/1280

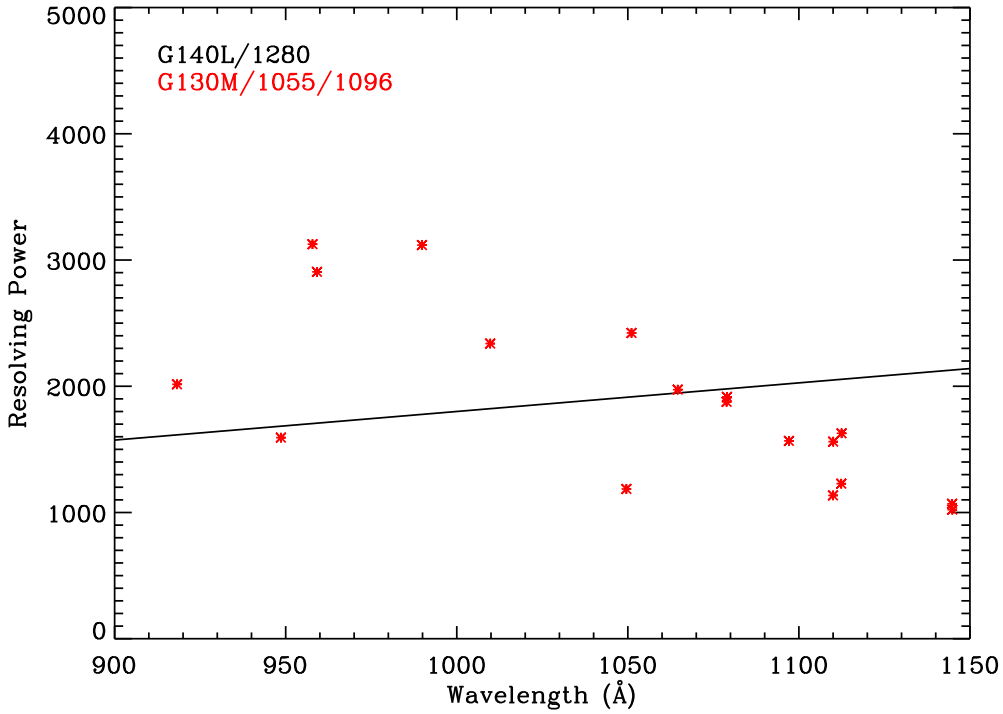

Resolving power (R = λ/FWHM) of the shortest-wavelength modes of G130M (red) and G140L (black). Values for G130M are derived from observations. Values for G140L are extrapolated from wavelengths longer than 1200 Å, which are themselves based on model LSFs.

5.1.5 Time-Dependent Sensitivity Changes

Observations of *HST* primary spectrophotometric standard stars show that there is a significant time dependence of the COS sensitivity for some spectrographic modes. The reflectivity of the G225M and G285M NUV gratings, which are coated with bare aluminum (rather than MgF_2 over aluminum like the other gratings), showed a time-dependent degradation before launch that has continued on orbit, decreasing at a rate of ~3% and ~10% per year respectively, independent of wavelength.

Throughout 2009, the FUV modes showed a wavelength-dependent sensitivity decline, falling ~3% per year below 1400 Å and as much as 11% per year at 1800 Å. The decline slowed to ~5% per year in 2010 and to 3% in 2011, independent of wavelength. Its characteristics are consistent with a degradation of the quantum efficiency of the CsI photocathode of the FUV detector. For details, see COS ISR 2011-02.

The COS data-reduction pipeline **calcos** includes a time-dependent sensitivity calibration, and regular monitoring of standard stars is used to update the sensitivity reference files. The ETC reflects the best estimate of the sensitivity for the middle of Cycle 20.

5.1.6 Zero-Order Image

The 1105 Å central-wavelength setting of grating G140L places the zero-order image from the grating on segment B of the FUV detector, violating detector count-rate limits, while a useful first-order spectrum falls onto segment A. For this central wavelength, observations can be made only in single-segment mode, with the high voltage for segment B reduced (Section 5.6). After final alignment of COS on-orbit, the zero-order image was also found to fall on segment B for the 1230 Å setting with `FP-POS=4`. In Cycle 18, `CENWAVE=1230` was replaced with `CENWAVE=1280` to keep the zero-order image off the detector. Two-segment observations are allowed for all FP-POS settings with `CENWAVE=1280`.

5.1.7 Internal Scattered Light

The internal scattered-light level within COS is quite low. In ground-test measurements, light scattered along the dispersion axis represents less than 1% of the nearby continuum. On orbit, the COS LSF dominates the scattered light (Chapter 3); scattering within the instrument is negligible (Kriss 2011).

5.1.8 Spatial Resolution and Field of View

The spatial resolution of COS is affected by the mid-frequency wavefront errors (MFWFEs) via the non-Gaussian wings they introduce (Section 3.3). The NUV channel corrects for the telescope's spherical aberration, but not for the MFWFEs. For PSA observations, the spatial resolution is ~ 0.07" for G185M and G230L, and 0.06" for G225M and G285M. For BOA observations, the spatial resolution is 0.29" for G185M, 0.22" for G225M, 0.24" for G285M, and 0.30" for G230L.

In the FUV, the situation is more complex, because of the uncorrected astigmatism in the cross-dispersion direction. Figure 5.7 shows the strong dependence of the spectral width on both the wavelength and central-wavelength setting for each of the FUV gratings. At wavelengths for which the profile width is large, the spectra of two objects separated by less than the profile width in the cross-dispersion (XD) direction would be combined.

The COS field of view is determined by the entrance apertures, which are 1.25 arcsec in radius, but the aberrated beam entering the aperture allows objects up to 2 arcsec from the center of the aperture to contribute to the recorded spectrum.

For additional information, please see "FUV Spectroscopic Performance" (COS ISR 2010-09, Ghavamian et al. 2010) and "NUV Spectroscopic Performance" (COS ISR 2010-08, Béland et al. 2010).

Figure 5.7: Cross-Dispersion Profile Widths for FUV Gratings

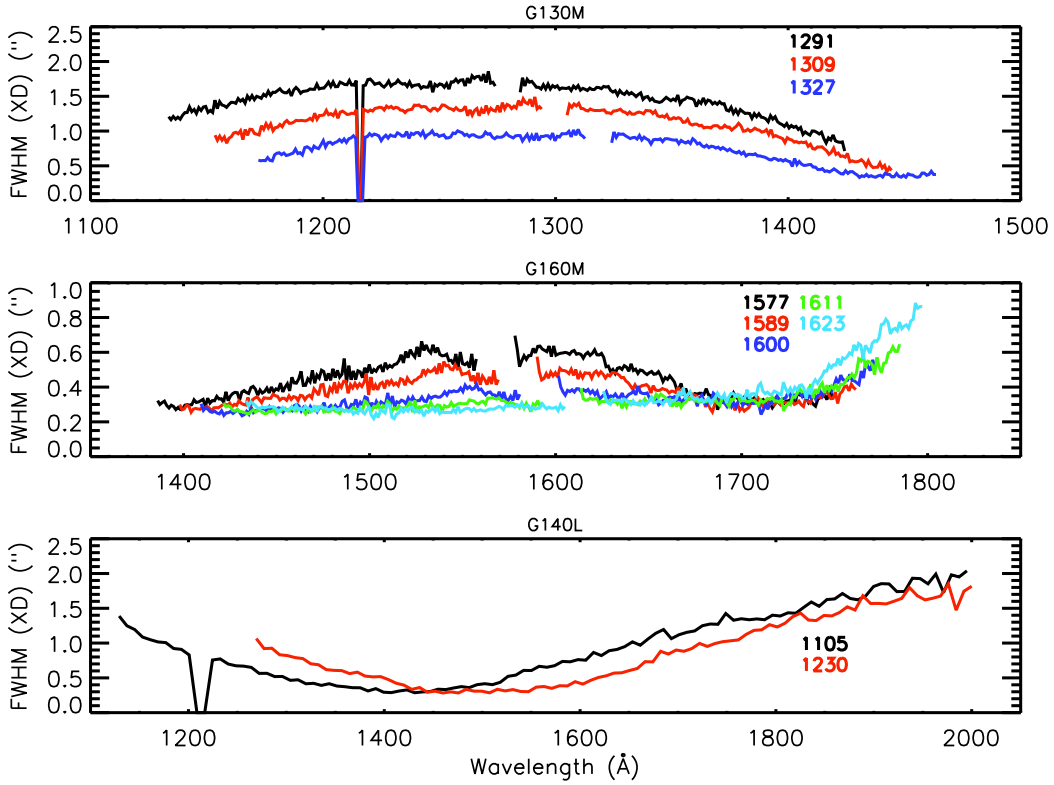

Variation in the width of the FUV spatial profile. The widths are obtained via Gaussian fits to the cross-dispersion profiles of a point source observed through the PSA. (Empirically-determined FWHM values may be slightly smaller.) Widths are plotted as a function of wavelength for each of the central-wavelength settings. Dips in the G130M and G140L spectra mark airglow features.

5.1.9 Photometric (Flux) Precision

Based on measurements made during SMOV, we estimate that the absolute flux calibration of COS is accurate to about 5% in the FUV, though uncertainties may be larger at wavelengths less than 1150 Å. In the NUV, the calibration is accurate to about 2% for the medium-resolution gratings; it is slightly less accurate in some parts of the G230L bandpass. Time-dependent sensitivity corrections should be accurate to about 2% (Section 5.1.5).

5.1.10 Wavelength Accuracy

The COS medium-resolution gratings are required to achieve a wavelength accuracy of 15 km/s. For G140L, the requirement is 150 km/s; it is 175 km/s for G230L. Analysis of COS data obtained on orbit suggest that these requirements are routinely met. To do so, targets must be properly centered in the desired aperture. Target acquisitions are discussed in Chapter 8.

Figure 5.8: Vignetting Profile for NUV M Gratings

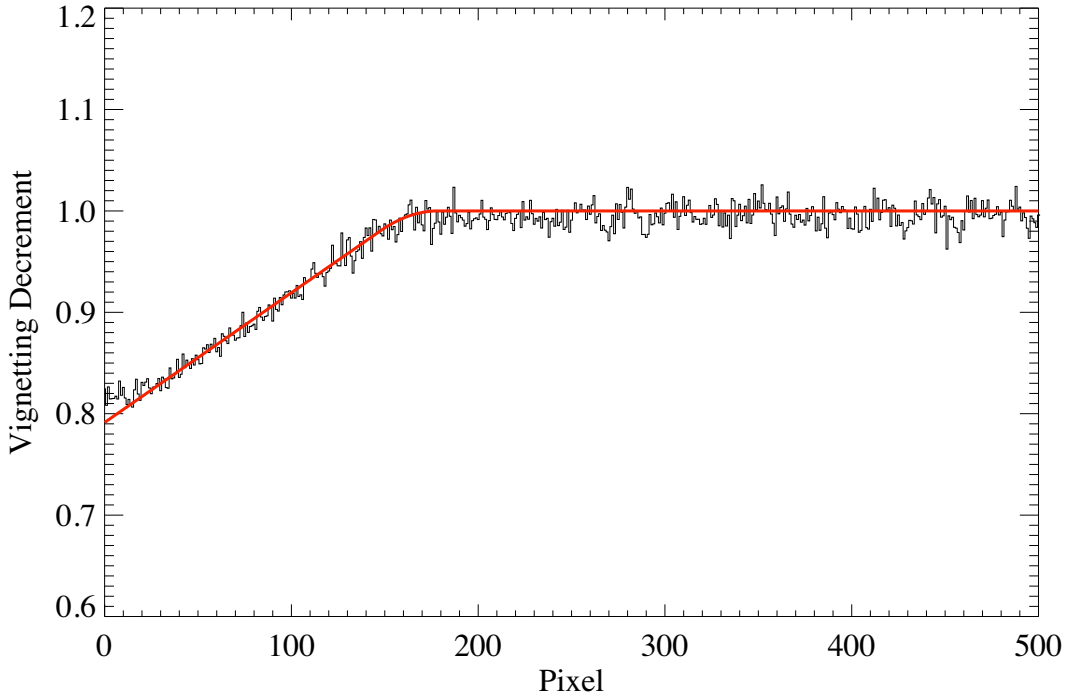

Vignetting profile of the medium-resolution gratings as a function of pixel location showing the linear decrease in throughput near the low-pixel edge of the NUV detector. The red line shows the best fit to the profile obtained from observations of the white dwarf G191-B2B.

5.1.11 Vignetting of the NUV Channel

After on-orbit alignment of COS in *HST*, fluxes of external targets in the PSA were found to be depressed at the short wavelength ends of the NUV stripes. For the medium-resolution gratings, the reduction is about 20% at the first pixel and rises linearly to expected levels over approximately the next 160 pixels (Figure 5.8). For G230L, the reduction is about 15% at the first pixel and extends about 110 pixels. (The slope is the same as in Figure 5.8; it is as though the ramp were shifted by 50 pixels.) The depression is thought to be due to vignetting of the beam at the NUV camera mirrors that image the spectrum on the detector. Corrections for this vignetting are not included in either the COS Exposure Time Calculator (ETC) or the **calcos** data-reduction pipeline. Users are advised to consult the COS Web pages, where additional information will be posted as it becomes available.

5.2 TIME-TAG vs. ACCUM Mode

COS exposures may be obtained in either a time-tagged photon-address mode (TIME-TAG), in which the position, arrival time, and pulse height (for FUV observations) of each detected photon are saved in an event stream, or in accumulation (ACCUM) mode, in which only the positions of the photon events are recorded.

5.2.1 TIME-TAG Mode

In TIME-TAG mode, each photon is kept as a separate event in a list in COS memory. Each entry in that list contains the (*x, y*) coordinates of the photon together with the pulse height of the charge cloud generated by it (for FUV observations). Time markers are inserted in the list every 32 ms by the instrument electronics. When data are processed by the ground system, arrival times are assigned to the events according to the time marker preceding the event.

COS observations should be obtained in TIME-TAG mode whenever possible, because it provides significant opportunities for temporal sampling, exclusion of poor quality data, and, for the FUV, improved thermal correction (by tracking the stim-pulse positions as a function of time) and background removal (by using the pulse-height information). TIME-TAG mode should always be used for exposures that will generate count rates of 21,000 counts/s or less from the entire detector (including both detector segments for the FUV). At count rates between 21,000 and 30,000 counts/s, TIME-TAG may be used to obtain properly flux-calibrated data, but the loss of some continuous time periods within extended exposures will occur (see the discussion under BUFFER-TIME below). At present, TIME-TAG should not be used for count rates greater than 30,000 counts/s. ACCUM mode should be used for such high count-rate targets.

We recommend that TIME-TAG mode always be used with FLASH=YES (the so-called TAGFLASH mode) unless circumstances prevent it (see Section 5.7.1).

Doppler Correction for TIME-TAG Mode

No on-board corrections are made for shifts in the spectrum due to the orbital motion of *HST* while in TIME-TAG mode; this is done later in pipeline processing.

Pulse-height Data for TIME-TAG

In FUV TIME-TAG mode, the pulse height of each photon event is recorded, along with the position and arrival time. Pulse heights are stored as 5-bit words, so their values range from 0 to 31. Post-observation pulse-height screening is useful for rejecting unwanted background events and can often improve the signal-to-noise ratio in the extracted science spectrum. Pulse-height information is not provided by the NUV detector.

5.2.2 ACCUM Mode

In ACCUM mode, an image of the detector is stored in a 16-bit memory buffer. As each photon arrives from the detector, the location in the buffer at coordinates *(x, y)* is incremented by one. Each location can hold at most 65,535 counts; the next event will cause the value to roll over to zero. To conserve memory, only a 16384 × 128 region of each segment is stored. Timing and pulse-height information is not saved, preventing the application of the data-correction techniques available in TIME-TAG mode.

ACCUM mode is designed for bright targets whose high count rates would fill the on-board buffer memory too rapidly if the data were taken in TIME-TAG mode. In some instances, one may observe a relatively bright object in TIME-TAG mode by using the BOA instead of the PSA, but the BOA degrades the spectroscopic resolution. Observers wishing to use ACCUM mode will be asked to justify doing so when submitting their Phase II program.

Observing Efficiencies with ACCUM

FUV ACCUM images do not include the entire detector. To conserve memory, photons are collected only from the stim regions and that portion of the detector actually illuminated by the target (1/8 of the full detector area, or 128 pixels in *y*). Each FUV ACCUM image fills one-half of the total COS memory, so it is possible to acquire two FUV images before dumping the on-board buffer.

NUV ACCUM images cover the entire detector. Because they are smaller, up to nine of them can be stored in the memory buffer. Unlike TIME-TAG mode, no data may be acquired during an ACCUM readout. NUV ACCUM mode is thus most efficient when repeated identical observations are stored in memory, then read out all at once. (Within APT, the Astronomer's Proposal Tool, one may easily schedule multiple iterations of an exposure using the Number_of_Iterations parameter.)

Doppler Correction for ACCUM Mode

In ACCUM mode, the COS flight software adjusts the pixel coordinates of detected events to correct for the orbital motion of *HST*. The correction (always by an integral number of pixels) is updated whenever *HST*'s velocity with respect to the target changes enough to shift the spectrum by an additional pixel. This is done via a small table, computed on the ground, that lists the time of each pixel shift, based on the orbital motion and the dispersion of the grating in use.

Note that ACCUM mode exposures longer than 900 seconds that use the G130M or G160M gratings may blur the FUV spectra by 1 to 2 pixels (about 1/6 to 1/3 of a resolution element) since shifts are performed in pixel, not wavelength, space.

Pulse-Height Distribution Data for ACCUM Mode Observations

Some pulse-height information is available for FUV ACCUM observations. A pulse-height histogram, consisting of 256 bins (128 bins for each detector segment) of 32 bits each, is dumped for every ACCUM mode image obtained with the FUV detector. (Why 128 bins? In ACCUM mode, individual pulse heights are stored as 7-bit words, so their values range from 0 to 127.) Pulse-height data are not provided for NUV exposures.

5.3 Valid Exposure Times

The minimum COS exposure duration is 0.1 seconds (but FLASH=YES TIME-TAG exposures impose a longer minimum; see Section 5.7.1). The maximum is 6,500 seconds. Between these extremes, COS exposure times must be integer multiples of 0.1 seconds. If the observer specifies an exposure time that is not a multiple of 0.1 seconds, its value is rounded *down* to the next lower integral multiple of 0.1 seconds, (or set to 0.1 seconds if a smaller value is specified). Exposure times larger than about 3,000 seconds are normally appropriate only for visits with the CVZ special requirement, because the visibility period of a typical orbit is ~ 50 minutes. See the *HST Primer* for information about *HST*'s orbit and visibility periods.

For TARGET=WAVE exposures, DEF (default) must be entered as the exposure time. The value appropriate for the optical configuration will be chosen from a table established at STScI for best performance. At present, TARGET=WAVE flash durations are identical to those given in Table 5.2.

5.4 Estimating the BUFFER-TIME in TIME-TAG Mode

COS maintains two on-board data buffers, each with a capacity of 9 MBytes (2.35×10^6 counts). The time set aside to fill one of these buffers is called the BUFFER-TIME. COS uses the BUFFER-TIME to establish the pattern and timing of memory dumps during a TIME-TAG exposure: For the first BUFFER-TIME of an exposure, counts are recorded in the first COS data buffer. At the end of this time, data recording switches to the second data buffer, and the first buffer is read out while the second is being filled.

For all external TIME-TAG observations, a value of the BUFFER-TIME must be specified in the Phase II proposal. The BUFFER-TIME is 2.35×10^6 counts divided by the anticipated count rate in photons per second. The BUFFER-TIME calculation should include counts from the detector dark current and stim pulses (for FUV) as well as the detected photon events, factoring in the instrument quantum efficiency and dead time. We recommend use of the COS ETC to compute an accurate value of the BUFFER-TIME. **Give yourself a margin of error of about 50%; i.e., multiply the ETC BUFFER-TIME by 2/3.**

If the BUFFER-TIME is overestimated, the buffer may fill before input switches to the other buffer. Subsequently-arriving photons will be lost, leaving a gap in the data. The pipeline will correct the exposure times for any such gaps, so flux calibrations will be correct, but the overall S/N will be lower than expected. If BUFFER-TIME is underestimated, input will switch to the second buffer before the first buffer is full. No data will be lost, but the resulting drain on spacecraft resources could preclude other activities, including parallel observations.

5.4.1 Faint Targets (BUFFER-TIME > Exposure Time)

For faint targets, the predicted BUFFER-TIME may be considerably longer than the exposure time. In such cases, set BUFFER-TIME equal to the exposure time. In orbits with multiple science exposures, you can minimize overheads – and squeeze out a few more seconds of observing time – by setting the BUFFER-TIME for each exposure to the exposure time minus 100 seconds. The buffer takes about 110 seconds to empty, so most of the data will be read out before the exposure is completed, leaving only a fraction for the end of the exposure. This allows the next exposure to begin sooner. You can test the effects of such trade-offs by trying them out within APT. See Section 9.7.5 for an example.

5.4.2 Bright Targets (BUFFER-TIME < 110 Seconds)

It takes 110 seconds to empty a COS data buffer. A `BUFFER-TIME` of 110 seconds corresponds to a count rate of 21,000 counts per second. If the count rate exceeds this value, then the second data buffer will be filled before the first buffer has been completely read out. In this situation, you have two options: You can shorten your exposure, or you can accept gaps in the recorded data stream. In either case, **calcos** will compute the actual exposure time and will calculate fluxes correctly, but the total number of collected counts, and hence the S/N, will be limited by the 21,000 counts per second rate.

- Option A: You wish to receive all the data and are willing to shorten the exposure time. In this case, use 2/3 of the `BUFFER-TIME` returned by the ETC. If the `BUFFER-TIME` is less than 111 seconds, APT will issue a warning and truncate the exposure time at 2 × `BUFFER-TIME` to ensure that all data are recorded.
- Option B: You can tolerate data drop-outs, but want control of the total exposure time. In this case, choose a `BUFFER-TIME` of 111 seconds. You will lose some fraction of the data during each `BUFFER-TIME` interval (see example below), but APT will not truncate your exposure.

As an example, suppose that 2/3 × (`BUFFER-TIME` returned by the ETC) is 100 seconds, and you want an exposure time of 360 seconds.

- With Option A, you would specify `BUFFER-TIME=100`. Because it takes longer than that to read out the buffer, APT limits you to an exposure time of 2 × 100 = 200 sec. In this case, COS records all the events that arrived during the exposure.
- With Option B, you would specify `BUFFER-TIME=111`. Since the COS buffer may be full after the first 100 seconds, the last 11 seconds of data may not be recorded and are lost each time the buffer fills. With this option you will get a series of data blocks as follows: **100**, *11*, **100**, *11*, **100**, *11*, **27**, where the bold numbers represent periods when the data are recorded, and the italic numbers represents periods when the data are lost. The COS shutter remains open for the full 360 seconds, and the data are properly flux calibrated by the pipeline.

5.4.3 Very Bright Targets (BUFFER-TIME < 80 Seconds)

The minimum allowed value of the BUFFER-TIME is 80 seconds. This value corresponds to a count rate of 30,000 counts per second over the entire detector, the maximum rate at which the flight electronics are capable of processing counts. If 2/3 of the ETC BUFFER-TIME is less than 80 seconds, then the source is very bright and should be observed in ACCUM mode. If your exposure is less than 80 seconds in length, set BUFFER-TIME=80. The buffer will be read out immediately after the exposure ends, and there will be no idle time.

The software and parameters that control dumps of the data buffer have been designed to avoid any loss of data from an observation. The duration and timing of data dumps depend on several factors, and observers are urged to experiment with APT to optimize the efficiency of their observations.

5.4.4 BUFFER-TIME and AUTO-ADJUST

If you use the AUTO-ADJUST feature in APT to set your exposure times, do it first, then adjust the BUFFER-TIME of each exposure according to the rules above.

5.5 Spanning the Gap with Multiple CENWAVE Settings

COS spectra exhibit wavelength gaps due to the physical layout of the detectors and the optics. The FUV detector consists of two segments whose active areas are separated by a gap approximately 9 mm wide. The optical image of the spectrum is continuous across the segments, but the wavelengths that fall in the gap are not recorded. These wavelengths can be brought onto the active area of the detector by choosing one of the alternate central-wavelength settings listed in Table 5.4. For the FUV M gratings, the gap (14-18 Å) is about twice the size of the difference in central wavelength shifts (9 Å). To span it, we recommend obtaining exposures at two or more FP-POS positions at each of two non-consecutive CENWAVE settings. For the G140L grating, both CENWAVEs are needed to obtain a complete spectrum.

For the NUV channel, dispersed light from the gratings is imaged onto the detector by three camera mirrors, resulting in three non-contiguous spectral stripes being recorded at once. The gaps between the stripes are approximately 64 Å for the G185M and G225M gratings, 74 Å for G285M, and 700 Å for G230L (Table 5.5). To acquire a complete medium-resolution spectrum requires six settings with G185M, six with G225M, and eight with G285M. A full spectrum with G230L requires all four CENWAVE settings. Such a complete spectrum can probably be acquired more efficiently with STIS, but COS may be a better choice when a limited number of specific wavelengths is desired.

5.6 FUV Single-Segment Observations

The FUV detector segments are operated and read out independently. For all FUV gratings, segment A detects the longer-wavelength light and segment B the shorter wavelengths. Normally, both segments are used for a science exposure, but there are circumstances in which operating with one detector segment at the nominal high voltage and the other effectively turned off may be beneficial. The `SEGMENT` optional parameter allows this choice. STScI strongly recommends use of both segments (the default for all but the G140L 1105 Å setting) unless special circumstances exist. Such circumstances include

- Sources with unusual spectral energy distributions at FUV wavelengths (bright emission lines or rapidly increasing/decreasing continuum slopes), for which the count rate on one detector segment exceeds the bright-object protection limit, while the other segment is safe for observing. In some cases, this problem may be mitigated by adjusting the central wavelength or `FP-POS` setting.
- Sources for which the count rate on one detector segment is high but safe, while the other segment has a relatively low count rate. If the science to be done were on the low count-rate segment, operating just that segment would reduce data losses due to dead-time effects and increase the S/N of the resulting spectrum.

The optional parameter `SEGMENT` specifies which segment of the FUV detector to use for an observation. A value of `BOTH` will activate both segments; this is the default setting. If `A` is selected, only segment A of the detector will be activated for photon detection, and the spectrum will contain data from only the long-wavelength half of the detector. If `B` is selected, only the short-wavelength segment B of the detector will be activated and used to generate data. Wavelength and flat-field calibration procedures remain the same for a particular segment whether or not the other segment is operating.

If grating G140L is specified with the 1105 Å wavelength setting, then the value must be `SEGMENT=A`. Switching from two-segment to single-segment operation (or back again) incurs a substantial overhead time; see Table 9.5.

5.7 Internal Wavelength Calibration Exposures

Three types of internal wavelength calibration exposures may be inserted in the observation sequence by the scheduling system or by the observer:

1. `FLASH=YES` (so-called TAGFLASH) lamp flashes (`TIME-TAG` observing with the PSA only),
2. AUTO wavecals, and
3. User-specified wavecals.

Note that *all* wavelength-calibration exposures are taken in TIME-TAG mode. Wavelength calibration exposure overheads are higher when the BOA is used for science observation, because the aperture mechanism must be moved to place the WCA in the wavelength-calibration beam.

While it is possible to suppress the taking of any wavelength-calibration spectra, doing so significantly lessens the archival quality of COS data and must be justified on a case-by-case basis.

5.7.1 Concurrent Wavelength Calibration with TAGFLASH

The Optional Parameter FLASH indicates whether or not to "flash" the wavelength calibration lamp during TIME-TAG exposures utilizing the PSA. These flashes provide data used by the **calcos** pipeline to compensate for drifts of the Optics Select Mechanisms. In this mode, when the external shutter is open to observe an external target, the wavecal lamp is turned on briefly at the beginning of and at intervals throughout the exposure. Light from the science target and the internal wavelength calibration source is recorded simultaneously on different portions of the detector. Other than the flash at the start, the timing of flashes is determined by the elapsed time since the last OSM motion. As a result, flashes may occur at different times in different exposures. The grating-dependent flash durations (Table 5.2) and the flash intervals are defined and updated as necessary by STScI. Observers may not specify either flash duration or interval. (Details of TAGFLASH execution are presented in COS ISR 2011-04.) When flashing is enabled, the exposure time must be at least as long as a single flash. Science exposures shorter than the flash durations listed in Table 5.2 may be obtained by setting FLASH=NO, in which case a wavecal exposure will automatically be inserted after the science exposure.

TIME-TAG sequences with FLASH=YES provide the highest on-target exposure time, as no on-target time is lost to wavelength-calibration exposures. We thus strongly recommend use of Optional Parameter FLASH=YES with all TIME-TAG observations through the PSA. (Since FLASH=YES is the default for TIME-TAG spectroscopic exposures, the observer need not specify it.) FLASH=YES may not be specified for ACCUM mode or when the BOA is selected.

5.7.2 AUTO Wavecals (when TAGFLASH is not used)

For ACCUM, BOA, or FLASH=NO TIME-TAG exposures, a separate wavelength calibration exposure will be automatically scheduled by APT for each set of external spectrographic science exposures using the same spectral element, central wavelength, and FP-POS value. These AUTO wavecals are always obtained in TIME-TAG mode with the external shutter closed. This automatic wavelength calibration exposure will be added before the first associated science exposure and after each subsequent science exposure if more than 40 minutes of visibility time has elapsed since the previous wavelength calibration exposure and if the same spectrograph set-up has been in use over that time. The calibration exposure will often use some science target orbital visibility. The calibration lamp configuration and exposure time will be based on the grating and central wavelength of the science exposure. Utilization of a GO

wavecal (see below) resets the 40 minute interval timer. Insertion of a FLASH=YES exposure in the time-line does not affect the 40-minute clock.

Table 5.2: TAGFLASH Exposure Durations

Grating	Central Wavelength (Å)	Flash duration (s)	Grating	Central Wavelength (Å)	Flash duration (s)
G130M	1055	102	G225M (cont.)	2339	12
	1096	35		2357	12
	1222	52		2373	22
	all others	12		2390	7
G160M	all	12		2410	7
G140L	all	7	G285M	2617	12
G185M	1786	12		2637	12
	1817	12		2657	7
	1835	12		2676	22
	1850	22		2695	22
	1864	32		2709	12
	1882	17		2719	7
	1890	12		2739	7
	1900	22		2850	22
	1913	17		2952	7
	1921	12		2979	17
	1941	12		2996	17
	1953	17		3018	22
	1971	17		3035	27
	1986	12		3057	32
	2010	12		3074	32
G225M	2186	7		3094	32
	2217	12	G230L	2635	7
	2233	7		2950	7
	2250	22		3000	7
	2268	12		3360	12
	2283	12	MIRRORA	...	7
	2306	12	MIRRORB	...	27
	2325	12			

AUTO wavecals may not be turned off by the observer. If there is a science requirement to turn off AUTO wavecals, specific permission must be sought from the STScI Contact Scientist.

FLASH=NO observations will be less efficient than FLASH=YES observations in terms of on-target utilization of orbital visibility and in the quality of their wavelength calibration due to possible OSM residual motions.

5.7.3 GO Wavecals (User-specified)

Observers may request additional wavelength-calibration exposures, called GO wavecals, by selecting TARGET=WAVE, EXPTIME=DEF, and FLASH=NO. The exposure must be made in TIME-TAG mode. GO wavecals use the same calibration lamp configuration and exposure times as the automatic wavelength calibrations discussed above. The default modes of operation automatically secure needed wavelength-calibration information to go with your science data, so GO wavecals are rarely required.

5.7.4 No-Cal Wavecals

The COS Pt-Ne wavelength-calibration lamps produce no lines on FUV segment B in the following observing modes:

- G130M, central wavelength 1055 Å, all FP-POS settings;
- G130M, central wavelength 1096 Å, all FP-POS settings;
- G140L, central wavelength 1280 Å, all FP-POS settings.

To these data, **calcos** assigns the wavelength shifts derived from the segment A spectrum. If no segment A data are present (*i.e.,* if SEGMENT=B), then no shift is assigned.

5.8 Fixed-Pattern Noise

The signal-to-noise ratio (S/N) of COS observations is improved through two techniques, flat fielding and coadding spectra taken at different central wavelengths or FP-POS settings. Flat fielding removes the high-frequency, pixel-to-pixel detector variations by dividing the data by a high S/N flat-field response image. FP-POS exposures smooth out the detector variations by combining in wavelength space data taken at different positions on the detector.

5.8.1 COS Flat Fielding

The internal flat-field calibration system consists of two deuterium lamps and the flat-field calibration aperture (FCA). The system was designed such that light from the lamps follows nearly the same optical path as that from an external target. The FCA is placed near the usual location of the PSA, and the lamp beam illuminates the gratings and mirrors from this slightly offset position.

The deuterium lamps are not bright enough to map out the flat field at FUV wavelengths, so the FUV flats are constructed from on-orbit observations of bright white dwarfs. A preliminary FUV flat is shown in Figure 5.9. The dark, vertical stripe

is a shadow cast by a grid wire in front of the detector (Section 4.1.1). A detector dead spot and the hexagonal pattern of the fiber bundles in the micro-channel plate are also visible. Although significant structure is present in the FUV flats, it is reproducible and can be removed during data reduction.

Figure 5.9: Section of a Flat-Field Image for the FUV XDL

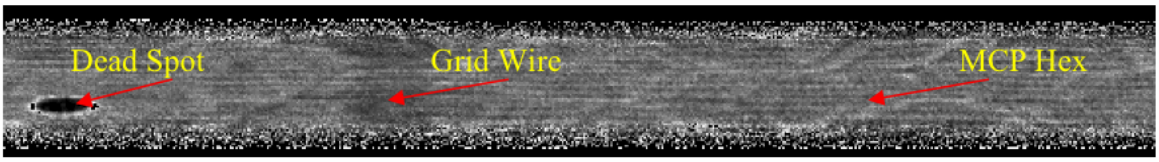

A section of the FUV flat field showing representative detector features and a grid wire.

Grid-wire shadows are the greatest source of fixed-pattern noise. In the past, **calcos** flagged these regions and eliminated their contributions to the final, summed spectra. During Cycle 18, a grid-wire flat-field calibration file was developed for the G130M and G160M gratings. Pixels affected by grid wires are still flagged by **calcos**, but their corrected values are included in the summed spectra. For the G140L grating, for which no flat field is yet available, the regions affected by grid-wire shadows are masked and rejected by **calcos** when it combines data obtained at different `FP-POS` settings. Figure 5.10 shows the effect of correcting the grid-wire shadows on a single G130M FUVB exposure of the white dwarf WD0320-539. This star has a relatively smooth continuum, making the corrections obvious. The upper (blue) spectrum contains grid-wire shadows (indicated by the vertical lines), which are corrected in the lower (green) spectrum. The affected regions are clearly improved, but residual structure, much of it fixed-pattern noise in the FUV detector, remains. This structure can be reduced through the use of multiple FP-POS settings (Section 5.8.2).

Figure 5.10: Correcting Grid-Wire Shadows with Flat-Field Reference File

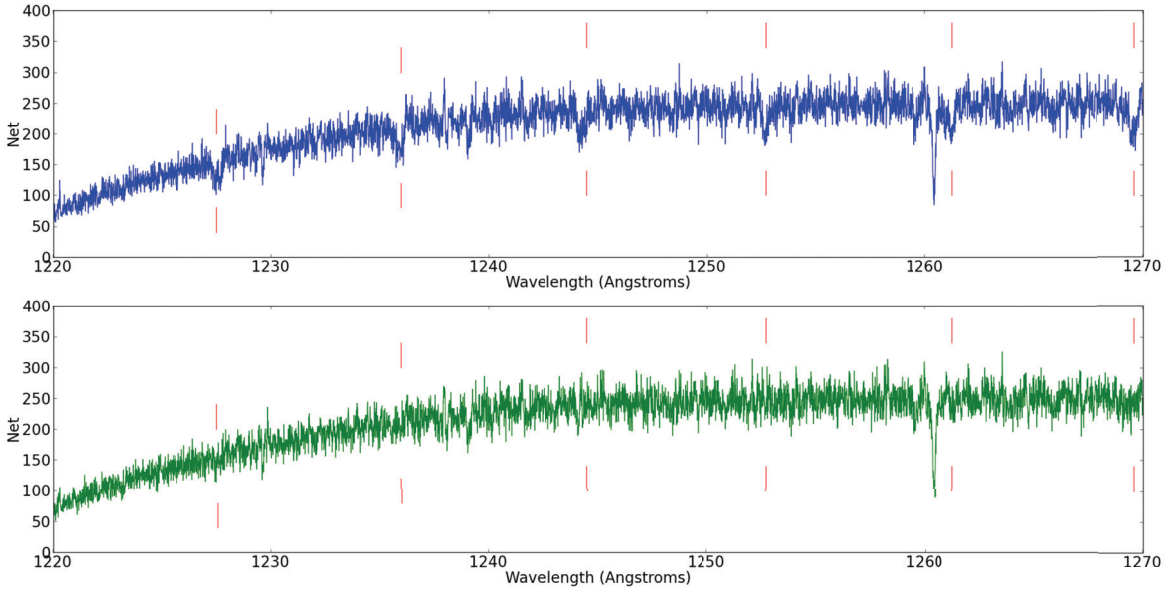

G130M FUVB exposure of the white dwarf WD0320-539. The upper (blue) spectrum contains grid-wire shadows (indicated by the vertical lines), which are corrected in the lower (green) spectrum.

Table 5.3: Limiting S/N for FUV Spectroscopy

Grating	FUVA	FUVB
Single FP-POS Exposure		
G130M	17.9	23.8
G160M	14.9	20.4
Combining 4 FP-POS Exposures		
G130M	35.7	47.6
G160M	29.9	40.8

Table 5.3 gives the limiting S/N for the G130M and G160M gratings when the grid-wire flat field is used, both with and without multiple FP-POS settings. To attain higher S/N ratios, special analysis procedures, such as those described in the 2011 January COS STAN, are required.

Because the grid wires are oriented perpendicular to the spectrum, their effect on the data is relatively insensitive to the location of the spectrum in the cross-dispersion direction. Much of the remaining fixed-pattern noise depends strongly on the spectrum location and will require considerably more effort to characterize and correct. Observers are advised to check the COS Web pages for the latest developments.

The NUV flat field used by **calcos** was built from a combination of external PSA deuterium lamp exposures taken on the ground and internal FCA observations taken

on the ground and on orbit. Figure 5.11 presents a comparison between two NUV flat-field frames, one obtained on orbit and one on the ground. Each image was divided by a low-order polynomial to isolate the high-order fringe pattern characteristic of the NUV detector. Their ratio is consistent with the noise in the on-orbit image, confirming that the two flat fields may be safely combined. Pre-flight ground tests with COS show that the NUV MAMA can deliver S/N up to about 50 without using a flat field. Using a flat field, S/N of 100 or more per resolution element should be routinely achievable.

Figure 5.11: Flat-Field Exposures for the NUV MAMA

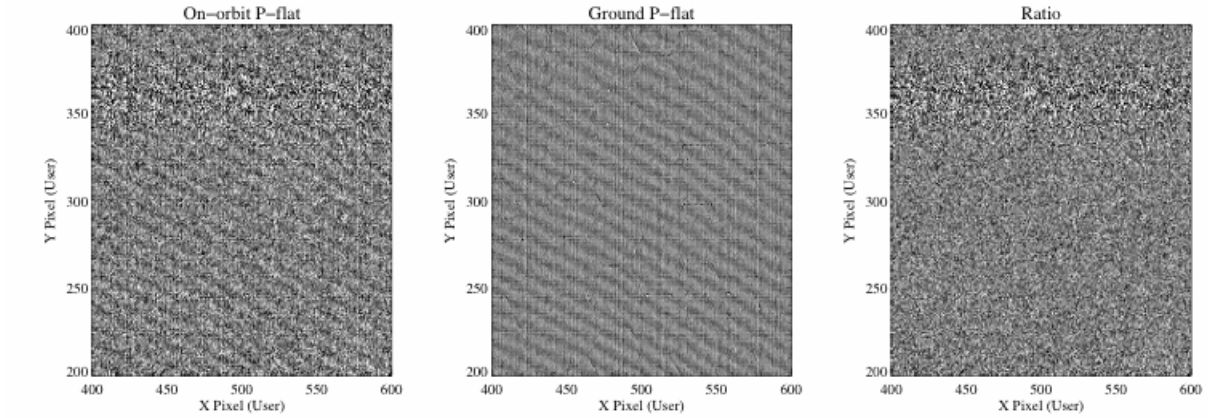

5.8.2 Use of Multiple FP-POS Settings

Fixed-pattern noise in the COS detectors limits the S/N that can be achieved in a single exposure to 15–25 per resolution element for the FUV and 50 for the NUV. To achieve higher S/N ratios, one can obtain a series of exposures, each slightly offset in the dispersion direction, causing spectral features to fall on a different part of the detector. For STIS and GHRS, these motions are known as FP-SPLITs. For COS, these motions are specified by the FP-POS optional parameter.

Four FP-POS offset positions are available: a nominal position (0), two positions toward longer wavelengths (–2 and –1), and one position toward shorter wavelengths (+1). Positions –2, –1, 0, and +1 are designated respectively as `FP-POS=1`, `2`, `3`, and `4`. The nominal position, `FP-POS=3`, is the setting used to define the wavelength range associated with the grating central wavelengths (Table 5.4 and Table 5.5). In pipeline processing, **calcos** creates individual calibrated spectra for each FP-POS position, then aligns and combines them into a merged spectral product, using only good-quality data at each wavelength.

The optical mechanism on which the grating is mounted is rotated by one step for each adjacent FP-POS position. The amount that a particular spectral feature moves in the dispersion direction on the detector is approximately 250 pixels per step for the FUV channel and 52 pixels for the NUV. The corresponding wavelength shifts for each grating are given in Chapter 13. There is a preferred direction for moving the grating mechanism; overheads are reduced if FP-POS exposures are obtained in

increasing order (see Section 9.5). When moving to a new grating or central-wavelength setting, you may select any FP-POS position without paying an additional overhead penalty. Thus, the most efficient order is `FP-POS=1,2,3,4`, as it requires no backward motion of the grating mechanism.

A wavelength calibration exposure will be obtained each time the FP-POS changes. For `FLASH=YES` exposures, the time-since-last-grating-motion clock is not reset by an FP-POS movement; however, there will always be at least one lamp flash during each individual `FP-POS` exposure. For `FLASH=NO` exposures, a separate wavelength calibration exposure will be taken for each FP-POS position change.

Requirements for Use of Multiple FP-POS Settings

The use of multiple FP-POS positions for each CENWAVE setting of the COS FUV detector is strongly encouraged, as it improves the limiting S/N and minimizes the effects of flat-field artifacts. The use of multiple FP-POS positions is especially important for G130M and G140L/1280 observations as, over time, exposure to the bright geocoronal Lyman α emission causes localized degradation of the COS FUV detector. Each FP-POS position of each CENWAVE setting projects Lyman α onto a different part of the detector, and spreading out this wear will extend the useful lifetime of the COS FUV channel. Proposers using the FUV channel of COS, but who do not intend to use **all four** FP-POS settings for each CENWAVE setting, must justify their observing strategy in their Phase I proposals.

5.9 COS Spectroscopy of Extended Sources

COS spectra of extended objects could have significantly lower resolution than those of point sources, depending on the spatial distribution of the source. For example, measurements of Lyman α airglow lines, which uniformly fill the COS aperture, show R = 1450 for G130M and R = 165 for G140L. Filled-aperture observations of SNR N132D confirm $R \sim 1500$ for both FUV M gratings (France et al. 2009, ApJ, 707, L27). In the NUV, the situation is much worse, because a source that fills the aperture will lead to cross-contamination among the three spectral stripes on the MAMA detector.

A similar situation arises when multiple point sources fall within the aperture. COS was designed to resolve two point sources separated by 1 arcsec in the cross-dispersion direction, but on-orbit measurements of the XD profile reveal that such observations are possible only for selected grating and central-wavelength settings (Section 5.1.8). Note that light from a point source falling more than 0.4 arcsec from the center of the PSA will be attenuated (Section 8.8.2).

The Optional Parameter `EXTENDED` (default = `NO`) sets a science header keyword to inform the **calcos** pipeline that the target is an extended source. The keyword may be used in the future to activate special data-reduction procedures, although none are currently in the pipeline. No aspect of on-board data-taking is affected by this parameter.

5.10 Wavelength Settings and Ranges

Table 5.4 and Table 5.5 show the wavelength ranges recorded on the detectors for each valid combination of grating and central-wavelength setting at the nominal `FP-POS=3` position (Section 5.8.2). The wavelength ranges spanned at other `FP-POS` settings may be estimated using the `FP-POS` step values provided in Chapter 13. Note, however, that uncertainties in the positioning of the Optics Select Mechanisms (Section 3.1.3) correspond to about half of an FP-POS step. These wavelength ranges are subject to change as the instrumental calibration evolves. The most recent measurements are available from the COS Web site.

Table 5.4: Wavelength Ranges for FUV Gratings for `FP-POS=3`

Grating	Central wavelength setting (Å)[1]	Recorded wavelengths[2]	
		Segment B	Segment A
G130M	1055	899 – 1040	1055 – 1196
	1096	940 – 1080	1096 – 1236
	1222	1067 – 1207	1223 – 1363
G130M (cont.)	1291	1134 – 1274	1291 – 1431
	1300	1144 – 1283	1300 – 1441
	1309	1154 – 1294	1309 – 1450
	1318	1163 – 1303	1319 – 1460
	1327	1172 – 1313	1328 – 1469
G160M	1577	1386 – 1559	1577 – 1751
	1589	1397 – 1571	1589 – 1762
	1600	1409 – 1581	1601 – 1774
	1611	1420 – 1594	1612 – 1786
	1623	1432 – 1606	1625 – 1798
G140L	1105	HV OFF	1118 – 2251[3]
	1280	<900 – 1165	1280 – 2391[3]

1. The central wavelength is (approximately) the shortest wavelength recorded on segment A.
2. All wavelength ranges quoted here are approximate, due to uncertainties in the position of the OSM1 mechanism.
3. G140L spectra are flux calibrated up to 2150 Å. At longer wavelengths, second-order light may be present (Section 5.1.3).

Table 5.5: Wavelength Ranges for NUV Gratings for `FP-POS=3`

Grating	Central wavelength setting (Å)[1]	Recorded wavelengths		
		Stripe A	Stripe B	Stripe C
G185M	1786	1670 – 1705	1769 – 1804	1868 – 1903
	1817	1701 – 1736	1800 – 1835	1899 – 1934
	1835	1719 – 1754	1818 – 1853	1916 – 1951
	1850	1734 – 1769	1833 – 1868	1931 – 1966
	1864	1748 – 1783	1847 – 1882	1945 – 1980
	1882	1766 – 1801	1865 – 1900	1964 – 1999
	1890	1774 – 1809	1872 – 1907	1971 – 2006
	1900	1783 – 1818	1882 – 1917	1981 – 2016
	1913	1796 – 1831	1895 – 1930	1993 – 2028
	1921	1804 – 1839	1903 – 1938	2002 – 2037
	1941	1825 – 1860	1924 – 1959	2023 – 2058
	1953	1837 – 1872	1936 – 1971	2034 – 2069
	1971	1854 – 1889	1953 – 1988	2052 – 2087
	1986	1870 – 1905	1969 – 2004	2068 – 2103
	2010	1894 – 1929	1993 – 2028	2092 – 2127
G225M	2186	2070 – 2105	2169 – 2204	2268 – 2303
	2217	2101 – 2136	2200 – 2235	2299 – 2334
	2233	2117 – 2152	2215 – 2250	2314 – 2349
	2250	2134 – 2169	2233 – 2268	2332 – 2367
	2268	2152 – 2187	2251 – 2286	2350 – 2385
	2283	2167 – 2202	2266 – 2301	2364 – 2399
	2306	2190 – 2225	2288 – 2323	2387 – 2422
	2325	2208 – 2243	2307 – 2342	2406 – 2441
	2339	2223 – 2258	2322 – 2357	2421 – 2456
	2357	2241 – 2276	2340 – 2375	2439 – 2474
	2373	2256 – 2291	2355 – 2390	2454 – 2489
	2390	2274 – 2309	2373 – 2408	2472 – 2507
	2410	2294 – 2329	2393 – 2428	2492 – 2527

Grating	Central wavelength setting (Å)[1]	Recorded wavelengths		
		Stripe A	Stripe B	Stripe C
G285M	2617	2480 – 2521	2596 – 2637	2711 – 2752
	2637	2500 – 2541	2616 – 2657	2731 – 2772
	2657	2520 – 2561	2636 – 2677	2751 – 2792
	2676	2539 – 2580	2655 – 2696	2770 – 2811
	2695	2558 – 2599	2674 – 2715	2789 – 2830
	2709	2572 – 2613	2688 – 2729	2803 – 2844
	2719	2582 – 2623	2698 – 2739	2813 – 2854
	2739	2602 – 2643	2718 – 2763	2837 – 2878
	2850	2714 – 2755	2829 – 2870	2945 – 2986
	2952	2815 – 2856	2931 – 2972	3046 – 3087
	2979	2842 – 2883	2958 – 2999	3073 – 3114
	2996	2859 – 2900	2975 – 3016	3090 – 3131
	3018	2881 – 2922	2997 – 3038	3112 – 3153
	3035	2898 – 2939	3014 – 3055	3129 – 3170
	3057	2920 – 2961	3036 – 3077	3151 – 3192
	3074	2937 – 2978	3053 – 3094	3168 – 3209
	3094	2957 – 2998	3073 – 3114	3188 – 3229
G230L	2635	1334 – 1733[2]	2435 – 2834	**1768 – 1967[3]**
	2950	1650 – 2050	2750 – 3150	**1900 – 2100[3]**
	3000	1700 – 2100	2800 – 3200	**1950 – 2150[3]**
	3360	2059 – 2458[4]	3161 – 3560[5]	**2164 – 2361[3]**

1. The central wavelength setting corresponds to the approximate midpoint of stripe B.
2. For central wavelength 2635 Å, the stripe A wavelengths are listed for completeness only (and in case a bright emission line falls onto the detector). The NUV detector's sensitivity at these wavelengths is extremely low. To obtain a low-resolution spectrum at wavelengths below ~ 1700 Å, we recommend the FUV grating G140L.
3. The values in shaded cells are wavelength ranges observed in second order. Their dispersion is twice that of the first-order spectrum. First-order flux, from wavelengths twice those of the listed range, will be present at the ~ 5% level.
4. Lyman α may be present in second order.
5. Longward of 3200 Å, second-order light may be present. At these wavelengths, the flux calibration applied by **calcos** is unreliable (Section 5.1.3).

CHAPTER 6:

Imaging with COS

In this chapter…

6.1 Introduction to COS Imaging

With a plate scale of 23.5 mas per pixel, the COS NUV channel provides the highest spatial sampling of any instrument aboard *HST*. Figure 6.1 shows an image of Pluto and its moon Charon obtained with COS. COS images are fully corrected for the telescope's spherical aberration, though not for the zonal (polishing) errors on its primary and secondary mirrors (Section 3.3). Because the optics image the sky onto the detector, rather than the aperture, COS images extend to a radius of 2 arcsec, but suffer considerable vignetting at radii greater than 0.5 arcsec, as shown in Figure 6.2.

To request an imaging observation, specify `CONFIG = COS/NUV` and `MODE = TIME-TAG` or `ACCUM`. In `TIME-TAG` mode, the minimum `BUFFER-TIME` is 80 seconds, which may be longer than the expected exposure time. `ACCUM` mode is recommended for such short exposures. The minimum COS exposure duration is 0.1 seconds, as discussed in Section 5.3. MIRRORB and/or the BOA can be used to obtain images of bright objects, but at some cost in spatial resolution; see Section 8.4 for details.

For longer exposures, drifting of the Optics Select Mechanisms (OSMs) can be significant, ~ 3.5 pixels in the X dimension with an *e*-folding time of ~ 50 minutes (COS ISR 2010-10). Observers taking images with exposure times longer than ~ 200 seconds are urged to use `MODE=TIME-TAG` and `FLASH=YES`; the resulting lamp flash will illuminate the WCA, allowing one to track the drift accurately. By default, `FLASH=NO` for all imaging modes.

COS imaging in `TIME-TAG` mode allows for high-speed NUV photometry with a temporal resolution of 32 msec. STIS is capable of much finer time resolution (125 microseconds), but at lower sensitivity.

Figure 6.1: Pluto and Charon Observed with COS

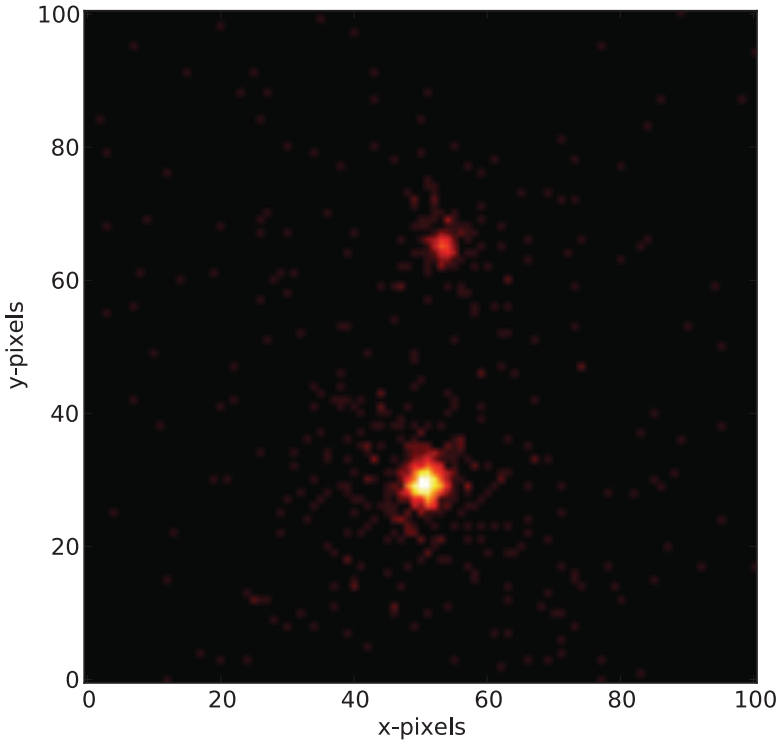

NUV exposure of Pluto and Charon, separated by 0.8”. The exposure time is 25 seconds. Note that the pixels numbers refer only to this sub-section of the full image. Image courtesy of J. Green.

Figure 6.2: Relative Throughput of the COS PSA in NUV Imaging Mode

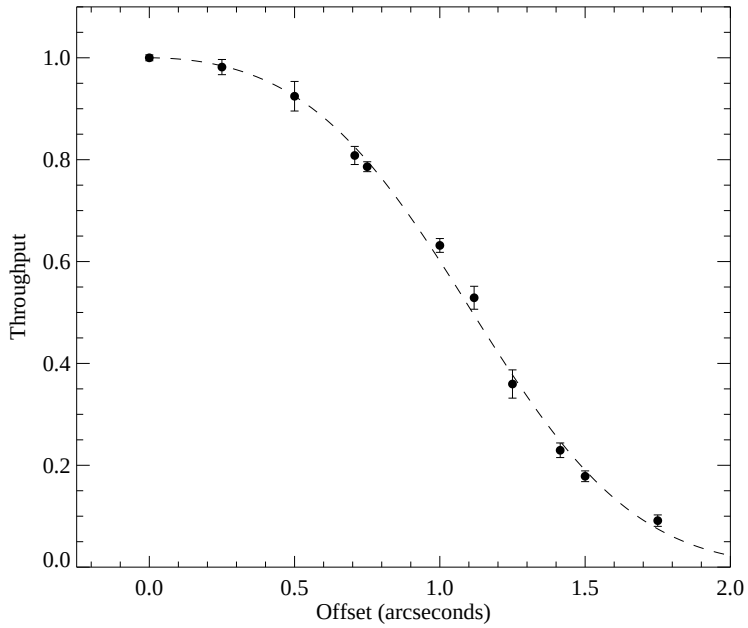

6.2 Sensitivity

When used in imaging mode, COS concentrates the target's NUV flux into a diffraction-limited image rather than dispersing the light. The local count rate limit for COS/NUV, 50 counts/s/pixel (Table 10.1), is easily reached, even for fairly faint objects. Observers should use the COS Exposure Time Calculator (ETC) to get an accurate estimate of expected count rates, but the following values will provide a guide. These have been calculated for a flat-spectrum source (flux independent of wavelength), and the limiting count rate is reached at the following approximate flux levels:

Aperture and Mirror	Flux Limit (erg cm^{-2} s^{-1} $Å^{-1}$)
PSA + MIRRORA	2×10^{-15}
BOA + MIRRORA	4×10^{-13}
PSA + MIRRORB	3×10^{-14}
BOA + MIRRORB	6×10^{-12}

When MIRRORA is used for imaging observations, sensitivity extends from about 1600 to 3300 Å, peaking at ~ 2300 Å (Figure 6.3). Care should be taken when observing cool stars (T_{eff} < 5,000 K) and other red objects, as high count rates at long wavelengths could damage the detector. When MIRRORB is employed, its use of a first-surface reflection allows short-wavelength light to reach the detector. Sensitivity extends to the NUV detector cut-off, about 1150 Å, for the primary image.

Figure 6.3: Effective Area for COS NUV Imaging with the PSA

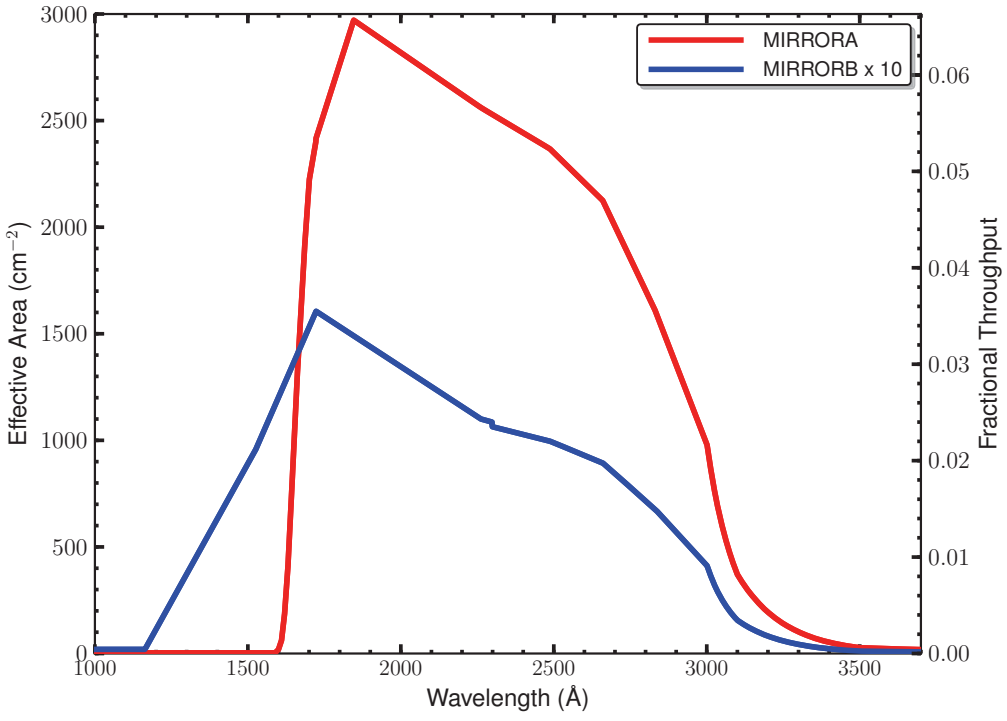

6.3 Image Characteristics

A two-dimensional Gaussian fit to a typical imaging PSF has a FWHM of 1.97 pixels (47.1 mas), with 13.4% of the light in the brightest pixel. Because the *HST* focus varies with orbital phase, FWHM values can range from 1.8 to 2.4 pixels.

As discussed in Section 3.3, mid-frequency wavefront errors (MFWFEs) contribute significantly to the PSF wings at wavelengths < 2500 Å, so the spatial resolution of a point source will depend somewhat on its spectral energy distribution. For an M star, which has little flux at the shortest wavelengths, the image would be close to diffraction limited. For a hot white dwarf, the MFWFEs would have the maximum impact on the spatial resolution.

Deep images reveal the detailed shape of the COS imaging PSF. Figure 6.4 shows the PSF, averaged over 180 degrees of azimuth and plotted on a log scale to reveal its extended wings. Figure 6.5 shows a 2-dimensional grey-scale image of a deep imaging observation that reveals two low-level "ghosts" located approximately 20 pixels to the right and the upper left of the center of the PSF. The peak intensity of the brightest of the two ghosts is roughly 0.1% of that of the main PSF. These features may complicate the analysis of faint objects located in the wings of a brighter object.

Figure 6.4: Extended Wings in the COS Imaging PSF

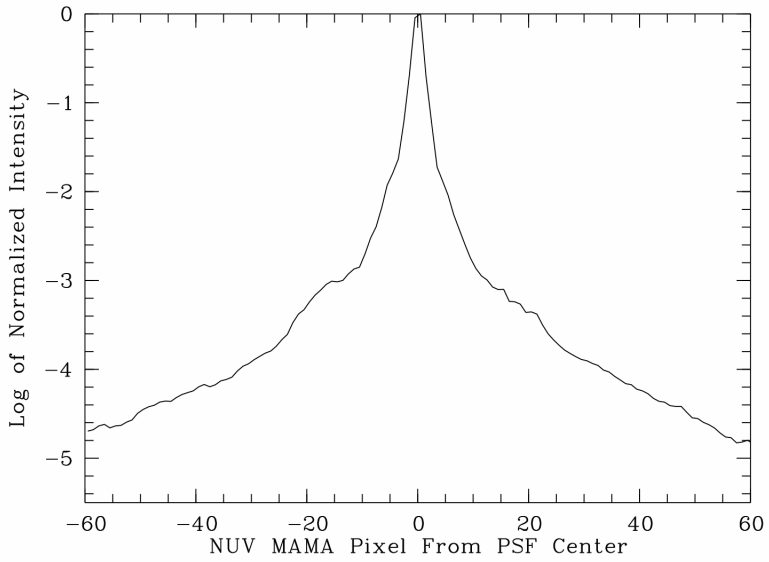

Azimuth-averaged COS imaging PSF plotted with a logarithmic intensity scale.

Figure 6.5: Ghosts in COS NUV Images

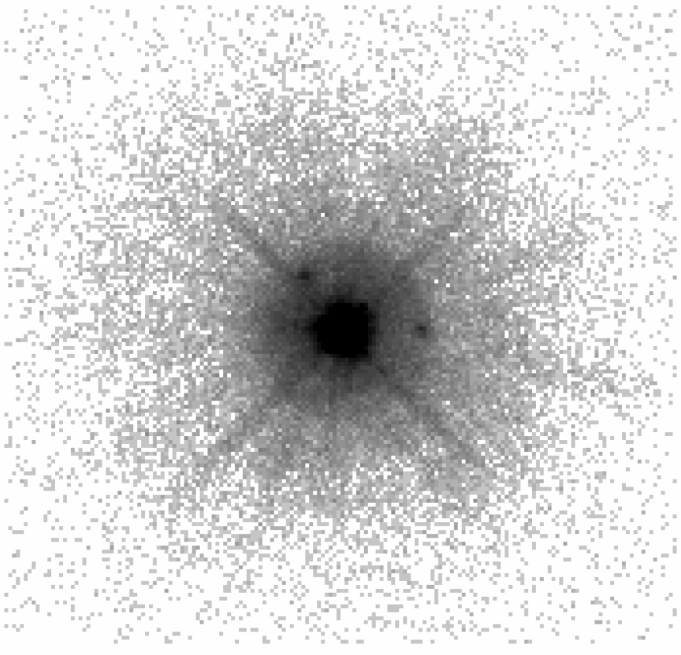

Negative grey-scale rendering of a deep COS NUV image of a point source. This figure is plotted with a logarithmic intensity scale and covers about 6.5 arcsec along each axis. Note the two ghost images to the right and upper left of the center of the PSF.

CHAPTER 7:

Exposure-Time Calculator (ETC)

In this chapter…

7.1 The COS Exposure Time Calculators

To help with proposal preparation, four COS Exposure-Time Calculators (ETCs) are available on the COS Web pages:

http://www.stsci.edu/hst/cos/software/planning/etc/

These calculators model spectroscopic and imaging exposures for both target acquisitions and scientific observations. They estimate count rates for given source and background parameters and calculate either the signal-to-noise ratio for a given exposure time or the exposure time needed to achieve a desired signal-to-noise ratio. If you have a calibrated spectrum of your source, you can upload it to the Exposure Time Calculators. The ETCs warn if your observations exceed local or global brightness limits (see Table 10.1). The ETCs offer extensive on-line help that provides instructions and explains their calculations.

A unique exposure ID is assigned to each calculation performed by the ETCs, allowing results from previous calculations to be retrieved easily. This number should be included in the appropriate box in your Phase II proposal to document your work and to facilitate Phase II review. Proposers are urged to check the COS ETC Web page for any updates or issues related to the COS ETCs before performing ETC simulations.

The spectroscopic ETC can display the input spectrum, a simulated one-dimensional output spectrum, the S/N as a function of wavelength, and the number of counts per resolution element for the selected instrument configuration and source. These outputs can be downloaded in ASCII format. The ETC also computes the BUFFER-TIME, which is required for TIME-TAG observations. Scale this value by 2/3 and enter it (or the exposure time, whichever is shorter) in APT (the Astronomer's Proposal Tool), as discussed in Section 5.4.

The imaging ETC allows for the selection of either the PSA or BOA and either MIRRORA or MIRRORB. It reports the count rate in the brightest pixel, total counts in the detector, and S/N per resolution element.

The target-acquisition ETCs return the acquisition exposure time to be entered in APT for both imaging and spectroscopic acquisitions. Target acquisition is described in Chapter 8.

7.2 Imaging Observations of Red Objects

As shown in Figure 6.3, the COS NUV channel is sensitive to wavelengths above 3200 Å, an important consideration when imaging red objects. For stars with effective temperatures above 6000 K, the effect is negligible, but it grows to about 20% at 5000 K, and below 5000 K it quickly becomes large.

If you upload a spectrum into the ETC to calculate exposure time of an imaging exposure, whether for a target acquisition or a scientific observation, be sure that the spectrum spans the full range of wavelengths to which the NUV channel is sensitive, from about 1600 Å to 12,000 Å. Failure to do so can produce a misleading result.

The COS ETC expects input spectra to extend out to 12,000 Å and will return a warning message ("Partial overlap between instrument throughput band and input spectrum") if they do not.

7.3 Sensitivity, Count Rate, and S/N

A complete theoretical discussion of the exposure time as a function of instrument sensitivity and signal-to-noise ratio is given in Chapter 6 of the *STIS Instrument Handbook* and will not be repeated here. However, COS has several characteristics that simplify signal-to-noise calculations.

Both COS detectors are photon counters, which means that they have no read noise. COS is optimized for point sources, and in this case the signal-to-noise ratio is given by,

$$\frac{S}{N} = \frac{C \cdot t}{\sqrt{C \cdot t + N_{pix}(B_{sky} + B_{det}) \cdot t}}$$

where

C = the signal from the astronomical source, in counts s^{-1}

t = the integration time, in seconds

N_{pix} = the total number of detector pixels integrated to achieve C

B_{sky} = the sky background, in counts s^{-1} $pixel^{-1}$

B_{det} = the detector dark count rate, in counts s^{-1} $pixel^{-1}$

With no detector read noise, the signal-to-noise ratio is proportional to the square root of the exposure time whether the target is bright or faint compared to the backgrounds and dark count.

Note that the detector dead-time effects discussed in Section 4.1.7 and Section 4.2.5 are not included in the ETC, which will over-predict the count rates and resulting S/N ratios for bright targets.

7.4 Detector and Sky Backgrounds

The primary background sources that affect COS observations are detector dark count, earthshine, zodiacal light, and airglow emission; neither of the COS detectors suffers from read noise. The ETC allows the user to select among several levels of intensity for each of the sky backgrounds, corresponding to a variety of observing environments.

7.4.1 Detector dark count

Table 7.1 lists the detector dark-count rates assumed by the ETC. The FUV values were measured in 2010 September, while the NUV values are projections for mid-Cycle 20 (2013 April). We assume that a resolution element, or "resel," spans 6 × 10 pixels on the FUV detector and 3 × 3 pixels on the NUV MAMA. Beginning with Cycle 20, the ETC uses separate dark rates for science observations and target acquisitions obtained with the FUV detector. **Calcos** filters the data by pulse height, while the COS flight software does not, so the effective dark rate for science data is lower than that for target acquisitions. In either mode, the dark rate on the FUV detector is truly small, due in part to its windowless design. The NUV detector has a window and thus a higher dark rate.

Table 7.1: Detector Dark Count Rates

	FUV in ACQ Mode	FUV in Science Mode	NUV
Dark rate (counts s^{-1})	1.56 per cm^2 2.25×10^{-6} per pixel 1.35×10^{-4} per resel	1.25 per cm^2 1.8×10^{-6} per pixel 1.1×10^{-4} per resel	128 per cm^2 8.0×10^{-4} per pixel 7.2×10^{-3} per resel

Figure 7.1: Sky Background Intensity as a Function of Wavelength

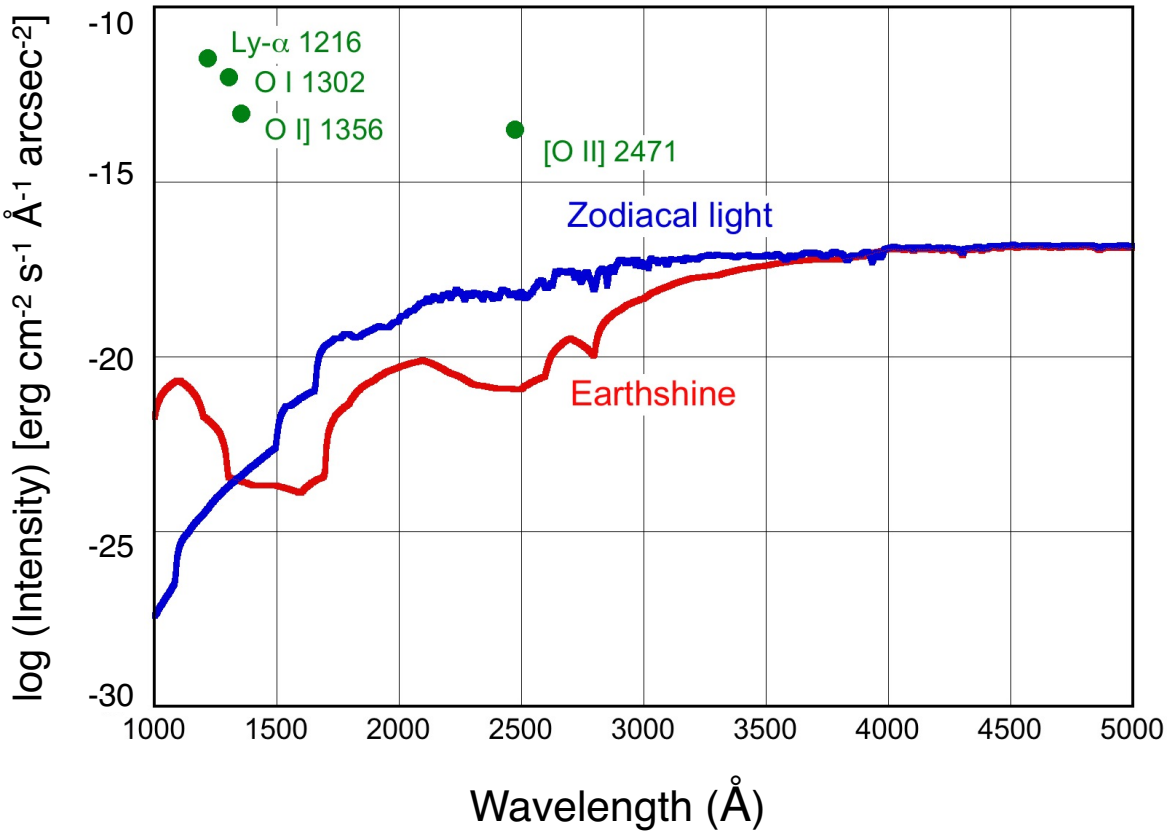

Earthshine for a target 24° above the limb of the sunlit Earth, corresponding to the "high" level in the ETC. Use Figure 7.2 to estimate background contributions at other angles. The zodiacal light level (m_V = 22.7 per arcsec^2, the "average" level in the ETC) corresponds to a helio-ecliptic latitude and longitude of 30° and 180°, respectively. The airglow line intensities are integrated fluxes, corresponding to the "Day" level in Table 7.4. The upper limit to the [OII] 2471 intensity is shown.

7.4.2 Earthshine

Four earthshine intensity levels, with scaling factors of (*none*, *average*, *high*, *extremely high*) = (0.0, 0.5, 1.0, 2.0), are available in the ETC. Earthshine intensity is a strong function of the angle between the target and the bright Earth limb. The earthshine surface brightness for a target 24° degrees above the limb, corresponding to the "high" level, is shown in Figure 7.1. The limb angle is approximately 24° when *HST* is aligned toward its orbit pole (*i.e.,* the center of the CVZ). The variation of earthshine with limb angle is shown in Figure 7.2.

Figure 7.2: Background Contributions from the Moon, Earth, and Zodiacal Light

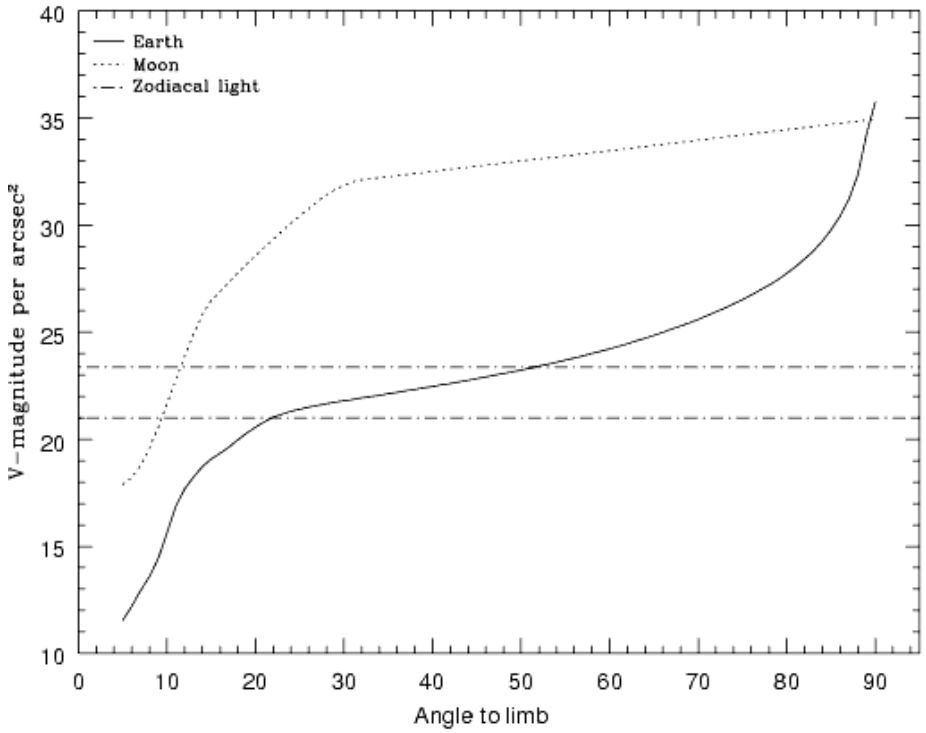

The values are V magnitude per square arcsec due to the moon and the sunlit Earth as a function of angle between the target and the limb of the bright Earth or moon. Zodiacal light levels range between m_V=22.1 and 23.3 mag arcsec^{-2}.

7.4.3 Zodiacal Light

Away from the airglow lines, at wavelengths between about 1300 and 3000 Å, the sky background is dominated by zodiacal light, which is generally fainter than the intrinsic detector background, especially for the NUV detector. Figure 7.1 shows the zodiacal light for the "average" level in the ETC. Table 7.2 gives the variation of the zodiacal background as a function of helio-ecliptic longitude and latitude. For a target near (50°,0°) or (–50°,0°), the zodiacal light is relatively bright at m_V = 20.9 mag arcsec^{-2}, about 9 times the polar value of m_V = 23.3 mag arcsec^{-2}. These limits are plotted in Figure 7.2. The intensity levels and the factors by which they are scaled in the ETC are (*none, low*, *average*, *high*) = (0.0, 0.576, 1.0, 1.738), corresponding to m_V = (none, 23.3, 22.7, 22.1) mag arcsec^{-2}.

Observations of the faintest objects may need the special requirement `LOW-SKY` in the Phase II observing program. `LOW-SKY` observations are scheduled during the part of the year when the zodiacal background is no more than 30% greater than the minimum possible value for the given sky position. `LOW-SKY` also invokes the restriction that exposures will be obtained at angles greater than 40° from the bright Earth limb to minimize earthshine and the UV airglow lines. The `LOW-SKY` requirement limits the times at which targets within 60° of the ecliptic plane will be scheduled and limits visibility to about 48 minutes per orbit.

Table 7.2: Approximate Zodiacal Sky Background (V mag arcsec^{-2}) as a Function of Helioecliptic Coordinates

Helioecliptic Longitude (deg)	Helioecliptic Latitude (deg)						
	0°	15°	30°	45°	60°	75°	90°
180°	22.1	22.4	22.7	23.0	23.2	23.4	23.3
165°	22.3	22.5	22.8	23.0	23.2	23.4	23.3
150°	22.4	22.6	22.9	23.1	23.3	23.4	23.3
135°	22.4	22.6	22.9	23.2	23.3	23.4	23.3
120°	22.4	22.6	22.9	23.2	23.3	23.3	23.3
105°	22.2	22.5	22.9	23.1	23.3	23.3	23.3
90°	22.0	22.3	22.7	23.0	23.2	23.3	23.3
75°	21.7	22.2	22.6	22.9	23.1	23.2	23.3
60°	21.3	21.9	22.4	22.7	23.0	23.2	23.3
45°	SA	SA	22.1	22.5	22.9	23.1	23.3
30°	SA	SA	SA	22.3	22.7	23.1	23.3
15°	SA	SA	SA	SA	22.6	23.0	23.3
0°	SA	SA	SA	SA	22.6	23.0	23.3

Note: A value of “SA” denotes positions in the solar avoidance zone

The ETC provides the user with the flexibility to adjust both the zodiacal (*none, low*, *average*, *high*) and earthshine (*none*, *average*, *high*, *extremely high*) sky background components to determine if the use of `LOW-SKY` is advisable for a given program. However, the absolute sky levels that can be specified in the ETC may not be achievable for a given target. As shown in Table 7.2, the minimum zodiacal background level for an ecliptic target is $m_V = 22.4$, which is brighter than both the low and average options with the ETC. By contrast, a target near the ecliptic pole would always have a zodiacal = *low* background in the ETC. The user is cautioned to consider sky levels carefully, as the backgrounds obtained in *HST* observations can span a significant range.

7.4.4 Airglow Emission

In the ultraviolet, the sky background contains important contributions from airglow emission lines, which vary from day to night and as a function of *HST* orbital position. These features originate mainly from hydrogen and oxygen atoms in the exosphere of the Earth. Airglow lines may be an important consideration for spectroscopic observations at wavelengths near the lines.

The brightest airglow line by far is Lyman α at 1216 Å. The strength of the Lyman α line varies between about 2 and 20 kilo-Rayleighs (i.e., between 6.3×10^{-14} and 6.3×10^{-13} erg/cm^2/s/arcsec^2, where 1 Rayleigh = 10^6 photons/cm^2/s per 4π steradians, which equals 3.15×10^{-17} erg/cm^2/s/arcsec^2 at Lyman α) depending on the time of the observation and the position of the target relative to the Sun. The next-strongest feature is the O I line at 1302 Å, which rarely exceeds 10% of Lyman α. The typical strength of the O I λ1302 line is about 2 kilo-Rayleighs (about 7×10^{-14} erg/cm^2/s/arcsec^2) on the daylight side and about 150 times fainter on the night side of the *HST* orbit. The O I] λ1356 and [O I] λ2471 lines may appear in observations on the daylight side of the orbit, but these lines are at least 10 times weaker than the O I λ 1302 line. The widths of the lines also vary, but a representative value for a temperature of 2000 K is about 3 km/s. Airglow emission from N I λ 1200 is also seen, particularly on the day side of the orbit, with fluxes up to 1.6×10^{-16} erg/cm^2/s/arcsec^2. The N I line is not included in the ETC. Airglow emission lines are essentially unresolved at the resolution of COS, but the emission fills the aperture in the spectral and spatial directions. For the FUV modes, the aperture width is approximately 114 pixels, or 1.12, 1.36, and 9.46 Å for G130M, G160M, and G140L, respectively. For the NUV modes, the aperture width is approximately 105 pixels, or 3.87, 3.46, 4.18, and 41.21 Å for G185M, G225M, G285M, and G230L, respectively.

The COS ETC provides four airglow intensity levels (*none, low*, *average*, *high*), whose scaling factors depend on the airglow line considered: (0.0, 0.1, 0.5, 1.0) for Lyman α, (0.0, 0.0667, 0.5, 1.0) for O I λ1302, (0.0, 0.006, 0.5, 1.0) for O I] λ1356, and (0.0, 0.005, 0.5, 1.0) for [O I λ2471.

It is possible to request that exposures be taken when *HST* is in the earth's shadow to minimize airglow emission (e.g., if you are observing weak lines at 1216 Å or 1302 Å) using the special requirement `SHADOW`. Exposures using this special requirement are limited to roughly 25 minutes per orbit, exclusive of the guide-star acquisition (or reacquisition) and can be scheduled only during a small percentage of the year. `SHADOW` reduces the contribution from the airglow emission lines by roughly a factor of ten, while the continuum earthshine is essentially nil. If you require `SHADOW`, you should request it in your Phase I proposal (see the *Call for Proposals*).

An alternate strategy for reducing the effects of airglow emissions is to use time-resolved observations, so that any data badly affected by airglow emission can simply be excluded from the final co-addition. This can be done either by using TIME-TAG mode, the default for all COS observations if the target is not too bright, or by taking a series of short (~ 5 min) ACCUM mode exposures over the course of each orbit.

As noted, geocoronal Lyman α is by far the strongest airglow feature. On the day side of the *HST* orbit, when Lyman α is at its strongest, it will produce a net count rate of 20 counts/s/resel, too faint to be a safety concern, but bright enough to make a significant contribution to gain sag on the FUV detector (Section 4.1.6).

7.4.5 Tabular Sky Backgrounds

Table 7.3 lists the *high* sky background numbers as plotted in Figure 7.1. The *high* sky values are defined as the earthshine at 24° from the limb and by the typical zodiacal light of m_V = 22.7. The quoted values represent the zodiacal and earthshine backgrounds (excluding the contributions from airglow emission lines) averaged over each wavelength interval. The line widths and intensities of some important airglow lines in the COS bandpass are listed in Table 7.4.

Table 7.3: Earthshine and Zodiacal Light in the COS PSA

Wavelength (Å)	Earthshine	Zodiacal Light	Total
1000	6.48 E–7	1.26 E –12	6.48 E –7
1100	1.66 E –6	6.72 E –11	1.66 E–6
1200	4.05 E–7	6.23 E–10	4.06 E –7
1300	2.66 E–8	3.38 E –9	2.99 E–8
1400	2.28 E –9	1.32 E–8	1.54 E–8
1500	1.95 E–9	2.26 E–7	2.28 E–7
1600	1.68 E–9	1.14 E–6	1.14 E–6
1700	6.09 E–8	3.19 E–5	3.19 E–5
1800	6.19 E–7	6.63 E–5	6.69 E–5
1900	2.30 E–6	1.05 E–4	1.07 E–4
2000	5.01 E–6	2.07 E–4	2.12 E–4
2100	6.97 E–6	5.95 E–4	6.02 E–4
2200	3.94 E–6	9.82 E–4	9.86 E–4
2300	1.83 E–6	9.67 E–4	9.69 E–4
2400	1.27 E–6	1.05 E–3	1.05 E–3
2500	1.37 E–6	1.01 E–3	1.01 E–3
2600	6.33 E–6	2.32 E–3	2.32 E–3
2700	2.66 E–5	4.05 E–3	4.08 E–3
2800	3.79 E–5	3.67 E–3	3.71 E–3
2900	2.17 E–4	7.46 E–3	7.68 E–3
3000	4.96 E–4	8.44 E–3	8.94 E–3
3100	1.04 E–3	9.42 E–3	1.05 E–2
3200	1.72 E–3	1.10 E–2	1.27 E–2
3300	2.18 E–3	1.34 E–2	1.56 E–2
3400	3.12 E–3	1.30 E–2	1.62 E–2
3500	4.06 E–3	1.31 E–2	1.72 E–2
3600	5.15 E–3	1.24 E–2	1.77 E–2

Table 7.3: Earthshine and Zodiacal Light in the COS PSA

Wavelength (Å)	Earthshine	Zodiacal Light	Total
3700	5.89 E–3	1.49 E–2	2.18 E–2
3800	6.19 E–3	1.41 E–2	2.03 E–2
3900	7.80 E–3	1.39 E–2	2.17 E–2
4000	1.14 E–2	2.07 E–2	3.21 E–2
4250	1.13 E–2	2.17 E–2	3.40 E–2
4500	1.33 E–2	2.53 E–1	3.86 E–2
4750	1.35 E–2	2.57 E–2	3.92 E–2
5000	1.30 E–2	2.50 E–2	3.80 E–2

These rates correspond to the *high* level in the ETC and are listed in units of 10^{-15} erg cm^{-2} s^{-1} $Å^{-1}$ for the total COS PSA, which is 4.91 $arcsec^2$ in area.

Table 7.4: Typical Strengths of Important Ultraviolet Airglow Lines

Airglow features	Intensity					
	Day			Night		
	Rayleighs	10^{-15} erg cm^{-2} s^{-1} $arcsec^{-2}$	10^{-15} erg cm^{-2} s^{-1} per PSA	Rayleighs	10^{-15} erg cm^{-2} s^{-1} $arcsec^{-2}$	10^{-15} erg cm^{-2} s^{-1} per PSA
O I λ911	17	0.7	3.5	8.3	0.35	1.7
O I λ989	161	6.2	30	0.6	–	–
H I λ1026	571	21	105	2.7	–	–
O I λ1027	64	2.4	12	0	–	–
O I λ1152	28	0.93	4.6	0	–	–
N I λ1200[1]	5.2	0.16	0.8	0.26	0.008	0.04
H I λ1216	20,000	630	3100	2,000	63	310
O I λ1302	2,000	59	290	13	0.38	1.9
O I] λ1356	204	5.8	28	12.5	0.35	1.7
O I λ2471	45	0.70	3.4	1	–	–

1. This feature is not included in the ETC.

7.5 Extinction Correction

Extinction can dramatically reduce the observed intensity of your source, particularly in the ultraviolet. Figure 7.3 shows A_λ/A_V values applicable to our Galaxy, taken from Cardelli, Clayton, & Mathis (1989, ApJ, 345, 245) assuming R = 3.1. This corresponds to the *Milky Way Diffuse (R_V=3.1)* selection of the ETC.

Extinction curves have a strong metallicity dependence, particularly at ultraviolet wavelengths. Sample extinction curves are presented in Gordon et al. [2003, ApJ, 594, 279 (LMC Average, LMC 30 Dor Shell, and SMC Bar)], Calzetti et al. [2000, ApJ, 533, 682 (starburst galaxies)], and references therein. At lower metallicities, the 2200 Å bump that is so prominent in the Galactic extinction curve disappears, and $A_\lambda/E(B–V)$ increases at shorter UV wavelengths.

The ETC allows the user to select among a variety of extinction curves and to apply the extinction correction either before or after the input spectrum is normalized.

Figure 7.3: Extinction in Magnitude as a Function of Wavelength

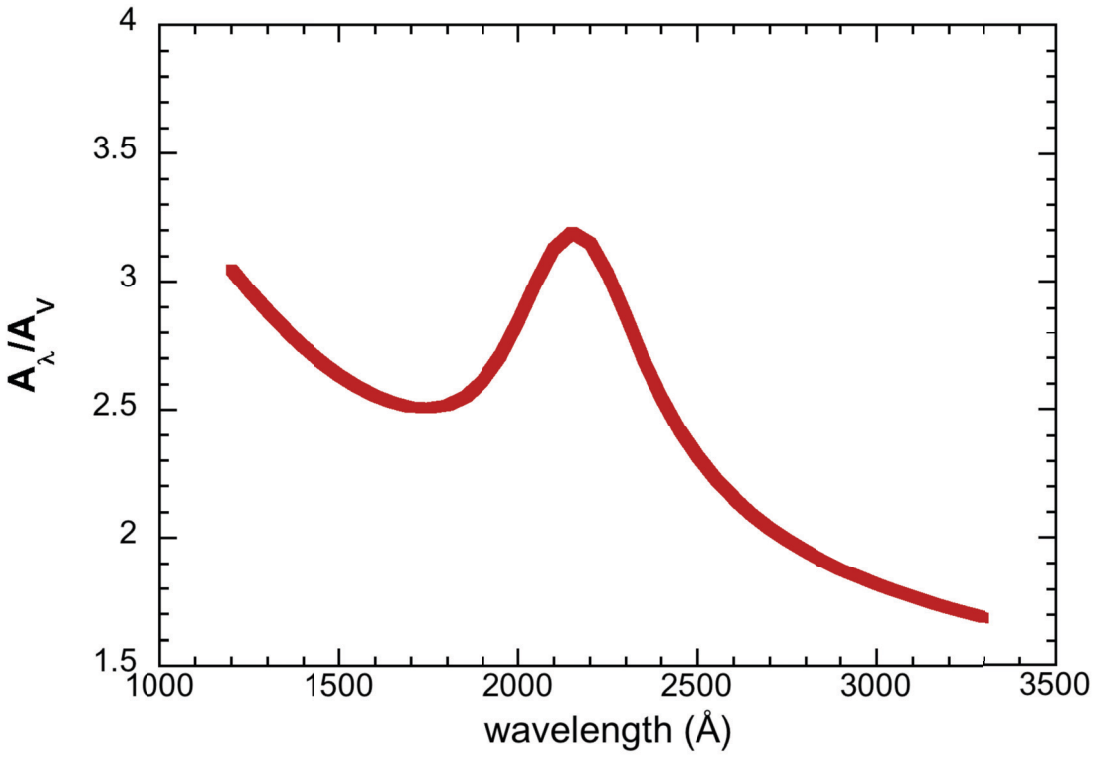

The Galactic extinction model of Cardelli et al. (1989), computed for R_V = 3.1.

7.6 Examples

In this section, we present a few examples of the way in which the COS ETCs may be used. They illustrate the information that is returned by the ETCs and how they can be used to plan your observations.

7.6.1 A Flat-Spectrum Source

One often does not know the exact spectrum shape of the object to be observed, so the answer to a simple question is desired: How long will it take to achieve a given signal-to-noise ratio at a given wavelength if the flux at that wavelength is specified? The easiest way to determine this is to use a flat spectrum as input. How long will it take to achieve S/N=10 per resolution element at 1320 Å with a source flux of 10^{-15} erg cm^{-2} s^{-1} $Å^{-1}$ using a medium resolution grating?

Only the G130M grating covers the desired wavelength at medium resolution, but several choices of central wavelength are available. We select the 1309 Å setting. We enter these values into the spectroscopic ETC, select the Primary Science Aperture (PSA), select "Exposure time needed to obtain a S/N ratio of 10.0," and enter the specified wavelength of 1320 Å. For the spectrum distribution, choose a flat continuum in F_λ. Make sure the reddening, E(B–V), is set to 0. Normalize the target to 10^{-15} erg cm^{-2} s^{-1} $Å^{-1}$. The zodiacal light, earthshine, and airglow were not specified, so we choose average values.

When this case is computed with the ETC, we find the required time is 12,586 seconds; the total count rates are 57 and 276 counts s^{-1} in detector segments A and B, respectively, well below the safety limit; the count rate in the brightest pixel is 0.104 counts s^{-1}, also well within the safe range (but see below); and the buffer time indicated by the ETC is 7075 seconds (COS.sp.178882).

What if somewhat higher *S/N* were desired and one were willing to devote 5 *HST* orbits to the observation? Assuming that each orbit allows 50 minutes of observing time (ignoring the acquisition time here), we find that in 15,000 seconds we will get *S/N* = 10.9 per resel. Note that $(15{,}000/12{,}586)^{1/2} = (10.9/10.0)$. That is, the *S/N* ratio scales as $t^{1/2}$, as stated in Section 7.3.

If a low-resolution observation is acceptable, then one could switch to the G140L grating. With a grating setting of 1105 Å and *S/N* = 10 per resel, we find the required exposure time is 2178 seconds, considerably less than the medium-resolution case required.

Note that the sensitivity of G130M is higher than that of G140L once resolving power is taken into account. In other words, a G130M spectrum that is rebinned to the same resolution as a G140L spectrum can be obtained in less time for a given S/N, although, of course, with diminished wavelength coverage. If only a limited portion of the source's spectrum is of interest, using G130M is more efficient than using G140L.

These cases also illustrate that the earthshine and zodiacal light are completely negligible in the FUV, unless the target flux is much lower than that considered here. This is also true of the airglow if the wavelength of interest is far from the airglow

lines. Of course, the airglow cannot be ignored in terms of the total count rate on the detector, or the local count rate if the source contributes at the same wavelengths as the airglow lines.

This is a toy example. For most targets, a more realistic model spectrum would be used to estimate exposure times and test for bright-object violations.

If only a limited portion of the source's spectrum is of interest, using G130M is more efficient than using G140L.

7.6.2 An Early-Type Star

We wish to observe an O5 star at medium spectral resolution at a wavelength of 1650 Å. We know that the star has a magnitude of $V = 16$. How long will it take to obtain $S/N = 15$?

We select the G160M grating with a central wavelength of 1623 Å. We select a Kurucz O5 stellar model and set the normalization to be Johnson $V = 16$. We find that the required exposure time is 785 seconds.

Suppose this star is reddened, with E(B–V) = 0.2. We select the *Milky Way Diffuse (R_V=3.1)* extinction law, which is shown in Figure 7.3. We must now decide if this extinction is to be applied before or after the normalization. Since the star has a measured magnitude, we want to apply the reddening before normalization. Otherwise, the extinction would change the V magnitude of the stellar model. Making this selection, we find that $S/N = 15$ can be obtained in 1864 seconds (COS.sp.178886). The ETC returns a `BUFFER-TIME` of 2376. To be conservative, we scale it by 2/3 to get 1584 s.

7.6.3 A Solar-Type Star with an Emission Line

We want to observe a solar-type star with a narrow emission line. Consider the Si II λ1810 feature with the following parameters: FWHM = 30 km s^{-1} or 0.18 Å at 1810 Å, and integrated emission line flux of 1×10^{-14} erg cm^{-2} s^{-1}. The measured magnitude of the star is $V = 12$. The desired exposure time is 1000 seconds.

In the ETC we select a G2V star and an NUV grating, G185M, set to a central wavelength of 1817 Å. We request an exposure time of 1000 s and specify that the *S/N* be evaluated at 1810 Å. We add an emission line with the line center at 1810 Å, FWHM=0.18, and an integrated flux of 10^{-14} erg cm^{-2} s^{-1}. We specify the normalization as Johnson $V = 12$. We set the zodiacal and earthshine to be *average*.

The ETC returns $S/N = 16.4$ per resel (COS.sp.178887). The local and global count rates are within safe limits. The recommended buffer time is 3036 seconds. This `BUFFER-TIME` exceeds the exposure time of 1000 s, so the `BUFFER-TIME` should be set to 1000.

7.6.4 A Faint QSO

An important science goal for the design of COS was to obtain moderate S/N spectra of faint QSOs in the FUV. In the ETC, use the FOS-based QSO spectrum and choose G130M at 1309 Å, S/N = 20, and a continuum flux of 10^{-15} erg cm^{-2} s^{-1} $Å^{-1}$ at 1320 Å. The indicated exposure time is 49,801 seconds, or about 16.6 orbits (COS.sp.178888). The source count rate is 0.001 (counts/s), with a background rate of 1.06×10^{-4} counts/s, 10 times lower than the source. The background is completely dominated by the dark current of the detector. The count rate over the entire detector is 350, well below any safety limits, and the maximum `BUFFER-TIME` is 6745 seconds. Scaling by 2/3 yields 4497 seconds for the `BUFFER-TIME`.

CHAPTER 8:

Target Acquisitions

In this chapter…

8.1 Introduction

The COS apertures are 2.5 arcsec in diameter. An observation will yield high-quality data only if the target is properly centered in the desired aperture. This chapter discusses the available target-acquisition (TA) methods, demonstrates the dependence of data quality on centering accuracy, and recommends acquisition scenarios for various combinations of target coordinate accuracy and brightness. Recommended parameters for all COS TA modes are presented in Section 8.9.

Based on recent improvements in the COS-to-FGS alignment, together with an analysis of the distribution of positional errors in the GSC2, we estimate that an *HST* guide-star acquisition will place a target in the COS aperture 98.5% of the time. As a result, we no longer require that all COS observations begin with an ACQ/SEARCH sequence if the uncertainty of the target coordinates is ≤ 0.4 arcsec. We do, however, recommend that some sort of target acquisition be performed to center the target in the aperture. APT (the Astronomer's Proposal Tool) will issue a warning if an acquisition is omitted. Target acquisition is required only once for a series of observations in contiguous orbits (i.e., once per visit). Moving targets require an acquisition at the beginning of each orbit.

Bright-Object Protection

The COS detectors are vulnerable to damage or performance degradation if exposed to too much light. Imaging acquisitions present a special risk because they concentrate the light of an object on a small area of the detector. Users of COS must demonstrate that their targets are safe. Information on bright-object protection and screening is provided in Chapter 10.

8.2 Target Acquisition Overview

COS has four TA modes:

- **ACQ/SEARCH** performs a spiral search by executing individual exposures at each point in a square grid pattern on the sky (details are in Section 8.3). This mode can use either dispersed-light or imaging exposures.
- **ACQ/IMAGE** obtains an NUV image of the target field, moves the telescope to center the object, and obtains a second NUV image as confirmation (details are in Section 8.4). This is generally the fastest and most accurate method of target acquisition, but covers a limited area on the sky.
- **ACQ/PEAKXD** determines the centroid of the dispersed-light spectrum in the cross-dispersion (XD) direction and moves the telescope to center the object in the XD direction (details are in Section 8.5).
- **ACQ/PEAKD** centers the target in the along-dispersion (AD) direction by executing individual exposures at each point in a linear pattern along the dispersion axis (details are in Section 8.6). `ACQ/PEAKXD` should always precede `ACQ/PEAKD`, and the two should always be performed together.

Coordinate accuracy and target brightness will inform your choice of target-acquisition strategy and optional parameters. Imaging acquisitions are fast and precise, but restrictions on the local count rate (Chapter 10) can prevent their use. While the TA modes can be used in any order or even repeated, the recommended strategies are given in Table 8.1. We suggest evaluating these strategies in the following order:

1. NUV imaging with the fastest allowable combination of aperture and mirror, even if the science to follow is performed with the FUV channel.
2. Dispersed-light acquisition using the same configuration as the first science exposure, if it will use less time overall.
3. Dispersed-light acquisition with a different configuration, if it will use less time overall.

The scenarios outlined here are for isolated point sources. See Section 8.10 for additional information regarding crowded or complex fields and offset-target TAs.

Table 8.1: Basic COS Target Acquisition Strategies

Type	Step 1	Step 2	Step 3
Imaging (if coordinates are good to 0.4”)	ACQ/IMAGE	none	none
Imaging (if coordinates are less accurate)	ACQ/SEARCH	ACQ/IMAGE	none
Dispersed-Light (coordinates good to 0.4”)	ACQ/PEAKXD	ACQ/PEAKD	none
Dispersed-Light (coordinates less accurate)	ACQ/SEARCH	ACQ/PEAKXD	ACQ/PEAKD
Either Imaging or Dispersed-Light	ACQ/SEARCH	2 × 2 × 1.767 ACQ/SEARCH	none

Please Note...

- It is the responsibility of the observer to provide coordinates and proper motions with the required accuracy. Be especially mindful of nearby white dwarfs, which generally have high proper motions, and binary stars, whose motions on the sky are highly non-linear. Observations that fail because of an inaccurate target position will not be repeated. STScI cannot be responsible for target-coordinate or proper-motion errors in published catalogs or in the literature. If there is any doubt that the available coordinates meet the required accuracy, then an ACQ/SEARCH should be performed.
- If a target falls near the edge of the aperture at the initial pointing, the ACQ/IMAGE and ACQ/PEAKXD algorithms may miscalculate its position. Users who require the best possible photometric or absolute wavelength accuracy may wish either to begin with an ACQ/SEARCH to ensure that the target is reasonably well centered before the final stages of the acquisition are performed, or to perform an extra ACQ/IMAGE or ACQ/PEAKXD in case the observation at the initial pointing was partially vignetted.
- At the present time, the new central-wavelength settings for G130M (1055, 1096, and 1222 Å) cannot be used for target acquisitions.
- For ACQ/IMAGE exposures, both the preliminary and confirmation images are downlinked and delivered to the observer. For the other three TA modes, no images or spectra are recorded.

8.3 ACQ/SEARCH Acquisition Mode

In ACQ/SEARCH mode, the telescope is moved in a spiral pattern on the sky to cover a square grid up to 5 × 5 steps in size. At each scan point, the telescope stops and data are collected. A two-dimensional array containing the total counts measured at each dwell point is constructed. After completion of the full n × n pattern, the target position is calculated as described below, and the telescope is moved to center the target. A 3 × 3 ACQ/SEARCH is illustrated in Figure 8.1.

Figure 8.1: Example of a 3 × 3 Spiral Search Pattern

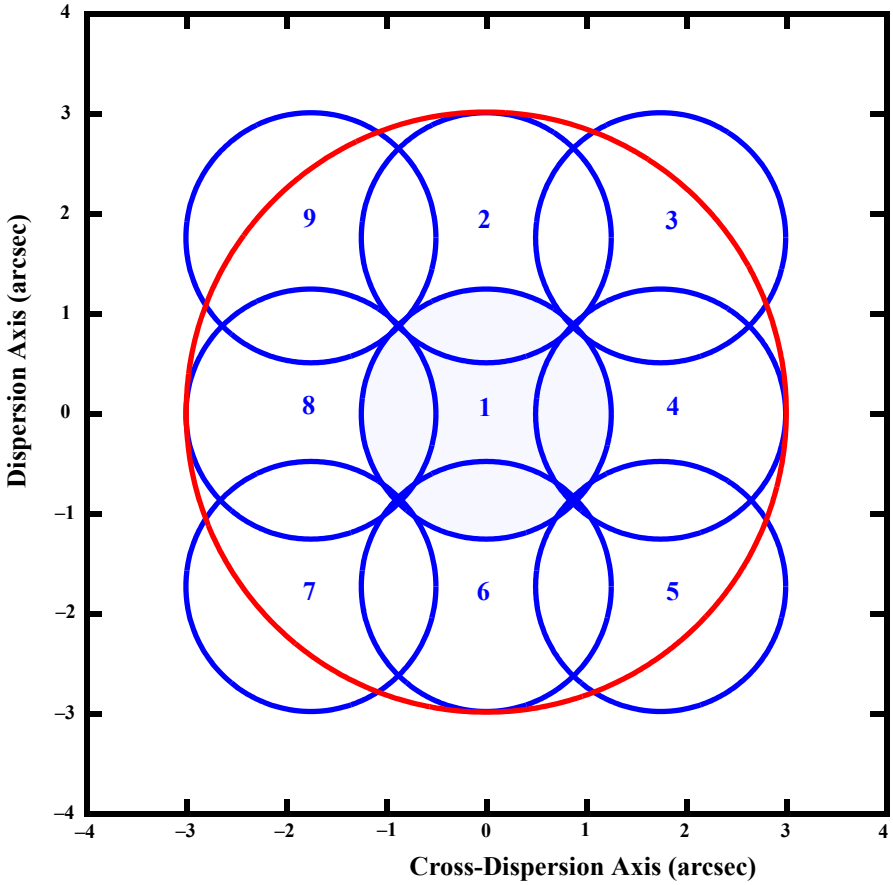

This 3 × 3 spiral search was executed with the default STEP-SIZE of 1.767 arcsec. The blue circles represent the nine positions of the 2.5 arcsec-diameter aperture, and the numbers show the sequence of steps on the sky. The large outer circle in red has a radius of ~ 3 arcsec.

For an ACQ/SEARCH, the user must specify

- The aperture to use, either PSA or BOA.
- The spectral element (grating or mirror) and the central-wavelength setting (if applicable). For a spectroscopic ACQ/SEARCH, these will generally be the grating and central wavelength of the initial science observation; however, an observer may specify ACQ/SEARCH with a different grating and central-wavelength setting if there are advantages to doing so.
- The SCAN-SIZE, which is 2, 3, 4, or 5, corresponding to spiral patterns of 2 × 2, 3 × 3, etc.

- The STEP-SIZE, or spacing between grid points. It may be any value from 0.2 to 2.0 arcsec, but we strongly recommend using the default value of 1.767 arcsec. This value has been chosen so that no part of the sky is missed, given the aperture diameter of 2.5 arcsec ($2.5/\sqrt{2} = 1.767$).
- The exposure time per dwell point.
- For FUV searches, users may choose to use just one of the segments, A or B, but the use of both (the default for all but G140L) is recommended.

Once the scan is complete, the flight software computes the centroid of the array and thus the position of the target. There are three centroiding options:

1. The first option is CENTER=FLUX-WT, which uses a flux-weighted centroiding algorithm to determine the center of light. It is the default for SCAN-SIZE=2.
2. A variation on CENTER=FLUX-WT is CENTER=FLUX-WT-FLR. In this case, a floor is subtracted from the counts at each dwell point before the centroid is computed. The floor is taken as the minimum number of counts seen in any one dwell point. FLUX-WT-FLR has the advantage of removing background counts, but leaves one or more points in the array with zero counts. As it can cause computational problems, FLUX-WT-FLR should not be used with SCAN-SIZE=2.
3. The last option for centering is CENTER=BRIGHTEST, which simply centers the dwell point with the most counts. This is straightforward but not as accurate as the other centroiding methods. CENTER=BRIGHTEST is appropriate if coordinates are uncertain and the ACQ/SEARCH is followed by a second ACQ/SEARCH using flux-weighted centering or an ACQ/IMAGE, or if the source is extended and it is only desired that the brightest point be in the aperture.

Table 8.2 presents the recommended ACQ/SEARCH parameters as a function of coordinate uncertainty. For all values of SCAN-SIZE > 2, we recommend CENTER=FLUX-WT-FLR, as it is slightly more accurate due to better sky and detector background suppression. Note that even SCAN-SIZE values (2 or 4) trigger additional overhead because of the telescope motion required to displace the aperture by half of a STEP-SIZE in both the dispersion and cross-dispersion directions, so that the overall pattern remains centered on the initial pointing.

Analysis of SMOV/Cycle 17 acquisitions indicate that a single ACQ/SEARCH acquisition, whether spectroscopic or imaging, provides a centering accuracy of 0.3 arcsec only 75% of the time. Additional TA stages are thus necessary to achieve the centering accuracy necessary to meet wavelength and photometric requirements.

Table 8.2: Recommended ACQ/SEARCH Parameters versus Coordinate Uncertainty

Coordinate uncertainty (arcsec)	SCAN-SIZE	STEP-SIZE	CENTER
$\sigma \leq 0.4$	ACQ/SEARCH not required.		
$0.4 < \sigma < 0.7$	2	1.767[1]	FLUX-WT
$0.7 < \sigma < 1.0$	3	1.767[2]	FLUX-WT-FLR
$1.0 < \sigma < 1.3$	4	1.767[2]	FLUX-WT-FLR
$1.3 < \sigma \leq 1.6$	5	1.767[2]	FLUX-WT-FLR

1. This is the default STEP-SIZE value and the largest to cover the search area without holes or gaps.
2. If target coordinate uncertainty is on the lower edge of the given range, the STEP-SIZE may be reduced slightly (*e.g.*, 1.5 arcsec) to improve centering accuracy at the expense of total area covered by the search.

8.4 ACQ/IMAGE Acquisition Mode

In ACQ/IMAGE mode, COS obtains an NUV image of the target field, moves the telescope to center the object, and obtains a second NUV image as confirmation. ACQ/IMAGE may use either the primary science aperture (PSA) or the bright object aperture (BOA) and either MIRRORA or MIRRORB. All four combinations are illustrated in Figure 8.2. Note the additional structure present in images obtained with MIRRORB and the BOA: The secondary image produced by MIRRORB is half the intensity of the primary image and is displaced by 20 pixels (about 0.5 arcsec) in the dispersion direction. The BOA produces a chevron-like image whose peak is displaced in both the dispersion and cross-dispersion directions. When the BOA is used with MIRRORB, two distorted peaks result. In this configuration, there is some overlap between the wings of the primary and secondary peaks, but they are well enough separated to allow for reliable acquisitions.

An ACQ/IMAGE exposure consists of the following steps:

1. An exposure of the internal Pt-Ne lamp is obtained through the WCA aperture. The onboard COS Flight Software (FSW) sets the exposure time for the lamp exposure automatically. The centroid of the WCA image is calculated by the FSW. Using the known offset between the center of the WCA and the science aperture (PSA or BOA), the location of the center of the science aperture on the detector is computed.

Figure 8.2: Point Sources Observed with all Four Aperture/Mirror Combinations

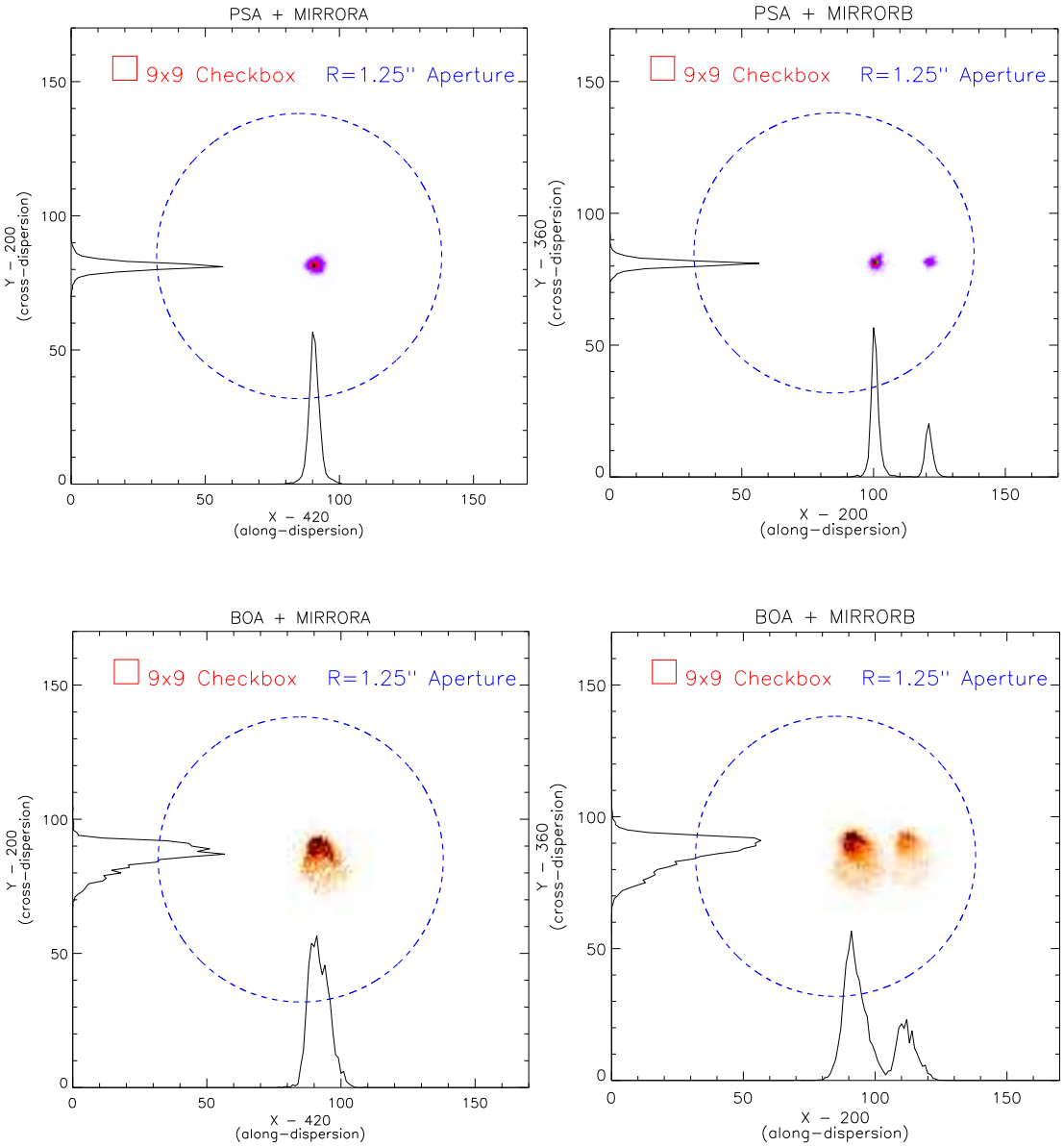

NUV images of point sources observed through the PSA (top) and BOA (bottom) using MIRRORA (left) and MIRRORB (right). The limits of each plot represent the 170 × 170 pixel image used by ACQ/IMAGE. Also shown are the COS aperture (blue circle of radius 1.25") and the 9 × 9 checkbox used by ACQ/IMAGE. Histograms show the AD and XD profiles. The pointing is typical of that expected after an ACQ/SEARCH, but before additional peak-ups.

2. The shutter is opened and a TA image of the field is obtained. The telescope is not moved, meaning that an acquisition using ACQ/IMAGE will be successful only if the target lies within (or just outside of) the aperture. An area of 170 × 170 pixels, which corresponds to approximately 4×4 arcsec^2, centered on the aperture, is read out. This image is recorded and downlinked and becomes part of the archived data package. (It is stored in the first extension of the _rawacq file.)

3. A 9 × 9 pixel checkbox array is then passed over the 170 × 170 pixel image. First, the checkbox with the most counts is identified. In the unlikely instance that two checkboxes have equal counts, the first one encountered is used. The brightest 9 × 9 array is then analyzed using a flux-weighted centroiding algorithm to calculate the target position.
4. Finally, *HST* is moved to place the calculated centroid at the center of the selected aperture. A second exposure, identical to the first, is taken and recorded for later downlink as a verification of the centering. (It is stored in the fourth extension of the `_rawacq` file.)

8.5 ACQ/PEAKXD Acquisition Mode

8.5.1 Description

An `ACQ/PEAKXD` sequence is used to improve centering in the cross-dispersion (XD) direction. The steps executed in an `ACQ/PEAKXD` sequence are

1. A short exposure of the Pt-Ne wavelength calibration lamp through the WCA aperture is obtained. The spectrum is collapsed along the dispersion direction, its centroid is calculated, and the center of the target aperture is computed.
2. A target spectrum is recorded for the user-specified time using a sub-array tailored to each grating and central wavelength (excluding edge effects and airglow lines). The spectrum is collapsed along the dispersion direction.
3. The target XD location is assumed to be the median (NUV) or mean (FUV) of the collapsed spectrum.
4. The slew required to move the target spectrum in the XD direction to the center of the aperture is computed.
5. The telescope is slewed by the calculated offset to center the target in the XD direction.

The user must specify the aperture (PSA or BOA, typically the same as for the science exposure), the grating and central wavelength, and the exposure time. The use of `MIRRORA` or `MIRRORB` is not allowed. For NUV `ACQ/PEAKXD` acquisitions, the stripe (`SHORT`, `MEDIUM`, or `LONG`, corresponding to stripes A, B, or C) to be used in the computation may be specified; however, the default stripe B (`MEDIUM`) is recommended, as it achieves the best centering. For FUV `ACQ/PEAKXD` acquisitions, only data from segment A are used to compute the centroid; data from segment B are ignored. For G140L, segment B is turned off by default.

Note: Because light from the three spectral stripes will overlap, PEAKXD acquisitions will fail—and should thus be avoided—for extended sources observed with the NUV detector.

8.5.2 Effects of FUV Detector Y Walk

As described in Section 4.1.6, the COS FUV detector is beginning to exhibit gain sag. One consequence of this effect is the mis-registration of photon events in the cross-dispersion (XD) or Y direction, commonly referred to as Y walk. While Y walk does not adversely affect science data, it can reduce the accuracy of target acquisitions obtained in dispersed light. If the target is centered in the aperture, but the Y walk shifts its spectrum in the XD direction, then the ACQ/PEAKXD algorithm will miscalculate its centroid and move the target away from the aperture center.

To combat the effects of Y walk, we have modified the algorithm used for FUV ACQ/PEAKXD exposures in two ways: First, it ignores data from detector segment B, which exhibits the greater gain sag. Second, it adds two pixels to the computed centroid to account for Y walk on segment A. (We will monitor the effects of Y walk and adjust this offset as necessary.) With these changes, all FUV gratings may now be used for dispersed-light target acquisitions. Furthermore, a signal-to-noise ratio of only 25 on segment A is required to compute an accurate spectral centroid.

8.6 ACQ/PEAKD Acquisition Mode

`ACQ/PEAKD` exposures are used to improve centering in the along-dispersion (AD) direction after an `ACQ/PEAKXD`. `ACQ/PEAKD` works much like `ACQ/SEARCH` except that, instead of a spiral, the spacecraft is moved linearly along the AD axis between exposures. An array containing the total counts at each dwell point is constructed. Its centroid is computed, and the telescope is moved to center the target in the aperture in the AD direction.

The user must specify the aperture, grating, central wavelength, and the exposure time at each dwell point. The use of `MIRRORA` or `MIRRORB` is not allowed. The number of steps, here called `NUM-POS`, may be 3, 5, 7, or 9. The `STEP-SIZE` is given in arc seconds. There are three options for the centering algorithm, `CENTER=FLUX-WT`, `FLUX-WT-FLR`, and `BRIGHTEST`, and they work just as described in Section 8.3.

For most applications, we recommend the use of `NUM-POS=5`, `STEP-SIZE=0.9`, and `CENTER=FLUX-WT-FLR`, as this combination is the least sensitive to high or variable background rates and covers a large area on the sky. Observers who wish to use `NUM-POS=3` are advised to use `STEP-SIZE`=1.3 and `CENTER=FLUX-WT`. The special parameter `CENTER=DEFAULT` sets `CENTER=FLUX-WT` if `NUM-POS=3` and `CENTER=FLUX-WT-FLR` if `NUM-POS=5, 7`, or `9`. For FUV `ACQ/PEAKD` acquisitions, either segment A or B may be used, but use of the `SEGMENT=DEFAULT` (both, except for G140L) is recommended.

8.7 Exposure Times

While the figures in this section will help you to estimate exposure times for various acquisition scenarios, the COS Exposure Time Calculator (ETC) should be used for all proposal preparation.

8.7.1 Imaging Acquisitions

Acquisition images obtained through the PSA should strive for a minimum S/N of 40. Due to the complex shape of images obtained through the BOA, a S/N > 60 is recommended. For MIRRORB acquisitions, the recommended S/N refers only to the primary image; the ETC performs this calculation appropriately. Figure 8.3 shows approximate exposure times needed to reach these S/N levels for various target fluxes. A flat source spectrum (F_λ = constant) is assumed.

Figure 8.3: Exposure Time Needed for an ACQ/IMAGE Acquisition

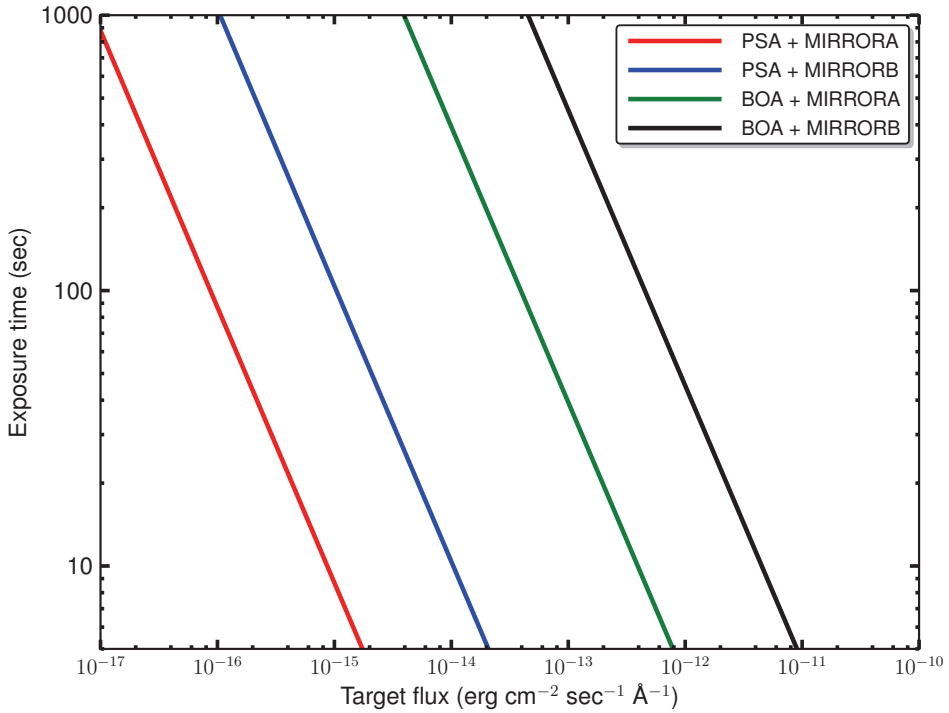

Approximate exposure time needed to achieve S/N = 40 (PSA) or 60 (BOA) as a function of target flux. This calculation assumes a flat source spectrum.

Figure 8.4: Exposure Time Needed for a Dispersed-Light Acquisition

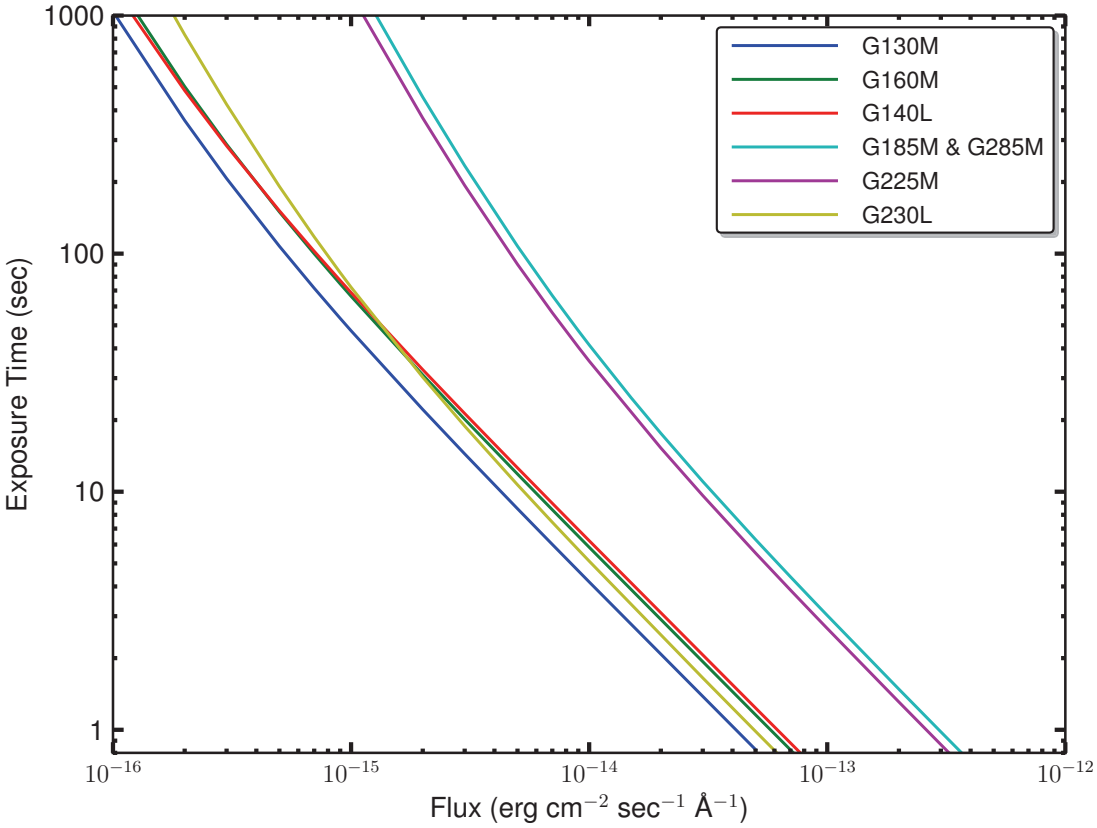

Approximate exposure time needed to achieve a S/N of 40, assuming a flat source spectrum.

8.7.2 Dispersed-Light Acquisitions

We recommend a minimum S/N of 40 for all dispersed-light acquisition exposures, except for FUV ACQ/PEAKXD exposures, which require only S/N = 25 in detector segment A (Section 8.5.2). STScI calibration programs routinely use up to S/N=100 to minimize the influence of Poisson noise and background when very precise pointing is required. Figure 8.4 is a guide to the exposure time needed for a dispersed-light acquisition, assuming a flat source spectrum (F_λ = constant). Note that these exposure times apply to each separate dwell point of a pattern, which is the quantity entered into APT in Phase II.

8.8 Centering Accuracy and Data Quality

A centering accuracy of 0.3 arcsec in the cross-dispersion (XD) direction is required to achieve optimum photometric accuracy and spectral resolution. In the along-dispersion (AD) direction, the minimum accuracy is set by velocity requirements: ±15 km/s for the medium-resolution modes, ±150 km/s for G140L, and ±175 km/s for G230L. Since the AD requirements are in units of km/s, they are detector and wavelength dependent. Assuming that the wavelength error budget is

split evenly between the COS TA and wavelength scale accuracy, the strictest pointing requirements are ±0.041 arcsec for the NUV channel and ±0.106 arcsec for the FUV channel.

8.8.1 Centering Accuracy and Wavelength Accuracy

To achieve a wavelength accuracy of ±15 km/s, the target should be centered to within about 0.04–0.07 arcsec for NUV observations and 0.1–0.2 arcsec for FUV observations. The throughput of COS is not affected by centering errors of less than 0.4 arcsec, so high centering precision is not strictly necessary if science goals do not require that the wavelength zero point be well constrained. For example, the spectra of some objects may include foreground interstellar or inter-galactic absorption lines that can be used to establish the zero point of the wavelength scale.

8.8.2 Centering Accuracy and Photometric Precision

Figure 8.5 shows the relative transmission of the PSA as a function of the displacement of a point source from the aperture center, as measured using each of the four NUV gratings. These and the corresponding FUV curves are nearly identical and show that the transmission of the COS apertures is essentially flat within the central ±0.4 arcsec, then tails off in a non-linear but approximately symmetrical profile (COS ISR 2010-09).

Figure 8.5: Relative Transmission of the COS PSA at NUV Wavelengths

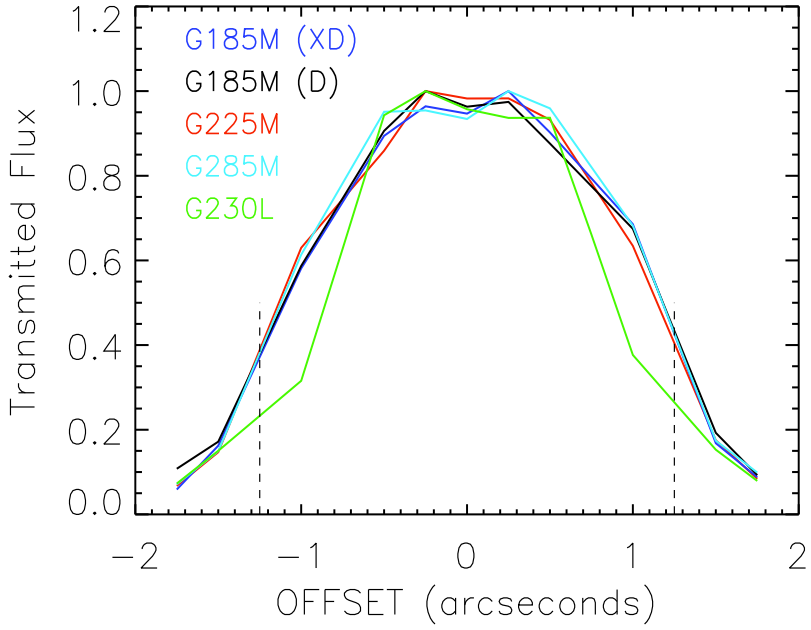

Transmitted flux as a function of displacement from aperture center for all four NUV gratings. The dotted lines mark the edge of the aperture (1.25”). The two curves labeled D and XD refer to offsets along the dispersion and cross-dispersion axes, respectively. The other curves trace offsets in the cross-dispersion direction. For all gratings, the absolute transmission for a centered point source is at least 95%.

8.8.3 Centering Accuracy and Spectroscopic Resolution

Targets placed within 0.4 arcsec of the aperture center will achieve maximum spectral resolution. Centering errors larger than 0.4 arcsec will lead to progressively poorer resolution. Targets at the edge of the aperture have approximately half the spectral resolution of well-centered targets.

8.9 Recommended Parameters for all COS TA Modes

As the result of our analysis of the target acquisition (TA) performance of COS during SMOV and Cycle 17, we have adjusted many COS TA parameters and have refined our recommendations and guidelines for routine COS TAs. We present these recommendations and guidelines in the previous sections and summarize the most significant changes below. Table 8.3 provides our recommended values for optional parameters for each COS TA type.

- All TA modes provide good centering. For maximum wavelength accuracy, use NUV imaging mode; otherwise, use the mode that is fastest, based on ETC simulations.
- Signal-to-noise (S/N) is important. Use S/N > 40 for PSA TAs and S/N > 60 for BOA TAs. A S/N of 25 on detector segment A is sufficient for FUV ACQ/PEAKXD exposures.
- A single ACQ/SEARCH is not sufficient to center a COS point-source target in the aperture. Always follow the first `ACQ/SEARCH` with an `ACQ/IMAGE`, `ACQ/PEAKXD+ACQ/PEAKD`, or a second 2 × 2 `ACQ/SEARCH`.
- `ACQ/SEARCH` exposures are not required for targets with coordinate accuracies of ±0.4 arcsec or better in the ICRS/GSC2 frame. Spending extra time to validate target coordinates is the best way to save TA time.
- If at all possible, use `STRIPE=MEDIUM` (stripe B) for NUV spectroscopic `ACQ/PEAKXD`s. (This is the default.)
- Use `SCAN-SIZE=5`, `STEP-SIZE=0.9`, and `CENTER=FLUX-WT-FLR` for most `ACQ/PEAKD` centerings. For the most accurate AD centering possible, use `SCANSIZE=9`, `STEP-SIZE=0.6`, and `CENTER=FLUX-WT-FLR`. When a fast TA is required and lower centering accuracy can be tolerated, use `SCAN-SIZE=3`, `STEP-SIZE=1.3`, and `CENTER=FLUX-WT`.

Table 8.3: COS Acquisition Modes, Options, and Recommended Values

Acquisition Type	Description	SCAN-SIZE or NUM-POS	STEP-SIZE (arcsec)	Optional Parameters	Recommended Values	Recommended S/N
ACQ/SEARCH	Spiral pattern; multiple exposures	2	1.767	CENTER=FLUX-WT, FLUX-WT-FLR, BRIGHTEST For FUV: SEGMENT=A, B, BOTH	FLUX-WT	40
		3[1]			FLUX-WT-FLR	
		4			FLUX-WT-FLR	
		5			FLUX-WT-FLR	
ACQ/IMAGE	Initial and confirmation images					40 (PSA) 60 (BOA)
ACQ/PEAKXD	One exposure			For NUV: STRIPE=SHORT, MEDIUM, LONG For FUV: SEGMENT=A, BOTH[2]	For NUV: STRIPE=MEDIUM For FUV: SEGMENT=BOTH (These are the default values.)	For NUV: 40 to 100 For FUV: 25 on segment A
ACQ/PEAKD	Linear pattern; multiple exposures	3	1.3	CENTER=FLUX-WT, FLUX-WT-FLR, BRIGHTEST, DEFAULT[3] For FUV: SEGMENT=A, B, BOTH	FLUX-WT	40 to 100
		5[1]	0.9		FLUX-WT-FLR	
		7	0.6		FLUX-WT-FLR	
		9	0.6		FLUX-WT-FLR	

1. Recommended number of acquisition steps.
2. For FUV exposures, data from detector segment B are ignored by the ACQ/PEAKXD centroiding algorithm, regardless of the value of the SEGMENT parameter.
3. For ACQ/PEAKD, use of the special parameter CENTER=DEFAULT is recommended. This parameter sets CENTER=FLUX-WT if NUM-POS=3 and CENTER=FLUX-WT-FLR if NUMPOS=5, 7, or 9.

8.10 Special Cases

8.10.1 Early Acquisitions and Preliminary Images

In some situations, an observer may need to obtain an independent ultraviolet image of a region in order to ensure that no objects violate safety limits and that the target to be observed can be acquired by COS successfully. Such an early acquisition should be included in the Phase I proposal, and the observation should not use a photon-counting detector. The UVIS channel on WFC3 is recommended, but observers are encouraged to consult with an STScI instrument scientist.

8.10.2 Extended or Multiple Targets

Because most COS target-acquisition schemes were developed with the implicit assumption that the target is a point source, acquisitions of extended or multiple sources may require more careful planning.

If the target is sufficiently uniform and its coordinates are well known, then a target acquisition may not be required. To ensure that the brightest region of an extended source falls into the aperture, an ACQ/SEARCH with `CENTER=BRIGHTEST` may be sufficient (Section 8.3). ACQ/PEAKXD acquisitions with the NUV detector should be avoided for extended sources, because light from the three spectral stripes will overlap on the detector (Section 8.5).

Complex targets—two nearby stars, multiple bright knots, etc.—may confuse the acquisition algorithms. In such cases, consider an offset target acquisition, discussed in Section 8.10.3.

8.10.3 Offset Target Acquisitions

When targets are faint or lie in crowded fields, direct acquisition of the primary science target may be difficult or uncertain. In such cases, an offset acquisition, in which acquisition of a nearby field target is followed by a short slew to the science target, may be appropriate.

The size of the offset is limited by the requirement that the guide stars remain within the fields of view of their respective FGSs. Offset acquisition slews routinely involve displacements up to 1 arcmin and can be larger. Offset slews have a typical accuracy of ±0.003 arcsec. The centering of the initial offset target should be refined (via either `ACQ/IMAGE` or `ACQ/PEAKXD+ACQ/PEAKD`) before the offset maneuver. For offset acquisitions, bright-object considerations apply over the entire offset region. Refer to Chapter 9 for a discussion of the modest overheads associated with the offset-acquisition spacecraft movement.

In unusual cases, including highly uncertain target coordinates or knotty, extended sources for which high wavelength accuracy is required, an offset target acquisition, followed by an additional `ACQ/IMAGE` or `ACQ/PEAKXD+ACQ/PEAKD` on the primary target, may be employed.

8.10.4 Acquisition Failure Actions and Diagnostics

Should any stage of the TA fail or a Local Rate Check (LRC) violation occur during a TA exposure, then the subsequent acquisition procedures in that visit (such as `ACQ/PEAKXD` or `ACQ/PEAKD`) will not be executed, but the science exposures will still occur. Note that *HST* will be left pointing at the last commanded position, which may differ substantially from the initial pointing.

Many quantities useful for evaluating the success of COS TAs are recorded in the COS TA data products (the `_rawacq` and `_spt` files). Table 5 of COS ISR 2010-14 lists these keywords and their meanings.

CHAPTER 9:

Scheduling Observations

In this chapter…

9.1 Introduction

Once you have established the series of target-acquisition, scientific, and (if necessary) calibration exposures required for your program, you are ready to determine the total number of orbits to request. Generally, this is a straightforward exercise: compile the overheads on the individual exposures, assign the exposures to orbits, and tally the results to determine your orbit request. In some cases, it may be an iterative process, as you refine your observing plan to use each orbit most efficiently. This chapter provides simple tools to help you perform these calculations.

Once your proposal has been accepted, you will return to this chapter to construct your Phase II proposal, the detailed observing plan that will eventually be transmitted to the telescope. Our goal is to help you schedule your observations as efficiently as possible.

Table 9.1: Phase I Estimates of Observatory and Instrument Overheads

Acquisition or Exposure	Overhead Time (minutes)	Notes
Guide-star acquisition	6	First orbit of each visit
Guide-star re-acquisition	4	Each subsequent orbit
ACQ/IMAGE	3	Typical imaging acquisition
ACQ/SEARCH	7	Imaging or dispersed, NUV or FUV
ACQ/PEAKXD + ACQ/PEAKD	7	Typical dispersed-light acquisition, NUV or FUV
Science (Imaging or Dispersed-Light)	5	First exposure in series
	2	Each subsequent exposure in series
	1	Add 1 minute for each instrument change (except to increment FP-POS)

9.1.1 Phase I Proposal

The *HST Primer* provides simple guidelines for estimating the overheads associated with a COS observation. These guidelines are summarized in Table 9.1. Each orbit must begin with a guide-star acquisition, which takes 6 minutes on the first orbit of a visit and 4 minutes on subsequent orbits. Next, the target must be acquired via an ACQ/SEARCH (7 min) and/or centered in the aperture via an ACQ/IMAGE (3 min) or a pair of ACQ/PEAKXD and ACQ/PEAKD exposures (7 min for both). The first science exposure requires 5 minutes of overhead. Subsequent identical exposures incur 2 minutes of overhead. Add 1 minute for each instrument change (e.g., new grating or central wavelength; incrementing the FP-POS takes only 3 seconds). If the same target is observed on contiguous orbits, a target acquisition is not required on the second and subsequent orbits.

These simple rules are remarkably successful at reproducing the total time required for a COS observation. To demonstrate, we list in Section 9.7 both the Phase I times and the final times predicted by APT for a series of observing scenarios. These rules assume that acquisition exposure times are on the order of 20 seconds. If your targets are extremely faint, you must increase the length of the acquisition exposures accordingly (Section 9.4). Finally, note that some instrument changes, such as turning a detector segment on or off, take considerably longer than 1 minute (Section 9.5).

Allowing sufficient time for overheads in your Phase I proposal is important; additional time to cover unplanned or overlooked overheads will not be granted later.

9.1.2 Phase II Proposal

Once your proposal is approved, you will be responsible for building the observing sequences that will be executed by the telescope. The APT (Astronomer's Proposal Tool) scheduling software is used to prepare the Phase II; it automatically incorporates the appropriate overheads into your observing plan. While all COS overheads are automatically scheduled by APT, it is useful to understand where they come from. To that end, this chapter discusses the various observatory and instrument overheads in some detail, and Section 9.7 provides observing scenarios as examples. Note that, when this chapter and APT disagree, the APT overheads are the definitive values.

Accounting properly for all the overheads involved in an observation can be complicated. The information provided here is meant only to be illustrative. Proposers are urged to use APT to derive a complete and accurate determination of overhead times.

9.2 Generic Observatory Overheads

The first time that you acquire an object, you must include a 6-minute overhead for the *HST* guide-star acquisition. In all subsequent orbits of the same visit, you must include the 4-minute overhead for the guide-star reacquisition. If you are observing an object in the Continuous Viewing Zone (CVZ), then no guide-star re-aquisitions are required.

You must allocate additional time for each deliberate movement of the telescope; e.g., if you are performing a target-acquisition exposure on a nearby object and then offsetting to your target, or if you are taking a series of exposures in which you move the target on the detector (`POS-TARG`), then you must allow time for telescope motion. The time varies depending on size of the slew; see Table 9.2.

Table 9.2: Generic Observatory Overhead Times

Action	Overhead type	Time needed
Guide-star acquisition	Initial acquisition	6 min
	Re-acquisition	4 min per orbit
Spacecraft movements	10 arcsec < Offset < 1.5 arcmin[1]	60 sec
	1.25 arcsec ≤ Offset ≤ 10 arcsec	30 sec
	Offset < 1.25 arcsec	20 sec

1. Spacecraft motions larger than ~ 1.5 arcmin are likely to result in the loss of guide stars.

9.3 Spectral Element Movement Overheads

For any COS exposure, including target-acquisition exposures, any change of spectral elements incurs an overhead. A transition from FUV to NUV requires movement of OSM1 to the NCM1 position, followed by a possible OSM2 movement. On the other hand, a transition from NUV to FUV requires only the movement of OSM1 from NCM1 to the desired FUV grating. Table 9.3 gives the times required for movement between OSM1 spectral elements and Table 9.4 gives the times for movement between OSM2 spectral elements.

All COS visits start with OSM1 at the G130M position (with central wavelength 1309 Å) and OSM2 at the G185M position. These gratings are highlighted in Table 9.3 and Table 9.4. OSM1 and OSM2 move sequentially, so the total overhead is the sum of the two separate overheads. The time required to move from one optical element to another is independent of the initial and final central-wavelength and FP-POS settings.

Table 9.3: Overhead Times for Motions Between OSM1 Spectral Elements

Movement times (s) from	to G140L	to G130M	to G160M	to NCM1
G140L	—	158	200	115
G130M	164	—	112	116
G160M	206	116	—	159
NCM1	121	109	154	—

Table 9.4: Overhead Times for Motions Between OSM2 Spectral Elements

Movement times (s) from	to G230L	to G185M	to G225M	to G285M	to MIRRORA	to MIRRORB
G230L	—	209	140	176	105	99
G185M	204	—	136	102	169	175
G225M	135	141	—	108	100	106
G285M	170	107	103	—	136	142
MIRRORA	100	174	105	141	—	71
MIRRORB	94	181	112	147	77	—

9.4 Acquisition Overheads

The various target-acquisition procedures are described in detail in Chapter 8. The exposure overheads associated with each are given below:

ACQ/SEARCH: Add 20 seconds to the exposure time and multiply by the number of dwell points. Add the grating-change overheads from Table 9.3 and Table 9.4. Even `SCAN-SIZE` values (2 or 4) trigger an additional overhead because of the telescope motion required to displace the aperture by half of a `STEP-SIZE` in both the dispersion and cross-dispersion directions, so that the overall pattern remains centered on the initial pointing.

ACQ/IMAGE: The associated overhead is 120 seconds plus twice the specified exposure time; this includes both the OSM1 and OSM2 movements and the overhead adjustment discussed in Section 9.6. The exposure time is doubled because, after *HST* is slewed to center the target, a confirmation image is obtained. Dumping the two images to memory requires an additional 58 seconds.

ACQ/PEAKXD: The overhead is 70 seconds (NUV) or 80 seconds (FUV) plus exposure time. Add the grating-change overhead from Table 9.3 and Table 9.4.

ACQ/PEAKD: Add 20 seconds to the exposure time and multiply by the number of dwell points. Add the grating-change overhead from Table 9.3 and Table 9.4. Add 39 seconds for memory readout.

9.5 Science Exposure Overheads

Science-exposure overheads are dominated by the time required to move OSM1 and OSM2 and to read out the on-board memory buffer at the end of each exposure. While the Phase II overheads computed by APT may be less than the values presented below, it is important to plan Phase I proposals using the conservative overheads given below to ensure adequate time for each exposure.

The full overhead calculation for science exposures depends upon a number of factors including generic exposure set-ups (which depend on the detector and observing mode), whether an aperture change is required, whether a grating change is required, whether the central wavelength setting for the grating is changed, and the directional sense of any required motion to implement an `FP-POS` change. Table 9.5 lists these additional overheads.

When moving to a new grating, you may specify any combination of central wavelength and FP-POS setting with no additional overhead penalty. As a result, the FP-POS sequence 1,2,3,4 is more efficient than 3,4,1,2, because no backward motion is required.

Table 9.5: Science Exposure Overhead Times

Overhead times (s)	FUV		NUV	
	TIME-TAG	ACCUM	TIME-TAG	ACCUM
Exposure set-up	71	79	36	38
Grating change	see Table 9.3		see Table 9.4	
Central wavelength change	72		75	
FP-POS forward[1]	3		3	
FP-POS backward[1]	70		70	
PSA – BOA Change	8		8	
WCS – BOA Change	10		10	
SEGMENT reconfiguration	330		N/A	
Memory readout[2]	116	108[2]	116	48[2]

1. "Forward" refers to the preferred direction of motion of OSM1 or OSM2 and "backward" to the opposite direction. The preferred direction is toward larger FP-POS values.
2. ACCUM mode readout overheads can be hidden within subsequent exposures under certain circumstances, but the rules are complex. Use these values as safe upper limits for proposals.

To estimate the overhead for an exposure, round the desired exposure time up to the next whole second and add the generic exposure setup overhead from Table 9.5. If a grating change has occurred from the previous exposure, add the appropriate values from Table 9.3 and/or Table 9.4. If a central wavelength change is made, add the appropriate value from Table 9.5. If an FP-POS movement is made, add the appropriate value for motion in the preferred direction (toward larger FP-POS) or non-preferred direction. Note that all dispersed-light target-acquisition exposures are obtained with FP-POS = 3. For all FUV observations except the G140L 1105 Å setting, both detector segments are powered on by default. To turn one of them off, set SEGMENT to A or B and add the associated overhead. Lastly, add the appropriate detector memory readout overhead.

9.6 First Exposure Overhead Adjustment

To increase observing efficiency, a special feature of the COS instrument commanding allows a portion of the instrumental overheads for the first exposure of a visit to be performed during the initial guide-star acquisition. These will usually be target-acquisition exposures. As a result, up to 340 seconds of instrumental overheads (Table 9.3, Table 9.4, and Table 9.5) but ***not*** observatory or acquisition overheads

(Table 9.2 and Section 9.4) may be hidden in this fashion. See Section 9.7 for examples.

9.7 Examples of Orbit Estimates

In this section, we present five example COS observations, using both detectors and all of the target-acquisition modes. Besides the topics discussed in the previous sections, we include examples of

- **Multiple FP-POS settings** (Section 5.8.2)**:** To minimize the damage to the FUV detector caused by strong Lyman α airglow lines and to improve the limiting S/N of an observation, observers are strongly encouraged to use multiple FP-POS settings for each CENWAVE setting. Observers should use at least two and, if possible, all four FP-POS positions of a given CENWAVE.
- **Adjusting the BUFFER-TIME (**Section 5.4.1**):** When the `BUFFER-TIME` is greater than the exposure time, one would normally set `BUFFER-TIME = EXPTIME`. In orbits with a series of long FUV exposures, one can minimize overheads by setting `BUFFER-TIME = EXPTIME-100`. The full buffer takes 116 seconds to empty, so most of the data will be read out before the exposure is completed. The post-exposure data dump then requires only 40 seconds. For the final exposure of an orbit, the buffer dump can occur during the occultation, so adjusting the `BUFFER-TIME` will not save time. See the example in Section 9.7.5.

While the overhead rules presented in this chapter may appear complex, the actual rules used by the *HST* scheduling software are even more so. It is thus imperative that you use APT to construct your Phase II proposal. In the examples that follow, we present three sets of overhead estimates: one using the Phase I rules (Section 9.1), one using the rules in this chapter (Sections 9.2 to 9.6), and one computed using APT version 19.2. The APT estimates should be considered definitive. COS is a relatively new instrument, and the overhead rules will continue to evolve as we learn how to use it more efficiently. The version of APT available for constructing Cycle 20 Phase II proposals may well return values that differ slightly from those given below.

9.7.1 Target Acquisition Using ACQ/IMAGE

In this example, we begin with an NUV ACQ/IMAGE target acquisition, then add two NUV TIME-TAG exposures using the same grating but different central wavelengths. For NUV observations, the use of multiple FP-POS settings is not required (though it useful to reduce flat-field noise).

Table 9.6: Overhead Values for ACQ/IMAGE Acquisition

Action	Phase I (s)	Chapter 10 (s)	APT Time (s)	Comment
Initial guide star acquisition	360	360	333	Required at start of a new visit
NUV ACQ/IMAGE with 2 s exposure	180	116 + 169 + 120 + 4 + 58 = 467	410 + 58 (dump)	COS starts at G130M on OSM1, so move to NCM1 requires 116 s. OSM2 home position is G185M, so move to MIRRORA takes 169 s. Add 2 min ACQ/IMAGE setup, twice the exposure time, and memory readout.
First exposure overhead adjustment	N/A	-(116 + 169) = -285	-333	OSM1 and OSM2 movements may be hidden in guide-star acquisition.
NUV G185M at 1850 Å, TIME-TAG, FP-POS=3, 1175 s exposure	300 + 1175	36 + 174+ 1175 + 116 = 1501	205 + 1175 + 116	Generic NUV TIME-TAG setup; change from MIRRORA to G185M (174 s); exp time; TIME-TAG memory readout
NUV G185M at 1817 Å, TIME-TAG, FP-POS=3, 1175 s exposure	120 + 60 + 1175	36 + 75 + 1175 + 116 = 1402	104 + 1175 + 116	Generic NUV TIME-TAG exposure setup; central-wavelength change (75 s); exp time; TIME-TAG memory readout
Total science time	2350	2350	2350	
Total time used in orbit	3370	3445	3359	

9.7.2 ACQ/SEARCH plus ACQ/IMAGE Acquisition

In this example, we begin with an NUV ACQ/SEARCH followed by an ACQ/IMAGE target acquisition. We obtain an NUV TIME-TAG exposure, then switch to the FUV channel for a pair of FUV TIME-TAG exposures. To minimize damage to the detector, we employ two FP-POS settings.

Table 9.7: Overhead Values for ACQ/SEARCH plus ACQ/IMAGE

Action	Phase I (s)	Chapter 10 (s)	APT Time (s)	Comment
Initial guide star acquisition	360	360	333	Required at start of a new visit
NUV ACQ/SEARCH, MIRRORA, 3 × 3 pattern, 10 s exposure	420	116 + 169 + 9×(20+10) = 555	677	COS starts at G130M on OSM1, so move to NCM1 requires 116 s. OSM2 home position is G185M, so move to MIRRORA takes 169 s. 9 ACQ/SEARCH sub-exposures, so overhead includes 9 slews (20 s each) plus 9 exposures (10 s each)
First exposure overhead adjustment	N/A	-(116 + 169) = -285	-291	OSM1 and OSM2 movements may be hidden in guide-star acquisition.
NUV ACQ/IMAGE with 10 s exposure	180	120 + 2×10 + 58 = 198	139 + 58 (dump)	No OSM2 movement; ACQ/IMAGE setup, twice exp time, and memory readout
NUV G225M at 2250 Å, TIME-TAG, FP-POS=3, 1200 s exposure	300 + 1200	36 + 105 + 1200 + 116 = 1457	136 + 1200 + 116	Generic NUV TIME-TAG setup; change from MIRRORA to G225M (105 s); exp time; TIME-TAG memory readout
FUV G130M at 1309 Å, TIME-TAG, FP-POS=2, 300 s exposure	120 + 60 + 300	71 + 109 + 300 + 116 = 596	177 + 300 + 116	Generic FUV TIME-TAG setup; OSM1 move from NCM1 to G130M (109 s); exp time; TIME-TAG memory readout
FUV G130M at 1309 Å, TIME-TAG, FP-POS=4, 300 s exposure	120 + 300	71 + 6 + 300 + 116 = 493	69 + 300 + 116	Generic FUV TIME-TAG setup; increment FP-POS by 2 settings (6 s); exp time; TIME-TAG memory readout
Total science time	1800	1800	1800	
Total time used in orbit	3360	3374	3446	

9.7.3 FUV Acquisition plus TIME-TAG

In this example, we begin with an FUV ACQ/SEARCH, followed by ACQ/PEAKXD and ACQ/PEAKD, all with G130M, then change to G140L and SEGMENT=A for a set of FUV TIME-TAG exposures using FP-POS=ALL.

Table 9.8: Overhead Values for FUV Acquisition and FP-POS=ALL

Action	Phase I (s)	Chapter 10 (s)	APT Time (s)	Comment
Initial guide-star acquisition	360	360	333	Required at start of a new visit
FUV ACQ/SEARCH, G130M at 1309 Å, 3 × 3 pattern, 15 s exposure	420	9 × (20 + 15) = 315	443	COS starts from G130M 1309 Å on OSM1, so no initial move. 9 ACQ/SEARCH sub-exposures, so overhead includes 9 slews (20 s each) plus 9 exposures (15 s each)
First exposure overhead adjustment	N/A	0	-12	No instrument movements prior to first exposure in this example.
FUV ACQ/PEAKXD, G130M at 1309 Å, 25 s exposure	420	80 + 25 = 105	111 + 25	PEAKXD overhead; exp time
FUV ACQ/PEAKD, G130M at 1309 Å, 5 steps, 25 s exposure		5 × (20 + 25) + 39 = 264	293 + 39	5 slews plus 5 exposures; memory readout
FUV G140L at 1280 Å, TIME-TAG, FP-POS=ALL, SEGMENT=A, 268 s exposure	330[1] + 300 + 268	330 + 71 + 164 + 268+ 116 = 949	300 (reconfig) + 232 + 268 + 116	SEGMENT reconfiguration change; generic FUV TIME-TAG setup; OSM1 grating change (164 s); exposure time; TIME-TAG memory readout (note: FP-POS=1)
	120 + 268	71 + 3 + 268 + 116 = 458	69 + 268 + 116	Generic FUV TIME-TAG setup; change to FP-POS=2 (3 s); exp time; TIME-TAG memory readout
	120 + 268	71 + 3 + 268 + 116 = 458	69 + 268 + 116	Same as above, but with FP-POS=3
	120 + 268	71 + 3 + 268 + 116 = 458	69 + 268 + 116	Same as above, but with FP-POS=4
Total science time	1472	1472	1472	
Total time used in orbit	3262	3367	3507	

1. We include the 330 s required to shut off detector segment B (Table 9.5).

9.7.4 FUV TIME-TAG with BOA and Multiple FP-POS

In this example, we start with an NUV ACQ/IMAGE, followed by a switch to the FUV channel and a TIME-TAG science exposure using G160M, FP-POS=ALL, the BOA, and, as required with the BOA, FLASH=NO. The science exposure will be followed automatically by a 12-second wavecal (see Table 5.2). As required, we obtain two exposures with FP-POS=1 and 2. In the second orbit (not shown), we obtain exposures with FP-POS=3 and 4.

Table 9.9: Overhead Values for FUV TIME-TAG Using the BOA

Action	Phase I (s)	Chapter 10 (s)	APT Time (s)	Comment
Initial guide-star acquisition	360	360	333	Required at start of a new visit
NUV ACQ/IMAGE with 2 s exposure	180	116 + 169 + 120 + 4 + 58 = 467	410 + 58 (dump)	OSM1 starts at G130M, so move to NCM1 requires 116 s. OSM2 starts at G185M, so move to MIRRORA takes 169 s. Add 2 min ACQ/IMAGE setup, twice the exposure time, and memory readout.
First exposure overhead adjustment	N/A	-(116 + 169) = -285	-333	OSM1 and OSM2 movements may be hidden in guide star acquisition.
FUV G160M at 1600 Å, TIME-TAG, BOA, FLASH=NO, FP-POS=1, 1100 s exposure	300 + 1100	71 + 154 + 8 + 116 + 1100 + 116 = 1449	218 + 1100 + 116	Generic FUV TIME-TAG setup; change from NCM1 to G160M (154 s); aperture change from PSA to BOA (8 s); exp time; TIME-TAG memory readout
FUV G160M at 1600 Å, TIME-TAG, AUTO WAVECAL, WCA, FP-POS=1, 12 s exposure	120 + 12	71 + 10 + 12 + 116 = 209	76 + 12 + 40	AUTO WAVECAL inserted, since FLASH=YES is not allowed with BOA; generic FUV TIME-TAG setup; aperture change from BOA to WCA (10 s); exp time; TIME-TAG memory readout
FUV G160M at 1600 Å, TIME-TAG, BOA, FLASH=NO, FP-POS=2, 1100 s exposure	120 + 1100	71 + 3+ 10 + 1100 + 116 = 1300	73 + 1100 + 116	Generic FUV TIME-TAG setup; increment FP-POS (3 s); aperture change from WCA to BOA (10 s); exp time; TIME-TAG memory readout
FUV G160M at 1600 Å, TIME-TAG, AUTO WAVECAL, WCA, FP-POS=2, 12 s exposure	120 + 12	71 + 10 + 12 + 116 = 209	76 + 12 + 40	Another AUTO WAVECAL required as FP-POS has changed; again generic FUV TIME-TAG exposure setup; aperture change from BOA to WCA (10 s); exp time; TIME-TAG memory readout
Total science time in orbit 1	2200	2200	2200	
Total time used in orbit 1	3424	3709	3447	
Note: Two additional exposures, using FP-POS=3 and 4 in a second orbit, are not shown.				

9.7.5 FUV TIME-TAG with Modified BUFFER-TIME

In this example, we begin with an NUV ACQ/IMAGE exposure, then switch to the FUV channel for four long G130M exposures, one at each FP-POS position. We use a couple of tricks to maximize the exposure time. First, we shorten the BUFFER-TIME for the first exposure of each orbit as described in Section 5.4.1, which reduces the length of the memory read-out following the exposure from 116 to 40 seconds. Second, we extend the exposure times, pushing the final memory read-out of each orbit into the occultation period. Note that we do not use FP-POS=ALL, because that would generate four identical exposures; instead, we increment the FP-POS by hand.

Table 9.10: Overhead Values for FUV TIME-TAG with Modified BUFFER-TIME

Action	Phase I (s)	Chapter 10 (s)	APT Time (s)	Comment
Initial guide star acquisition	360	360	333	Required at start of a new visit
NUV ACQ/IMAGE with 10 s exposure	180	116 + 169 + 120 + 20 + 58 = 483	426 + 58	OSM1 starts at G130M, so move to NCM1 requires 116 s. OSM2 starts at G185M, so move to MIRRORA takes 169 s. Add 2 min ACQ/IMAGE setup, twice the exposure time, and memory readout.
First exposure overhead adjustment	N/A	-(116 + 169) = -285	-333	OSM1 and OSM2 movements may be hidden in guide star acquisition.
FUV G130M at 1327 Å, TIME-TAG, FP-POS=1, BUFFER-TIME=1210, 1310 s exposure	300 + 1310	109 + 71 + 1310 + 40 = 1530	177 + 1310 + 40	Move OSM1 from NCM1 to G130M (109 s); generic TIME-TAG set-up (71 s); exposure time; short TIME-TAG memory read-out (40 s)
TIME-TAG, FP-POS=2, BUFFER-TIME=1310, 1310 s exposure	120 + 1310	71 + 3 + 1310 + 116 = 1500	69 + 1310 + 116	Generic TIME-TAG set-up; move to FP-POS=2 (3 s); exp time; TIME-TAG memory readout
Total science time in orbit 1	2620	2620	2620	
Total time used in orbit 1	3580	3588	3506	
Guide star re-acquisition	240	240	222	Required at start of next orbit
TIME-TAG, FP-POS=3, BUFFER-TIME=1398, 1498 s exposure	120 + 1498	71 + 3 + 1498 + 40 = 1612	69 + 1498 + 40 - 5 (hidden)	As for FP-POS=2, but with short TIME-TAG memory read-out
TIME-TAG, FP-POS=4, BUFFER-TIME=1498, 1498 s exposure	120 + 1498	71 + 3 + 1498 + 116 = 1688	69 + 1498 + 116	As for FP-POS=2
Total science time in orbit 2	2996	2996	2996	
Total time used in orbit 2	3476	3540	3507	

CHAPTER 10:

Bright-Object Protection

In this chapter…

10.1 Introduction

Both the FUV XDL and the NUV MAMA detectors are subject to damage or destruction by excessive illumination. An excessive local count rate can permanently reduce the sensitivity of the affected detector region; the most likely causes are a bright spectral emission line (XDL or MAMA) or a bright source observed in direct imaging (MAMA). A global over-illumination of the detector can result in its loss. To protect the detectors, onboard software monitors the local and global count rates, shuttering the instrument in case of a local violation, and lowering the high voltage if a global count-rate violation is detected. The local rate is checked before an exposure is begun, while the global rate is monitored continuously during the exposure. Under certain circumstances, damage could result despite the onboard safety measures, and in any event lowering the high voltage will disrupt the *HST* schedule and operations. Therefore, all proposed COS observations must meet count-rate screening limits with safety margins to allow for uncertainties. COS is currently the only *HST* instrument to use UV detectors for target acquisitions; such acquisitions must be screened, as well. It is the responsibility of the observer to screen all proposed targets and fields during Phase II preparation, and of STScI to check and enforce these limits. The COS Bright Object Protection (BOP) policies and procedures are described in this chapter.

Table 10.1: COS Count Rate Screening Limits

Detector	Source type	Type of limit	Limiting count rate (counts/s)
FUV	predictable	global	15,000 per segment
		local	0.67 per pixel
	irregular	global	6,000 per segment
		local	0.67 per pixel
NUV	predictable	global	170,000 (imaging) or 30,000 per stripe (spectroscopic)
		local	50 per pixel[1] (imaging) or 70 per pixel (spectroscopic)
	irregular	global	68,000 (imaging) or 12,000 per stripe (spectroscopic)
		local	50 per pixel (imaging) or 70 per pixel (spectroscopic)

1. For imaging acquisitions, a count rate of 360 counts/s in the 9×9-pixel box surrounding the target (as computed by the COS Imaging Acquisition ETC) represents an equivalent safe upper limit.

10.2 Screening Limits

The global and local count-rate screening limits for each COS configuration are given in Table 10.1. The limits are independent of observing mode (TIME-TAG or ACCUM). Compliance with these limits must be checked for all proposed COS targets by means of the Exposure Time Calculator (ETC), which issues warnings if they are exceeded. In Phase I, all proposed targets must be screened against these limits. In Phase II, the results of more detailed target and field checks must be submitted with the observing proposal; details are provided in Section 10.6.

10.3 Screening versus Data-Rate Limits

It is useful to compare the BOP limits with the 30,000 counts/s limit on TIME-TAG exposures discussed in Section 5.2.1. In the FUV, a steep spectrum could exceed the BOP limit of 15,000 counts/s per detector segment without exceeding the TIME-TAG limit. In the NUV, the BOP limit is considerably higher; a target that is perfectly safe could be far too bright to observe in TIME-TAG mode.

10.4 Source V Magnitude Limits

In the following tables, the screening limits in Table 10.1 are converted into V magnitude limits for a variety of sources. These values are not meant to be a substitute for the ETC, but rather an indication of whether a given object may be near the limit. The most sensitive spectroscopic setting and lowest rate limit (global or local) determine the listed values. Stellar spectra are assumed to be unreddened. Table 10.2 corresponds to spectroscopy through the PSA, Table 10.3 through the BOA, and Table 10.4 to NUV imaging for both apertures.

Table 10.2: V Magnitude Limits for PSA Spectroscopy

Spectral Class	FUV			NUV			
	G130M	G160M	G140L	G185M	G225M	G285M	G230L
O5 V	14.7	14.0	15.1	10.1	9.5	8.7	12.5
O7 V	14.5	13.8	14.9	10.0	9.5	8.6	12.4
O9 V	14.2	13.6	14.7	9.9	9.4	8.5	12.3
B0 V	14.2	13.5	14.6	9.8	9.3	8.4	12.2
B1 V	13.8	13.1	14.3	9.4	9.0	8.2	11.9
B3 V	12.8	12.5	13.4	8.8	8.4	7.7	11.3
B5 V	12.0	11.9	12.7	8.3	8.0	7.4	10.8
B8 V	10.9	11.0	11.5	7.5	7.2	6.7	10.0
A1 V	8.5	8.9	9.3	6.4	6.2	5.8	9.0
A3 V	6.4	7.8	8.3	6.1	6.0	5.6	8.7
A5 V	2.9	6.9	7.3	5.8	5.8	5.5	8.5
F0 V	-0.1	4.9	5.7	4.8	5.2	5.2	7.8
F2 V	-1.2	4.0	5.0	4.5	5.0	5.2	7.6
F5 V	-3.4	1.9	3.2	3.7	4.4	5.0	7.3
F8 V	-4.8	0.5	2.0	3.2	4.1	4.8	7.1
G2 V (Solar)	1.8	-0.5	3.4	1.4	2.7	4.4	6.8
G8 V (Tau Ceti)	3.0	-0.4	4.7	0.5	2.2	3.9	6.4
K2 V (Epsilon Eri)	4.0	-0.1	5.8	-0.8	1.1	3.2	6.1
KM III (Eta Ser)	-1.5	-1.4	0.2	-0.7	1.0	2.9	5.7
KM III (Alpha Boo)	-0.8	-2.3	0.9	-3.1	-1.1	0.9	4.7
KM III (Gamma Aql)	-2.3	-4.5	-0.5	-5.4	-3.9	-2.3	3.8
KM III (HD 146051)	-3.1	-5.0	-1.4	-7.0	-5.1	-3.1	3.3
KM III (Alpha Cet)	0.2	-1.5	1.9	-4.2	-1.9	-1.0	3.3
KM III (HD 123023)	0.0	-1.0	1.6	-3.2	-1.2	-0.3	3.7
KM III (Beta Gru)	-0.2	-0.6	1.5	-2.9	-1.0	0.7	3.4
T~50000 Blackbody	14.6	14.0	15.0	10.1	9.5	8.6	12.5
$F_\lambda \sim \lambda^{-1}$	11.0	10.6	11.5	7.2	7.2	6.7	9.9
F_λ= const surface brightness	11.1	10.9	11.8	7.7	8.0	7.6	10.7
F_λ= const point source	9.3	9.2	10.0	6.0	6.3	5.9	9.0

Table 10.3: V Magnitude Limits for BOA Spectroscopy

Spectral Class	FUV			NUV			
	G130M	G160M	G140L	G185M	G225M	G285M	G230L
O5 V	9.4	8.5	9.8	4.6	3.8	2.8	6.9
O7 V	9.2	8.4	9.6	4.4	3.7	2.7	6.8
O9 V	9.0	8.2	9.4	4.3	3.6	2.7	6.7
B0 V	8.9	8.0	9.3	4.2	3.5	2.6	6.6
B1 V	8.5	7.7	9.0	3.9	3.3	2.4	6.2
B3 V	7.5	7.0	8.1	3.2	2.7	1.9	5.6
B5 V	6.7	6.5	7.4	2.7	2.2	1.5	5.1
B8 V	5.5	5.5	6.2	1.9	1.5	0.8	4.3
A1 V	3.1	3.4	3.8	0.8	0.4	-0.1	3.3
A3 V	1.0	2.2	2.8	0.5	0.2	-0.3	3.0
A5 V	-2.5	1.4	1.8	0.2	0.0	-0.4	2.8
F0 V	-5.6	-0.7	0.1	-0.8	-0.6	-0.7	2.0
F2 V	-6.7	-1.6	-0.6	-1.2	-0.8	-0.8	1.7
F5 V	-8.8	-3.7	-2.4	-2.0	-1.4	-1.0	1.4
F8 V	-10.2	-5.0	-3.6	-2.5	-1.7	-1.1	1.2
G2 V (Solar)	-3.6	-6.1	-1.9	-4.3	-3.1	-1.5	0.8
G8 V (Tau Ceti)	-2.3	-5.9	-0.6	-5.2	-3.6	-2.0	0.3
K2 V (Epsilon Eri)	-1.2	-5.6	0.5	-6.4	-4.7	-2.7	0.1
KM III (Eta Ser)	-6.9	-6.9	-5.2	-6.3	-4.8	-3.1	-0.4
KM III (Alpha Boo)	-6.1	-7.8	-4.4	-8.7	-6.9	-5.1	-1.3
KM III (Gamma Aql)	-7.6	-10.0	-5.9	-11.1	-9.7	-8.2	-2.2
KM III (HD 146051)	-8.5	-10.5	-6.8	-12.6	-10.9	-9.0	-2.8
KM III (Alpha Cet)	-5.1	-7.0	-3.4	-9.7	-7.7	-7.0	-2.8
KM III (HD 123023)	-5.4	-6.5	-3.7	-8.8	-7.0	-6.4	-2.3
KM III (Beta Gru)	-5.6	-6.1	-3.8	-8.6	-6.8	-5.2	-2.6
T~50000 Blackbody	9.3	8.5	9.7	4.5	3.7	2.8	6.9
$F_\lambda \sim \lambda^{-1}$	5.7	5.1	6.2	1.6	1.4	0.8	4.2
F_λ= const surface brightness	5.8	5.4	6.4	2.2	2.2	1.7	5.0
F_λ= const point source	4.1	3.7	4.6	0.5	0.5	0.0	3.3

Table 10.4: V Magnitude Bright-Object Limits for Imaging

Spectral Class	PSA+MirrorA	PSA+MirrorB	BOA+MirrorA	BOA+MirrorB
O5 V	19.2	16.3	13.5	10.7
O7 V	19.1	16.1	13.4	10.5
O9 V	19.0	16.0	13.3	10.4
B0 V	18.9	15.9	13.2	10.3
B1 V	18.6	15.6	12.9	10.0
B3 V	18.1	15.0	12.4	9.3
B5 V	17.6	14.5	11.9	8.9
B8 V	16.9	13.7	11.1	8.0
A1 V	15.8	12.6	10.1	6.9
A3 V	15.6	12.3	9.9	6.6
A5 V	15.3	12.0	9.6	6.2
F0 V	14.7	11.3	8.9	5.5
F2 V	14.4	11.0	8.6	5.2
F5 V	14.0	10.6	8.1	4.7
F8 V	13.7	10.3	7.8	4.4
G2 V (Solar)	13.0	9.6	7.1	3.7
G8 V (Tau Ceti)	12.6	9.1	6.6	3.2
K2 V (Epsilon Eri)	11.8	8.3	5.8	2.4
KM III (Eta Ser)	11.4	8.0	5.5	2.0
KM III (Alpha Boo)	9.6	6.1	3.6	0.2
KM III (Gamma Aql)	7.1	3.6	1.1	-2.3
KM III (HD 146051)	6.2	2.7	0.2	-3.3
KM III (Alpha Cet)	8.0	4.6	2.1	-1.3
KM III (HD 123023)	8.7	5.2	2.7	-0.7
KM III (Beta Gru)	8.9	5.5	3.0	-0.4
T~50000 Blackbody	19.2	16.2	13.5	10.6
$F_\lambda \sim \lambda^{-1}$	16.8	13.6	11.0	7.9
F_λ= const surface brightness	10.9	8.0	5.1	2.3
F_λ= const point source	15.8	12.6	10.1	6.9

10.5 Tools for Bright-Object Screening

10.5.1 The Bright Object Tool (BOT)

STScI has developed a Bright Object Tool (BOT) to facilitate field checking prior to COS program implementation. The BOT is implemented within APT (the Astronomer's Proposal Tool), using the Aladin interface, and reads target and exposure information from the proposal. Help files and training movies are available within APT. The BOT is based on displays of the Digital Sky Survey (DSS) and on automated analysis of the field using data from two catalogs: the second Guide Star Catalog (GSC2) and the *GALEX* catalog.

GSC2 provides two magnitudes (photographic J and F), hence one color, for most fields down to about magnitude 22, which, combined with conservative assumptions about spectral type vs. color, allow expeditious target and field checks. In some cases, the GSC2 is inadequate because of crowding or the absence of one filter. The APT/BOT automatically clears stars with only a single GSC2 magnitude if they are safe based on the assumption that the target is an unreddened O5. Any other unknown targets must be cleared by hand.

Automated *GALEX* screening is now available within the APT/BOT. The AIS (all-sky) sources are screened as unreddened O5 stars and reported as either safe, unsafe, or unknown. Because it is based directly on UV fluxes, *GALEX* screening can reveal, for example, previously unknown hot companions to late-type stars. If the field passes the BOT check, it is safe; unsafe and unknown objects require further investigation. ***Caveats:*** (1) The *GALEX* catalog does not cover the whole sky, so check that your field is fully covered. (2) *GALEX* fluxes represent upper limits in crowded regions because of the instrument's relatively low spatial resolution. (3) The *GALEX* detectors suffer local non-linear effects at high count rates. The fluxes and magnitudes in the current version of the *GALEX* catalog are not corrected for these effects and may be underestimated for the brightest stars. A preliminary correction is presented in Morrissey et al. (2007, ApJS, 173, 682). The BOT now applies this correction to the *GALEX* catalog. As a result, it may report *GALEX* magnitudes that are brighter than those given in the *GALEX* catalog itself.

In general, a COS pointing with unconstrained telescope orientation requires the clearance of a field 43 arcsec in diameter. If any displacements from the default pointing (*e.g.,* acquisition scans, POS TARGs, patterns, or mosaics) are specified, then the field to be cleared increases commensurately. Because both the PSA and BOA are exposed to the sky at all times, no unsafe or unknown star may fall within 7 arcsec of either aperture. The BOT automatically accounts for the reduced throughput of the BOA.

Note: Always check the science target with the ETC, rather than relying on the BOT field report. When constructing your Phase II proposal within APT, include the ETC exposure ID number to document your work and to facilitate the Phase II review.

10.5.2 The Exposure Time Calculator (ETC)

Should the tools available within the BOT be insufficient to clear a field object, its safety may be confirmed using the ETC.

An existing UV spectrogram of the target or class may be imported directly into the ETC. When using *IUE* data as input spectra in the ETC, consider only low-resolution spectra taken through the large aperture. Note that the ETC does not convolve imported spectra to the COS resolution. To be conservative, one must assume that the entire flux of an emission line falls within a single COS resolution element.

If model spectra are used in the ETC, the original Kurucz (not Castelli & Kurucz) models should be used for early-type stars. None of the provided models is adequate for late-type stars, since the models lack chromospheric emission lines; actual UV data must be used for them when possible. If a given star has only a V magnitude, it must be treated as an unreddened O5 star. If one color is available, it may be processed as a reddened O5 (which will always have a greater UV flux than an unreddened star of the same color).

If two colors are available, then the spectral type and reddening can be estimated separately. In some cases, the 2MASS JHK may be the only photometry available for an otherwise unknown star. The ETC supports direct entry of observed J and H magnitudes with E(B-V). It is also possible to estimate V and E(B-V) from those data on the assumption of a reddened O5 star, and thus determine its count rates in the ETC. Martins & Plez (2006, A&A, 457, 637) derive $(J-H)_0 = -0.11$ for all O stars and $(V-J)_0 = -0.67$, $(V-H)_0 = -0.79$ for early O types. (The K band should be avoided for BOP because of various instrumental and astrophysical complications.) Bessell & Brett (1988, PASP, 100, 1134), Appendix B, give relationships between the NIR reddenings and E(B-V).

10.6 Policies and Procedures

All COS exposures, whether target-acquisition, spectroscopic, or imaging, must be checked for bright objects. Any COS targets or fields that cannot be demonstrated to be safe to a reasonable level of certainty in the judgment of the contact scientist (CS) will not be observed. In that case, it is possible that equivalent alternative targets may be approved upon request. Any observations that trigger the onboard safety mechanisms will not be rescheduled.

Before the Phase II deadline, a COS GO must send to his/her CS the results of ETC calculations for each discrete target (the "ETC run #" is now a required field within APT), and reports on any unsafe or unknown stars from APT/BOT for each field, either showing that the observations are safe or documenting any unresolved issues. (An exception is moving-target fields, which cannot be cleared until the scheduling windows have been established.) It is not expected that all such issues will be resolved by the Phase II deadline, but they should at least be identified and have planned resolutions by then.

Light from a bright nearby source could scatter into the PSA. For example, a target that is safe for the BOA may scatter enough light into the PSA to violate our screening limits. The region of concern is an annulus extending 5 to 15 arcsec from the center of the PSA. Any field object falling in this annulus may not produce a global count rate in excess of 1×10^5 counts/s per segment for the FUV channel or 2×10^5 counts/s for the NUV, or a local count rate over 3.3 counts/s/pixel in the FUV or 250 counts/s/pixel in the NUV. At present, the APT/BOT does not search for such objects, so they must be checked by hand. In such cases, count rates must be estimated using the ETC as though the source were at the center of the PSA.

In worst cases, new ground-based data or *HST* CCD UV exposures may be required to clear the fields for BOP; in general, the latter must be covered by the existing Phase I time allocation.

For unsafe targets, one solution is to change to a less-sensitive instrument configuration: one could use the BOA, MIRRORB, or both (though the BOA reduces image quality; see Figure 8.2), a higher-resolution grating, or a less-sensitive wavelength setting. Note that the medium-resolution gratings actually have higher throughput than G140L when the data are rebinned, but are subject to brighter limits.

For unsafe field objects that threaten to fall into the non-target aperture, an orientation restriction (ORIENT) may be used to constrain the spacecraft roll angle and thus the position of the non-target aperture, but such constraints will limit the scheduling of the observation.

GOs planning COS observations of unpredictably variable targets, such as cataclysmic variables, should be aware of the special BOP procedures in effect for such cases. These include quiescence verification immediately preceding the COS observations, as detailed in ACS ISR 2006-04, which applies to all *HST* detectors subject to BOP. Observations of flare stars are allowed with COS (and STIS) only if the Contact Scientist is convinced that the target would not violate BOP limits even in its brightest state.

A pointing or configuration change after the targets and fields have been cleared by the STScI BOP review must be approved by the COS Team on the basis of a specific scientific justification and a new BOP review by the GO, which may be submitted via the CS.

10.7 On-Orbit Protection Procedures

Should an overly-bright object be observed with COS, on-board software will typically act to protect the instrument from damage. The most serious response is to reduce the high voltage of the affected detector; subsequent observations will not take place until COS undergoes a safe-mode recovery procedure that is run from the ground. Activating any of the instrument protection levels listed below is regarded as a serious breach of our health and safety screening procedures and is cause for an investigation. Observers are responsible for ensuring that their observations do not endanger the instrument.

FUV Bright Object Protection

There are five levels of protection for the COS FUV detector:

1. At the lowest level are the screening limits imposed on observers in order to provide a margin of safety for the instrument. The screening limits (Table 10.1) are set a factor of two or more below actual risk levels, and we expect observers to work with us to ensure these limits are adhered to. They are determined by estimating the expected count rate from an object, both globally over the detector and locally in an emission line if appropriate. The COS ETC is the tool used for this check.
2. At the next level, within COS the "Take Data Flag" (TDF) is monitored during an exposure. If an event occurs that causes the TDF to drop (such as loss of lock on a guide star, which could lead to the telescope's drifting), then the exposure will continue with the COS external shutter closed. Subsequent exposures in the visit may also be lost.
3. Next comes local rate monitoring. It is possible to permanently damage a localized region of the micro-channel plates without necessarily exceeding the global rate limits. This could occur if an object with bright emission lines were observed, for example. At the beginning of each exposure, the COS flight software bins the FUV spectrum by 4 pixels in x and 1024 in y; if the count rate in any bin exceeds 1000 counts per 15 seconds, the external shutter is closed and the calibration lamps turned off. All subsequent exposures until the next grating change or target acquisition are lost.
4. Global rate monitoring is next. The COS flight software continuously monitors the total event rate for both FUV detector segments. If the rate for either segment exceeds 600,000 counts in 10 seconds, the high voltage to both segments is turned off. Special commanding is required to turn on the FUV detector high voltage, so subsequent FUV observations will be lost, and the *HST* schedule will be disrupted.
5. At the highest level, the instrument is protected by software that senses an over-current condition in the high-voltage power supply; if triggered, the software shuts down the high voltage.

NUV Bright Object Protection

Similar protections also apply to the NUV detector:

1. At the lowest level are the screening limits imposed on observers to provide a margin of safety for the instrument. The screening limits (Table 10.1) are set a factor of two or more below actual risk levels, and we expect observers to work with us to ensure these limits are adhered to. They are determined by estimating the expected count rate from an object, both globally over the detector, and locally in an emission line if appropriate. The COS ETC is the tool used for this check.

2. At the next level, within COS the "Take Data Flag" (TDF) is monitored during an exposure. If an event occurs that causes the TDF to drop (such as loss of lock on a guide star, which could lead to the telescope's drifting), then the exposure will continue with the COS external shutter closed. Subsequent exposures in the visit may also be lost.
3. Next comes local rate monitoring. It is possible to permanently damage a small region of a micro-channel plate without exceeding the global rate limits. This could occur if an object with bright emission lines were observed, for example. Before each observation, the flight software takes a 0.3-second exposure, bins it in "superpixels" of 4×4 pixels each, and analyzes it in two passes. During the first pass, the flight software checks that each superpixel does not exceed the threshold values of 225 counts and 390 counts for imaging and spectroscopic observations, respectively. During the second pass, the software steps a box (of 1×2 superpixels for spectroscopic exposures and 2×2 pixels for imaging exposures) across the image, checking that the same limits are not exceeded in the larger area. The purpose of the second pass is to ensure that bright sources at the edge of the superpixels are not missed. This 0.3-second exposure is not recorded. If the local rate limit is exceeded, the COS flight software closes the external shutter and all subsequent exposures until the next grating change or target acquisition are lost.
4. Global rate monitoring is next. The COS flight software continuously monitors the total event rate for the NUV MAMA. If the total count rate exceeds 20,000 in 0.1 sec the high voltage to the MAMA is turned off, the external shutter is closed, and the calibration lamps are turned off. The NUV detector can resume operations only after a safe-mode recovery procedure, so subsequent NUV exposures will be lost, and the *HST* schedule disrupted.
5. At the highest level, the NUV MAMA is protected by the detector electronics. The Bright-Scene Detector (BSD) monitors the output of 2 of every 32 anode wires across the detector. The wires are parallel to the dispersion axis. If the total count rate exceeds 17,000 in 138 msec, then the high voltage is turned off. COS can resume operations only after a safe-mode recovery procedure. BSD differs from global-rate monitoring in two ways: it is done in hardware, not software, and what is measured is not a digitized count rate, but current in the anode grid wires.

CHAPTER 11:

Data Products and Data Reduction

In this chapter…

11.1 Overview

Raw COS data are processed through the STScI **OPUS** pipeline. Data first undergo Generic Conversion, by which bits from individual exposures are unpacked and combined into files containing raw, uncalibrated data. Next, the raw files are processed through the COS calibration pipeline, **calcos**, which performs image and spectroscopic reduction to produce output files useful for scientific analysis. Finally, the data are ingested into the Hubble Data Archive through the Data Archive and Distribution System (DADS). This system populates a database containing header keywords that is accessible to users via the Multimission Archive at STScI (MAST). Both calibrated and uncalibrated data are then available for distribution by MAST to the user.

11.2 COS Data Files

When data are taken in TIME-TAG mode (the default), the raw data are in the form of a table of photon events containing the arrival time, *x* and *y* pixel coordinates, and pulse height (for FUV data) for each photon detected. Raw `ACCUM` data are in the form of a 2-D image. For FUV data, there will be two raw files for each exposure, one file for segment A and one for segment B. For NUV data, there will be one raw file for each exposure.

The calibrated data have the same general format for both FUV and NUV, although there are differences in detail. There is a "corrtag" file (the file name contains the string "`corrtag`") containing a corrected events table. The corrtag table includes all of the columns from the raw data file, plus these additional columns: a weight that accounts for the flat-field and dead-time corrections, a data-quality column, and a column that gives the pulse-height amplitude of each event. (Codes for the DQ flags are listed on the COS Web page.) The corrtag file provides several sets of corrected pixel coordinates for each event. These include X[Y]CORR, which are corrected for thermal drifts in the detector electronics and geometric distortions in the detector; XDOPP, which are the *X* coordinates corrected for orbital Doppler motions; X[Y]FULL, which are the XDOPP and YCORR coordinates recast into a coordinate system defined by the WAVECAL spectrum; and WAVELENGTH, which provides the wavelength corresponding to the XFULL coordinate. The corrtag file has a separate extension containing timeline information. It provides second-by-second values for the spacecraft position, solar and target altitudes above the horizon, and count rates for the most prominent airglow lines and the background. The data in this extension can be useful when reprocessing TIME-TAG data, allowing the user to exclude, for example, data obtained during orbital day. For ACCUM data, the corrtag table has the same format, but all the values in the TIME column are a constant, half the exposure time. There is one row in this pseudo-TIME-TAG table for each count in the raw ACCUM image.

Additional calibrated files include the `flt` and `counts` images, which are created by binning the events in the corrtag table. Both images have units of counts/s, but the `flt` image may also be corrected for flat-field and dead-time effects. For spectroscopic data, a 1-D extracted spectrum (or three spectra, for NUV exposures) will be written to an `x1d` file for each exposure. For data in an association (whereby multiple exposures are processed together—the usual case), the 1-D spectra for separate exposures will be averaged and written to an `x1dsum` table. If multiple FP-POS settings are used, there will be one `x1dsum` file for each FP-POS (`x1dsum[1,2,3,4]`), even if only one spectrum was obtained at each position. The distinction between the x1d and x1dsum files in such cases is that the data-quality weights, the DQ_WGT column of the x1d files, are used to eliminate bad or suspect data (such as detector dead spots). The `x1dsum` file without a number is the final sum of all of the exposures. It can be a weighted mean of all the `x1dsum[n]` files or, if a single exposure was obtained at a single FP-POS setting, a copy of the `x1d` file with the DQ_WGTs applied.

By default, **calcos** will combine data taken at different FP-POS settings, but not at different central wavelengths. A new association is created when either the grating or central wavelength is changed, and **calcos** combines only data within an association. In early 2012, a version of **calcos** will be released that can combine data from multiple central wavelengths; to use it, one must modify the association table to include all of the data files to be combined. Another tool for combining spectra is the "splice" task in the `ctools` package of IRAF/PyRAF. This program was written for STIS data, but it can be run on COS data, though not all of the input columns will be preserved.

Wavelength calibration can be performed in either of two ways. The default (specified as FLASH=YES) is to take line-lamp exposures ("wavecal" exposures) simultaneously with the science data. In this case, the wavecal spectra will be extracted and saved in lampflash tables. The alternative is to take separate wavecal exposures interspersed with the science exposures. These wavecals will be calibrated in the same way as science exposures, except that the calibrated wavecal data (`corrtag`, `flt`, `counts`, `x1d`) will not be corrected for the offset of the spectrum from the template, and no `x1dsum` file will be created for a wavecal.

11.3 Additional COS Files

Several additional files are used in the processing of COS data. These include association files (`asn`), which are used to control calibration processing; engineering support files (`spt`), which contain information used in the pipeline processing; and lampflash files (`lampflash`), which contain extracted wavelength calibration spectra used in the processing of `TIME-TAG` data with `FLASH=YES`. For a full description of these and other files, see the *COS Data Handbook*.

CHAPTER 12:

The COS Calibration Program

In this chapter...

12.1 Introduction

In this chapter, we provide a brief overview of the calibration observations obtained during ground testing and on-orbit through Cycle 19. Potential Cycle 20 observers should assume that all of these calibrations will be completed by the time that Cycle 20 begins.

Observers wishing to use instrument configurations that are not addressed by these calibration plans should assess their specific calibration needs and include time in their Phase I proposal for any additional calibrations that are required. Proposers who believe that more extensive calibration observations or analysis may be of general benefit to the COS user community should consider submitting a Cycle 20 Calibration Outsourcing Proposal (see the Cycle 20 Call for Proposals for details).

12.2 Ground Testing and Calibration

The COS Instrument Definition Team (Principal Investigator, James Green, University of Colorado) was responsible for the ground testing and ground calibration of COS. Most of the ground test data was obtained in 2003 and 2006 during thermal vacuum testing at Ball Aerospace and Goddard Space Flight Center, respectively. These tests characterized the basic properties of the optics, the detectors, and the mechanisms. While some measurements (e.g., FUV full-detector flat-field images) cannot be repeated in orbit, most of the ground-test data have been superseded by on-orbit measurements obtained during SMOV4.

12.3 SMOV4 Testing and Calibration

The primary goal of the Observatory Verification program for Servicing Mission 4 (SMOV4) was the timely commissioning of *HST* for normal science operations. For the newly-installed COS, this included testing the focus (internal and external), verifying the target-acquisition procedures, monitoring instrument stability (both in terms of image motions and sensitivity), and measuring plate scales, line-spread functions, and other instrument parameters. SMOV4 observations were completed in 2009 October, and a series of Instrument Science Reports (ISRs) detailing the results of their analysis have been published. Those ISRs and the observing programs on which they are based are listed in Table 12.1.

Table 12.1: COS ISRs Resulting from SMOV Calibration Program

Number	Title	Author	Associated SMOV Programs
2009-01	Preliminary Characterization of the Post-Launch Line Spread Function of COS	Ghavamian et al.	11489, 11476
2010-01	SMOV Absolute Flux Calibration of the COS NUV Mode	Massa et al.	11479
2010-02	SMOV Absolute Flux Calibration of the COS FUV Modes	Massa et al.	11492
2010-03	COS Near-UV Flat Fields and High S/N Determination from SMOV Data	Ake et al.	11478, 11481
2010-04	SMOV: COS NUV On-Orbit Optical Alignment	Hartig et al.	11468, 11469
2010-05	SMOV: COS NUV Wavelength Calibration	Oliveira et al.	11470, 11474, 11475
2010-06	SMOV: COS FUV Wavelength Calibration	Oliveira et al.	11485, 11488, 11487
2010-07	SMOV: COS FUV Focus Determination	Lennon et al.	11484
2010-08	NUV Spectroscopic Performance	Beland & Ghavamian	11476, 11477
2010-09	FUV Spectroscopic Performance	Ghavamian et al.	11489, 11490
2010-10	SMOV: COS NUV Imaging Performance	Goudfrooij et al.	11473
2010-11	FUV Darks	Sahnow et al.	11356, 11482, 11484, 11895
2010-12	NUV Darks	Sahnow et al.	11355, 11466, 11894
2010-13	NUV/FUV Structural and Thermal Stability	Smith & Keyes	11480, 11493
2010-14	COS Target Acquisition Guidelines, Recommendations, and Interpretation	Keyes & Penton	11471, 11472, 11486

12.4 Cycle 17 Calibration Program

The Cycle 17 calibration program continued the testing begun during SMOV. It included long-term programs to monitor the sensitivity and wavelength scale of both the NUV and FUV detectors. Midway through Cycle 17, additional calibration programs were added. Brief descriptions of these programs are presented in Table 12.2. A comprehensive review of the Cycle 17 calibration program will be published in an upcoming ISR (Osten et al. 2011).

Table 12.2: Cycle 17 Calibration Program

Program ID	Title	Accuracy Achieved	Products
11891	NUV MAMA Fold Distribution	< 5% in peak of fold distribution	None
11894	NUV Detector Dark Monitor	0.2% in global dark-rate uncertainty	ISR, Reference file
11895	FUV Detector Dark Monitor	0.1% in global dark-rate uncertainty	ISR, Reference file
11896	NUV Spectroscopic Sensitivity Monitor	min S/N of 30 per resel at λ_{cen}	COS ISR 2010-15, Reference file
11897	FUV Spectroscopic Sensitivity Monitor	S/N per resel of 30 at λ_{cen} for G140L and G130M; S/N ~ 23 for G160M	COS ISR 2010-15, Reference file
11899	NUV Imaging Sensitivity	S/N ~ 60, observed to predicted count-rate accuracy of ±1%	ISR, Reference file
11900	NUV Internal/External Wavelength Scale Monitor	7.2 to 15.5 pixel wavelength zero-point accuracy	ISR, Reference file
11997	FUV Internal/External Wavelength Scale Monitor	wavelength zero-point accuracy of 5.7-7.5 pixels for G130M, 5.8-7.2 for G160M, 7.5-12.5 for G140L	Calibration Workshop paper, Reference file
12010	COS FUV Line Spread Function Characterization	Continuum S/N = 9.2 near 1530 Å	COS ISR 2009-01, tables of LSF models
12052	COS NUV Grating Efficiency Test	Few percent uncertainty in count-rate ratios	Calibration Workshop paper, ISR
12080	G140L Focus Sweep	30% uncertainty in autocorrelation FWHM of spectra	ISR
12081	COS Flux Calibration Below 1150 Å with G140L/1280	3% for 900-1150 Å, 10% for 300-700 Å	ISR, Reference file
12082	Extending COS/ G130M Coverage Down to 905 Å with Two New Central Wavelengths	wavelength scale: ± 0.5 Å, sensitivity: ± 5-10%, resolution: 20-30%	ISR, Reference file
12083	G140L/1280 Wavecal Template	N/A	Reference file
12084	G140L/1280 Internal-to-External Wavelength Scales	7.5-12.5 pixel wavelength zero-point accuracy	Reference file
12085	STIS/E230M Data to Determine Internal-to-External Offsets in COS/G230L	Unknown	Reference file
12086	Generation of 1-D Fixed-Pattern Templates	2%	Reference file, ISR
12096	COS FUV Detector Lifetime Position Test	min S/N per resel of 30 at λ_{cen}	ISR

12.5 Cycle 18 Calibration Program

The Cycle 18 calibration program continued the calibration and monitoring observations performed in Cycle 17, including long-term programs to monitor the sensitivity and wavelength scale of both the NUV and FUV detectors. Brief descriptions of these programs are presented in Table 12.3.

Table 12.3: Cycle 18 Calibration Program

Program ID	Title	Desired Accuracy	Products
NUV Monitors			
12419	NUV MAMA Fold Distribution	< 5% in peak of fold distribution	
12420	NUV Detector Dark Monitor	< 5%	ISR, Reference file
12421	NUV Spectroscopic Sensitivity Monitor	S/N = 30 at λ_{cen}	ISR, Reference file
12422	NUV Internal/External Wavelength Scale Monitor	Wavelength zero-point accuracy to a few pixels	ISR, Reference file
FUV Monitors			
12423	FUV Detector Dark Monitor	few counts per exposure	ISR, Reference file
12424	FUV Spectroscopic Sensitivity Monitor	S/N = 30 at λ_{cen}	ISR, Reference file
12425	FUV Internal/External Wavelength Scale Monitor	Wavelength zero-point accuracy to a few pixels	ISR, Reference file
Special Programs			
None[1]	COS Observations of Geocoronal Lyman α Emission	G140L: S/N =2 per pixel at 1200 Å, G130M: S/N = 2 per pixel at 1213 Å	List of exposures on the COS Web site that GOs may use to model and subtract Ly α
12426	FUV Sensitivity Characterization	1% over 2 Å bands	ISR, Reference file
12432	COS FUV Detector Gain Sag vs. High Voltage	1% over 2 Å bands	Decision on change of voltage or lifetime position

1. Coordinated parallel with a STIS calibration program.

12.6 FUV Lifetime Position Calibration Program

As described in Section 4.1.6, gain sag is beginning to affect spectra obtained with the FUV detector. To address this problem, the COS team is exploring the possibility of moving the Aperture Mechanism so that FUV spectra fall on a different part of the detector, called a lifetime position. This work is divided into three phases. Table 12.4 lists the programs that will be used to determine the location of the new lifetime position, enable science at that location, and finally calibrate observations obtained there.

Table 12.4: Lifetime Position Calibration Program

I. Identify the New Lifetime Position
12676 - COS/FUV Characterization of Detector Effects
12677 - COS/FUV Mapping of the Stray PtNe Light through FCA
12678 - COS/FUV Characterization of Optical Effects
COS/NUV Mapping of Stray Light through the FCA
COS/NUV Characterization of Optical Effects on Spectra
COS/NUV Characterization of Optical Effects on Imaging
II. Enable Science at the New Lifetime Position
COS/FUV High Voltage Sweep to Maximize Lifetime
COS/NUV and FUV Target Acquisition Algorithm Updates
COS/FUV Focus Sweep
III. Calibrate the New Lifetime Position
COS/FUV Wavelength Calibration and Lamp Template Spectra
COS/FUV Flux Calibration, Flat Fielding, and Bad Pixel Regions
COS/FUV Spectral and Spatial Resolution

Phase I is currently underway (Cycle 18). Program IDs have been assigned to the FUV programs; the NUV programs are still under development. Phases II and III will take place during Cycle 19.

12.7 Cycle 19 Calibration Program

The Cycle 19 calibration program, currently under development, will continue the routine calibration and monitoring observations performed in Cycle 18. The draft Cycle 19 calibration programs, together with two approved GO calibration programs to develop new short-wavelength observing modes, are listed in Table 12.5.

Table 12.5: Cycle 19 Calibration Programs

NUV MAMA Fold Distribution
NUV Detector Dark Monitor
NUV Flat Field Monitor
NUV Spectroscopic Sensitivity Monitor
NUV Internal/External Wavelength Scale Monitor
NUV Detector Recovery after Anomalous Shutdown
FUV Detector Dark Monitor
FUV Spectroscopic Sensitivity Monitor
FUV Internal/External Wavelength Scale Monitor
FUV Detector Recovery after Anomalous Shutdown
COS Observations of Geocoronal Lyman α Emission
12501 - COS G140L CENWAVE=800: A Gapless Low-Astigmatism Mode for Observations to the Lyman Limit
12505 - COS Observations below 1150 Å with R > 10,000: Calibrations for a New G130M/1222 Central Wavelength

12.8 Cycle 20 Calibration Plans

The Cycle 20 calibration plans for COS will continue the routine calibration and monitoring observations performed in Cycles 17–19. The priorities assigned to the calibration of various COS modes will be determined by the approved GO programs in each cycle.

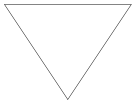

If your program requires calibrations beyond those beyond those described here, then you should explicitly include this calibration in your Phase I proposal.

CHAPTER 13:

Spectroscopic Reference Material

In this chapter...

13.1 Introduction

The information in this chapter will help you to select a detector, grating configuration, and observing aperture and to develop your observing plan. For each grating, the following information is provided:

- A brief description of the grating, with special considerations for its use.
- Grating parameters, including the dispersion and plate scale.
- Plots showing the available central-wavelength settings and the range of wavelengths covered by each setting and (for the FUV gratings) `FP-POS` position.
- Plots and tables of sensitivities and effective areas as a function of wavelength.
- Plots of signal-to-noise ratio as a function of STMAG, F_λ, and exposure time.

Note that the quoted sensitivities are estimates for mid-Cycle 20 (2013 April). The COS Exposure Time Calculator (ETC) will be updated as the instrument's sensitivity continues to evolve. See the COS Web site for the latest information.

13.2 Using the Information in this Chapter

13.2.1 Grating Parameters

For each grating, the resolving power and dispersion are taken from Table 5.1. Plate scales are derived from data obtained during SMOV.

13.2.2 Wavelength Ranges

For each grating, we plot the wavelengths sampled by each central-wavelength setting. For the NUV gratings, the central wavelength is the approximate midpoint of stripe B. For the FUV gratings, the central wavelength is (approximately) the shortest wavelength recorded on segment A. Wavelength ranges for each central wavelength at `FP-POS=3` are provided in tabular format in Table 5.4 and Table 5.5.

For the FUV gratings, the wavelength ranges sampled at each `FP-POS` position are plotted separately. For the NUV gratings, the total wavelength range sampled by all `FP-POS` positions is plotted for each central-wavelength setting.

13.2.3 Grating Sensitivities and Effective Areas

This section presents sensitivities and effective areas as a function of wavelength for each grating. The target is assumed to be a point source centered in the PSA. For both the FUV and NUV detectors, the total systemic[1] *spectroscopic point-source sensitivity,* S^p_λ, has units of counts pix_λ^{-1} sec^{-1} per incident erg cm^{-2} sec^{-1} $Å^{-1}$, where

- pix_λ = a pixel in the dispersion direction, and
- counts refer to the total counts from a point source integrated over the PSF in the direction perpendicular to the dispersion.

The count rate per pixel is simply the product of the target flux and the point-source sensitivity at a given wavelength. To estimate the S/N ratio achieved at a given count rate and exposure time, follow the directions in Section 7.3 or use the S/N plots in this chapter.

The effective area has units of cm^2.

13.2.4 Signal-to-Noise Plots

For each grating, a plot is provided to help you estimate the signal-to-noise ratio (S/N) that can be achieved from a point source observed at a fiducial wavelength near the peak of the effective-area curve. The fiducial wavelength is indicated in the ordinate label of each plot. To estimate S/N at other wavelengths, scale your source flux or magnitude by the relative sensitivities at the wavelength of interest and at the fiducial. The plots show S/N as a function of F_λ and of STMAG for a range of

1. COS plus *HST* Optical Telescope Assembly (OTA).

exposure times. $STMAG_\lambda$ is the color-dependent correction from V magnitude to STMAG at wavelength λ. Values of $STMAG_\lambda$ for various stellar and extragalactic sources are presented in Table 13.1 and Table 13.2, respectively. In producing these plots, we assumed an average sky background (as described in Chapter 7) and the dark current appropriate for each detector. These plots should be used only for rough estimates of exposure times. When constructing your proposal, use the COS Exposure Time Calculator (ETC) to estimate S/N values.

Note the following:

- The point source S/N has been calculated per resolution element and has been integrated over the PSF to contain all of the flux in the cross-dispersion direction.
- The symbols in the S/N figures delineate regions of parameter space where the dark current contributes more than half the source counts.
- The vertical shaded area indicates the bright-object screening limit given in Table 10.1.

Follow these steps to use the S/N plots:

1. Look up in Table 13.1 the effective temperature and wavelength region of interest (e.g., 5000 K @ 2000 Å). Interpolate in the table to get $STMAG_\lambda$.
2. Add the V magnitude of the target to get STMAG.
3. Find the appropriate plot for the desired grating and locate STMAG on the horizontal axis. Read off the S/N for the desired exposure time, or vice-versa. Alternatively, use F_λ directly on the horizontal axis.
4. To get accurate values for repeated or `FP-POS` exposures, use the sub-exposure time when consulting the plot, and then multiply the resulting S/N by $\sqrt{N}$, where N is the number of sub-exposures to be averaged.

For example, consider a V=15 star of spectral type B0 V, for which we want to derive the S/N achieved in a 100 sec exposure using the NUV grating G230L. The S/N calculations for G230L are presented in Figure 13.27, where we learn that the fiducial wavelength for this grating is 3000 Å. Assuming an effective temperature of 30,000K, we obtain $STMAG_\lambda \sim -2.1$ at 3000 Å from Table 13.1, making STMAG = 12.9. Returning to Figure 13.27, we find this value on the horizontal axis. For an exposure time of 100 seconds, the S/N ~ 9.5.

Table 13.1: STMAG$_\lambda$ as a Function of Wavelength for Stellar Objects

Temp (K)	Wavelength (Å)									
	1000	**1200**	**1500**	**2000**	**2500**	**3000**	**3500**	**4000**	**4500**	**5000**
45000	-5.87	-5.46	-4.79	-3.87	-3.02	-2.36	-1.76	-1.27	-0.79	-0.37
30000	-5.38	-4.92	-4.37	-3.50	-2.70	-2.13	-1.56	-1.23	-0.76	-0.35
20000	-3.90	-3.38	-3.45	-2.73	-2.14	-1.66	-1.18	-1.13	-0.72	-0.33
15000	-1.68	-1.24	-2.68	-2.08	-1.53	-1.21	-0.83	-1.05	-0.68	-0.31
10000	9.18	6.27	-0.72	-0.68	-0.26	-0.21	-0.03	-0.88	-0.62	-0.29
9000	12.84	8.67	1.81	-0.19	0.15	0.05	0.16	-0.75	-0.58	-0.26
8000	17.10	11.79	6.33	0.51	0.58	0.21	0.24	-0.56	-0.46	-0.20
7000	20.97	15.07	9.29	1.86	1.26	0.36	0.24	-0.34	-0.32	-0.12
6000	N/A	19.44	14.17	5.50	2.92	0.94	0.47	0.02	-0.15	-0.04
5000	N/A	N/A	20.15	9.80	6.24	2.74	1.24	0.50	0.04	0.10
4000	N/A	N/A	N/A	14.74	9.70	5.53	2.37	0.97	0.24	0.58
3000	N/A	N/A	N/A	17.85	11.46	5.69	2.22	0.71	0.25	0.82

Table 13.2: STMAG$_\lambda$ as a Function of Wavelength for Non-Stellar Objects

Spectrum	Wavelength (Å)							
	1500	**2000**	**2500**	**3000**	**3500**	**4000**	**4500**	**5000**
Elliptical	3.35	3.19	4.17	2.92	1.60	0.70	0.17	0.15
S0	4.63	3.95	3.27	2.23	1.61	0.71	0.18	0.13
Sa	2.64	2.27	2.39	1.78	1.31	0.36	0.12	0.07
Sb	1.70	2.59	2.04	1.32	1.12	0.43	0.17	0.10
Sc	-0.18	0.44	-0.17	-0.68	-0.67	-0.51	-0.44	-1.25
Starburst, E(B-V)<0.1	-1.71	-1.15	-0.68	-0.43	-0.13	-0.42	-0.23	-1.24
Starburst, 0.25 < E(B-V) < 0.35	-0.95	-0.87	-0.33	-0.10	0.08	-0.19	-0.19	-0.28
Starburst, 0.51 < E(B-V) < 0.60	-0.40	-0.18	0.01	0.23	0.03	-0.14	-0.12	-0.36
Starburst, 0.61 < E(B-V) < 0.70	0.05	0.31	0.31	0.15	0.27	-0.17	-0.13	-0.11

The STMAG$_\lambda$ values of Table 13.1 are derived from the stellar models of Castelli and Kurucz (2003, 2004), assuming solar metallicity ([Fe/H] = 0.0) and a surface gravity log (g) = 4.5. The STMAG$_\lambda$ values of Table 13.2 are based on observed spectra of each object type.

13.3 Gratings

For each COS grating, we present the resolving power, dispersion, plate scale, the wavelength range covered at each central wavelength setting and `FP-POS` position, sensitivities, effective areas, and a tool for estimating S/N. Advice on use is provided where appropriate.

Note that the quoted sensitivities are estimates for mid-Cycle 20 (2013 April). The COS Exposure Time Calculator (ETC) will be updated as the instrumental sensitivity evolves.

Wavelengths in this handbook and in COS data products are always measured in vacuum.

Gratings:

FUV Grating G130M

Description

The G130M grating samples wavelengths between about 1150 and 1450 Å. (Its use at shorter wavelengths is discussed below.) It offers higher resolution and effective area than the G140L grating, but less spectral coverage.

Special Considerations

The gap between segments A and B spans 14.3 Å. To fill this gap requires exposures separated by two central-wavelength settings.

Grating	Resolving Power $R = \lambda/\Delta\lambda$	Dispersion (mÅ pixel^{-1})	Plate Scale (milliarcsec pixel^{-1})		FP-POS Step (Å step^{-1})
			Disp. Axis	Cross-Disp. Axis	
G130M	16,000 - 21,000	9.97	22.9	100	2.5

Figure 13.1: Wavelength Ranges for the G130M Grating

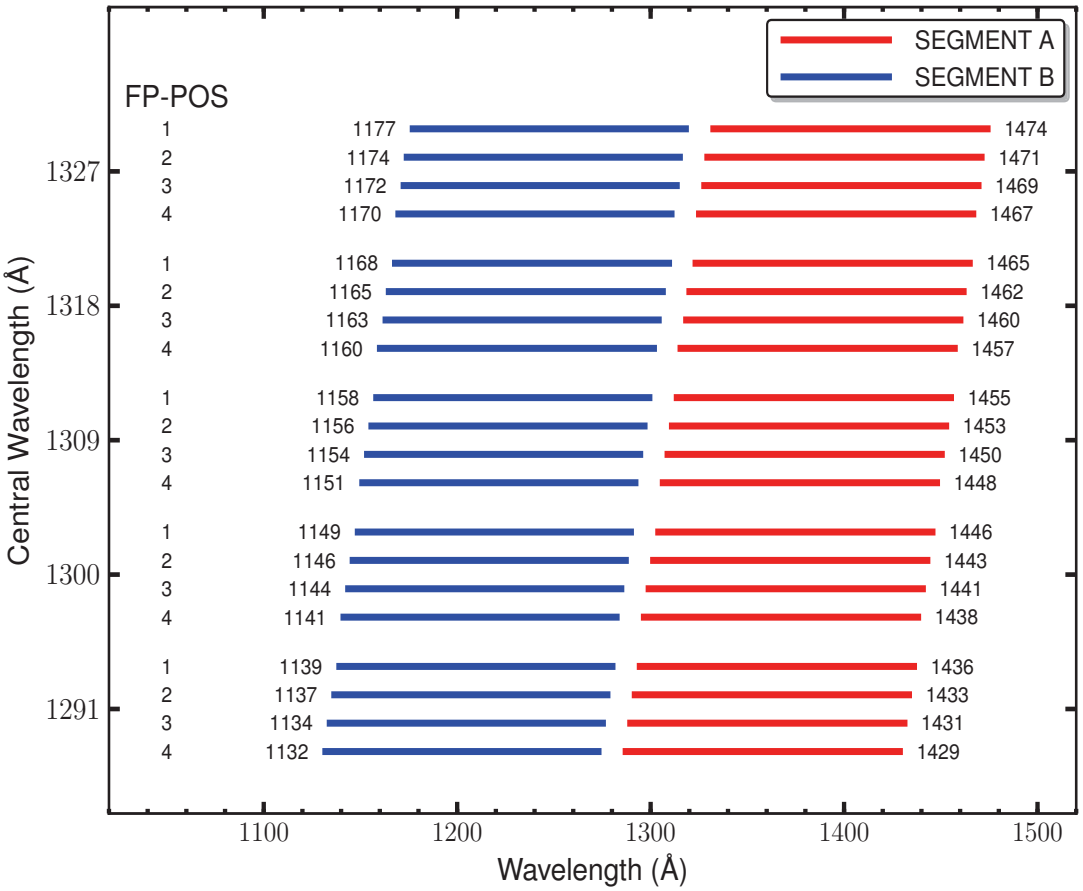

G130M Point-Source Sensitivity

Table 13.3: G130M Point-Source Sensitivity for PSA

Wavelength (Å)	Throughput	Sensitivity (counts pixel^{-1} sec^{-1} per erg cm^{-2} sec^{-1} Å^{-1})	Effective Area (cm^2)
1150	3.230E-02	8.4E+11	1.46E+03
1200	4.530E-02	1.2E+12	2.05E+03
1250	5.643E-02	1.6E+12	2.55E+03
1300	5.235E-02	1.5E+12	2.37E+03
1350	4.406E-02	1.3E+12	1.99E+03
1400	3.814E-02	1.2E+12	1.73E+03
1450	2.917E-02	9.6E+11	1.32E+03

Figure 13.2: G130M Point-Source Sensitivity for PSA and BOA

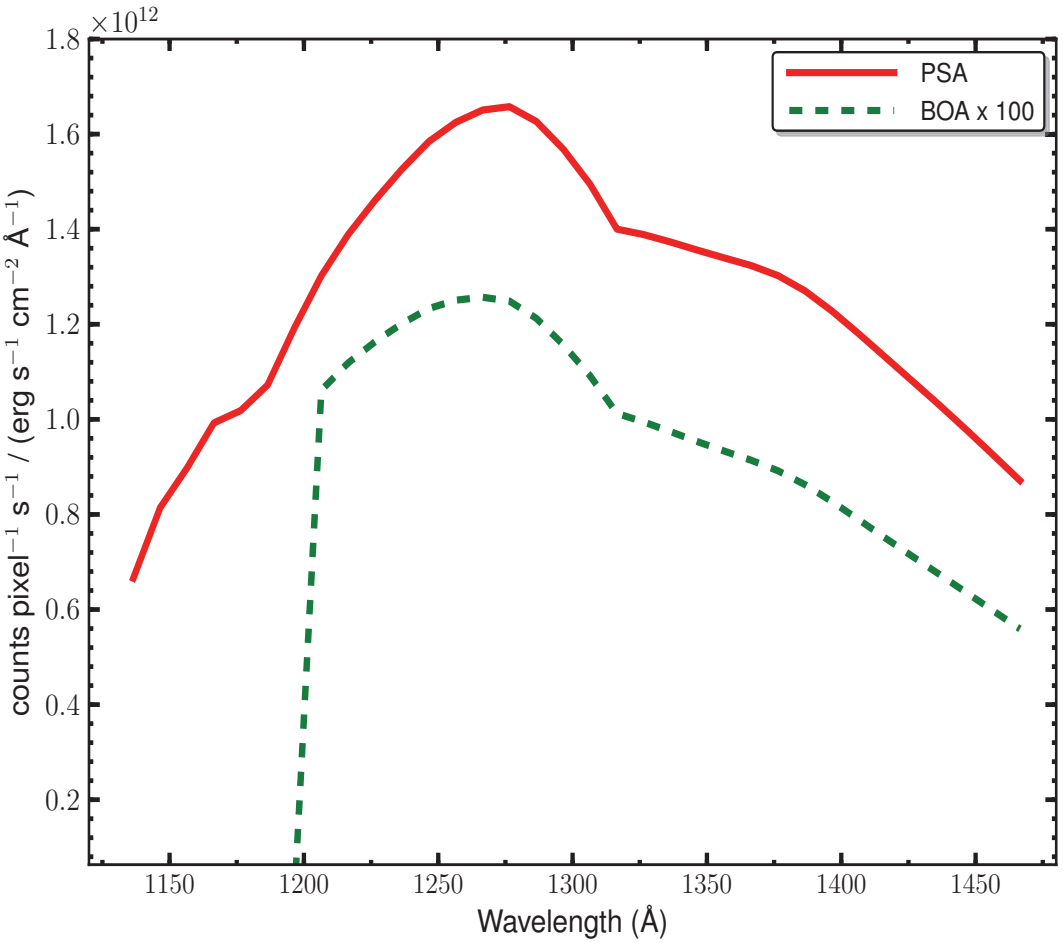

The throughput of the BOA is poorly characterized below 1200 Å and close to zero below 1150 Å.

G130M Signal-to-Noise Ratio

Figure 13.3: Point-Source Signal-to-Noise as a Function of STMAG for G130M at 1310 Å

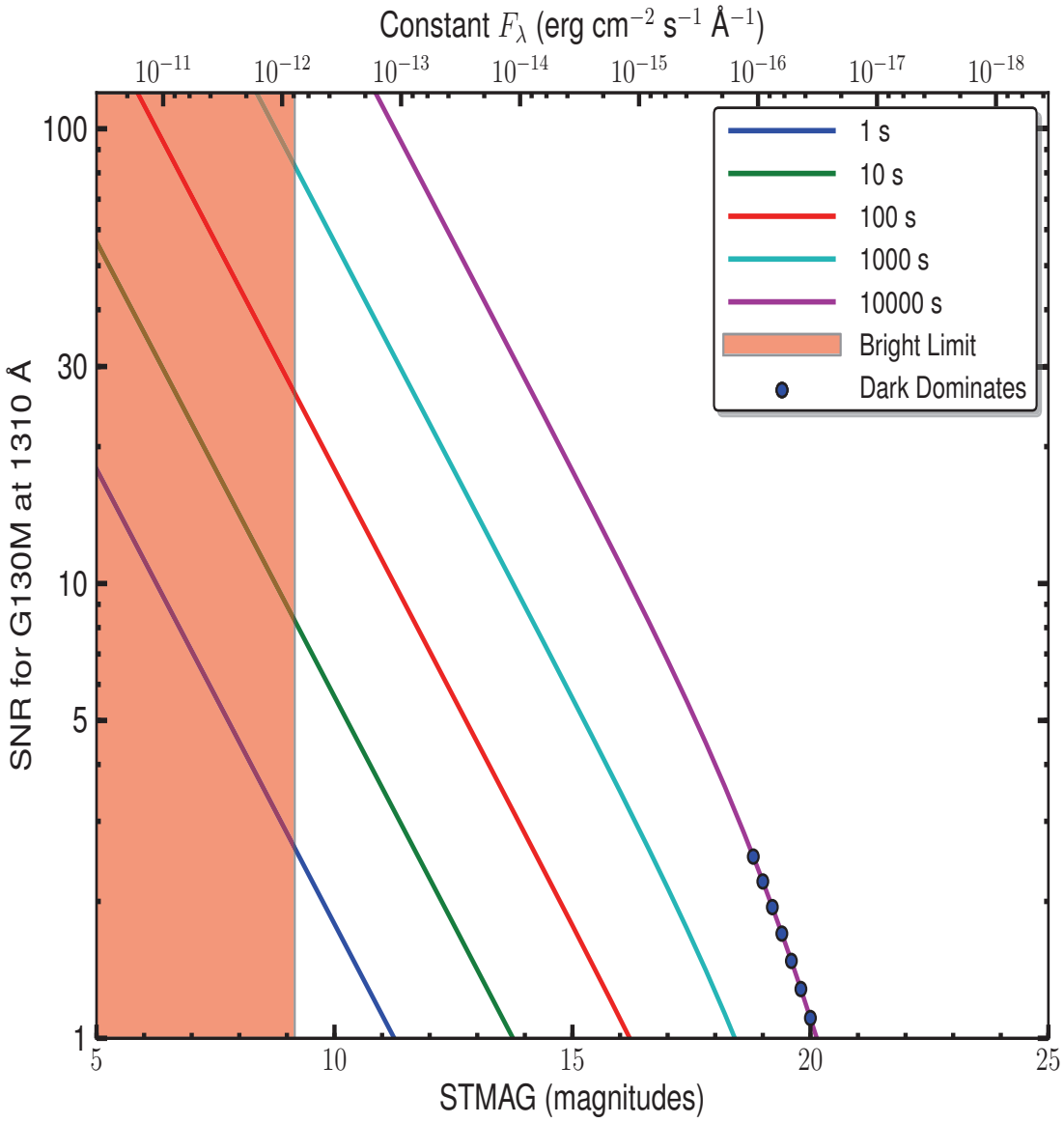

The top axis displays constant F_λ values corresponding to the STMAG units (V+STMAG$_\lambda$) on the bottom axis. Recall that STMAG=0 is equivalent to F_λ = 3.63E-9 erg cm^{-2} s^{-1} Å^{-1}. Colors refer to exposure times in seconds. The edge of the shaded area corresponds to the bright-object screening limit. Use of the PSA is assumed.

FUV Grating G130M with CENWAVE=1222

Description

When used with a central wavelength of 1222 Å, grating G130M samples wavelengths between about 1065 and 1365 Å with a resolving power R > 10,000. Its sensitivity is comparable to that of other G130M modes and considerably higher than G140L. Preliminary measurements indicate that the resolving power of this mode is R > 13,000 at 1135 Å and R > 10,000 at 1340 Å, but this is a lower limit; predicted values exceed 14,000 at 1065 Å and 17,000 at 1135 Å.

Special Considerations

A key advantage of this observing mode is that it places the Lyman α airglow line in the gap between detector segments A and B, eliminating this source of damaging high-intensity flux.

Grating	Resolving Power $R = \lambda/\Delta\lambda$	Dispersion (mÅ pixel^{-1})	Plate Scale (milliarcsec pixel^{-1})		FP-POS Step (Å step^{-1})
			Disp. Axis	Cross-Disp. Axis	
G130M	13,000 - 10,000	9.97	22.9	100	2.7

Figure 13.4: Wavelength Ranges for the G130M/1222 Mode

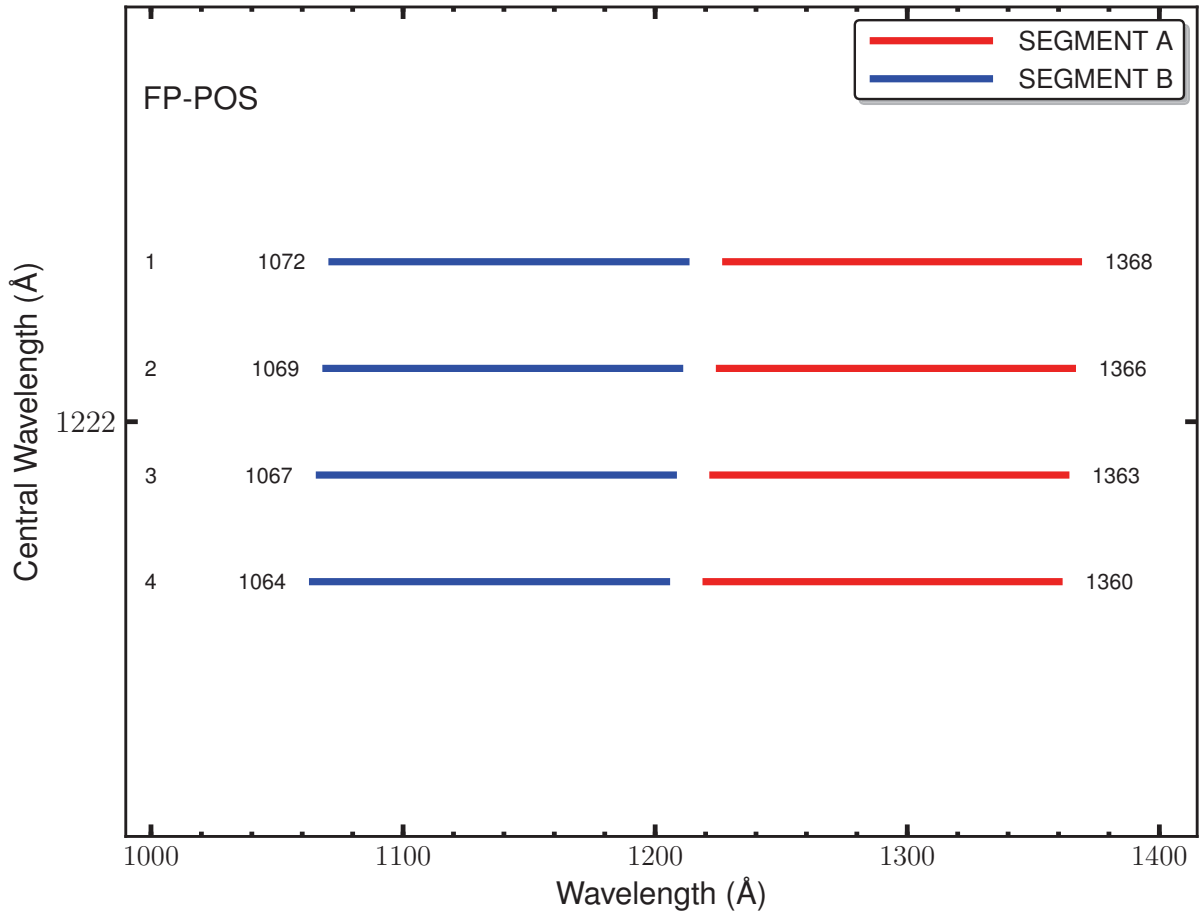

G130M/1222 Point-Source Sensitivity

Table 13.4: G130M/1222 Point-Source Sensitivity for PSA

Wavelength (Å)	Throughput	Sensitivity (counts pixel^{-1} sec^{-1} per erg cm^{-2} sec^{-1} Å^{-1})	Effective Area (cm^2)
1067	7.456E-04	1.8E+10	3.37E+01
1100	7.474E-03	1.9E+11	3.38E+02
1150	4.064E-02	1.1E+12	1.84E+03
1200	4.627E-02	1.3E+12	2.09E+03
1250	5.013E-02	1.4E+12	2.27E+03
1300	4.819E-02	1.4E+12	2.18E+03
1350	4.065E-02	1.2E+12	1.84E+03

Figure 13.5: G130M/1222 Point-Source Sensitivity for PSA

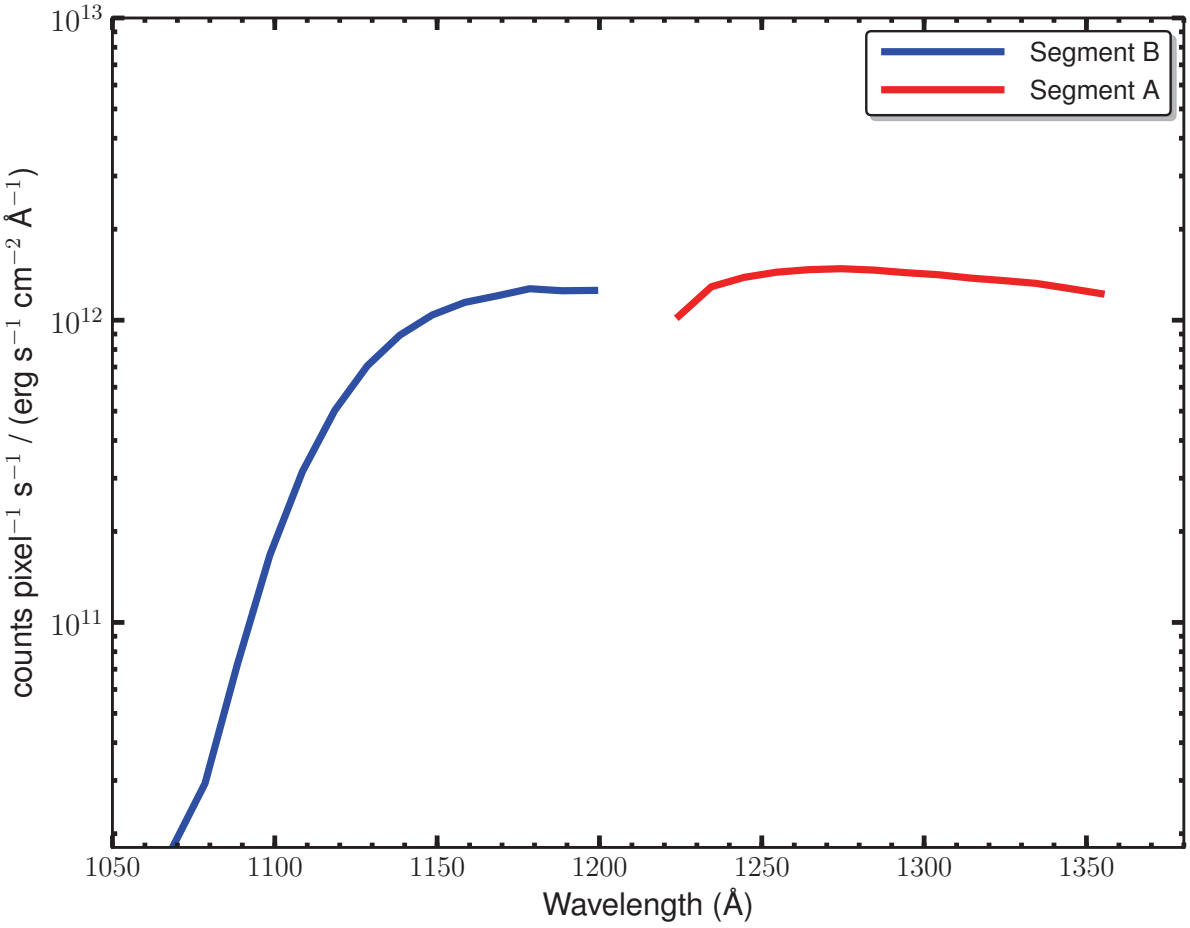

The sensitivity through the BOA is not shown, as its MgF_2 filter is opaque at wavelengths $\lambda < 1150$ Å.

G130M/1222 Signal-to-Noise Ratio

Figure 13.6: Point-Source Signal-to-Noise as a Function of STMAG for G130M at 1135 Å

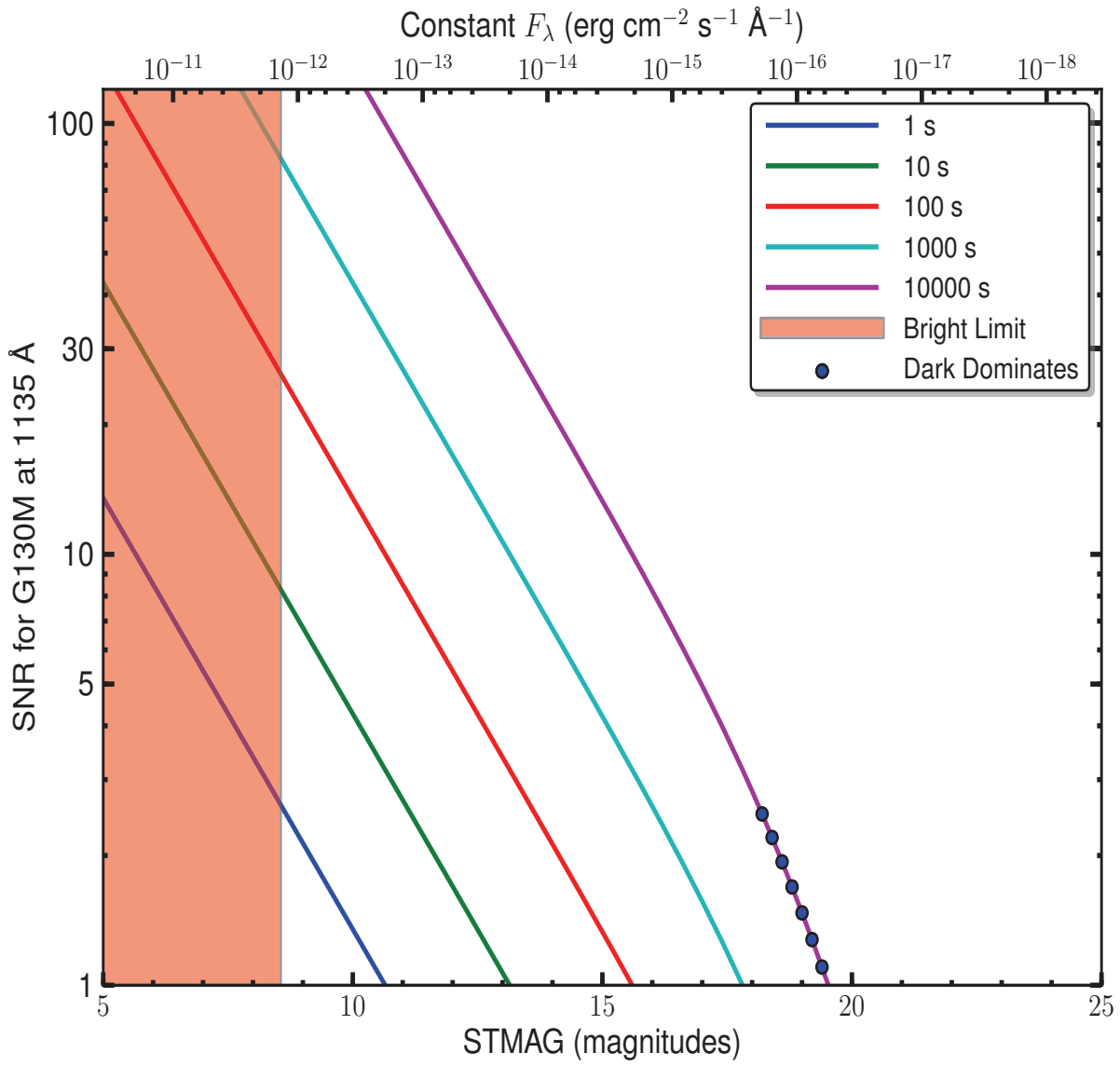

The top axis displays constant F_λ values corresponding to the STMAG units (V+STMAG$_\lambda$) on the bottom axis. Recall that STMAG=0 is equivalent to F_λ = 3.63E-9 erg cm^{-2} s^{-1} Å^{-1}. Colors refer to exposure times in seconds. The edge of the shaded area corresponds to the bright-object screening limit. Use of the PSA is assumed.

FUV Grating G130M with CENWAVE=1055 or 1096

Description

When used with a central wavelength of 1055 or 1096 Å, grating G130M samples wavelengths between about 900 and 1200 Å. Its resolution and effective area are higher than those of the G140L grating, but lower than those of G130M when used at longer central wavelengths.

Special Considerations

The COS sensitivity rises steeply between 1070 and 1150 Å. To observe bright targets near the Lyman limit, turn off detector segment A and use only segment B.

Grating	Resolving Power $R = \lambda/\Delta\lambda$	Dispersion (mÅ pixel^{-1})	Plate Scale (milliarcsec pixel^{-1})		FP-POS Step (Å step^{-1})
			Disp. Axis	Cross-Disp. Axis	
G130M	3000 - 1000	9.97	22.9	100	2.5

Figure 13.7: Wavelength Ranges for the G130M/1055 and 1096 Modes

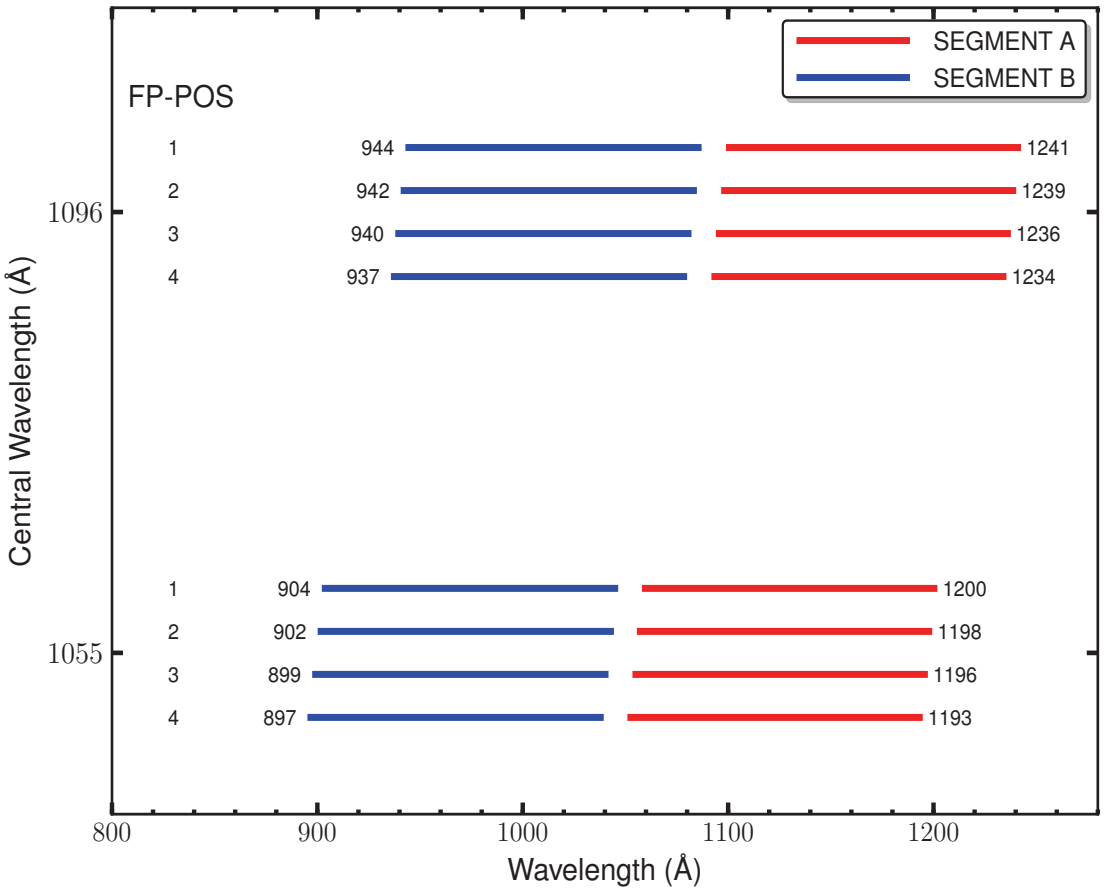

G130M/1055 and 1096 Point-Source Sensitivity

Table 13.5: G130M/1055 and 1096 Point-Source Sensitivity for PSA

Wavelength (Å)	Throughput	Sensitivity (counts pixel^{-1} sec^{-1} per erg cm^{-2} sec^{-1} Å^{-1})	Effective Area (cm^2)
900	3.142E-04	6.4E+09	1.42E+01
950	5.775E-04	1.2E+10	2.61E+01
1000	3.764E-04	8.5E+09	1.70E+01
1050	7.522E-04	1.8E+10	3.40E+01
1100	5.777E-03	1.4E+11	2.61E+02
1150	3.230E-02	8.4E+11	1.46E+03
1200	4.530E-02	1.2E+12	2.05E+03

Figure 13.8: G130M/1055 and 1096 Point-Source Sensitivity for PSA

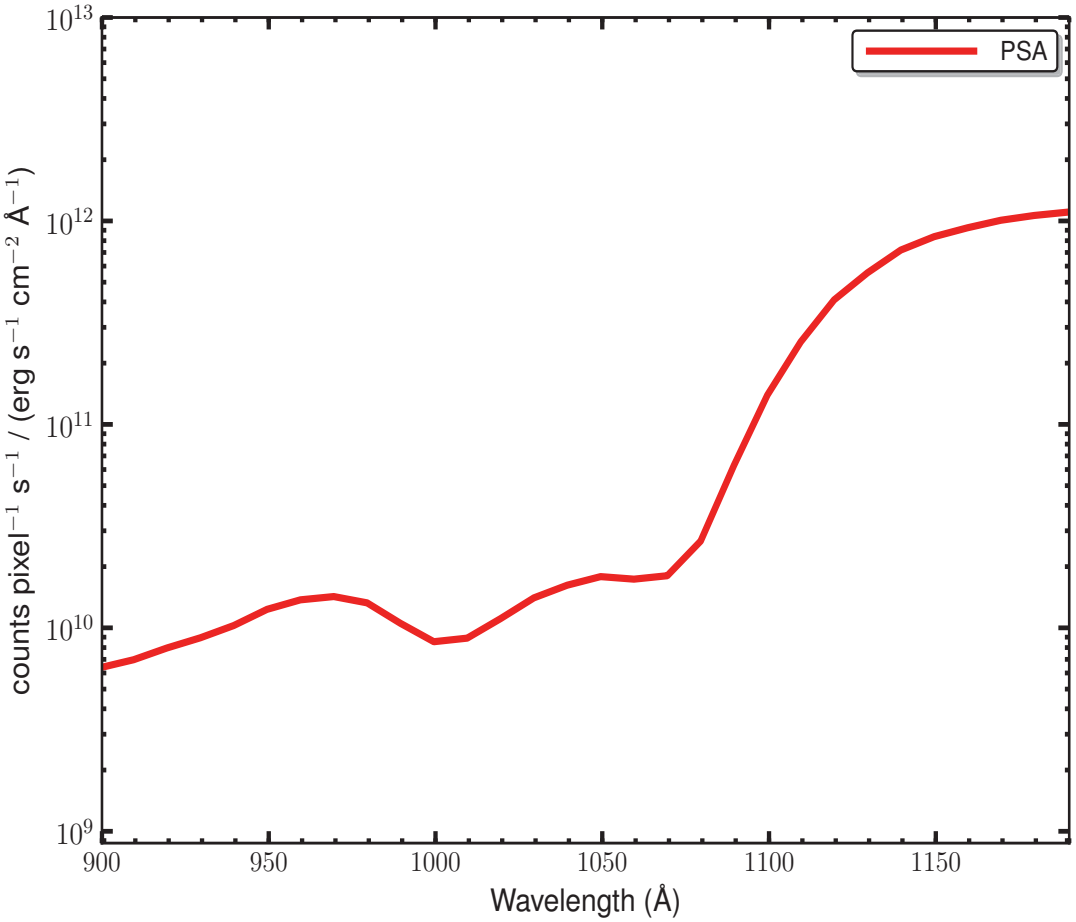

The sensitivity through the BOA is not shown, as its MgF_2 filter is opaque at these wavelengths.

G130M/1055 and 1096 Signal-to-Noise Ratio

Figure 13.9: Point-Source Signal-to-Noise as a Function of STMAG for G130M at 1030 Å

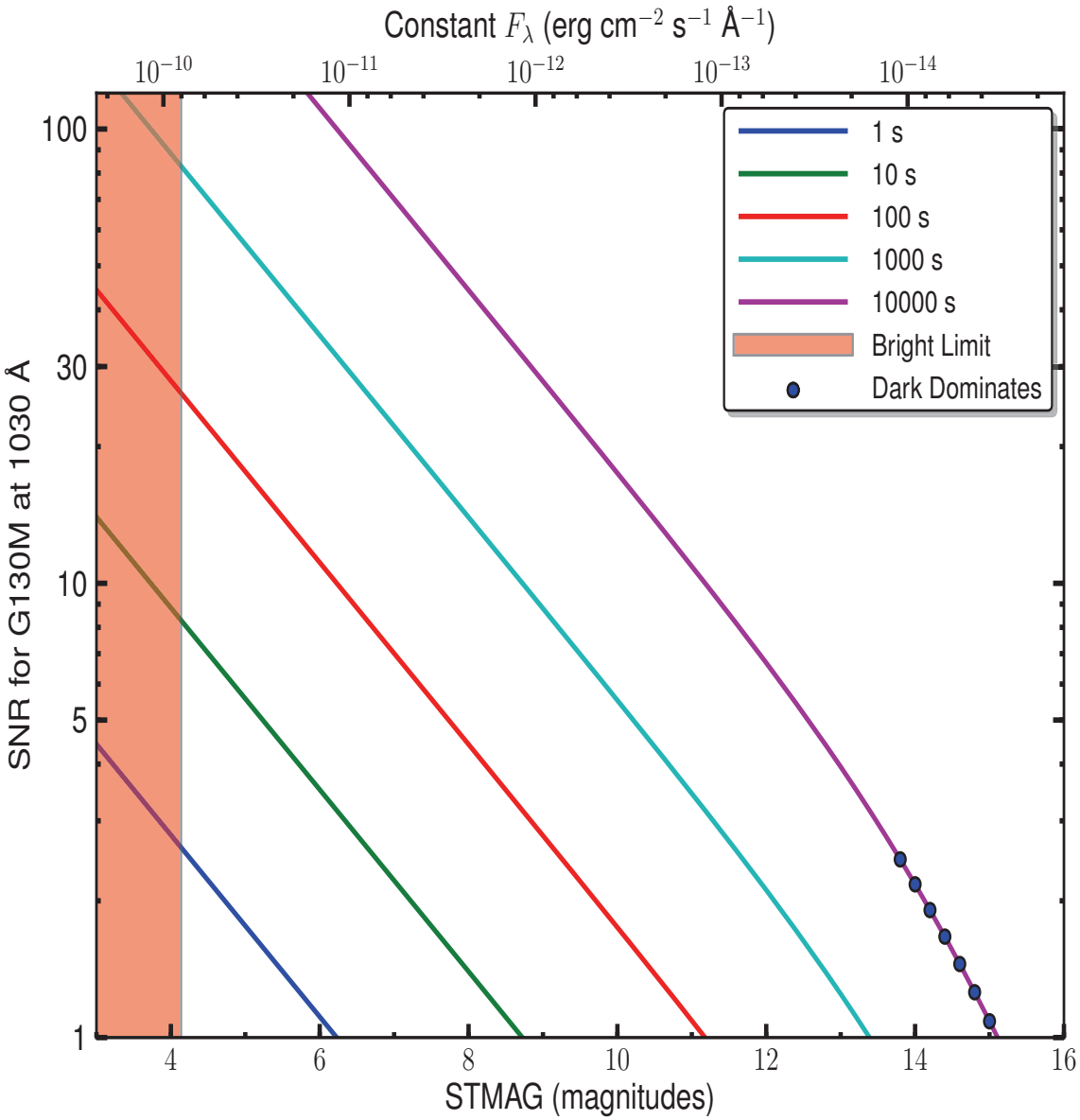

The top axis displays constant F_λ values corresponding to the STMAG units (V+STMAG$_\lambda$) on the bottom axis. Recall that STMAG=0 is equivalent to F_λ = 3.63E-9 erg cm^{-2} s^{-1} Å^{-1}. Colors refer to exposure times in seconds. The edge of the shaded area corresponds to the bright-object screening limit. Use of the PSA is assumed.

FUV Grating G160M

Description

The G160M grating samples wavelengths between about 1405 and 1775 Å. It offers higher resolution and effective area than the G140L grating, but less spectral coverage.

Special Considerations

The gap between segments A and B spans 18.1 Å. To fill this gap requires exposures separated by two central-wavelength settings.

Grating	Resolving Power $R = \lambda/\Delta\lambda$	Dispersion (mÅ pixel^{-1})	Plate Scale (milliarcsec pixel^{-1})		FP-POS Step (Å step^{-1})
			Disp. Axis	Cross-Disp. Axis	
G160M	16,000 - 21,000	12.23	24.3	90	3.2

Figure 13.10: Wavelength Ranges for the G160M Grating

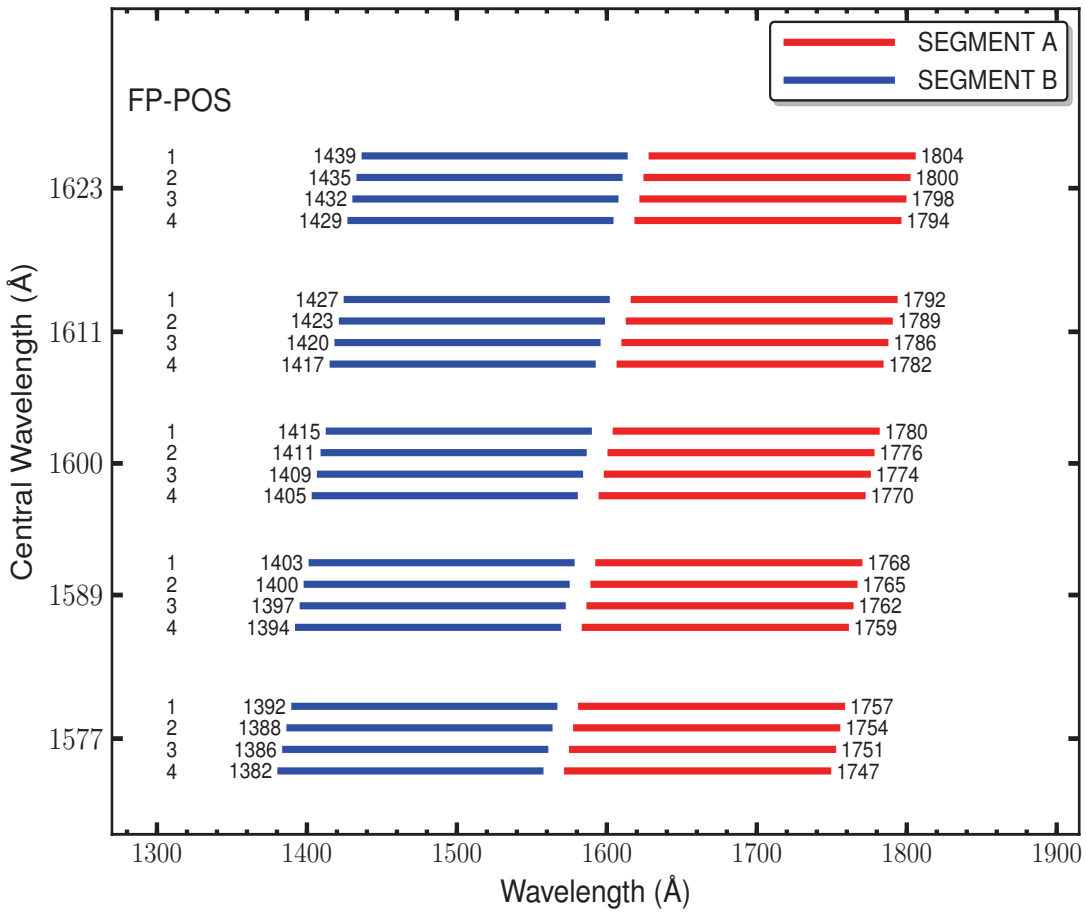

G160M Point-Source Sensitivity

Table 13.6: G160M Point-Source Sensitivity for PSA

Wavelength (Å)	Throughput	Sensitivity (counts pixel^{-1} sec^{-1} per erg cm^{-2} sec^{-1} Å^{-1})	Effective Area (cm^2)
1400	4.024E-02	1.6E+12	1.82E+03
1450	3.488E-02	1.4E+12	1.58E+03
1500	2.616E-02	1.1E+12	1.18E+03
1550	2.078E-02	9.0E+11	9.40E+02
1600	1.588E-02	7.1E+11	7.18E+02
1650	1.216E-02	5.6E+11	5.50E+02
1700	9.991E-03	4.7E+11	4.52E+02
1750	8.343E-03	4.1E+11	3.77E+02

Figure 13.11: G160M Point-Source Sensitivity for PSA and BOA

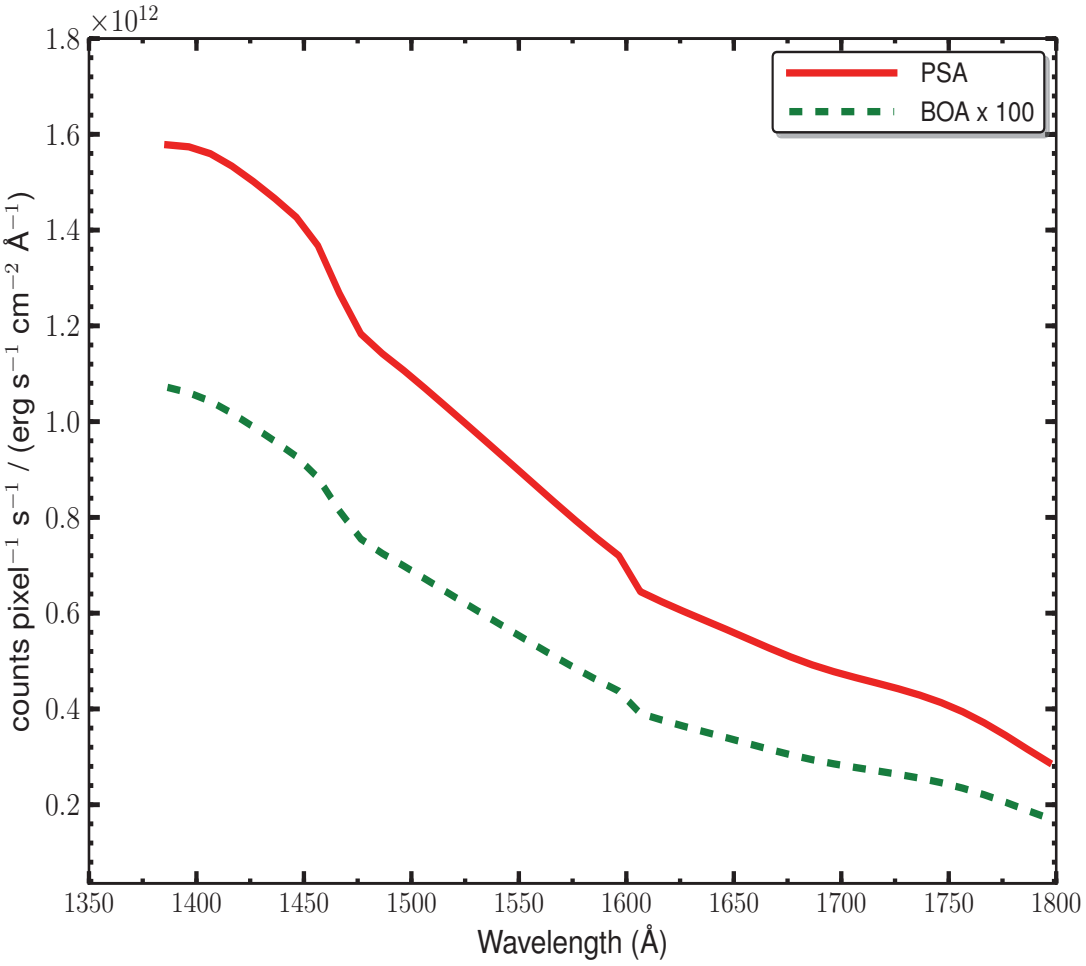

G160M Signal-to-Noise Ratio

Figure 13.12: Point-Source Signal-to-Noise as a Function of STMAG for G160M at 1610 Å

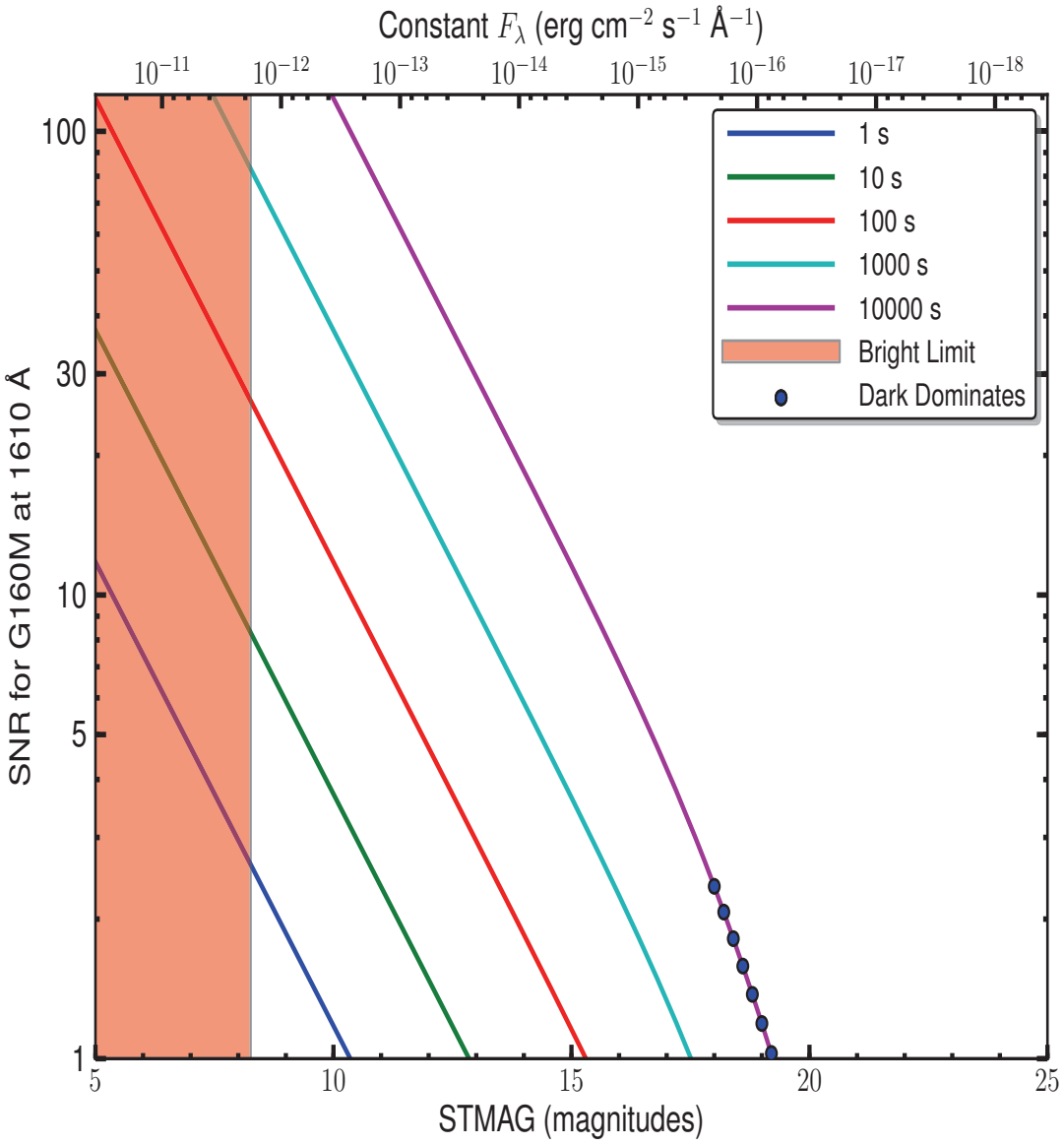

The top axis displays constant F_λ values corresponding to the STMAG units (V+STMAG$_\lambda$) on the bottom axis. Recall that STMAG=0 is equivalent to F_λ = 3.63E-9 erg cm^{-2} s^{-1} Å^{-1}. Colors refer to exposure times in seconds. The edge of the shaded area corresponds to the bright-object screening limit. Use of the PSA is assumed.

FUV Grating G140L

Description

G140L is a low-resolution grating (R~2,000) with wavelength coverage extending to 900 Å—and perhaps below. Its sensitivity at EUV wavelengths—marked in light blue in Figure 13.13—has not yet been calibrated. The grating has two central-wavelength settings, 1105 and 1280 Å.

Special Considerations

The gap between segments A and B spans 105 Å. To fill this gap requires exposures at both central-wavelength settings. When setting 1105 is used, the high voltage on Segment B must be lowered to avoid a dangerously high count rate from zero-order light. Wavelengths longer than 2150 Å may be contaminated by second-order light.

Grating	Resolving Power $R = \lambda/\Delta\lambda$	Dispersion (mÅ pixel^{-1})	Plate Scale (milliarcsec pixel^{-1})		FP-POS Step (Å step^{-1})
			Disp. Axis	Cross-Disp. Axis	
G140L	1,500 - 4,000	80.3	23.0	90	19.6

Figure 13.13: Wavelength Ranges for the G140L Grating

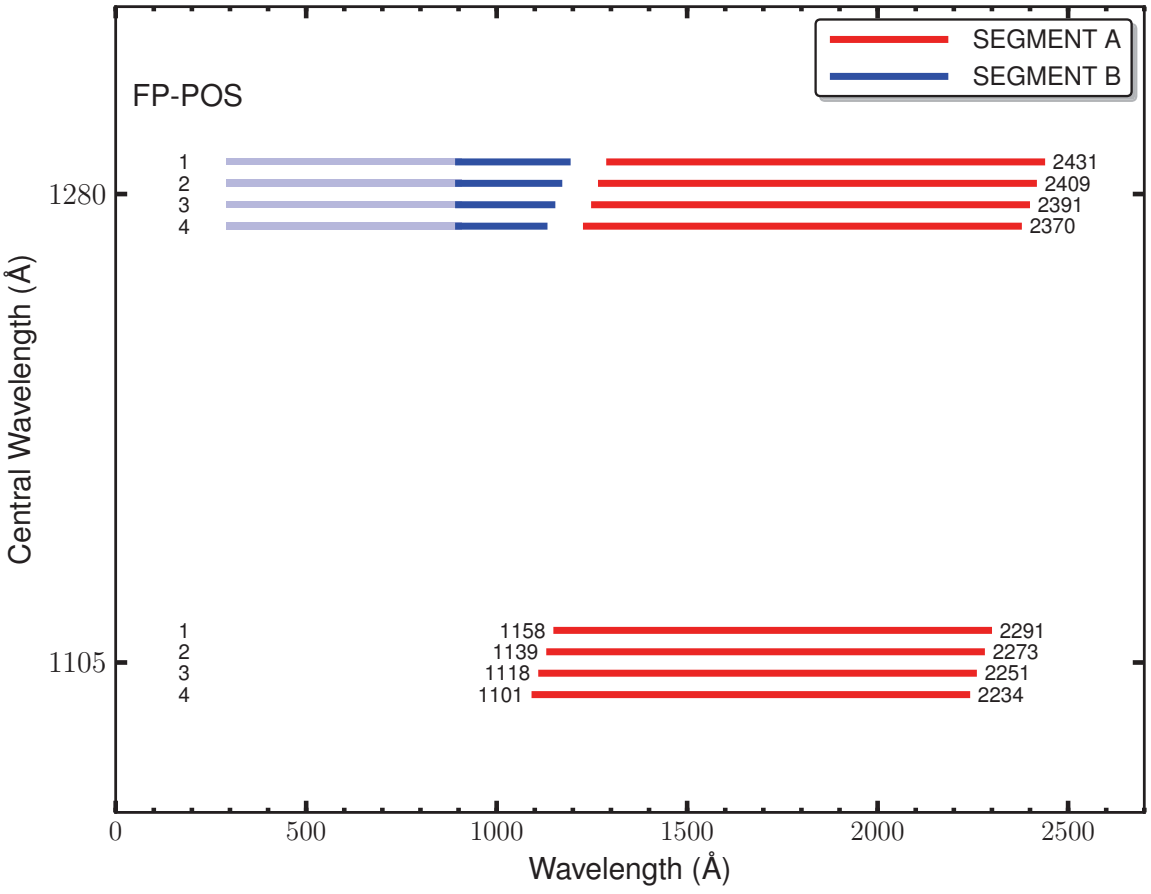

The COS sensitivity at EUV wavelengths (marked in light blue) is not yet known.

G140L Point-Source Sensitivity

Table 13.7: G140L Point-Source Sensitivity for PSA

Wavelength (Å)	Throughput	Sensitivity (counts pixel^{-1} sec^{-1} per erg cm^{-2} sec^{-1} Å^{-1})	Effective Area (cm^2)
950	1.565E-04	2.7E+10	7.08E+00
1000	1.338E-04	2.4E+10	6.05E+00
1100	5.054E-03	1.0E+12	2.29E+02
1200	2.987E-02	6.5E+12	1.35E+03
1300	3.319E-02	7.8E+12	1.50E+03
1400	2.286E-02	5.8E+12	1.03E+03
1500	1.497E-02	4.1E+12	6.77E+02
1600	8.962E-03	2.6E+12	4.05E+02
1700	6.026E-03	1.9E+12	2.73E+02
1800	3.932E-03	1.3E+12	1.78E+02
1900	2.046E-03	7.0E+11	9.26E+01
2000	4.337E-04	1.6E+11	1.96E+01
2100	2.886E-05	1.1E+10	1.31E+00

Figure 13.14: G140L Point-Source Sensitivity for PSA and BOA

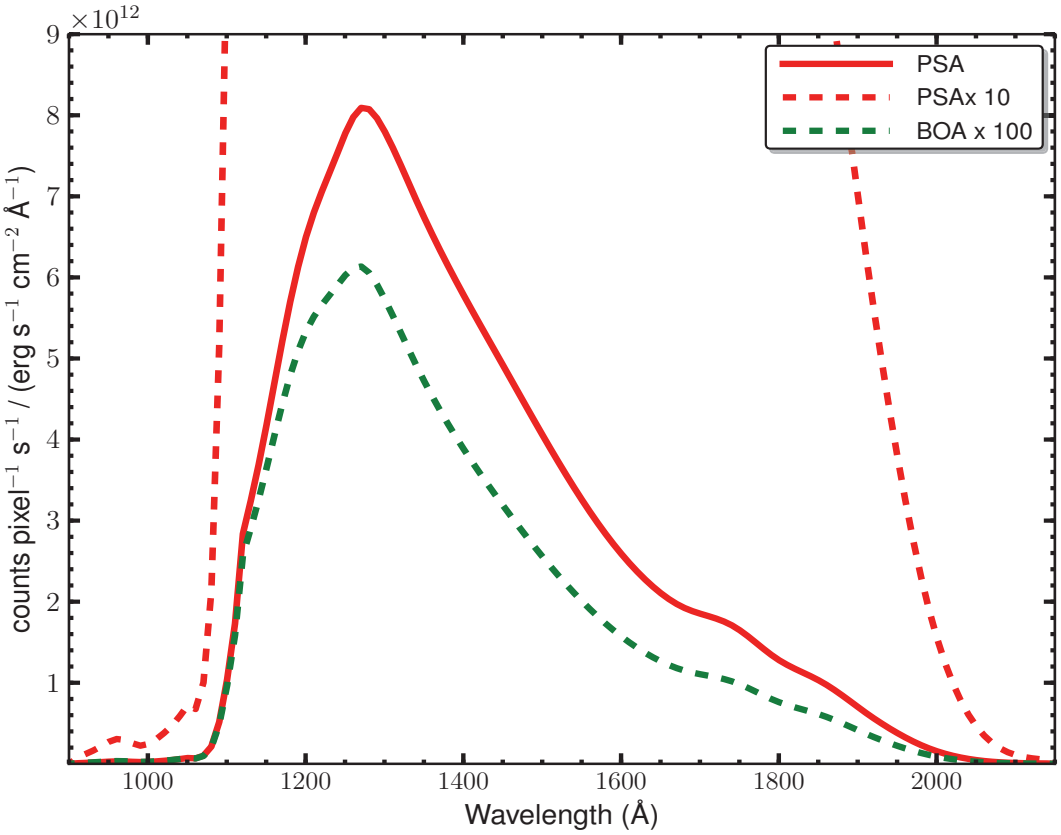

PSA × 10 is plotted to show sensitivity below 1100 Å.

G140L Signal-to-Noise Ratio

Figure 13.15: Point-Source Signal-to-Noise as a Function of STMAG for G140L

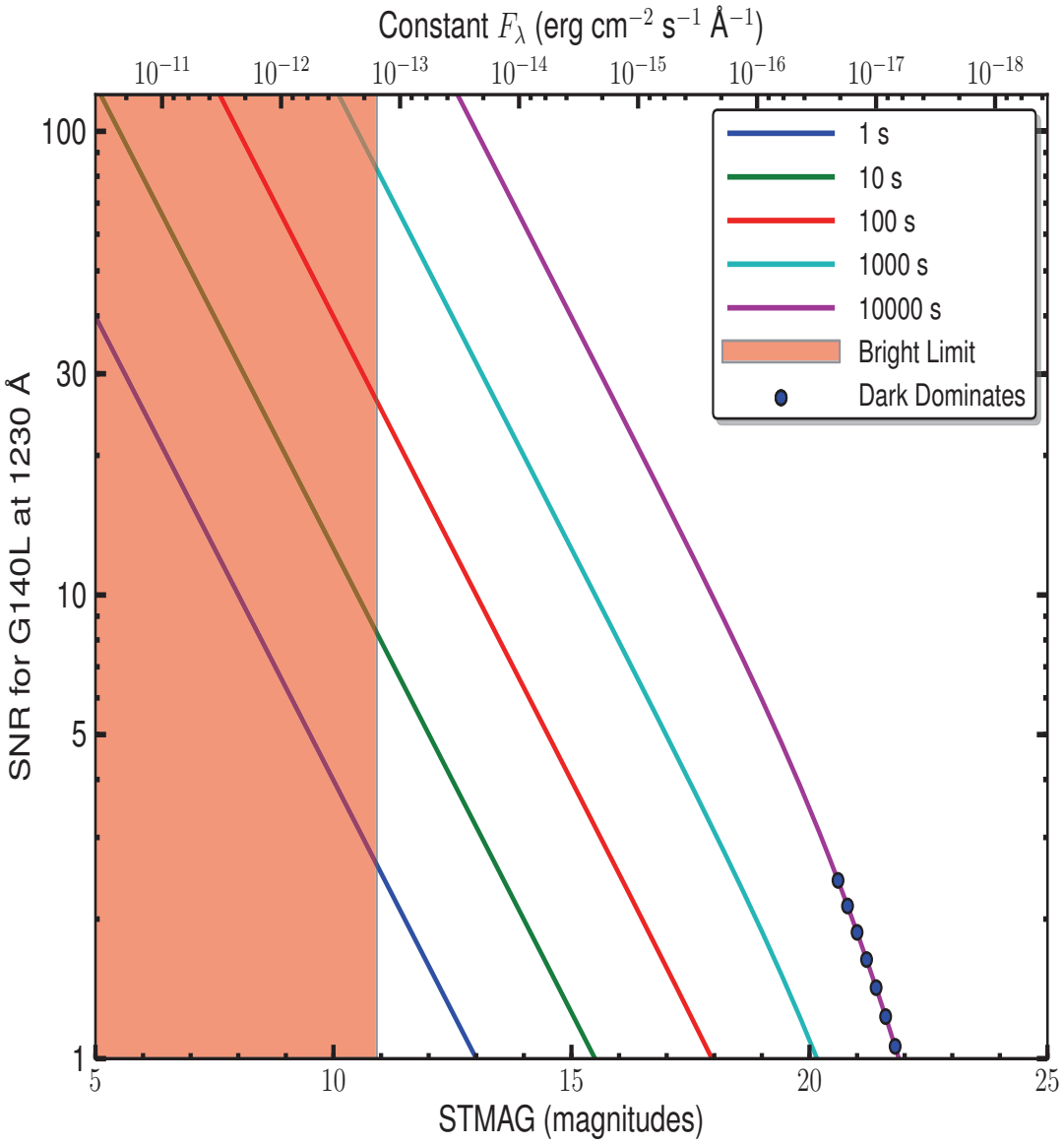

The top axis displays constant F_λ values corresponding to the STMAG units (V+STMAG$_\lambda$) on the bottom axis. Recall that STMAG=0 is equivalent to F_λ = 3.63E-9 erg cm^{-2} s^{-1} Å^{-1}. Colors refer to exposure times in seconds. The edge of the shaded area corresponds to the bright-object screening limit. Use of the PSA is assumed.

NUV Grating G185M

Description

The G185M grating samples wavelengths between about 1700 and 2100 Å. The grating has 15 central wavelength settings.

Special Considerations

G185M spectra consist of three 35-Å stripes separated by two 64-Å gaps. To acquire a complete spectrum requires the use of six central-wavelength settings.

Grating	Resolving Power $R = \lambda/\Delta\lambda$	Dispersion (mÅ pixel^{-1})	Spatial Resolution (milliarcsec pixel^{-1})	Plate Scale (milliarcsec pixel^{-1})		FP-POS Step (Å step^{-1})
				Disp. Axis	Cross-Disp. Axis	
G185M	16,000 - 20,000	37	75 ± 4	24.3	23.8	1.9

Figure 13.16: Wavelength Ranges for the G185M Grating

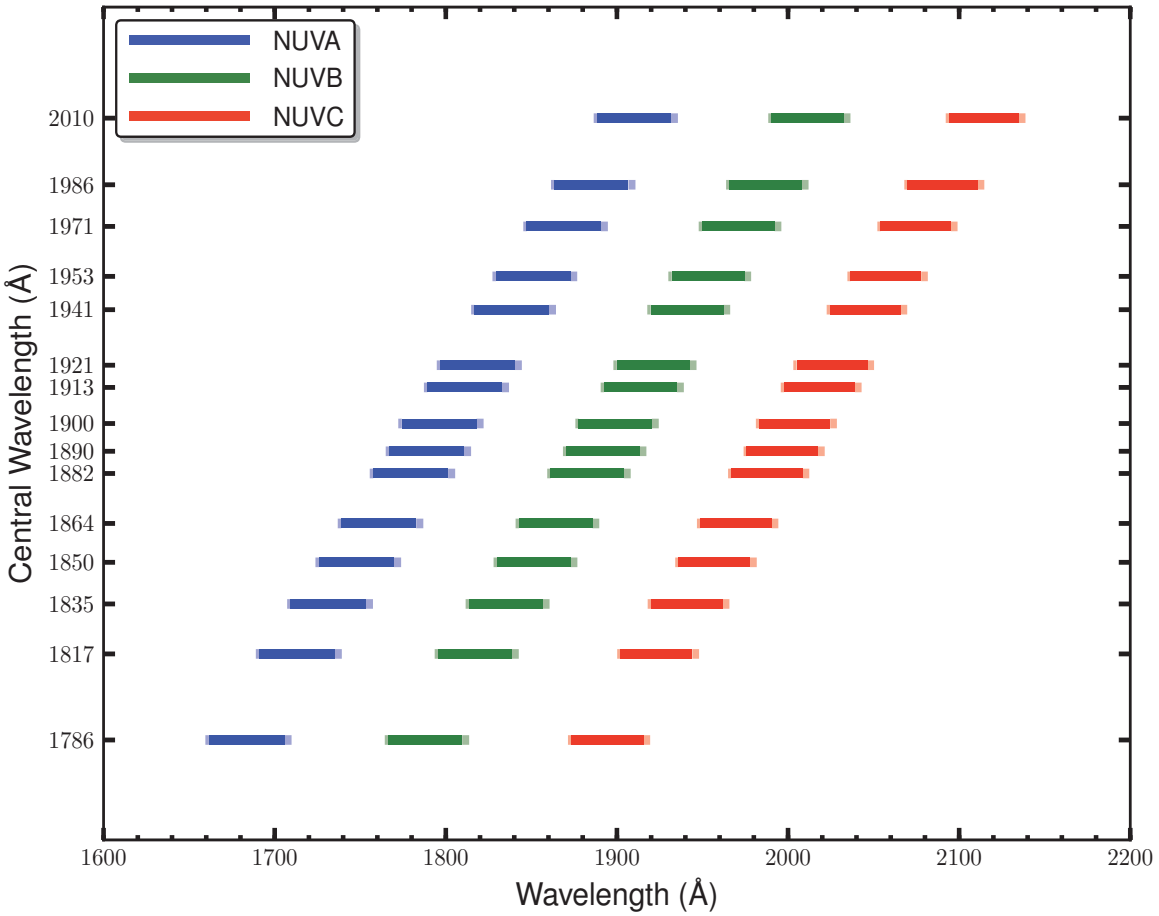

Dark lines represent wavelengths sampled by all four FP-POS positions.

G165M Point-Source Sensitivity

Table 13.8: G185M Point-Source Sensitivity for PSA

Wavelength (Å)	Throughput	Sensitivity (counts pixel^{-1} sec^{-1} per erg cm^{-2} sec^{-1} Å^{-1})	Effective Area (cm^2)
1670	3.097E-03	4.3E+11	1.40E+02
1700	7.851E-03	1.1E+12	3.55E+02
1750	1.082E-02	1.6E+12	4.90E+02
1800	1.255E-02	1.9E+12	5.68E+02
1850	1.323E-02	2.0E+12	5.99E+02
1900	1.307E-02	2.1E+12	5.91E+02
1950	1.259E-02	2.0E+12	5.70E+02
2000	1.228E-02	2.0E+12	5.56E+02
2050	1.154E-02	2.0E+12	5.22E+02
2100	1.060E-02	1.9E+12	4.80E+02

Figure 13.17: G185M Point-Source Sensitivity for PSA and BOA

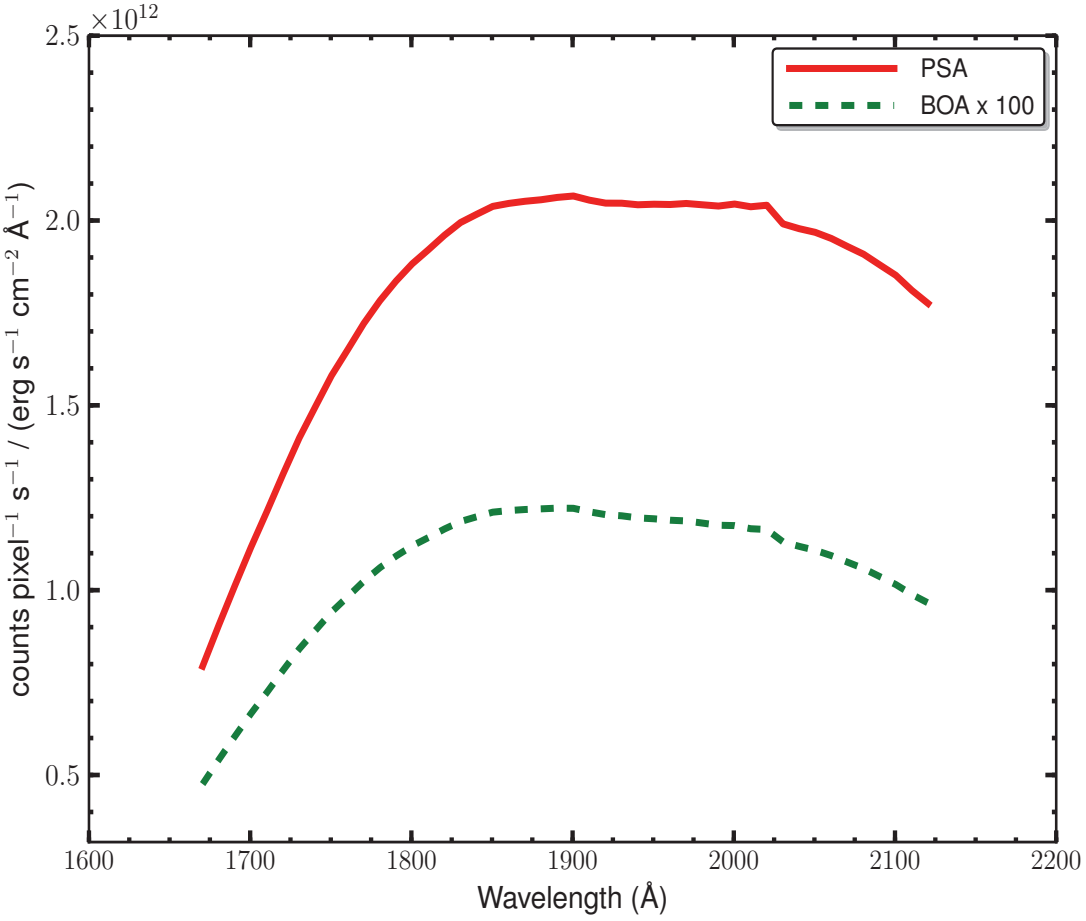

G185M Signal-to-Noise Ratio

Figure 13.18: Point-Source Signal-to-Noise as a Function of STMAG for G185M

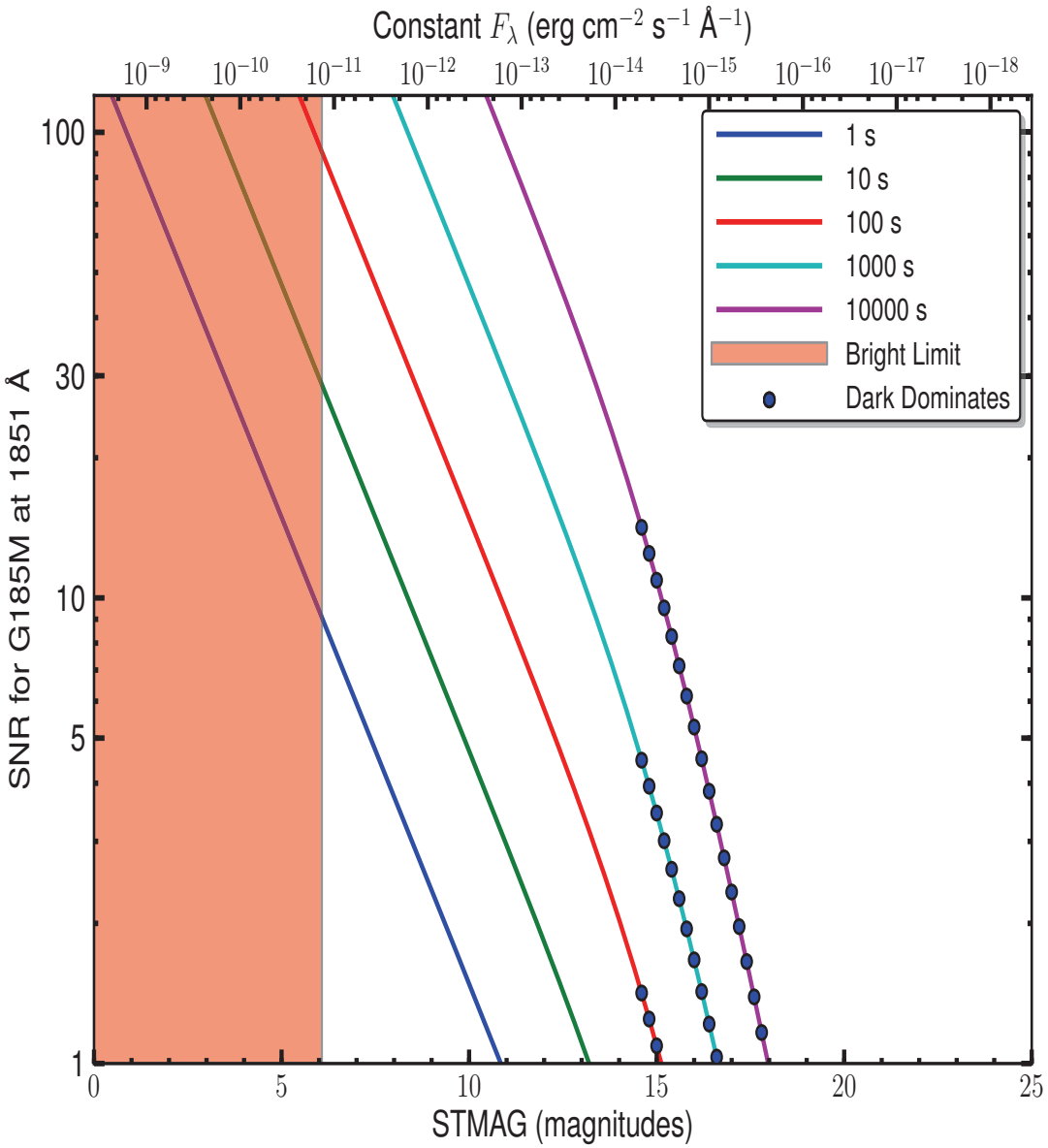

The top axis displays constant F_λ values corresponding to the STMAG units (V+STMAG$_\lambda$) on the bottom axis. Recall that STMAG=0 is equivalent to F_λ = 3.63E-9 erg cm^{-2} s^{-1} Å^{-1}. Colors refer to exposure times in seconds. The edge of the shaded area corresponds to the bright-object screening limit. Use of the PSA is assumed.

NUV Grating G225M

Description

The G225M grating samples wavelengths between about 2100 and 2500 Å. The grating has 13 central wavelength settings.

Special Considerations

G225M spectra consist of three 35-Å stripes separated by two 64-Å gaps. To acquire a complete spectrum requires the use of six central-wavelength settings.

Grating	Resolving Power $R = \lambda/\Delta\lambda$	Dispersion (mÅ pixel^{-1})	Spatial Resolution (milliarcsec pixel^{-1})	Plate Scale (milliarcsec pixel^{-1})		FP-POS Step (Å step^{-1})
				Disp. Axis	Cross-Disp. Axis	
G225M	20,000 - 24,000	33	58 ± 2	24.3	23.1	1.7

Figure 13.19: Wavelength Ranges for the G225M Grating

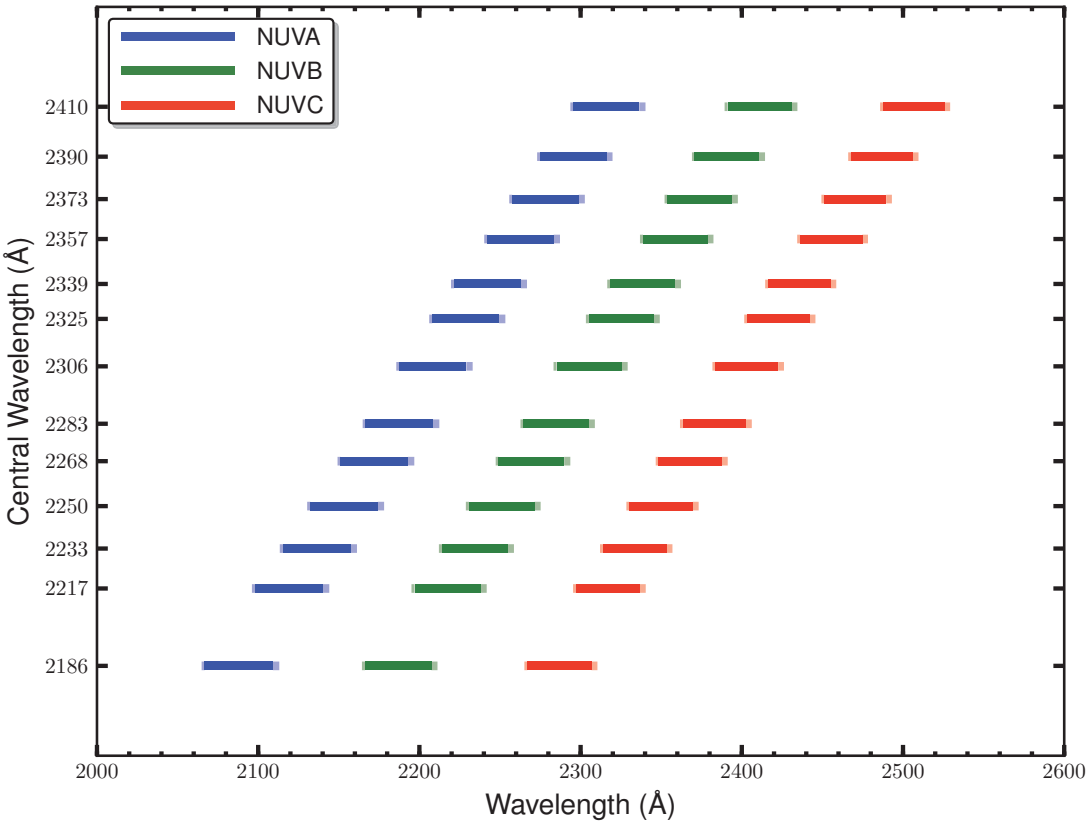

Dark lines represent wavelengths sampled by all four FP-POS positions.

G225M Point-Source Sensitivity

Table 13.9: G225M Point-Source Sensitivity for PSA

Wavelength (Å)	Throughput	Sensitivity (counts pixel^{-1} sec^{-1} per erg cm^{-2} sec^{-1} Å^{-1})	Effective Area (cm^2)
2100	6.099E-03	1.0E+12	2.76E+02
2150	7.552E-03	1.3E+12	3.42E+02
2200	9.430E-03	1.6E+12	4.27E+02
2250	1.078E-02	1.9E+12	4.88E+02
2300	1.181E-02	2.1E+12	5.34E+02
2350	1.246E-02	2.3E+12	5.64E+02
2400	1.275E-02	2.4E+12	5.77E+02
2450	1.264E-02	2.4E+12	5.72E+02
2500	1.276E-02	2.5E+12	5.77E+02

Figure 13.20: G225M Point-Source Sensitivity for PSA and BOA

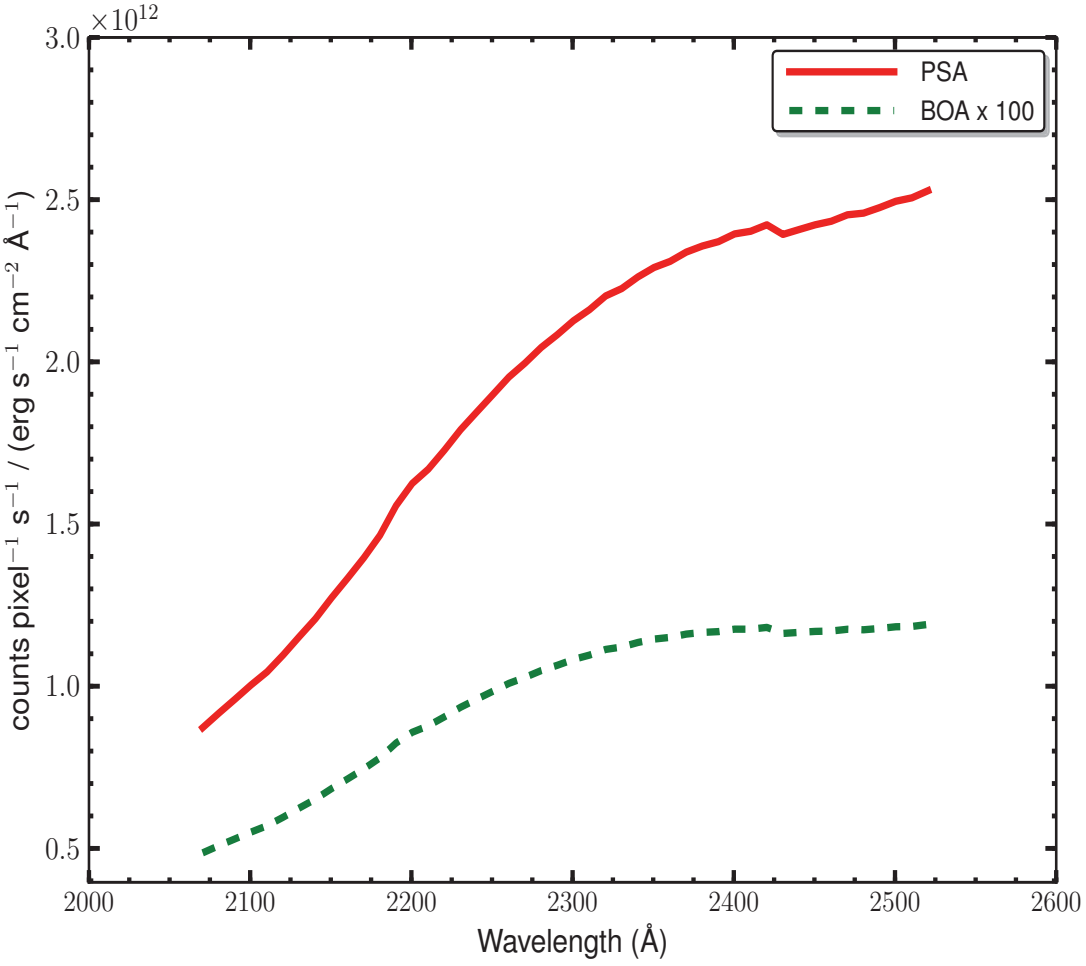

G225M Signal-to-Noise Ratio

Figure 13.21: Point-Source Signal-to-Noise as a Function of STMAG for G225M

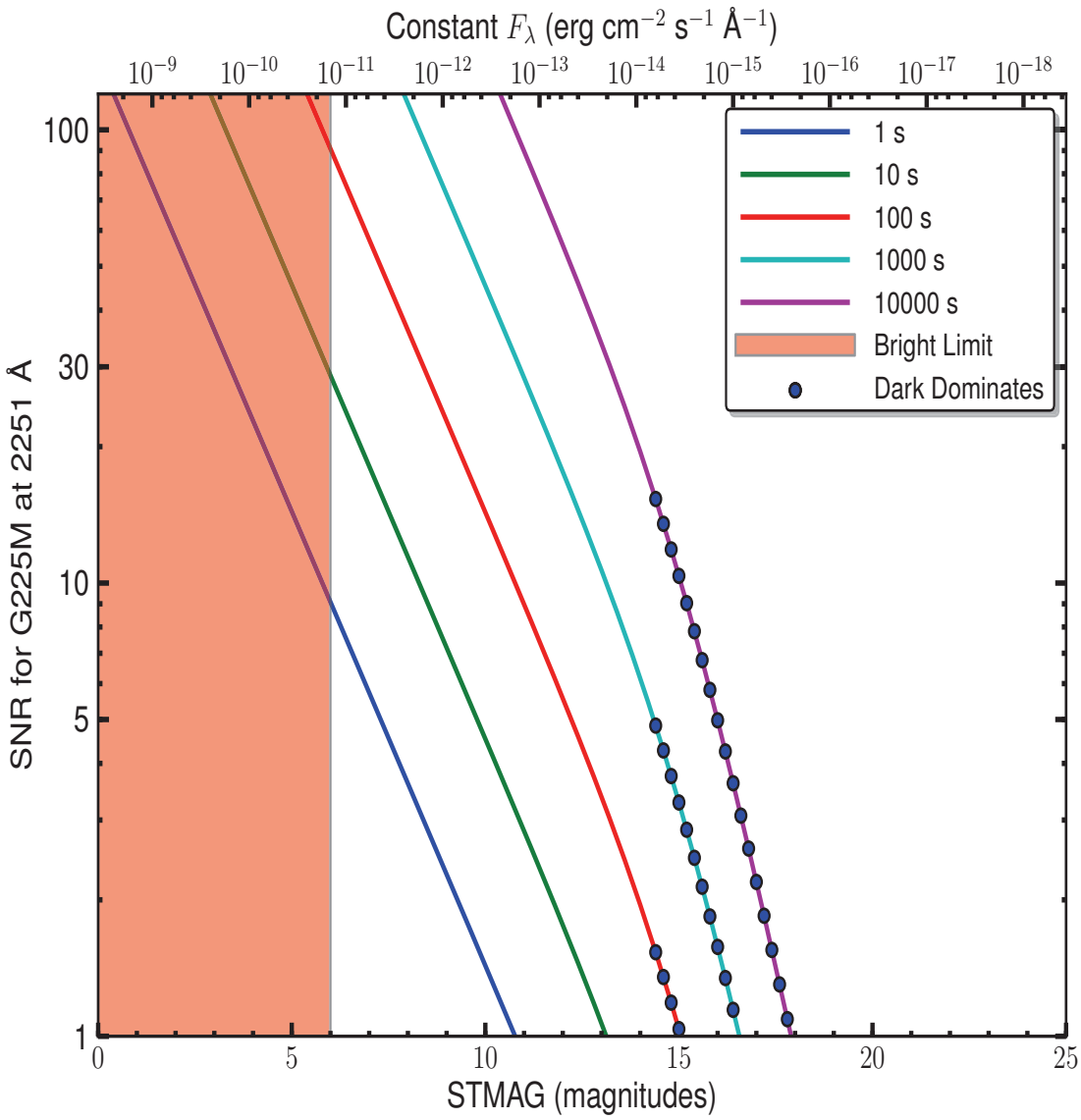

The top axis displays constant F_λ values corresponding to the STMAG units (V+STMAG$_\lambda$) on the bottom axis. Recall that STMAG=0 is equivalent to F_λ = 3.63E-9 erg cm^{-2} s^{-1} Å^{-1}. Colors refer to exposure times in seconds. The edge of the shaded area corresponds to the bright-object screening limit. Use of the PSA is assumed.

NUV Grating G285M

Description

The G285M grating samples wavelengths between about 2500 and 3200 Å. The grating has 17 central wavelength settings.

Special Considerations

G285M spectra consist of three 41-Å stripes separated by two 74-Å gaps. To acquire a complete spectrum requires the use of eight central-wavelength settings.

Grating	Resolving Power $R = \lambda/\Delta\lambda$	Dispersion (mÅ pixel^{-1})	Spatial Resolution (milliarcsec pixel^{-1})	Plate Scale (milliarcsec pixel^{-1})		FP-POS Step (Å step^{-1})
				Disp. Axis	Cross-Disp. Axis	
G285M	20,000 - 24,000	40	56 ± 1	24.3	24.4	2.1

Figure 13.22: Wavelength Ranges for the G285M Grating

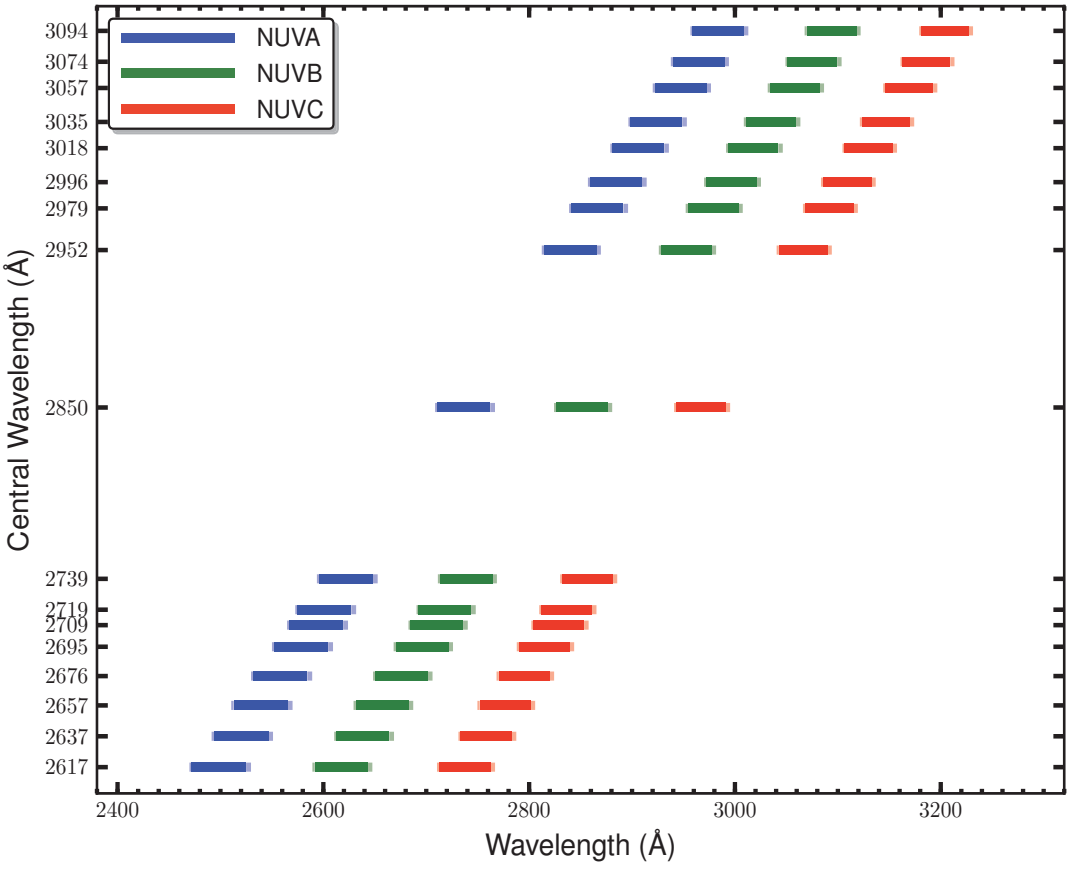

Dark lines represent wavelengths sampled by all four FP-POS positions.

G285M Point-Source Sensitivity

Table 13.10: G285M Point-Source Sensitivity for PSA

Wavelength (Å)	Throughput	Sensitivity (counts pixel^{-1} sec^{-1} per erg cm^{-2} sec^{-1} Å^{-1})	Effective Area (cm^2)
2500	4.206E-03	9.7E+11	1.90E+02
2600	4.859E-03	1.2E+12	2.20E+02
2700	5.060E-03	1.3E+12	2.29E+02
2800	4.697E-03	1.2E+12	2.12E+02
2900	4.165E-03	1.1E+12	1.88E+02
3000	3.186E-03	8.8E+11	1.44E+02
3100	2.002E-03	5.7E+11	9.06E+01
3200	1.033E-03	3.1E+11	4.67E+01

Figure 13.23: G285M Point-Source Sensitivity for PSA and BOA

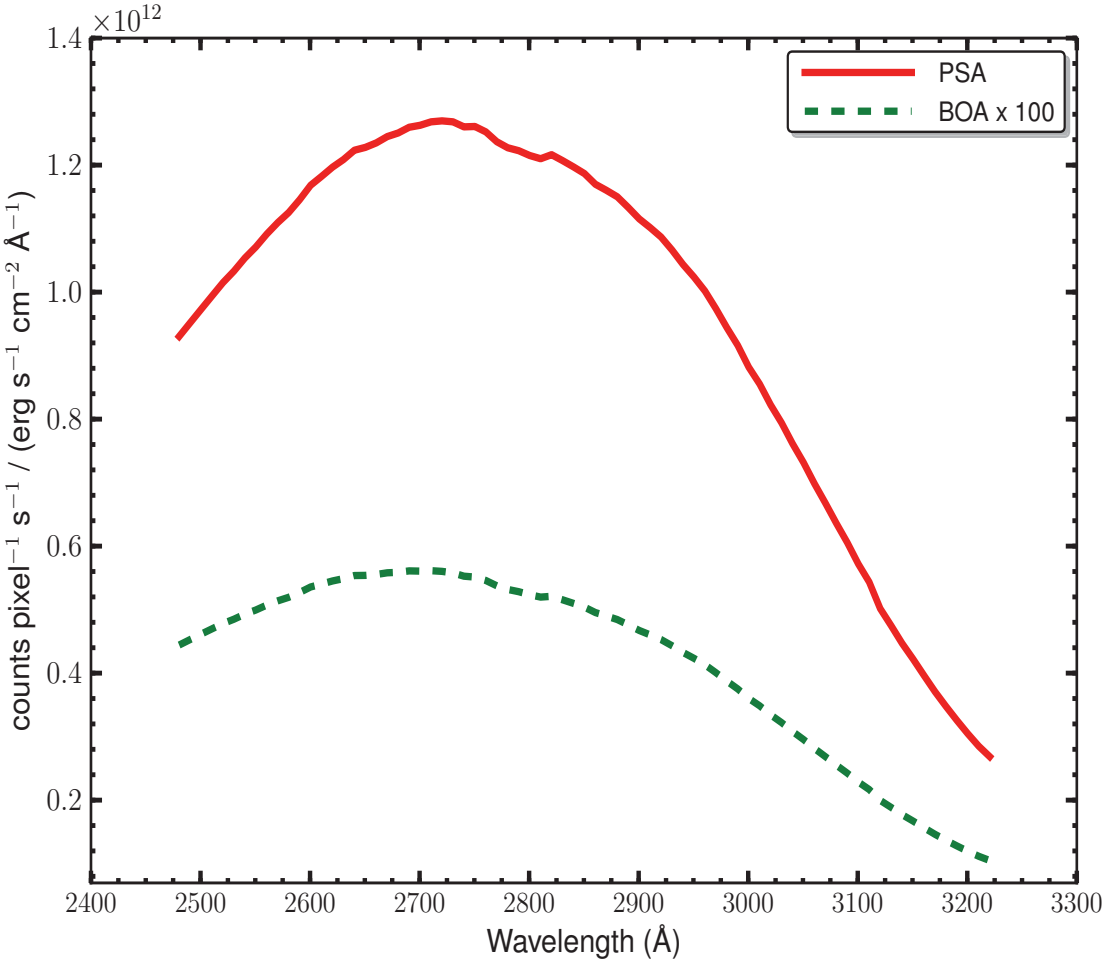

G285M Signal-to-Noise Ratio

Figure 13.24: Point-Source Signal-to-Noise as a Function of STMAG for G285M

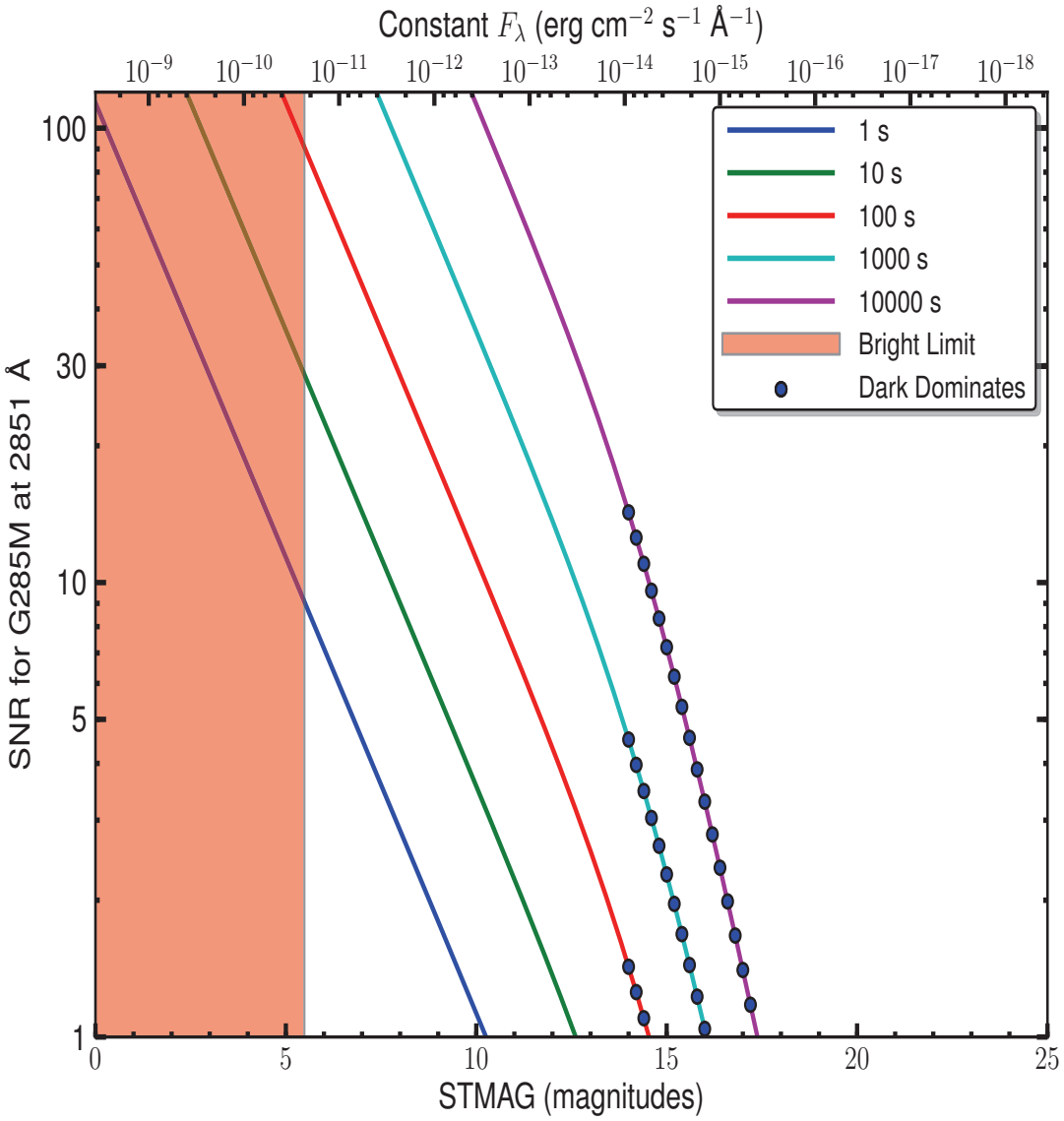

The top axis displays constant F_λ values corresponding to the STMAG units (V+STMAG$_\lambda$) on the bottom axis. Recall that STMAG=0 is equivalent to F_λ = 3.63E-9 erg cm^{-2} s^{-1} Å^{-1}. Colors refer to exposure times in seconds. The edge of the shaded area corresponds to the bright-object screening limit. Use of the PSA is assumed.

NUV Grating G230L

Description

G230L is a low-resolution grating (R~3000) with wavelength coverage extending from about 1650 to 3200 Å. The grating has four central-wavelength settings.

Special Considerations

G230L spectra consist of three 400-Å stripes separated by two 700-Å gaps. To acquire a complete spectrum requires the use of all four central-wavelength settings.

Only stripes A and B record first-order light, and even they may be contaminated by second-order light when central wavelength 3360 is used. See Table 5.5.

Grating	Resolving Power $R = \lambda/\Delta\lambda$	Dispersion (mÅ pixel^{-1})	Spatial Resolution (milliarcsec pixel^{-1})	Plate Scale (milliarcsec pixel^{-1})		FP-POS Step (Å step^{-1})
				Disp. Axis	Cross-Disp. Axis	
G230L	2,100 - 3,900	390	81 ± 1	24.3	24.0	20.3

Figure 13.25: Wavelength Ranges for the G230L Grating

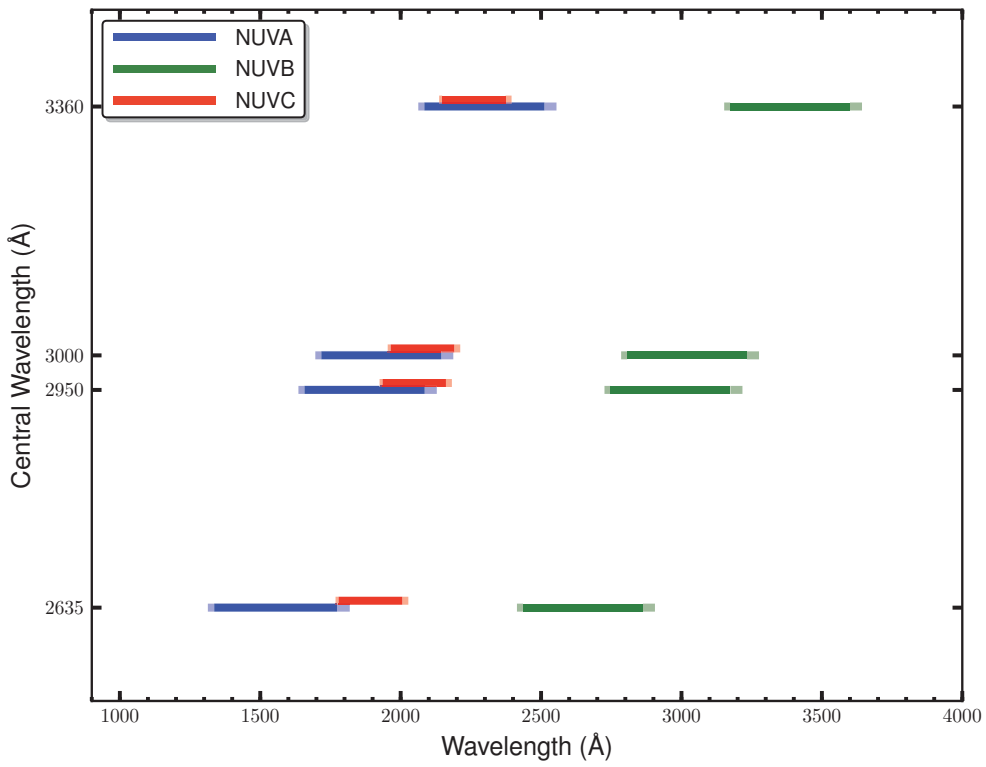

Dark lines represent wavelengths sampled by all four FP-POS positions. Wavelengths above 3200 Å may be contaminated by second-order light.

G230L Point-Source Sensitivity

Table 13.11: G230L Point-Source Sensitivity for PSA

Wavelength (Å)	Throughput	Sensitivity (counts pixel^{-1} sec^{-1} per erg cm^{-2} sec^{-1} Å^{-1})	Effective Area (cm^2)
1600	1.316E-04	1.6E+11	5.95E+00
1800	9.462E-03	1.3E+13	4.28E+02
2000	1.342E-02	2.0E+13	6.07E+02
2200	1.495E-02	2.4E+13	6.76E+02
2400	1.438E-02	2.6E+13	6.50E+02
2600	1.244E-02	2.4E+13	5.63E+02
2800	9.304E-03	1.9E+13	4.21E+02
3000	4.995E-03	1.1E+13	2.26E+02
3200	1.336E-03	3.2E+12	6.04E+01
3400	3.127E-03	7.9E+12	1.41E+02

Figure 13.26: G230L Point-Source Sensitivity for PSA and BOA

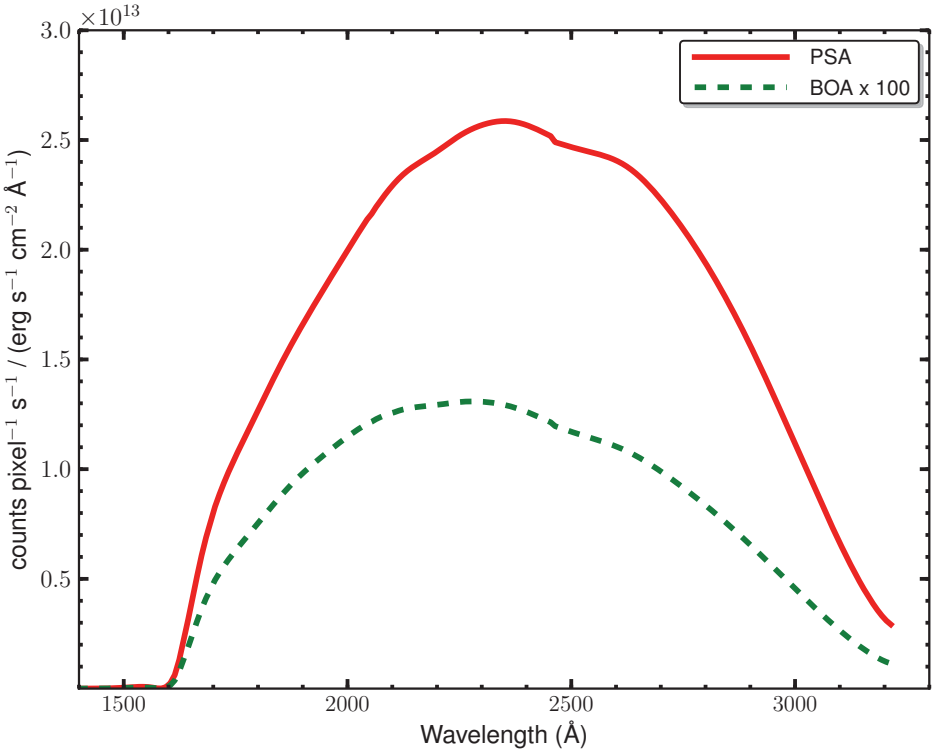

G230L Signal-to-Noise Ratio

Figure 13.27: Point-Source Signal-to-Noise as a Function of STMAG for G230L

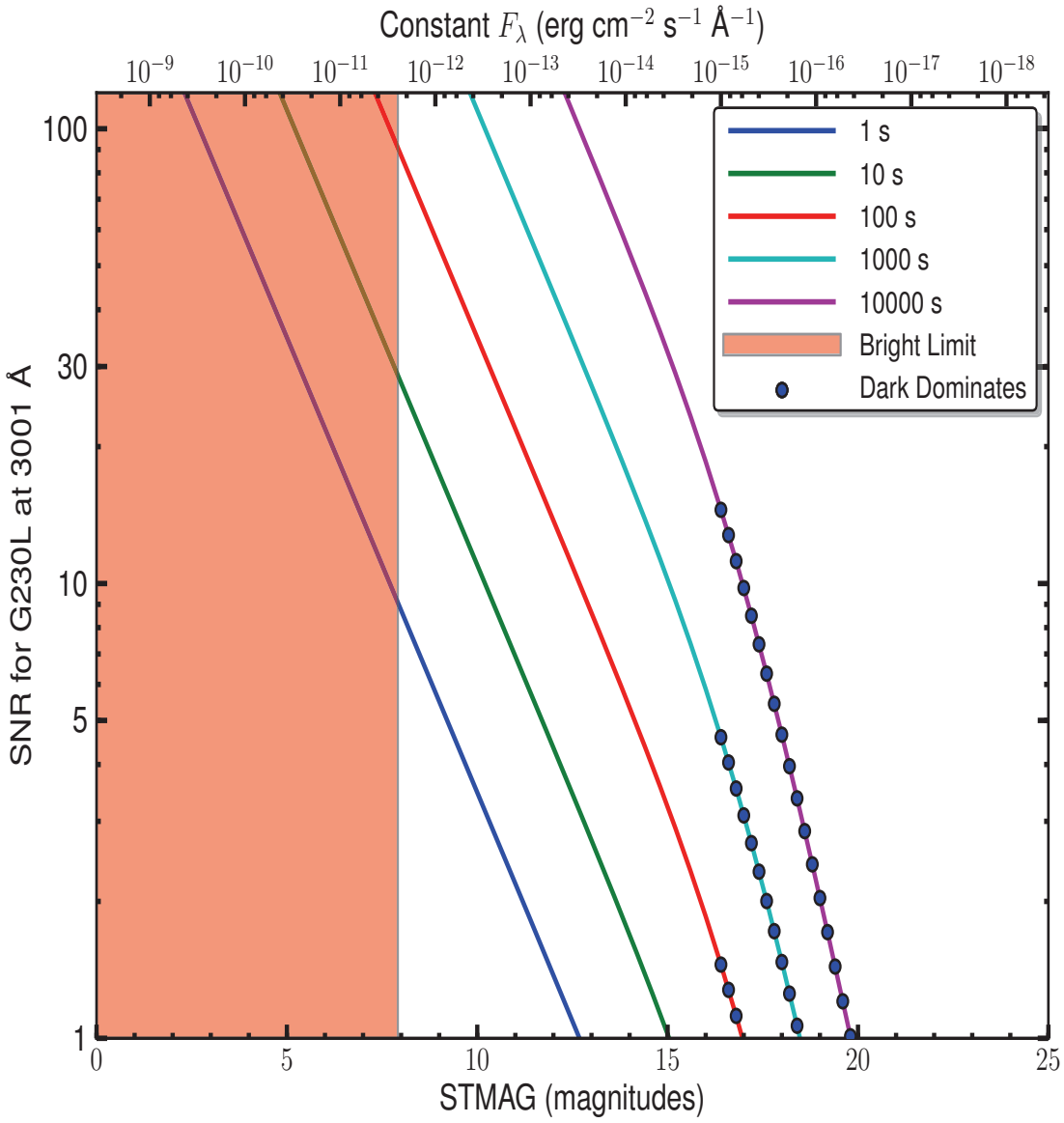

The top axis displays constant F_λ values corresponding to the STMAG units (V+STMAG$_\lambda$) on the bottom axis. Recall that STMAG=0 is equivalent to F_λ = 3.63E-9 erg cm^{-2} s^{-1} Å^{-1}. Colors refer to exposure times in seconds. The edge of the shaded area corresponds to the bright-object screening limit. Use of the PSA is assumed.

13.4 Spectrograph Design Parameters

13.4.1 FUV Channel

Table 13.12 presents design parameters of the FUV spectrograph and gratings. The FUV gratings are concave and have holographically-generated grooves to provide dispersion and correct for astigmatism. The gratings have aspherical surfaces to correct for *HST*'s spherical aberration. The FUV "M" gratings have been ion etched to produce triangular groove profiles for better efficiency. The G140L grating has grooves with a laminar profile. All FUV gratings are coated with MgF_2 over aluminum.

The surface of the optic is a sphere of the quoted radius, but with a deviation of $\Delta z = a_4 r^4 + a_6 r^6$, where z is measured along the vertex normal. The quantities γ, δ, r_c, and r_d are the standard positions of the recording sources as defined in Noda, Namioka, and Seya (1974, J. Opt. Soc. Amer., 64, 1031).

Table 13.12: Design Parameters for the FUV Spectrograph and Gratings

Dimension	G130M	G160M	G140L
secondary mirror vertex to aperture (z, mm)	6414.4		
V_1 axis to aperture (mm)	90.49		
aperture to grating (mm)	1626.57		
α (degrees)	20.1	20.1	7.40745
β (degrees)	8.6466	8.6466	–4.04595
$\alpha - \beta$ (degrees)	11.4534		
grating to detector (mm)	1541.25		
detector normal vs. central ray (degrees)	9.04664		
nominal groove density (lines mm $^{-1}$)	3800	3093.3	480
radius of curvature (mm)	1652	1652	1613.87
a_4	1.45789×10^{-9}	1.45789×10^{-9}	1.33939×10^{-9}
a_6	-4.85338×10^{-15}	-4.85338×10^{-15}	1.4885×10^{-13}
γ (degrees)	–71.0	–62.5	10.0
d (degrees)	65.3512	38.5004	24.0722
r_c (mm)	–4813.92	–4363.6	3674.09
r_d (mm)	5238.29	4180.27	3305.19
recording wavelength (Å)	4880		

13.4.2 NUV Gratings

Table 13.13 presents design parameters of the NUV gratings. The NUV gratings are flat and were not constructed holographically. The NUV MAMA has low but measurable sensitivity at FUV wavelengths, and with some gratings second-order light could contaminate the spectrum. To minimize this effect, the coated optics are optimized for wavelengths above 1600 Å. Given the four reflections used in the NUV channel, wavelengths below 1600 Å, including geocoronal Lyman α, are effectively eliminated. In addition, gratings G230L and G285M have order-blocking filters mounted directly on them to block the second-order spectra below 1700 Å. Even with these filters, it is possible for second-order light to appear on the NUV MAMA when G230L is used, especially in the long-wavelength stripe.

Table 13.13: Design Parameters for the NUV Gratings

Dimension	G185M	G225M	G285M	G230L
groove density (mm^{-1})	4800	4800	4000	500
α (degrees)	27.24	33.621	35.707	5.565
β (degrees)	25.85	32.23	34.32	1.088
coating	Al + MgF_2	Al only	Al only	Al + MgF_2

13.5 The Location of COS in the *HST* Focal Plane

The location of the COS aperture in the *HST* focal plane is shown in Figure 13.28. Note the relative orientation of the *HST* V_2 and V_3 axes (the V_1 axis is along *HST*'s optical axis), as well as the relative locations and orientations of the other instruments. The COS aperture lies ~ 325 arcsec from the V_1 axis in the $+V_2, -V_3$ quadrant.

Figure 13.28: A Schematic View of the *HST* Focal Plane

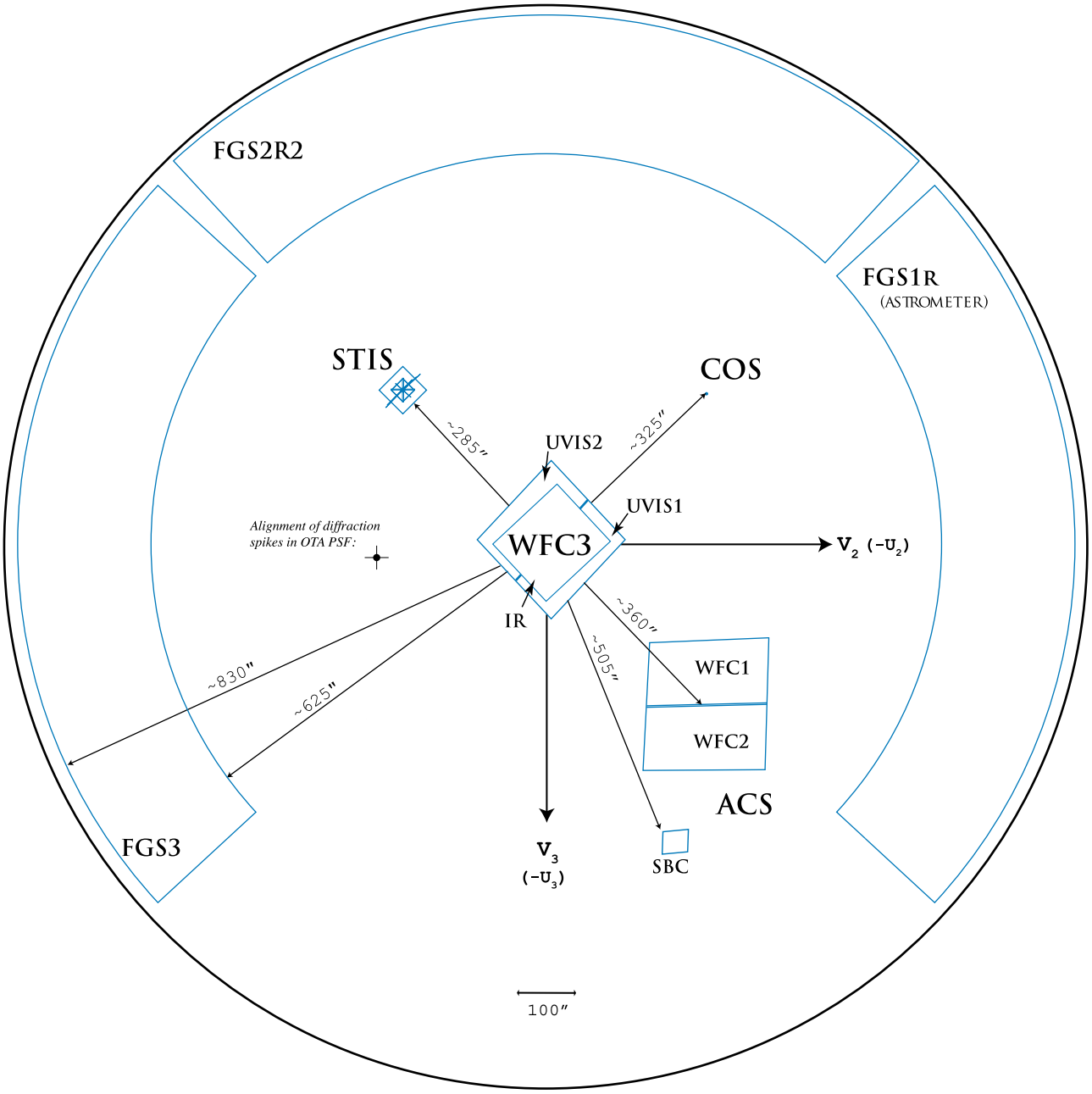

This drawing shows the entire *HST* focal plane and the apertures of the scientific instruments. The view is from the rear of the telescope looking forward toward the sky, the opposite of the sense of Figure 13.29.

13.6 The COS User Coordinate System

Figure 13.29 presents a schematic layout of the COS focal plane. In this figure, the *x* and *y* axes denote the COS user coordinate system. In this system, *x* lies along the wavelength (dispersion) axis and increases with increasing wavelength for both the FUV and NUV channels. For the NUV channel, *y* increases with increasing wavelength in the cross-dispersion (XD) direction. All references to COS (including POS TARG specifications in APT, the Astronomer's Proposal Tool, detector pixel coordinates, and science header keywords) employ the user coordinate system.

Figure 13.29: Schematic Layout of the COS Detectors

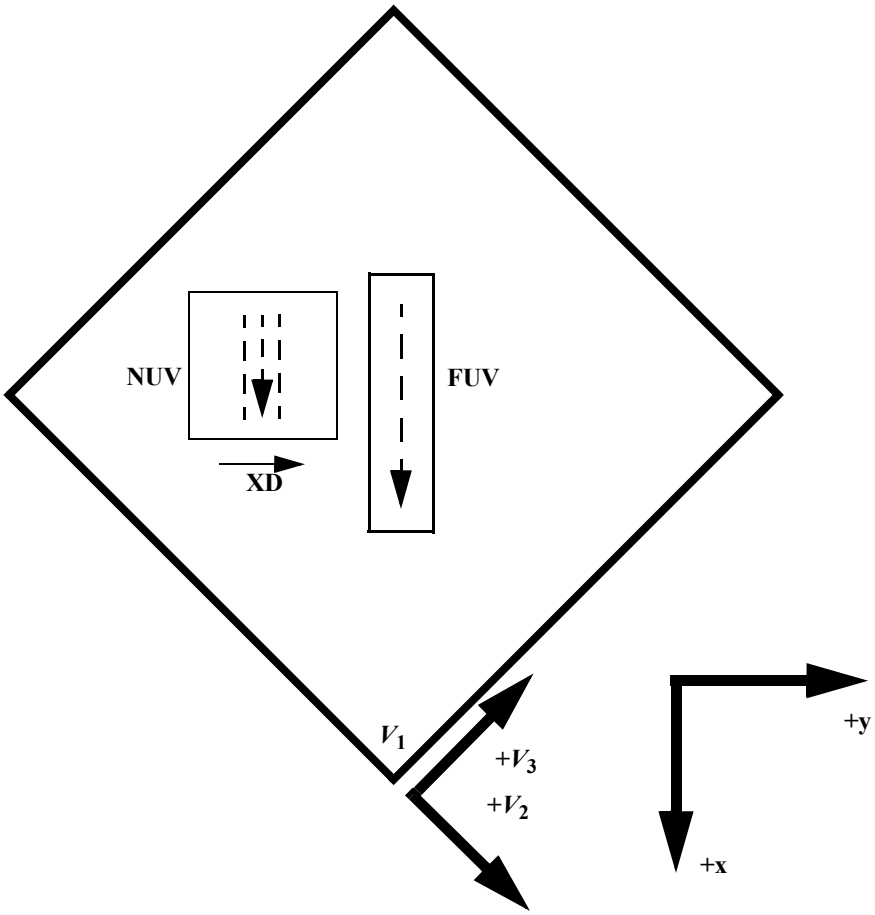

This view is from the front of the telescope looking aft. The dashed arrows show the direction of increasing wavelength for the two detectors, and "XD" indicates the direction of increasing wavelength for the NUV cross-dispersion direction. The *x* and *y* axes denote the COS user coordinate system. For both the FUV and NUV channels, wavelength increases in the +*x* or ($+V_2$, $-V_3$) direction.

Note that this diagram is purely schematic and it is intended to show only relative directions. This diagram does **not** show the locations of apertures. The bottom corner of this square (at V_1) corresponds to the center of the WF3 camera (see Figure 13.28).

Glossary

A Glossary of Terms and Abbreviations

ACCUM

Operating mode for COS in which only the locations of detected photons are recorded; no time information is recorded. ACCUM mode is designed for bright objects with high count rates. See also TIME-TAG.

Along Dispersion (AD)

The dispersion direction, corresponding to the X axis on both the FUV and NUV detectors.

Aperture Mechanism (ApM)

The Aperture Mechanism is used to place either the BOA or PSA into position as the science aperture. The ApM is also moved to place the FCA into position if a flat-field exposure is to be taken.

APT

The Astronomer's Proposal Tool, software provided by STScI for writing Phase I proposals and Phase II programs. The use of APT is encouraged in all cases, even for Phase I proposals, because it provides an accurate estimate of the actual time needed to obtain an observation. For more information, go to

`http://apt.stsci.edu`

BOA

The Bright Object Aperture is 2.5 arcsec in diameter with a neutral-density filter that attenuates flux by a factor of about 200.

calcos

The COS calibration pipeline, a software package that performs image and spectroscopic data reduction to produce output files useful for scientific analysis.

central wavelength

For the NUV gratings, the central wavelength is the approximate midpoint of the stripe B spectrum. For the FUV gratings, the central wavelength refers to the shortest wavelength recorded on segment A (though that value is subject to change as the instrument calibration improves).

channel (FUV or NUV)
One of the two COS optical systems, FUV and NUV, including mirrors, gratings, and detectors.

ETC
Exposure Time Calculator, software provided by STScI to estimate exposure times needed to achieve, say, a given signal-to-noise level on a source. Although information is provided in this handbook on exposure estimation, the ETC provides the most accurate way to determine the exposure times required to acquire or observe an object. The ETC is used together with the APT to plan *HST* observations. For more information, go to

http://www.stsci.edu/hst/cos/software/planning/etc

FCA
Flat-field Calibration Aperture, the aperture through which the on-board deuterium lamps illuminate the COS optical system.

FGS
Fine Guidance Sensor. By tracking guide stars, the three FGSs can maintain the pointing stability of *HST* with a precision of 2 mas or less.

FP-POS
A command used to move the spectrum on the detector (in the dispersion direction) to reduce the effects of fixed-pattern noise.

FUSE
Far Ultraviolet Spectroscopic Explorer, a moderate-resolution (*R ~ 15,000*), far-UV spectrograph that used micro-channel plate detectors similar to those employed by the FUV channel of COS.

FUV
The far-ultraviolet channel of COS can observe wavelengths from less than 900 to 1800 Å.

Galex
Galaxy Evolution Explorer, a NASA mission observing the sky in two ultraviolet bandpasses. *Galex* data are useful for determining the UV fluxes of COS targets. For more information, go to

http://www.galex.caltech.edu

GSC2/IRCS
Guide Star Catalog II / International Celestial Reference System. The GSC2 is an all-sky optical catalog based on 1” resolution scans of the photographic Sky Survey plates from the Polomar and UK Schmidt telescopes. The ICRS is the fundamental celestial reference system adopted by the International Astronomical Union for high-precision astrometry. Uncertainties in this system are dominated by the 0.3” uncertainty of the GSC2.

GTO

Guaranteed Time Observer, a member of the COS science team who has been granted a share of telescope time as part of their involvement in designing and building COS.

home position

The default position for a mechanism. COS is reconfigured at the start of each visit, and mechanisms are returned to their home positions. For the ApM, the home is the PSA; for OSM1, home is G130M, `CENWAVE=1309`; and for OSM2, home is G185M, `CENWAVE=1850`.

IDT

Instrument Development Team, NASA's term for the group that proposed and built COS.

LSF

Line Spread Function, the shape of a spectral feature emitted by a monochromatic point source.

MAMA

Multi-Anode Micro-channel Array, a photon-counting UV detector, used in the NUV channel.

MAST

The Multi-mission Archive at Space Telescope, which makes available data from a number of NASA missions, including *HST*. Go to

`http://archive.stsci.edu`

MCP

Micro-Channel Plate, a resistive glass plate with 10-15 micron-sized holes used within both the XDL and MAMA detectors to amplify photo-electrons into charge pulses large enough for electronic processing.

MIRRORA, MIRRORB

MIRRORA and MIRRORB are used for NUV imaging in COS. MIRRORA provides the highest throughput. MIRRORB uses a reflection off of the order-sorting filter of MIRRORA to get lower throughput, which can be helpful when observing bright targets.

NUV

The near-ultraviolet channel of COS can observe wavelengths from ~1650 to 3200 Å.

OSM1, OSM2

The Optics Select Mechanisms place gratings or mirrors in the optical path.

OTA

Optical Telescope Assembly, *HST*'s optical system of primary and secondary mirrors, plus the structure that holds them and maintains alignment.

pixel
The basic stored unit of data. In the NUV channel, MAMA pixels correspond to physical portions of the detector. In the FUV channel, the position of a detected event is assigned to a pixel based on calculations, but there are no physical pixels as such.

PHD
Pulse-Height Distribution, a histogram of the charge cloud sizes collected in a particular exposure or portion thereof. The PHD is a useful measure of data quality and is recorded as a data product for FUV exposures. PHD data are not available for NUV exposures.

POS TARG
The "`POS TARG X, Y`," special requirement is used to request a target offset in APT. POS TARG offsets are specified in the COS user coordinate system, which is used in all COS data products (Section 13.6). Note that the POS TARG coordinates represent motion of the target in the aperture; the telescope moves in the opposite direction.

PSA
Primary Science Aperture, a circular aperture 2.5 arcsec in diameter and completely open.

PSF
Point Spread Function, the two-dimensional distribution of light produced by the *HST*+COS optics.

resel
Resolution element of a spectrum or image. For spectra, a resel corresponds to the FWHM of a narrow emission line. Using pre-flight data, resels were determined to be roughly 6 pixels wide (dispersion direction) by 10 tall for the FUV channel and 3×3 pixels for the NUV. On-orbit data suggests that the FUV resel is somewhat larger than this, while the NUV resel is somewhat smaller. Note that spectra are recorded in pixel units and that any rebinning into resels is performed on the ground during data reduction.

segment
The COS FUV detector consists of two independent segments. In all spectroscopic modes, the long-wavelength end of the spectrum falls on segment A, and the short-wavelength end on segment B.

SMOV
Servicing Mission Observatory Verification, the period immediately following a servicing mission in which *HST*'s instruments are activated, tested, and made ready for science observing. Only a minimal set of calibrations are done in SMOV to confirm instrument performance; more detailed calibrations are performed in the ensuing cycle.

stim pulse

Artificially-induced events on each segment of the FUV detector. The stim pulses allow for the correction of thermal distortion and aid in determining the dead-time correction.

STMAG

In this system, the flux density is expressed per unit wavelength, and the reference spectrum is flat in F_λ. *STMAG = -2.5 log* F_λ *- 21.10*.

stripe

To accommodate the NUV detector format, COS NUV spectra are split into three non-contiguous stripes, each of which covers a relatively small range in wavelength.

TAGFLASH

Use of TIME-TAG mode with FLASH=YES selected. In this mode, wavelength-calibration spectra are obtained at periodic intervals during a PSA TIME-TAG observation so that any drifts of the spectrum due to residual motion of the optics can be removed.

TIME-TAG

A COS observing mode in which the locations (pixels) and times (to the nearest 32 msec) are recorded for each detected photon. Doing this consumes memory but allows great flexibility in reducing and analyzing the data.

wavecal

A wavelength calibration exposure; i.e., an exposure of the Pt-Ne wavelength calibration lamp through the WCA.

WCA

Wavelength Calibration Aperture, which is illuminated by a Pt-Ne wavelength calibration lamp.

XD

Cross-dispersion direction, corresponding to the Y axis on both the FUV and NUV detectors.

XDL

Cross Delay Line, the type of detector used in the FUV channel of COS.

Index